EXPERIMENTAL STUDIES OF INTRINSIC KINETICS AND DIFFUSION DURING METHANE STEAM REFORMING

Kaihu Hou

Department of Chemistry and Applied Chemistry

Science Research Institute

University of Salford, Salford, UK

TO MY WIFE, LANZHI, AND MY SON, SHAOBO

CONTENTS

LIST OF TABLES

LIST OF FIGURES

ACKNOWLEDGEMENTS

ABSTRACT

The intrinsic kinetics and diffusion behaviour of methane steam reforming have been investigated in this work. Measurements of effective diffusivities of the gases present in methane steam reforming have been carried out by using the steady-state technique over wide ranges of temperature and pressure in a modified Wicke-Kallenbach (W-K) type diffusion apparatus. The effects of diffusion limitation on the reactions were examined at atmospheric pressure in a pellet reactor; and the intrinsic kinetics of methane steam reforming have been studied on a commercial nickel/alumina catalyst (ICI 57-4) in an integral reactor. A simulation study has been carried out to determine the effects of hydrogen removal on the performance of a membrane reactor and the catalyst activity for methane steam reforming.

For the measurements of effective diffusivities, the temperature and pressure dependencies of effective diffusivities of gases measured have been obtained, and the tortuosities of pellets used for the gases measured have been estimated by using the parallel path pore model. At ambient pressure, the temperature exponent values range from 1.0 to 1.25. This indicates that the diffusion occurs in the transition region. At pressures up to 1MPa, the diffusion lies mainly in the bulk diffusion region. The pressure exponent was generally less than 1.0 with values lying between 0.4 and 0.85 except for gas-water vapour pairs where it is close to 1.0. The tortuosities estimated for the pellets varied from 1.84 to 2.51 for different gases at ambient pressure, but decreased with increase in pressure.

Using the pellet reactor that couples the diffusion and reaction for methane steam reforming, experimental results, which were obtained over catalyst pellets without holes, show that the diffusion rate of methane into the catalyst pellets almost totally controlled the reaction rate.

Under such diffusion limitation, other conditions did not show any apparent effects on the reaction. For catalyst pellets that contained four holes, the diffusion limitation on reaction was considerably reduced. However, catalyst activity did not play an important role in affecting the reaction. It was found that the effects of diffusion limitation on the catalyst pellet with a higher activity are greater than on catalyst pellet with a lower activity.

For the study of the intrinsic kinetics of methane steam reforming, the effects of temperature, pressure, and ratio of steam/methane on reactions have been investigated experimentally under condition of no diffusion limitation. The effects of total pressure on initial reaction rates indicated that the rate controlling steps of steam reforming are surface reactions between adsorbed species. The experimental results confirmed that both CO and CO_2 are primary products of steam reforming. Six detailed reaction mechanisms were considered by combining different adsorption behaviour of methane and steam on the nickel catalyst. For methane steam reforming, accompanied by water gas shift on the catalyst used, intrinsic rate equations were derived by using the Langmuri-Hinshelwood-Hougen-Watson (LH-HW) approach and Freundlich's non-ideal adsorption concept. Applying the method of parameter estimation and model discrimination, the new model was determined and the parameters in this model were determined as statistically significant and thermodynamically consistent.

The influence of hydrogen removed on the catalyst deactivated by hydrogen sulphide poisoning and carbon formation has been simulated for methane steam reforming in a tubular catalytic reactor with a hydrogen permeable wall. The effects of the main variables on H_2S tolerance and the tendency to carbon formation on the catalyst have been investigated. The simulation demonstrated that the hydrogen removed by the membrane

may cause more extensive catalyst deactivation with the H_2S tolerance decreasing and the tendency to carbon formation increasing as the proportion of hydrogen removal increased. The simulation also showed that the benefit of using a membrane reactor may not be achieved for feedstocks with a high H_2S level when a high proportion of hydrogen is removed. A higher applied pressure and a more efficient desulphurisation technique need to be employed to compensate for the influence of significant hydrogen removal on the catalyst activity for methane steam reforming in a membrane reactor operated at low temperatures.

CHAPTER 1 GENERAL INTRODUCTION

Catalytic steam reforming of hydrocarbons has grown during the last six decades into one of the world's great catalytic processes. It is of major economic significance since the products from it form the feed for a number of other major processes. Ammonia synthesis is still the largest consumer of synthesis gas, but the growing interest in C_1 chemistry, in large-scale conversion of natural gas into liquid products, and in the increasing availability of light hydrocarbon and natural gas around the world has created a need to explore the limits of the reforming technology to make it more cost effective.

It is well known that the reformer represents the 'heart' of the steam reforming process. This item of equipment is expensive and account for more than 50% of the total cost of the process due to the high temperatures and pressures necessarily applied. Therefore, one of the most important factors in determining the capital cost of the process is the design of the reformer. The process economy would be greatly improved if the process could be run under optimum operating conditions that change with change in feed composition or desired products. The optimum operating conditions can be determined most readily by the simulation of the reformer. Both the design and the simulation of the reformer are based on four elements, i.e., reaction kinetics, and transfer of mass, heat and momentum. Hence, a thorough understanding of these four elements is essential for any process optimisation.

In this thesis, attention is focussed on the two important aspects namely the intrinsic kinetics and mass transfer in the catalyst particles for steam reforming of methane on a commercial nickel catalyst (ICI 57-4). The main objectives of this study were to derive the intrinsic kinetics of methane steam reforming over the catalyst used, to obtain reliable

values of the effective diffusivities of the gases present in methane steam reforming, and to examine the effects of diffusion limitation on the reforming reaction.

Organisation of the thesis:

Chapter 2 presents a review of the literature of steam reforming. It is divided into three sections: the first section presents a review of early published papers on the kinetics and catalyst development for steam reforming; the second section is concerned with the literature on the reaction kinetics from 1950 to date; the last section gives a brief survey on the catalyst deactivation by sulphide poisoning and carbon formation, recent developments for increasing the catalyst stability, and attempts to apply new reactor configurations (e.g., catalytic membrane reactors) for methane steam reforming.

Chapter 3 reviews the diffusion literature and that for effective diffusivity measurement. The emphasis of the review is to describe the various theories of gas diffusion in porous solids and the associated methods of effective diffusivity measurement.

Methane steam reforming is a very typical heterogeneous gas-solid catalytic reaction. Relatively large sizes of catalyst pellets are used in order to minimise the pressure drop in the catalyst tubes during the process. Hence, diffusion of the reactants and products in the catalyst plays an important role in this reaction. Reliable values of the effective diffusivities of these gases are necessary to facilitate an understanding of the reaction kinetics of methane steam reforming. The experiments made and a discussion of effective diffusivity measurements obtained are described in Chapter 4. The effects of temperature and pressure on effective diffusivity were investigated.

An attempt to probe the effects of diffusion limitation on the methane steam reforming for catalysts of different activities and shapes is given in Chapter 5. The experimental measurements were carried out in a single pellet reactor.

A change of catalyst composition changes not only the values of the parameters of the kinetic model but also changes the model formulation through a change in the mechanism. Hence, it would be very useful for industrial practice to study specific kinetic mechanism of methane steam reforming for a given catalyst. Experiments of methane steam reforming in an integral reactor under the elimination of diffusion limitation and the derivation of kinetic model for a specified commercial catalyst (ICI 57-4) are presented in Chapters 6 and 7, respectively.

The influence of hydrogen removal on catalyst deactivation and on the performance of a membrane reactor for methane steam reforming is simulated in Chapter 8.

Finally, Chapter 9 gives the conclusions from this study and recommendations for future work.

CHAPTER 2 REVIEW OF LITERATURE ON METHANE

STEAM REFORMING

2.1 Introduction

The catalytic reforming of hydrocarbons in the presence of steam has been developed in the last sixty years into one of the most important industrial processes which provides different types of gas products for other processes. Ammonia, methanol, Fischer-Tropsch synthesis, hydrogen for petroleum refining, reducing gas for metal ores and town gas are the worldwide consumers of the product from catalytic steam reforming reactions. Among these processes, ammonia production consumes a very large proportion of the hydrogen produced from hydrocarbon steam reforming. Because of the increasing availability of light hydrocarbons and natural gas around the world and the increasing demands for synthesis gas and hydrogen, the catalytic reaction of steam reforming has been extensively investigated. Since hydrocarbons and natural gas are made up of a number of components, the reaction mechanism of the reforming process is extremely complex. Under industrial process conditions, higher alkanes, such as C_2H_6, C_3H_8 etc., give very fast and complete conversion of the feedstock with methane as the only surviving alkane in the product. A general observation which has been made when reforming higher alkanes is that, provided the contact time is long enough, the exit gas composition is that which approximately corresponds to the chemical equilibrium involving only methane steam reforming. Based on these facts, most research work on the kinetics of the steam reforming and the modelling and simulation of the reformer have been carried out with regard to methane steam reforming.

Therefore in this chapter, a review of the steam reforming process is mainly concerned with methane steam reforming. The chapter is divided into three sections; the first section briefly reviews the early kinetic studies and catalyst development for methane steam reforming; the second section discusses the kinetic investigations of methane steam reforming from the 1950s to up to date; finally, some recent studies on the catalyst and the particular application of a membrane reactor for methane steam reforming are given in the final section.

2.2 Early Kinetic Studies and Catalyst Development for Methane Steam Reforming.

The steam reforming process converts hydrocarbons into hydrogen, carbon dioxide, carbon monoxide, and methane in various proportions depending on the reaction conditions dictated by the end use of the gas mixtures desired. The pertinent stoichiometrical equations describing the system are:

$$C_nH_m + n\,H_2O = n\,CO + (n + m/2)\,H_2 \tag{1}$$

$$CO + H_2O = CO_2 + H_2 \tag{2}$$

$$C_nH_m + 2n\,H_2O = n\,CO_2 + (2n + m/2)\,H_2 \tag{3}$$
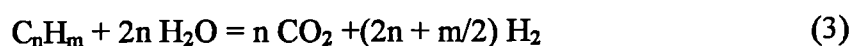
For higher hydrocarbons (n ≥ 2), it is assumed that the hydrocarbon is chemisorbed on a dual site followed by successive scission of the carbon-carbon bonds. The resulting C_1-species react with adsorbed steam as the methane steam reforming reaction (Rostrup-Nielsen, 1984).

Light hydrocarbons and specifically methane tend to be stable molecules, due to their chemical stucture. Since the reaction of hydrocarbon with steam has to break its C-H and/or C-C bond to produce permanent gases of hydrogen, carbon dioxide, and carbon

monoxide, a high temperature and catalysts are necessary for the reaction to proceed. Hence the developments of appropriate catalysts have been given a very high priority in early investigations of hydrocarbon steam reforming. Van Hook (1980) gave a brief state of the art summary in the area of steam reforming prior to the 1930s. Hydrocarbon interaction with catalytic metals was observed in 1817 during the development of the mine safety lamp, and the production of hydrogen when hydrocarbons and steam are passed over calcium oxide was described in 1868. The application of nickel for this process was claimed in 1889. A steam reforming patent (British patent, 1927) claimed low operating temperature conditions by using catalysts of iron, cobalt, or nickel promoted with chromia, vanadia, alkali, or alkaline. Based on the experiments before the 1930s, catalysts of supported nickel or cobalt were rated as the best materials. Using nickel catalysts, theoretical values for equilibrium in the methane steam reforming reaction were verified in 1924, and experimental demonstrations of the effect of temperature and pressure on system equilibrium were reported in 1931. Intraparticle diffusion limitation and severe catalyst deactivation were also encountered in this period.

In 1933 Fujimoto (from Van Hook, 1980) reported on methane steam reforming and methane decomposition over a broad temperature range of 673 to 1273 K using reduced nickel foil and a 90% nickel-alumina catalyst at atmospheric pressure. For steam reforming at a steam/carbon ratio of about 2.5 and constant feed rate conditions, equilibrium methane conversions were achieved using both catalysts. However, increasing the temperature beyond 866 K with nickel foil resulted in a serious loss in activity with a methane conversion of only a few percent being attained between 977 and 1172 K. The nickel foil had been seriously damaged with carbon above 866 K, whereas the 90% nickel-alumina catalyst withstood 250 hr of operation at 973 K and maintained the equilibrium conversion.

Ipatieff et al (1950) examined various catalysts for methane steam reforming in the 755-1089 K range, at 1 and 18 bar pressure for steam/methane ratios of 5, 11,and 30. Among the catalysts based on copper, iron, cobalt, nickel and several combinations of these metals, nickel on Kieselguhr catalysts showed high activity. Life tests indicated that a 7.4% copper, 65%nickel on Kieselguhr was the best and showed the beneficial effect of copper promotion on the life of the catalyst. Operating pressure, even at steam/methane ratios beyond 30, severely affected catalyst life, especially the nonpromoted nickel catalyst.

From their experiments on the activities of nine commercial catalysts for the steam reforming of methane at atmospheric pressure and a steam/methane ratio of 2.5, Arnold et al (1952) found that catalysts with higher nickel content generally had higher activity. Attempts to undertake experiments at 1422 K resulted in rapid plugging of the reactor with carbon and all catalysts were seriously damaged at 1338 K.

Pioneering attempts to develop sulphur-resistant steam reforming catalysts were carried out by Sabastian and Riesz (1951). Supported nickel, cobalt, molybdenum, chromium, and combinations of these metals were tested. Using their best sulphide nickel on silica catalyst (Ni/Si = 1/3 atom ratio), they achieved a high rate of propane conversion in the presence of 2500 ppm H_2S at the lowest temperature studied (922 K).

A reasonable mechanistic scheme, based on Fujimoto's data for nonporous nickel foil (A) and high activity porous nickel-alumina catalysts (B) was suggested by Van Hook (1980) as follows;

(A) Methane decomposition/steam reforming on nonporous foil:

$$CH_4 \underset{k_b}{\overset{fast}{\rightleftharpoons}} \text{Intermediate} \nearrow \overset{k_1}{\longrightarrow} C + H_2$$
$$\searrow_{+H_2O, k_2} CO + CO_2 + H_2$$
$$+ H_2O, k_3 \quad \text{1072 K and higher; essentially irreversible to gasified products}$$
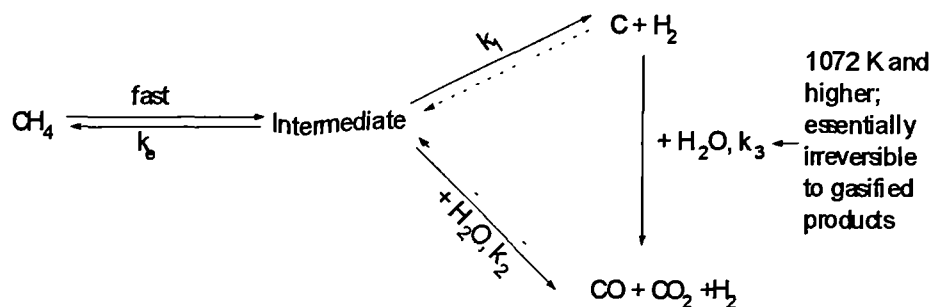
where the intermediate concentration $= k_e P_{CH_4} / P_{H_2}^x$ and $k_2 > k_1 > k_3$;

(B) Methane/steam reaction on porous catalyst with diffusion limitations:

$$CH_4 \overset{k_d}{\longrightarrow} \text{Intermediate} \nearrow \overset{k_1}{\longrightarrow} C + H_2$$
$$\searrow_{+H_2O, k_2} CO + CO_2 + H_2$$
$$+ H_2O, k_3$$
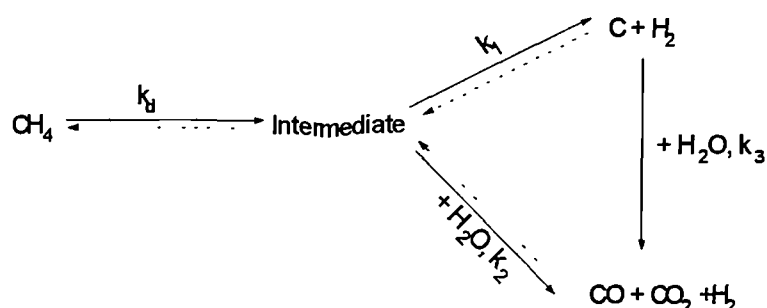
where k_d is the internal pore diffusion rate constant.

Fujimoto's data also indicated that methane steam reforming could be approximated by reversible first order kinetics over both catalysts. An Arrhenius plot of methane decomposition (thermodynamic equilibrium used on the basis of carbon, as graphite, at unit activity) for the nickel foil gave an excellent straight line from 977-1172 K with an apparent activity energy of 181 kJ/mole. However, an activation energy of only 22 kJ/mole was obtained for methane decomposition over the nickel-alumina catalyst in the 672 to 866 K. This means that the serious intraparticle diffusion limitation greatly reduced the apparent activation energy.

Experiments were performed for the CH_4/steam and CH_4/CO_2 reforming reactions using finely divided copper on silica in a fluid bed, and early mechanistic suggestions were developed by Lewis et al (1949). They indicated that the kinetics show first order dependence in both steam (or CO_2) and methane. The poor performance of copper as a catalyst was confirmed by the low conversion rates of 0.01 to 0.03 moles CH_4 converted /(g cat hr p_{CH_4}) at 1089 K. Noteworthy in this early work for both CO_2 and steam reforming of methane is the high activation energy of 200kJ/mole for finely divided catalyst and the appearance of inhibition terms of CO_2, H_2O, H_2 in the rate expressions.

Reversible first order (in methane) kinetics were also given from Arnold et al.'s studies (1952). Based on their experiments at various space velocities and temperatures between 977 and 1089 K using 16/20 mesh 6% nickel on alumina/silica at atmospheric pressure, an activation energy of at least 140 kJ/mole was suggested. However, a lower activation energy of 60.6 kJ/mole was obtained from the experiments using 7/16 × 7/16 in. extruded catalyst (24% Ni on $Ca/SiO_2/Al_2O_3$). This is probably the earliest published result showing a change of activation energy with a change in catalyst particle size.

From pilot plant investigations and thermodynamic calculations, Reitmeier et al (1948) produced plots and equations which make possible the selection of reacting mixtures of light hydrocarbons, steam, and/or carbon dioxide to produce synthesis gas having a wide range of compositions without the deposition of carbon on the catalyst. Additional plots make possible the selection of reacting compositions to produce synthesis gas of any desired composition. Their results also demonstrated the importance of selecting equipment and operating conditions that assist in preventing carbon deposition on the catalyst.

Since early studies were limited because of the analytic equipment available, it was difficult to investigate the kinetic mechanism of methane steam reforming and to reveal the reasons for catalyst deactivation in more detail. However, the main questions relating to steam reforming had been answered, including the reaction order with respect to methane, catalyst deactivation due to carbon formation and sulphide poisoning. It was also established that nickel was the best catalyst for steam reforming, and that alumina and magnesia were uniformly superior supports for the nickel.

2.3 Studies of the Kinetics of Methane Steam Reforming

The kinetic mechanisms of methane steam reforming on a nickel catalyst have been extensively studied for various catalysts by various means, and a large number of rate equations has been reported in the literature since the 1950s.

Akers and Camp (1955) performed the first extensive study of the kinetics of methane steam reforming. The work was carried out in an integral reactor at atmospheric pressure and a temperature range of 613 to 911 K using commercial 1/8 inch pellets of nickel supported on Kieselguhr. The study did not suggest any mechanism, but they found that the reaction rate is first order with respect to methane with no dependencies on other reactants and the rate controlling step was stated to be the dissociative adsorption of methane. On the basis of thermodynamic analysis and their experimental results, they concluded that reactions (1) and (3) are the primary reactions, i.e. both CO and CO_2 are primary reaction products, and if reaction (2) is proceeding, the rate of this is slower. Thus both steam reforming reactions producing CO and CO_2, (1) and (3) are involved rather

than one with the other product being produced through the reaction (2). The lower reaction rate constant and an apparent activation energy of 36.8 kJ/mol reported by the authors suggest the possibility of diffusion limitation in this study (Van Hook, 1980)

Following Akers and Camp's work on methane steam reforming, Bodrov et al (1964, 1967, and 1968) performed a series of systematic studies on the reaction of methane and steam using nickel foil as catalyst in order eliminate the bias due to pore limitation, and also used porous nickel catalysts of various sizes in order to investigate any pore diffusion limitations. They found that there is a certain correlation with the partial pressures of CO, H_2O, and H_2, and their influence varies with temperature:

(a) for 673 K < T < 773 K

$$r = kP_{CH_4} / P_{H_2} \qquad (2.1)$$

(b) for 773 K < T < 873 K

$$r = \frac{kP_{CH_4}}{P_{H_2}^{0.5}} \qquad \text{with E= 151 kJ/mol} \qquad (2.2)$$

(c) for 873 K < T < 1173 K

$$r = \frac{kP_{CH_4}}{1 + aP_{H_2O} / P_{H_2} + bP_{CO}} \qquad \text{with E= 82.1 kJ/mol} \qquad (2.3)$$

These forms of rate equation suggest that the inhibition due to H_2, which is a product, decreases with temperature increase. When the temperature is higher than 973 K, as the H_2 concentration increases, the rate of reaction increases and so indicates some kind of autocatalysis. Since hydrogen is a product of a reversible reaction it is more appropriate that the increase of hydrogen concentration will decrease the rate through

(1) the reversible reaction step.

(2) hydrogen adsorption to decrease the concentration of vacant active sites.

The rate equation (2.3) was derived from the following mechanism

$$CH_4 + s - CH_2(s) + H_2 \qquad (2.4)$$

$$H_2O + s = O(s) + H_2 \qquad (2.5)$$

$$CH_2(s) + O(s) = CO(s) + 2H_2 + s \qquad (2.6)$$

$$CO(s) = CO + s \qquad (2.7)$$

$$CO + O(s) = CO_2 + s \qquad (2.8)$$
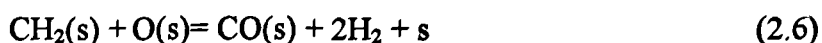
Where s is an active site of the catalyst. Based on their study, Bodrov et al proposed that at lower temperatures (673-873 K), the rate controlling step is the surface reaction between the adsorbed oxygen and the adsorbed CH_2 radical, while at higher temperatures the rate controlling step is methane adsorption and partial dissociation on active nickel. Their study also implies that the reaction is of first order with regard to methane, and only CO is a primary product of the reactions, whereas CO_2 is possibly produced through the water gas shift reaction. The latter contradicts the conclusion reported by Akers and Camp (1955).

Dependence of the extent of the methane steam reforming reaction upon the partial pressures of methane, hydrogen, and water was investigated by Agnelli et al (1985). The experiments were accomplished over an alumina-supported nickel catalyst at atmospheric pressure and a temperature range of 915 to 1010 K in a flow reactor. A conclusion that the reaction is of first order with respect to methane was given, since in their experiments the extent of reaction did not depend on the inlet concentration of methane. They also noticed that the extent of reaction increases as hydrogen partial increases at 915 and 980 K, whereas at 1010 K the variation of hydrogen partial pressure has no effect on the extent of reaction. A mechanism differing from Bodrov's was proposed, which assumed that adsorption of methane occurred with complete dissociation to the carbon atom.

$$CH_4 + 7s = C(s_3) + 4 H(s) \qquad (2.9)$$

$$4H(s) = 2H_2 + 4 s \qquad (2.10)$$

$$H_2O + s = O(s) + H_2 \qquad (2.11)$$

$$C(s_3) + O(s) = CO(s) + 3s \qquad (2.12)$$

$$CO(s) = CO + s \qquad (2.13)$$

$$CO(s) + O(s) = CO_2 + S \qquad (2.14)$$

By postulating that methane adsorption with dissociation was the rate controlling step, one rate equation was derived as follows:

$$r = \frac{kP_{CH_4}}{\left(1 + K_{H_2O} \dfrac{P_{H_2O}}{P_{H_2}} + K_{CO}P_{CO}\right)^7} \qquad (2.15)$$

where K_{H_2O} and K_{CO} are adsorption coefficients.

Their mechanism also implies that carbon dioxide is produced through adsorbed CO reacting with adsorbed oxygen, and is not a primary product originating from methane directly. It was found that different reduction and oxidation treatment of the catalyst had no influence on the extent of reaction, i.e. on the catalyst activity. This observation differs from Bartholomew's (1976, 1980). The activation energy of 184 kJ/mol obtained indicates that the experiments were carried out under conditions with no pore diffusion limitation.

Ross and Steel (1972) studied the mechanism of the steam reforming of methane over a coprecipitated nickel alumina catalyst (75Ni %) in powder form (250-335 μm). The reaction was carried out at low total pressures (0-10 mm Hg), in the temperature range of 773-873 K and at a low steam/methane ratio (2.0-0.2). The kinetics obtained fitted the following expression:

$$r = \frac{kP_{CH_4}}{P_{H_2O}^{0.5}} \qquad (2.16)$$

This rate equation shows a first order reaction with respect to methane, and no inhibition due to products. The dependence on steam (which is a reactant) is of negative order (-0.5). This is most probably due to competitive adsorption between methane and steam for the active sites. The authors proposed the following mechanism

$$H_2O + s = OH(s) + 0.5\ H_2 \qquad (2.17)$$

$$CH_4 + s = CH_x(s) + (4-x)/2\ H_2 \qquad (2.18)$$

$$CH_x(s) + OH(s) = CO + (1+x)/2\ H_2 \qquad (2.19)$$
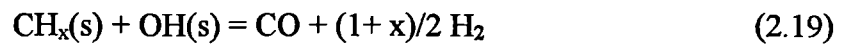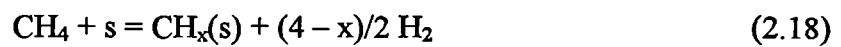
where step (2.18), the adsorption-dissociation of methane, is the rate controlling step. In this case the very low activation energy (28.9 kJ/mol) indicates that they worked under the pore diffusion limitation zone due to the high activity of the catalyst (75 Ni %) used.

Experiments on methane steam reforming were performed over 3/16 inch pellets of a Ni/alumina catalyst in a continuous stirred tank reactor at 1-2 atm and 623-723 K (Quach and Rouleau, 1975). Based on the assumption that the rate controlling step is reaction between the surface adsorption of methane and the steam in the gas phase which produces adsorbed hydrogen and CO_2 in the gas phase, they suggested the following equation:

$$r = \frac{k\left(P_{CH_4}P_{H_2O}^2 - \dfrac{P_{CO_2}P_{H_2}^4}{K_{p3}}\right)}{1 + K_{CH_4}P_{CH_4}} \qquad (2.20)$$

Their postulated equation contradicts the results of other investigators (Leach et al., 1980; Schouten et al., 1979) which suggest complete dissociation of the adsorbed methane, together with the assumption that the reaction occurs between adsorbed methane and steam in the gas phase. The denominator of the rate equation implies none or very weak

adsorption of CO and H_2, while in fact CO and H_2 are usually strongly adsorbed on a nickel catalyst with competition between these products (Kester and Falconer, 1984).

Using a recirculation reactor at 1 bar and 973-1173 K with a Ni commercial catalyst of size 0.25-0.63 mm, Kopsel et al (1980) found that the reaction rate is first order with respect to methane, while hydrogen indirectly inhibits the reaction and steam promotes the reaction. By assuming that methane adsorption is the rate controlling step, the rate equation was given as

$$ r = \frac{kP_{CH_4}}{1 - 11.6\dfrac{P_{H_2O}}{P_{H_2}}} \tag{2.21} $$

The authors did not report any diffusion limitation in their results. The activation energy for the temperature range of 973-1173 K was found to be 146.5 ± 20.9, which suggests the absence of diffusion effects. A question would be raised from the rate equation reported: when the term value of $11.6\dfrac{P_{H_2O}}{P_{H_2}}$ is larger than one, the denominator will be negative. This means that the rate equation can only be applied to a case of a very high hydrogen concentration in the feed.

Natural gas steam reforming was studied by Atroshchenko et al. (1969) using an integral reactor under pressures of 2 to 6 bar and in the temperature range 873-1023 K. A commercial catalyst GIAP-3 (containing Ni supported on alumina) was used with particle sizes of 3-4 mm and a surface area of 5 m^2/g. Atroshchenko suggested the following mechanism

$$ H_2O + s = O(s) + H_2 \tag{2.22} $$

$$ O(s) + CH_4 = CO + 2H_2 + s \tag{2.23} $$
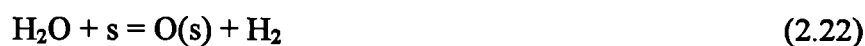
This mechanism assumes that first step is very rapid and the second step is the rate controlling step, which could proceed in a series of consecutive chain reactions. An expression was given to calculate the reaction rate at a close approach to equilibrium as follows.

$$r = \frac{kP_{CH_4}P_{H_2O}}{P_{H_2}}\left(1 - \frac{P_{CO}P_{H_2}^3}{K_{P1}P_{CH_4}P_{H_2O}}\right) \quad (2.24)$$

Pore diffusion limitations were not examined. The apparent activation energy was determined to be about 93 kJ/mol, which indicates the experiments were carried out in the transition region between intrinsic kinetics and strong pore diffusional controlled kinetics. Analysis of the rate equation shows that it takes into consideration the reversible reaction step in steam reforming. The rate equation also implies that the forward reaction is first order with respect to methane and steam, and inhibited by hydrogen. The reversible reaction is independent of the methane concentration, and is second order in hydrogen and first order in CO.

The effect of the support on the reaction kinetics of methane steam reforming was studied recently by Al-Ubaid (1984). The experiments were carried out on nickel supported by different materials (in powder form) at atmospheric pressure within the temperature range 723-823 K. These supports had a wide range of acidity. The results obtained showed that the support has a major effect on the reaction rate functionality of the reactants. A positive order for steam was found on the acidic support (Y-zeolite), whereas a negative order for steam was produced with a less acidic support (Ni/spinel). Of course, these results cannot be generalised since for a negative order of steam this dependence cannot extend over the whole range of concentration because steam is a reactant. At the same time, they found that the reaction order with respect to methane is decreased with support acidity. However, the

dependence on hydrogen is not affected by the support type, indicating the absence of

hydrogen competition with the reactants for the reduced nickel sites. For the less acidic

support, the following mechanism was proposed

$$CH_4 + s = C(s) + 2H_2 \tag{2.25}$$

$$H_2O + s = O(s) + H_2 \tag{2.26}$$

$$C(s) + O(s) = CO(s) + s \tag{2.27}$$

$$CO(s) + O(s) = CO_2 + 2s \tag{2.28}$$
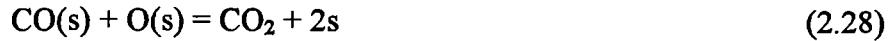
Assuming the rate controlling step is the surface reaction between the adsorbed carbon and

oxygen to produce carbon monoxide, the rate equation for above mechanism is

$$r = \cfrac{kP_{CH_4}P_{H_2O}}{P_{H_2}^3\left(1 + K_1\cfrac{P_{CH_4}}{P_{H_2}^2} + K_2\cfrac{P_{H_2O}}{P_{H_2}} + K_3\cfrac{P_{CO_2}P_{H_2}}{P_{H_2O}}\right)^2} \tag{2.29}$$

furthermore, if

$$1 + K_1\frac{P_{CH_4}}{P_{H_2}^2} + K_3\frac{P_{CO_2}P_{H_2}}{P_{H_2O}} \ll K_2\frac{P_{H_2O}}{P_{H_2}}$$

the following simplified rate expression is obtained

$$r = \frac{k^{\bullet}P_{CH_4}}{P_{H_2O}P_{H_2}} \tag{2.30}$$

This mechanism implies that carbon dioxide is not a direct primary product from methane,

but is produced from reaction between adsorbed CO, which is a primary product, and

adsorbed oxygen.

A bifunctional mechanism was suggested by Al-Ubaid (1984) for the highly acidic support

$$H_2O + Support = H_2O(support) \tag{2.31}$$

$$CH_4 + s = C(s) + 2H_2 \tag{2.32}$$

$$C(s) + H_2O(support) = HCO(s) + 0.5 H_2 + support \tag{2.33}$$

$$HCO(s) + H_2O(support) = HCOO(s) + H_2 + support \qquad (2.34)$$

$$HCOO(s) = CO_2 + 0.5\ H_2 + s \qquad (2.35)$$
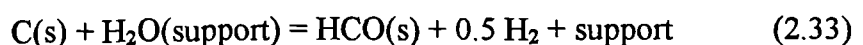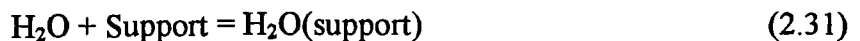
The overall rate equation obtained by assuming step (2.35) as the rate controlling step is as follows

$$r = \frac{kP_{CH_4}P_{H_2O}^2}{P_{H_2}^{3.5}\left(1 + K_1\dfrac{P_{CH_4}}{P_{H_2}} + K_2\dfrac{P_{CH_4}P_{H_2O}}{P_{H_2}^{2.5}} + K_3\dfrac{P_{CH_4}P_{H_2O}}{P_{H_2}^{3.5}}\right)} \qquad (2.36)$$

If the following inequality is satisfied,

$$K_2\frac{P_{CH_4}P_{H_2O}}{P_{H_2}^{2.5}} \gg 1 + K_1\frac{P_{CH_4}}{P_{H_2}} + K_3\frac{P_{CH_4}P_{H_2O}}{P_{H_2}^{3.5}}$$

the following simplified rate equation can be obtained

$$r = k^\bullet\frac{P_{H_2O}}{P_{H_2}} \qquad (2.37)$$

Based on the mechanism postulated by author, this suggests that carbon dioxide is a primary product from methane, whereas CO would be produced from the reverse water gas shift reaction. Comparing the two mechanisms reported by Al-Ubaid above, one conclusion is that the properties of the support affect the formation of primary products, and also changes the mechanism of steam reforming.

On the assumption that desorption of products was the rate controlling step, a kinetic mechanism and rate equations for methane steam reforming were derived by Allen et al (1975). The experiments were carried out over a commercial nickel catalyst (G-56B) of 3/16×3/16 inch pellets in a fixed bed integral reactor at a temperature of 915 K and six levels of pressure from 1 to 18 bar. By analysis of the correlation of conversion data at different pressures, they concluded that the overall rate is controlled by a step involving desorption of products due to the initial rates of reaction and which appears to be

independent of the total pressure. To derive the rate equations, the following mechanism was proposed

$$H_2O + s = H_2O(s) \tag{2.38}$$

$$CH_4 + H_2O(s) = CO(s) + 3H_2 \tag{2.39}$$

$$CO(s) + H_2O(s) = CO_2(s) + H_2 \tag{2.40}$$

$$CO(s) = CO + s \tag{2.41}$$

$$CO_2(s) = CO_2 + S \tag{2.42}$$
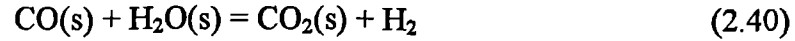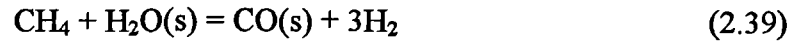
Applying the method of Hougen and Watson, and assuming desorption of CO and CO_2 as the rate controlling steps, they derived the rate expressions as follows

$$r_{CO} = \frac{k_{CO}\left(P_{CH_4}P_{H_2O} - \dfrac{P_{CO}P_{H_2}^3}{K_{P1}}\right)}{P_{H_2}^3\left(1 + K_1 P_{H_2O} + K_2 \dfrac{P_{CH_4}P_{H_2O}}{P_{H_2}^3} + K_3 \dfrac{P_{CH_4}P_{H_2O}^2}{P_{H_2}^4}\right)} \tag{2.43}$$

$$r_{CO_2} = \frac{k_{CO_2}\left(P_{CH_4}P_{H_2O}^2 - \dfrac{P_{CO_2}P_{H_2}^4}{K_{P3}}\right)}{P_{H_2}^4\left(1 + K_1 P_{H_2O} + K_2 \dfrac{P_{CH_4}P_{H_2O}}{P_{H_2}^3} + K_3 \dfrac{P_{CH_4}P_{H_2O}^2}{P_{H_2}^4}\right)} \tag{2.44}$$

It is worth noticing that there is a big difference from the results of other investigators reviewed above, in which methane does adsorb on the catalyst, whereas the present results propose it is present in the gas phase and reacts with adsorbed steam. Methane adsorption with dissociation on the nickel catalyst has indeed been confirmed by many investigators so their proposed mechanism could hardly be accepted.

Numaguchi and Kikuchi (1988) studied methane steam reforming in an integral fixed bed reactor over a nickel catalyst at temperatures varying from 674 to 1160 K, pressures ranging from 1.2 to 25.5 bar and steam/methane ratios in the feed between 1.44 and 4.5.

By assuming surface reactions to be the rate controlling steps for steam reforming, they proposed hybrid rate expressions of Langmuir-Hinshelwood form and power expressions based on the Freundlich adsorption rate expression. No details of mechanisms were suggested in their paper. For reaction (1), in which reaction between methane and steam produces CO and H_2

$$r_1 = \frac{k_1(P_{CH_4}P_{H_2O} - P_{CO}P_{H_2}^3 / K_{P1})}{P_{H_2O}^{0.596}} \qquad (2.45)$$

For reaction (2), i.e., the water gas shift reaction

$$r_2 = k_2(P_{CO}P_{H_2O} - P_{CO_2}P_{H_2} / K_{P2}) \qquad (2.46)$$

From equations (2.45) and (2.46), the positive reaction order with respect to steam is found in both equations, and hydrogen retards the reaction rates via backward reaction and not via the competitive adsorption with other reactants. Only CO is a primary product as suggested. The activation energies for reaction (1) and (2), which are 106.87 kJ/mol and 54.53 kJ/mol, respectively, were determined by the calculation of mass and heat balances considering interphase diffusions by using a numerical method based on the non-linear two-point boundary value problem. Their results suggest that best way to probe the mechanism of methane steam reforming is by combining the Langmuir ideal adsorption theory and the Freundlich adsorption concept to determine the mechanism of methane steam reforming.

In the study by De Deken et al (1982), great care was taken to eliminate the diffusion limitation while still working at the near industrial conditions of 823-913 K and 5 to 15 bar. The experiments were performed over a commercial catalyst ($Ni/\alpha Al_2O_3$) in a tubular reactor operated in the integral mode and at steam/methane ratios of 3 to 5. Molar ratios of hydrogen to methane in the feed were maintained between 1.0 and 2.25 during the

experimentation to avoid any carbon deposition or reoxidation of the catalyst. The following mechanism was suggested

$$CH_4 + s = C(s) + 2H_2 \qquad (2.47)$$

$$H_2O + s = O(s) + H_2 \qquad (2.48)$$

$$C(s) + O(s) = CO(s) + s \qquad (2.49)$$

$$C(s) + 2O(s) = CO_2(s) + 2s \qquad (2.50)$$

$$CO(s) = CO + s \qquad (2.51)$$

$$CO_2(s) = CO_2 + s \qquad (2.52)$$

The authors chose the two necessary conversions for defining component composition to be the total conversion of methane and the conversion of methane into carbon dioxide. After discrimination over 150 Hougen-Watson based models, the following rate expressions were obtained

$$r_{CO} = \frac{k_{CO}\left(P_{CH_4}P_{H_2O} - \dfrac{P_{CO}P_{H_2}^3}{K_{P1}}\right)}{P_{H_2}^3\left(1 + K_{CO}P_{CO}\right)^2} \qquad (2.53)$$

$$r_{CO_2} = \frac{k_{CO_2}\left(P_{CH_4}P_{H_2O}^2 - \dfrac{P_{CO_2}P_{H_2}^4}{K_{P3}}\right)}{P_{H_2}^4\left(1 + K_{CO}P_{CO}\right)^3} \qquad (2.54)$$

where K_{P1} and K_{P3} are the equilibrium constants for the reactions producing CO and CO_2, (i.e., reactions (1) and (3), respectively), k_{CO} and k_{CO_2} are the corresponding reaction rate constants and K_{CO} is the adsorption constant of CO. They concluded that the rate controlling steps are the surface reactions between adsorbed carbon atoms and adsorbed oxygen atoms from complete dissociation of methane and steam, and that CO_2 and CO are formed simultaneously. However, the mechanism excluded the water gas shift reaction.

A more general intrinsic kinetic model was developed by Xu and Froment (1989). Experimental temperatures were in the range of 773-848 K for methane steam reforming and 573-673 for the reverse water gas shift reaction, respectively. Other experimental conditions were pressures from 5-15 bar, a steam/methane ratio of 3-5 and a hydrogen/methane ratio of 1.25. Operation was in the integral mode and the catalyst used was a commercial nickel catalyst supported on magnesium spinel with 15.2% Ni. The two main reactions of steam reforming together with the water gas shift reaction were taken into consideration by these authors. A large number of reaction mechanisms were tested, first from thermodynamic considerations and then by model discrimination and parameter estimation procedures. None of the reactions was taken to be at equilibrium. Thermodynamic analysis suggested that neither the direct production of CO_2 from CO, nor the independent parallel production of CO and CO_2 from CH_4, were likely to occur alone. Based on the mechanism of an adsorption/surface reaction/desorption model in 13 steps with intermediates of CH_2O and CHO, and assuming that the surface reactions were the rate controlling steps, the following equations were obtained

$$r_1 = \frac{k_1 \left(P_{CH_4} P_{H_2O} - \frac{P_{CO} P_{H_2}^3}{K_{P1}} \right)}{P_{H_2}^{2.5} (den)^2} \tag{2.55}$$

$$r_2 = \frac{k_2 \left(P_{CO} P_{H_2O} - \frac{P_{CO_2} P_{H_2}}{K_{P2}} \right)}{P_{H_2} (den)^2} \tag{2.56}$$

$$r_3 = \frac{k_3 \left(P_{CH_4} P_{H_2O}^2 - \frac{P_{CO_2} P_{H_2}^4}{K_{P3}} \right)}{P_{H_2}^{3.5} (den)^2} \tag{2.57}$$

Where $den = 1 + K_{CO} P_{CO} + K_{H_2} P_{H_2} + K_{CH_4} P_{CH_4} + K_{H_2O} \frac{P_{H_2O}}{P_{H_2}}$.

The 13 step mechanism used suggests a competition for the active sites between methane and steam, and thus leads to the functional dependence of the rate of reaction shown above, which can give non-monotonic dependence of reaction rate upon the partial pressure of steam and methane (Elnashaie, et al 1990).

Soliman et al (1992) studied the intrinsic kinetics of methane steam reforming in an integral reactor over a Ni/Ca aluminate spinel catalyst developed in-house at 748-823 K and 1-3 bar. A mechanism similar to Xu and Froment's was suggested, and the final rate equations were determined by model discrimination as follows:

$$r_1 = 0 \tag{2.58}$$

$$r_2 = \frac{k_2\left(P_{CO}P_{H_2O} - \dfrac{P_{CO_2}P_{H_2}}{K_{P2}}\right)}{P_{H_2}^{2.5}(den)^2} \tag{2.59}$$

$$r_3 = \frac{k_3\left(P_{CH_4}P_{H_2O}^2 - \dfrac{P_{CO_2}P_{H_2}^4}{K_{P3}}\right)}{P_{H_2}^{3.5}(den)^2} \tag{2.60}$$

Where $den = 1 + K_{CO}P_{CO} + K_{H_2O}\dfrac{P_{H_2O}}{P_{H_2}}$. This model implies that for the catalyst used the primary product is carbon dioxide, which is then converted to carbon monoxide by the reverse water gas shift reaction. This is in contradiction to many previous investigations where the product was considered to be carbon monoxide. The authors accredited this difference as due to the different catalysts used.

Among the results of kinetic studies selected here on methane steam reforming, there is a general agreement that the reaction is first order in methane. However, there are quite different conclusions on the initial products, the rate controlling steps, the dependence of

the reaction rate upon the steam and hydrogen and the behaviour of steam and methane on the catalyst.

Seven investigators (Bodrov et al., 1967 and 1968, Agnelli et al., 1985, Ross and Steel, 1972, Atroshchenko et al., 1969, Al-Ubaid, 1984 (for less acidic support), Allen et al., 1975, Numaguchi et al., 1988) reported that carbon monoxide only is a primary product, while some investigators (Quach et al., 1975, Al-Ubaid 1984 (for high acidic support), Soliman et al.,1992) suggest that carbon dioxide only is a primary product. Akers and Camp (1955), De Deken et al. (1982) and Xu and Froment (1989) reported that both carbon dioxide and carbon monoxide are primary products.

The conclusions on the rate controlling steps can be roughly grouped into two categories. Surface reactions between adsorbed steam (or adsorbed oxygen) and adsorbed carbon (or adsorbed CH_x- an adsorbed intermediate) are the rate controlling steps, reported by Bodrov et al. (1968), Atroshchenko et al.(1969), AL-Ubaid (1984), Numaguchi et al.(1988), De Deken et al.(1982), Xu and Froment (1989), and Soliman etal. (1992), whereas that methane adsorption with partial/complete dissociation is the rate controlling step was the view shared by Akers and Camp (1955), Bodrov et al. (1964, 1967), Agnelli etal. (1985), Ross and steel (1972), and Kospel et al. (1980). The only exception is that of Allen et al. (1975) who suggested that the desorption of products is the rate controlling step.

From the literature review on kinetic studies of methane steam reforming above, the different possibilities for steam and methane reaction on the catalyst were postulated. Steam:

(a) The steam reacts while in the gas phase. This means that it is not adsorbed (Quach et al. 1975)

(b) Steam is adsorbed with dissociation on the catalyst (Bodrov et al., 1967, Atroshchenko et al., 1969, Agnelli et al. 1985, De Deken et al., 1982, Xu and Froment, 1989, Soliman et al., 1992):

$$H_2O + s = O(s) + H_2$$
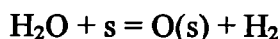
or according to Ross and Steel (1972)

$$H_2O + s = OH(s) + 0.5 H_2$$

(c) Steam is adsorbed on the catalyst (Allen et al. 1975, Al-Ubaid, 1984)

$$H_2O + s = H_2O(s)$$
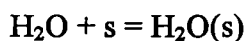
Methane

(a) Methane reacts while in the gas phase (Allen et al., 1975), i.e. it is not adsorbed on the catalyst.

(b) Methane is adsorbed on the catalyst (Quach et al. 1975)

$$CH_4 + s = CH_4(s)$$
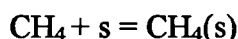
(c) Methane is adsorbed on the catalyst with dissociation into H_2 and CH_2 or C (Bodrov, et al., 1967, Ross and Steel, 1972, Al-Ubaid, 1984, De Deken et al., 1982, and Xu and Froment, 1989)

$$CH_4 + s = CH_2(s) + H_2$$

or $\qquad\qquad CH_4 + s = C(s) + 2H_2$
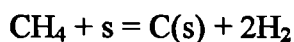
Different conclusions on the dependence between steam partial pressure and the reaction rate can be derived from literature reviewed above. Two investigators (Akers and Camp, 1955, Bodrov et al. 1967) reported zero order dependence of the rate of reaction upon

steam partial pressure, six reported positive order dependence (Quach and Rouleau, 1975, Atroshchenko et al. 1969, Kospel et al., 1980, Al-Ubaid, 1984, De Deken, et al. 1982, Numaguchi et al., 1988), and four reported negative order dependence (Bodrov et al. 1967,Ross and Steel, 1972, Al-Ubaid, 1984, and Agnelli, et al. 1985), whereas the non-monotonic dependence of the reaction rate upon the partial pressure of steam was given by Allen et al. (1975), Xu and Froment(1989), and Soliman et al.(1992).

Since the study of the kinetics of the methane/steam reaction was carried out with catalysts of different compositions prepared by various methods and of different particle size, and over wide ranges of temperature and pressure, it is not surprising that different mechanisms have been suggested. The reasons for this are twofold: (1) the change of catalyst composition changes not only the values of the parameters of the kinetic model, but it also changes the structure of the kinetic model through changes in the mechanism (Soliman et al. 1992); (2) a lack of appreciation of the diffusion limitation often results in misunderstandings of the kinetic mechanism (Twigg, 1989). This makes it very difficult, if indeed possible, to develop a generalised kinetic model, which can be applied to different catalysts with a change in parameters to suit each catalyst. The change in the structure of the kinetic model and the mechanism makes it mandatory to study the mechanism and the kinetic model for each type of steam reforming catalyst. Therefore, in order to obtain the best understanding of the kinetic mechanism of methane steam reforming on a specified commercial catalyst (ICI 57-4), the experimental study in the present work has been carried out under two kinds of condition, i.e., a) where the diffusion limitation is eliminated or b) by using a specially designed reactor, which can couple the diffusion effect into the kinetic study.

2.4 Studies on the Catalyst Stability and Membrane Reactor Performance for Methane Steam Reforming

2.4.1 Deactivation of nickel steam catalysts

Like most catalysts, nickel reforming catalysts may be deactivated by coking (or carbon formation) from some reactions, poisoning from impurities and ageing. Even without coking and poisoning, it is inevitable that the catalysts are slowly deactivated by ageing effects, such as sintering and loss of active metal.

Nickel reforming catalysts are sensitive to certain impurities, such as sulphur, arsenic, halogens, phosphorus, and lead, which can be found in the feedstocks. Some of these cause permanent damage to the catalyst; others have only a temporary effect, with catalytic activity returning to normal when feedstock purity is restored.

Sulphur is the severest poison of these impurities because sulphur compounds are strongly chemisorbed on the metal surface. Small amounts of sulphur seem to have greater effects on the more active catalyst. The reason for this is primarily twofold: (1) if most of the Ni surface is occupied by sulphur, this prevents further adsorption of reactant molecules, and (2) the reconstruction of Ni surface may modify or lower the adsorption rates of reactant gases.

The adsorption of hydrogen sulphide on the nickel surface has been extensively studied. The investigations (Saleh, et al., 1961, Den Besten, et al., 1962, Rostrup-Nielsen, 1968,

Ng, et al., 1978, Fowler, et al., 1979) suggest that H_2S strongly adsorbs with complete dissociation on the nickel surface even below room temperature:

$$H_2S \text{ (gas)} + nNi = S\text{-}(Ni)_n + H_2(gas) \qquad (2.61)$$
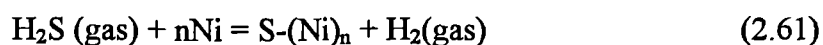
Different values of n have been reported. Saleh et al.(1961) reported a three-site mechanism in the temperature range 355-375 K, whereas a four-site mechanism was suggested by Den Besten and Selwood (1962) in the temperature range of 375 to 498 K, and Ng et al (1978) at room temperature. At high temperatures (825-925 K), Rostrup-Nielsen found that the value of n would be equal to one. Accounting for the effect of temperature on the adsorption mechanism of H_2S on the nickel surface, it is possible that the value of n may change with temperature. It appears that H_2S adsorption decreases with temperature and is not affected by total pressure, while hydrogen, which is a product of H_2S adsorption with dissociation, inhibits the adsorption of H_2S.

Hydrogen sulphide adsorption (poisoning) is reversible, and there is a H_2S concentration below which no detectable poisoning occurs, depending on the operating temperature. Sensitivity to poisoning is increased as operating temperatures are lowered. In practice, a lower H_2S concentration and higher operating temperatures are preferred for avoiding H_2S poisoning to the catalyst.

Normally, sulphur which is present in natural gas can be purified effectively to a tolerable content preceding steam reforming. For example, about 5 ppm of sulphur is present in natural gas from North Sea Oil Fields, and this has to be reduced to less than 0.5 ppm to the reformer (Twigg, 1989); and this is usually accomplished using a hydrodesulphurization catalyst in combination with a bed of zinc oxide. In the first step, sulphur compounds in natural gas are transformed into hydrocarbons and hydrogen

sulphide by hydrodesulphurization over the nickel or cobalt molybdate catalyst. Some typical reactions for a number of different sulphur compounds are shown below.

$$C_2H_5SH + H_2 = C_2H_6 + H_2S \qquad (2.62)$$

$$C_6H_5SH + H_2 = C_6H_6 + H_2S \qquad (2.63)$$

$$CH_3SC_2H_5 + 2H_2 = CH_4 + C_2H_6 + H_2S \qquad (2.64)$$

$$C_4H_4S + 4H_2 = C_4H_{10} + H_2S \qquad (2.65)$$
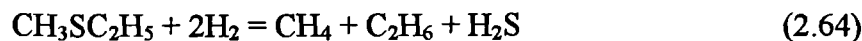
Hydrogen sulphide is then removed by adsorption in beds of zinc oxide. Zinc oxide reacts almost completely with hydrogen sulphide to form zinc sulphide as shown below.

$$ZnO + H_2S = ZnS + H_2O \qquad (2.66)$$

According to the thermodynamics of the above reaction, temperature and water vapour have strong effects on the equilibrium H_2S concentration over zinc oxide. Hence, a lower operating temperature and a dried natural gas are used in the purification process in order to guarantee the quality of feed to the reformer.

Deactivation of nickel reforming catalysts by carbon formation is a major problem in steam reforming. Its causes are generally threefold: (1) fouling of the metal surface, (2) blockage of catalyst pores and voids, and/or actual physical disintegration of the catalyst support. Carbon may be formed via different routes, each influencing the morphology of carbon. According to Rostrup-Nielsen (1984), three different kinds of carbon species are observed in steam reforming: (1) whisker-like carbon, (2) encapsulating carbon, and (3) pyrolytic carbon. Whisker carbon is formed by diffusion of C through the Ni crystallites, and growth occurs with the Ni crystallites at the top of the whisker. It does not deactivate the catalyst but causes a break-down of the catalyst. Encapsulating carbon results from slow polymerisation of radicals containing C on the Ni surface, and leads to a progressive deactivation of the catalyst. Pyrolytic carbon (C-precursor) is deposited by thermal

cracking of hydrocarbons, and encapsulates the catalyst particle and deactivates the catalyst.

The kinetic mechanisms of carbon formation are very complicated, particularly for higher hydrocarbons such as in naphtha steam reforming. For natural gas steam reforming, the important reactions of carbon formation are presented by:

Methane decomposition

$$CH_4 = C + 2H_2 \tag{4}$$

CO disproportionation (Boudouard reaction)

$$CO = C + CO_2 \tag{5}$$

and CO reduction

$$CO + H_2 = C + H_2O \tag{6}$$

The methane decomposition reaction is endothermic and experiences an increase in the number of moles; hence it is favoured by high temperatures and low pressures. Both the CO disproportionation and reduction reactions are exothermic and result in a decrease in mole number, hence these reactions are favoured by low temperatures and high pressures.

Combining the main reactions of methane steam reforming with carbon formation reactions, it is possible to determine a carbon formation free region, which is a compromise between the two kinds of carbon formation reactions, by thermodynamic equilibrium calculations according to the "equilibrium gas principle" (Bartholomew, 1982). However, this is certainly not valid for all cases because the activity of carbon is considered to be unity, as in graphite, in thermodynamic equilibrium calculations.

The presence of either H_2 or H_2O (both as products of carbon formation reactions) can very substantially reduce or eliminate the carbon formation in steam reforming. In industry, the high ratios of steam/hydrocarbon are used to control carbon formation. However, excess steam must be recycled and it is desirable to minimise the magnitude of the recycle steam for economy purpose.

Both the nickel and the support play dual roles, contributing to the steam reforming reactions and also to the carbon formation reactions. The nickel catalyst, depending on its activity, will catalyse the reaction of steam with intermediates, but will also promote decomposition and polymerisation to produce carbon. Acidity in the support is known to facilitate both kinds of steam reforming and carbon formation reactions. This problem was solved by ICI (Twigg, 1989) by adding an alkali metal component into the catalyst. This accelerates the reverse reaction of CO reduction, i.e., accelerates the gasification reaction of carbon, and at the same time the alkali neutralises the acidity in the catalyst support, so retarding decomposition and polymerisation. The most effective alkali was found to be K_2O (potash). The K_2O is effective by being mobile on the catalyst surface. Accurate formulation combines the potassium as a complex potassium alumina-silica (e.g. Kalsilite, $K_2O.Al_2O_3.SiO_2$) and monticellite ($CaO.MgO.SiO_2$). The potassium is liberated at a very slow rate as involatile K_2CO_3 which is hydrolysed as fast as it is formed, producing KOH, which is very mobile on the catalyst surface and is the effective carbon –removing agent.

Another way for controlling carbon formation is by addition of promoters into the catalysts. In principle, promoters, which enhance the adsorption of H_2 or H_2O and /or the rate of gasification of adsorbed carbon or coke precursors by H_2 or H_2O, or reduce the solubility and rate of diffusion of carbon in the metal particles, should minimise the

deposition of carbon. The better selectivity of urania –promoted catalyst was related to their ability to enhance steam adsorption and gasification (Bhatta et al., 1969). Rostrup-Nielsen (1974) observed that formation of coke in steam reforming was delayed and occurred at lower rates on nickel catalyst promoted with alkali or supported on MgO. This effect was also attributed to enhanced steam adsorption and more efficient gasification of adsorbed carbon from the decomposition of hydrocarbons in the presence of these promoters. Ruthenium and Rhodium catalysts showed very high reforming activity while producing no coke. This was attributed to reduced mobility/or solubility of carbon in the metal particles (Rostrup-Nielsen, 1974).

Baker and Chludzinski (1980) investigated the effects of various oxide additives on the carbon produced via the decomposition of hydrocarbon on nickel-iron particles (5-50 nm diameter) supported on a silica. Three different kinds of behaviour were observed for the specimens containing oxide additives: (1) Al_2O_3 and TiO_2 films provided a physical barrier toward hydrocarbon adsorption and decomposition on the surface below 650°C, but were not effective at higher temperatures due to spalling; (2) MoO_3, WO_3 and Ta_2O_5 inhibited the rate of carbon formation (at 1120 K) by factors 10-50, presumably by reducing carbon solubility in the metal particles; and (3) SiO_2 was most effective in reducing the carbon formation at 1120 K by 200-fold, apparently by lowering both the solubility and rate of diffusion of the carbon in the metal particle.

Wood and co-workers (1980) reported that the Ir-promoted Ni/Al_2O_3 showed less of coking tendency. Gardner and Bartholomew (1981) found that the rate of carbon deposition on Ni/Al_2O_3 was decreased by addition of Pt. Borowieck et al. (1994, 1997) also observed that the introduction of small amounts of molybdenum and tungsten

compounds (of less than or equal to 0.1 wt %) into the nickel steam catalyst considerably reduced the detrimental effect of carbon formation, while entailing no change in the catalyst activity. With large amounts, a decrease in the catalyst activity was observed, although that was much smaller than the reduction of the coking rate. The properties of the $Ni\text{-}Mo/Al_2O_3$ catalysts depended on the hydrogen/steam ratio in the reaction mixture which affects the mean degree of oxidation and distribution of various molybdenum states on the surface.

Two poisons, sulphur and $Fe(CO)_5$, are known to affect the deposition of carbon in steam reforming, although the precise nature of their influence is not well understood from the somewhat sparse literature on this subject. Rostrup-Nielsen (1984) reported that very little carbon formation occurred on a sulphur poisoned $Ni/Al_2O_3.MgO$ catalyst under steam reforming conditions for which thermodynamics would predict significant amounts to occur. He explained that this was due to a blockage of the nickel surface by sulphur atoms preventing dissolution and diffusion of carbon atoms through the nickel crystallite. Further, Rostrup-Nielsen speculated that at high coverage of sulphur there are insufficient large metal ensembles available for dissociative adsorption of hydrocarbons, although smaller ensembles are sufficiently available to activate hydrocarbon molecules for further reaction with steam. Trimm (1997) also claimed that doping with traces of sulphur that concentrated on the nickel surface would reduce carbon formation significantly. Further research on how sulphur affects the adsorption of hydrocarbons and deposition of carbon should be done.

The surface structure and metal particle size have an effect on the rate of carbon formation in steam reforming. In general, carbon formation is apparently favoured on rough surfaces.

Data reported by Gardner and Bartholomew (1981) show that the carbon deposition rate is greater on smaller particles of nickel on alumina. However, a conflicting conclusion was suggested recently by Yamazaki et al.(1996). They found that the catalyst with a low nickel content and with very small particles of metallic nickel kept its activity for 60 hr or more at 1123 K and at a steam to carbon ratio of 1.0, gave little coke on the catalyst (<1 wt %), whereas the commercial steam reforming catalyst under the same reaction conditions lost its activity at 20 hr because of severe coking under the identical conditions. Hence, a study of the effect of the size of nickel particle on carbon deposition should also be of interest.

2.4.2 Catalytic membrane reactors for methane steam reforming

For methane steam reforming, the methane conversion is limited by thermodynamics. To achieve a high methane conversion the reaction should be carried out at high temperatures and low pressures. As regards the economics of the total process, a high applied pressure is to be preferred in most ammonia and hydrogen plants. Under a high applied pressure, a high temperature has to be used in order to obtained the desired conversion of methane. Consequently, the energy consumed for this process is relatively high. The economics of the process would be greatly improved if the reactions could be carried out at low temperatures provided a high conversion could be obtained. Considerable attention has focused recently on the application of steam reforming in the production of hydrogen for fuel cells. Since most of the fuel cells operate at low temperatures, high overall thermal efficiency would be expected if steam reforming could be carried out at comparatively low temperatures.

If a reversible reaction reaches a state of chemical equilibrium at any fixed conditions, no further change in the composition with time can occur. Nevertheless, if one or more of the products can be separated from the reacting mixtures by employing a selective gas permeation membrane, the reaction will advance in the forward direction and will finally break the equilibrium limitation. Raymont (1975) has suggested a similar concept for increasing the decomposition yield of hydrogen sulphide, whose equilibrium conversion is quite low (only several percent at 1000 K). Following this, Kameyama et al. (1981) succeeded in improving experimentally the decomposition yield of hydrogen sulphide using a microporous Vycor glass membrane, through which one of the products, hydrogen gas, can pass more easily than other gaseous species. Since then, applications of membranes in heterogeneous catalytic reactions have been extensively studied. Main interests have been concentrated in two areas: (1) removal of one and more products from the reaction system to improve the reaction conversion; (2) controlled addition of one or more reactants to reaction system to influence the reaction path for enhancing the reaction selectivity. Examples of the first kind include dehydrogenation reactions, where removal of the product hydrogen increases the conversion of reactant. An application of the second type occurs in many oxidation processes. Use of a membrane leads to a controlled addition of oxidant and therefore increases selectivity to the desired product.

Inorganic membranes which may be used in catalytic membrane reactors are of two main types, that is, dense membranes and porous membranes. Dense membranes exhibit specific permeability properties to certain gases, such as palladium and palladium alloys for hydrogen permeation and silver for the permeation of oxygen. The permeation of gases through dense membranes follows a solution-diffusion mechanism. Porous membranes may be made from glass alumina, zirconia, silver and stainless steel with a wide variation

of pore diameters. Gases diffuse through the membranes by molecular or Knudsen diffusion, by bulk flow, or surface diffusion, etc. which process dominates depends mainly on the pore size and the operating pressure(s).

Applications of membrane reactors with dense or porous membranes to methane steam reforming have been carried out for nearly ten years (Uemiya, et al., 1991; Adris, et al., 1991; Chai, et al., 1993; Shu, et al., 1994; Barbieri, et al., 1997). These investigations demonstrate that the supported palladium and palladium alloys membranes promoted the steam reforming reaction more effectively than porous membranes. The difference between these two types of membranes is attributed to their hydrogen permeabilities. In the temperature range of 573 to 873 K, dense membrane reactors attained a methane conversion twice as high as the equilibrium value of the packed bed reactor system as a result of the selective removal of hydrogen from the reaction system. Under the same conditions porous membranes have shown little effect on the shift of equilibrium unless their pore sizes were very small. A near complete conversion of methane can be achieved in the dense membrane reactor if a high flow rate of sweep gas and high reaction pressure could be used.

The benefit of removal of hydrogen on methane steam reforming has been demonstrated by these studies. However, little attention has been directed to the effect of removal of hydrogen on the catalyst poisoning by sulphur compounds adsorption and of carbon formation from methane decomposition. It has been pointed out that the adsorption of hydrogen sulphide on nickel catalysts is very strong at low temperatures and its fractional coverage fractional on the active sites of the catalyst depends on the value of P_{H_2S}/P_{H_2} while the tendency of methane decomposition is restrained by the $\left(P_{H_2}\right)^2/P_{CH_4}$ (Rostrup-

Nielsen, 1968 and 1984; Bartholomew et al., 1979; Fowler, et al., 1979, McCarty, et al., 1980). The removal of hydrogen produced will favour the adsorption of hydrogen sulphide and the reaction of methane decomposition so that it will influence the catalyst activity and stability as well as modify the advantages of membrane reactor operation.

An examination of the effects of the main variables, including H_2S content, the extent of hydrogen removal, the temperature and pressure, on the H_2S tolerance and the tendency of carbon formation, carried out by simulation, or experimentally would be of use in any future work on methane steam reforming.

CHAPTER 3 DIFFUSION OF GASES AND VAPOUR IN POROUS SOLID

AND MEASUREMENT OF EFFECTIVE DIFFUSIVITY

3.1 Introduction

The diffusion of gases and vapour in porous particles is of great importance in chemical reaction systems, separation processes and drying operations. Reliable knowledge of this intraparticle mass transfer process is important for the development, design and optimization of these processes.

When molecules of gas or vapour pass through a porous solid, there are not only collisions between molecules and between the molecules and the wall of pores of solid but possible absorption and desorption of molecule on the inner surface of solid may occur as well. Thus the transportation of gas molecules in porous solids may undergo a succession of these steps. In general, diffusion of a gas or vapour through a porous solid may be described by one of the following mechanisms:

1. Ordinary or bulk diffusion.

2. Knudsen diffusion.

3. A combination of 1 and 2 above (transition region).

4. Surface diffusion

Diffusivity, which is an ability of a gas to diffuse through a porous solid under certain conditions, can be measured or predicted. To account for the effects of porosity and the

complex structure of the porous solid, such as porous catalysts, the effective diffusivity is to be used in practice. The effective diffusivity can be obtained directly by experiments under steady or unsteady state methods. Some models are available for roughly estimating the effective diffusivity. In this chapter, a brief review on diffusion of gases, and the measurement and prediction of the effective diffusivity is presented.

3.2. Diffusion of Gases in Porous Solids

3.2.1 Ordinary or bulk diffusion

Ordinary or bulk diffusion occurs if the pores are large and the density of the gas is relatively large. Diffusion of gases will take place if there is a change in concentration between regions of a mixture. Gases diffuse in a tendency to make the concentration uniform in the system. The molar flux of species i is a vector quantity denoting the flow of moles of species i through a unit area per unit time. The molar fluxes relative to stationary coordinate are

$$N_i = C_i u_i \qquad (3.1)$$

The molar fluxes relative to the molar average velocity u^* are:

$$J_i^* = C_i \left(u_i - u^* \right) \qquad (3.2)$$

But since

$$u^* = \left(\sum C_i u_i \right) / \left(\sum C_i \right)$$

Therefore

$$J_i^* = N_i - y_i \sum N_i \qquad (3.3)$$

So for a binary mixture of A and B

$$J_A^* = N_A - y_A(N_A + N_B)$$ (3.4)

If the gas mixture has a symmetrical distribution and is in random motion, Fick's law of diffusion will apply and

$$J_A^* = -CD_{AB}\frac{\partial y_A}{\partial z}$$ (3.5)

Therefore:

$$N_A = y_A(N_A + N_B) - CD_{AB}\frac{\partial y_A}{\partial z}$$ (3.6)

The vector $y_A(N_A + N_B)$ is the molar flux of A resulting from the bulk motion of the fluid and

the vector $(-CD_{AB}\frac{\partial y_A}{\partial z})$ is the molar flux of A resulting from diffusion superimposed on the

bulk flow. Equation (3.6) can be integrated if the ratios of the fluxes and the pressure are constant and diffusion is in one direction, to give:

$$N_A = -\frac{CD_{AB}}{\alpha Z}\ln\frac{1-\alpha y_{A0}}{1-\alpha y_{Az}}$$ (3.7)

where

$$\alpha = 1 + N_B/N_A$$

For a given process α is determined by the chemical stoichiometry. For instance if $A \to B$ then $\alpha=0$, but if $A \to B$ and B is adsorbed on the surface of porous solid, then $\alpha=1$. Also for equimolar diffusion $\alpha=0$ since $N_A=-N_B$, equation (3.6) will reduce to:

$$N_A = -CD_{AB}\left(\frac{dy_A}{dz}\right)$$ (3.8)

For a binary mixture, Hoogschagen(1955) and Dullien and Scott(1962) have showed that the ratio of the fluxes is equal to the square roots of the inverse of the molecular weight ratio of the two diffusing gases, i.e

$$\alpha = 1 + N_B/N_A$$

$$= 1 - \left(M_A/M_B\right)^{0.5}$$

The bulk diffusivity D_{AB} can be measured but may also be predicted theoretically. For the latter purpose, the best known formula is the Chapman-Enskog equation (Hirschfelder, et al., 1954)

$$D_{AB} = \frac{1.8583 \times 10^{-5} T^{1.5} \left(\dfrac{1}{M_A} + \dfrac{1}{M_B}\right)^{0.5}}{P\sigma_{AB}^2 \Omega_{AB}}$$ (3.9)

Where D_{AB}: Diffusivity, m^2/s

P: pressure, kPa

σ_{AB}: collision diameter, $\overset{\circ}{A}$

ω_{AB}: collision integral, K

M_A, M_B: the molecular weights of A and B respectively.

Another equation was developed by Fuller et al (1966) which has been claimed to be more accurate than others. This is:

$$D_{AB} = \frac{10^{-5} T^{1.75} \left(\dfrac{1}{M_A} + \dfrac{1}{M_B}\right)^{0.5}}{P\left(\left(\sum v\right)_A^{1/3} + \left(\sum v\right)_B^{1/3}\right)^2}$$ (3.10)

Where $(\sum v)_A, (\sum v)_B$ are the special diffusion volumes of A and B respectively. This

diffusion volume is the sum of parameters that can be assigned to atoms, groups and other

structural features of the species. Units of D_{AB} and P in the equations (3.9) and (3.10) are m^2/s

and kPa, respectively.

Diffusion in multicomponent systems often occurs in chemical reaction processes. For this

case, if the multicomponent system consists of species A_1, A_2,......, A_n, and species A_i

diffuses into the mixture of the other n-1 species, the diffusivity D_{im} of species i is predicted

by following equation as :

$$\frac{1}{D_{im}} = \frac{\sum\limits_{\substack{j\neq i}}^{n} \frac{y_j}{D_{ij}}}{1 - y_i}$$ (3.11)

where D_{ij} is given by equation (3.9) or (3.10).

3.2.2 Knudsen diffusion

If the pores are small and the gas has a low density, collisions will occur primarily between

molecules and the pore wall. In bulk diffusion it is the gas - gas collisions which are limiting,

and the gas - wall collisions are negligible. The usual rough criterion for Knudsen diffusion is

that the mean free path of the gas molecule is much larger than the pore diameter. For bulk

diffusion the criterion is that the mean free path is smaller than the pore diameter. Most real

cases of diffusion probably lie between these two limiting cases.

Under the Knudsen diffusion mode, based on the kinetic theory of gases the Knudsen

diffusivity may be estimated by the equation:

$$D_{KA} = \frac{2}{3} r_p \bar{V}_A$$
(3.12)

where

$$\bar{V}_A = \left(\frac{8RT}{\pi M_A} \right)^{0.5}$$

and units of r_p and $\bar{V}_A$ are m and m/s, respectively. Combining above two equations gives a working expression for D_{KA} in a straight circular pore of radius r_p in m²/sec:

$$D_{KA} = 97 \, r_p \, (T/M_A)^{0.5}$$
(3.13)

3.2.3 Transition region

By comparing the pore size and the mean free path of gas, the type of diffusion may be determined. However, in dealing with diffusion in a given catalyst particle or pellet, it is very rare to find one single mode of diffusion. It is often probable that both types of diffusion are important. This is known as the " transition region ". When the pressure is reduced, the change from bulk to Knudsen diffusion does not occur suddenly when the mean free path of the gas molecules becomes equal to the pore radius. The theory of this region between bulk and Knudsen diffusion has been reported by Scott and Dullien(1962). These authors suggested that the following equation be used for the binary gas diffusion in a porous solid at constant total pressure:

$$\frac{1}{D_A} = \frac{1-\alpha}{D_{AB}} + \frac{1}{D_{KA}}$$
(3.14)

For equimolar counter diffusion $\alpha = 0$, equation (3.14) will reduce to

$$\frac{1}{D_A} = \frac{1}{D_{AB}} + \frac{1}{D_{KA}}$$ (3.15)

Whether Knudsen or bulk diffusion predominates depends on the ratio D_{AB}/D_{KA} and not solely on the pore size. If D_{AB}/D_{KA} is very large, equation (3.15) reduces to

$$D_A = D_{AB}$$ (3.16)

On the other hand, if D_{AB}/D_{KA} is very small, the equation (3.15) reduces to

$$D_A = D_{KA}$$ (3.17)

3.2.4 Surface diffusion

Surface diffusion may take place if one of the molecular species is adsorbed on the surface to a considerable extent. The transport by movement of molecules over a surface is called " surface diffusion" and the direction of transport is that of decreasing surface concentration. Equilibrium adsorption is a function of the partial pressure of the adsorbed component in the gas adjacent to the surface, and both tend to decrease in the direction of diffusion. Surface and gas phase diffusion proceed in parallel. The available data shows that it contributes little to overall transport through a porous mass at high temperature unless appreciable adsorption occurs and yet if adsorbed molecules are held so strongly to be essentially immobile, surface diffusion becomes insignificant.

The surface diffusion flux per unit-section area of porous solid N_s may be expressed as:

$$N_s = -\frac{D_s}{\tau_s} \rho_p S_g \frac{dC_s}{dz}$$ (3.18)

where

$$D_s = D_o \exp\left(-\frac{E_s}{RT}\right)$$

and τ_s accounts for the tortuous path of surface diffusion, C_s is the surface concentration

$(kmol/m^2)$, D_s is the surface diffusivity in m^2/sec and the product $\rho_p S_g = S_v$ is the surface area

per unit volume of solid (m^2/m^3). D_s varies somewhat with surface concentration because of

variations of E_s, but approaches some limiting value as surface coverage is decreased. Surface

diffusion is likely to be significant with high area and therefore fine pore solids.

The surface diffusion of propane and other hydrocarbon through a well-characterized porous

matrix of molybdenum sulfide has been studied by Reed and Butt (1971) under conditions of

known and controlled surface coverage. They found that surface diffusion contributions for

propane were 32% and 11% of the total flux at 293 K and 343 K respectively; for 2,2-

dimethylpropane were 42% and 11% of the total flux at 293 K and 343 K respectively; and

were independent of surface coverage for coverages below 1%

3.3 The Prediction and Measurement of Effective Diffusivity of Gases in Porous Catalyst

The geometrical structure of a porous catalyst is very complicated, consisting of large number

of interconnected pores with irregular shapes, different diameters and a proportion of dead-end

pores. Also the length of the tortuous diffusion path in real pores is greater than the distance

along a straight line in the mean direction of the diffusion. All these factors cause the flux to

be less than would be possible in a uniform pore of the same length and mean radius. By

assuming that the ratio of real diffusion area to total cross-section area is equal to the porosity

of a porous solid, the following expression may be employed to give the flux compared to the

total cross-section of porous solid:

$$D_{Ae} = \frac{\varepsilon_p}{\tau} D_A$$

where

ε_p: porosity of porous catalyst particle or pellet

τ: tortuosity factor

Here D_A is the diffusivity which may be the bulk or Knudsen diffusivity, or a combination of the two, while D_{Ae} is the effective diffusivity.

Because of the lack of experimental data it is frequently necessary to estimate the effective diffusivity (D_e) from the physical properties of the catalyst. To do this, the first step is to evaluate the diffusivity for single cylindrical pore; a geometrical model of the pore system is then used to convert D to De for the porous pellet. In fact, a model is necessary because of the complexity of the pore structure. Various models are available for estimating D_e. Because predicted values typically deviate from experimental values by a factor of two, and occasionally by the order of magnitude discrepancies observed by Brown (1969) and Satterfield (1968). A large number of methods have been developed to measure the effective diffusivity in the absence of reaction. These methods can be grouped under two different categories: the steady state method and the unsteady state method. Each has its merits. While the steady state methods are generally less difficult to interpret, more information is potentially available from the unsteady state methods. Variations exist in each category. In the following review, typical predictive models and measuring techniques are outlined briefly.

.

3.3.1 Models for predicting effective diffusivity

3.3.1.1 Wheeler model

In this model it is assumed that diffusion occurs through a number of capillaries all of which are of the same length and radius. Wheeler suggested the following equation to estimate the effective diffusivity:

$$D_{Ae} = \frac{\varepsilon_p}{\tau} \frac{D_{AB}D_{KA}}{D_{AB} + D_{KA}}$$ (3.20)

Values of D_{AB} are calculated by using equation (3.9) or (3.10). Equation (3.14) is employed for determining D_{KA}, and the r_p is determined from.

$$r_p = (2\varepsilon_p)/(S_g\rho_p)$$ (3.21)

Prediction of D_{Ae} by this model is somewhat limited because of the uncertainty in τ. Estimated data shows that the tortuosity τ varies, on average from 2 to 6 (τ can not be measured directly).

3.3.1.2 Random Pore Model (Wakao-Smith model)

Many catalyst particles are formed by tableting, extruding, or by compaction in some other manner of a highly microporous powder (the "microparticles") to obtain a pellet having two separately identifiable pore structures. The voids inherent in the microparticles are termed the "micropores", whereas the voids due to spaces between the compacted microparticles are

designed as " macropores". Such bidispersed structured catalysts are described in terms of two diffusivities. The effective diffusivity has to include the micropore and macropore diffusion.

Wakao and Smith (1962) proposed the Random Pore Model for the predicting diffusivity at constant pressure in bidisperse porous media. This represents the diffusion flux as being the sum of that through macropores, micropores and that by a series through both. The model gives the effective diffusivity for isobaric diffusion as:

$$D_{Ae} = \varepsilon_a^2 D_a + \frac{\varepsilon_i^2 (1 + 3\varepsilon_a)}{1 - \varepsilon_a} D_i \tag{3.22}$$

where

$$D_a = \frac{1}{\dfrac{1 - \alpha y_A}{D_{AB}} + \dfrac{1}{D_{KA}}}$$

$$D_i = \frac{1}{\dfrac{1 - \alpha y_A}{D_{AB}} + \dfrac{1}{D_{Ki}}}$$

and ε_a: the porosity of macropores

             ε_i: the porosity of micropores

For pellets containing micropores only, $\varepsilon_a = 0$ and equation (3.22) reduces to:

$$D_{Ae} = \varepsilon_i^2 D_i \tag{3.23}$$

For pellets without micropores, $\varepsilon_i = 0$ and equation (3.22) becomes :

$$D_{Ae} = \varepsilon_a^2 D_a \tag{3.24}$$

The Random Pore Model has been confirmed experimentally by measurements of the effective diffusivities for a series of Boehmite alumina pellets pressed at different densities (Satterfield,

1970). It is however less accurate for the prediction of pellet diffusivities for different sizes of pressed Boehmite pellets (Smith and Robertson, 1963).

3.3.1.3 Parallel Pore Model (Johnson and Stewart, 1965)

This method predicts the rate of diffusion of a binary gas mixture through a porous solid at constant temperature and pressure. The rate of diffusion in each pore is predicted by the "dusty gas" theory of Evans,Watson and Mason(1961), and the total diffusion rate is given by integration over the pore-size distribution. Surface diffusion is neglected. The model predicts the effective diffusivity as follows:

$$D_{Ae} = \frac{\varepsilon_p}{\tau} \int \left(\frac{1 - \alpha y_A}{D_{AB}} + \frac{1}{D_{KA}} \right)^{-1} f(r_p) dr_p \qquad (3\,25)$$

Where $f(r_p)dr_p$ is the fraction of void volume occupied by pores with a radius between r_p and $r_p + dr_p$.

For one-dimensional diffusion, according to Fick's law:

$$N_A = -\frac{D_{Ae} P}{RT} \frac{dy_A}{dz} \qquad (3.26)$$

Combining equations (3.26) and (3.25), gives

$$N_A = -\frac{P\varepsilon_p}{\tau RT} \left[\int \left(\frac{1 - \alpha y_A}{D_{AB}} + \frac{1}{D_{KA}} \right)^{-1} f(r_p) dr_p \right] \frac{dy_A}{dz} \qquad 3\,27)$$

Integration of equation (3.27) from z = 0 to z = Z gives

$$N_A = \frac{P\varepsilon_p D_{AB}}{\tau RTZ} \int \ln\left(\frac{1 - \alpha y_{AL} + \frac{D_{AB}}{D_{KA}}}{1 - \alpha y_{A0} + \frac{D_{AB}}{D_{KA}}}\right) f(r_p) dr_p \qquad (3.28)$$

Equation (3.28) can be used to evaluate τ from experimental measurements if ε_p and the pore size distribution are known, or to predict the diffusion rate if τ is known.

3.3.2 The Measurements of effective diffusivity

A large number of methods have been developed to measure the effective diffusivity in the absence of reaction. These methods can be grouped in two different categories: the steady method and the unsteady state method.

3.3.2.1 The steady state method

The most commonly used steady state method is the Wicke-Kallenbach technique. In this method the ends of a cylindrical pellet are exposed to two gas streams flowing at steady state. The two faces of the pellet are maintained at equal total pressure in order to eliminate the convective term. One or both of the gas streams leaving the pellet are analyzed. From the analysis and the measured flow rates of the streams, the flux of gas through the pellet can be obtained. The most critical component of the Wicke-Kallenbach method is the diffusion cell. Stagnant layers and boundary layer resistance in series with the pellet resistance must be eliminated. Wicke and Kallenbach used this technique to measure the effective diffusivity of carbon monoxide in nitrogen over porous pellets. Hoogschagen (1955) found that the diffusion

fluxes are inversely proportional to the square roots of the molecular weight for bulk diffusion as well as in Knudsen diffusion. Rothfeld (1963) measured the flux over a range of total pressure for both sides of a pellet, and found that the flux ratio in steady state counter diffusion was independent of pressure.

The W-K technique provides a measure of effective diffusivity regardless of the mechanism of diffusion. However, apart from this it suffers from a number of problems. The sample must be of such size and geometric shape that it can be mounted leak-free in the diffusion cell, and the material of construction requirements usually impose a limitation upon the maximum temperature of measurement.

3.3.2.2 The unsteady state methods

The unsteady state methods can conveniently be categorized in term of three classifications- moment methods, sorption rate methods and gas chromatography methods.

The moment methods originated from time-lag methods. The latter developed first by Barrer(1953), have been used frequently and subsequent modifications were made by Goodknight and Fatt(1961), Beveridge and Goldie(1972) and other invesigators. In the moment methods popularized by Smith and co-workers (Dogu and Smith, 1976; Burghardt and Smith, 1979; Wang and Smith, 1983), one side of the Wicke-Kallenbach diffusion cell is subjected to an impulse of diffusing component, and the response on the opposite side is recorded. The effective diffusivity is achieved by analysis of the first and second moments of

the normlized response curse, which can be calculated from numerical integration of the experimental response curve.

The sorption rate methods which are particularly suitable for measurements of effective diffusivity in powders and granular materials and involve an experimental determination of the adsorption or desorption of a pure compound or a component of a mixture. Several variations of the techniques are popular. These may be roughly categorized according to whether the measurement is made at constant volume or constant pressure (Haynes, 1988). In the constant-volume experiment (Riekert, 1971; Satterfield and Margetts, 1971; Ma, et al,1973 , 1976), at time zero a step change in pressure is introduced into the experimental system; for a single-component gas the pressure response is recorded while for a gas mixture samples of fluid are collected from the system periodically and their composition is determined as a function of time. From a knowledge of the pressure (or composition) versus time curve one can calculate the sorption rate (or sorption uptake). The sorption uptake is also recorded gravimetrically (Heering, et al., 1982). In the constant-pressure experiment (Ruthven and co-workers,1972, 1980, 1981, 1982; Satterfield, et al.,1967; Kondis and Dranoff, 1971), the sorption uptake is determined gravimetrically or volumetrically. Effective diffusivities can be calculated from experimental uptake curves (Kocirik, et al., 1973 and 1974; Garza, et al., 1983).

Gas chromatography has been used as a popular tool for evaluating effective diffusivities in heterogeneous catalysts over the past three decades (Davis and Scott, 1965; Suzuki and Smith, 1971; Hsu and Haynes, 1981; Sarmah and Haynes, 1989). Instead of the diffusion cell used in the moment methods a column which contains fine particles of catalyst is used to measure an

effective diffusivity of a gas through the catalyst. Extensive studies on this subject have been done by Haynes and co-workers (Haynes and Sarma, 1973; Hsiang and Haynes, 1977; Hsu and Haynes, 1981; Haynes, 1986, Fu and Haynes, 1986). Similarly to the moment method experiments, a pulse of diffusing component is injected into inlet stream and the effluent pulse is recorded. Based on analysis of the moments of the response curve, the effective diffusivity can be obtained. Like the moment method, the principal advantage of the method is that the measurement can be easily conducted at elevated temperatures and pressures.

Unsteady state methods should not applied when diffusion is rapid. In such situations the experimental results may be controlled or at least modifed by extraparticle transport resistances and instrument response factors

CHAPTER 4 . MEASUREMENTS OF EFFECTIVE DIFFUSIVITIES OF GASES IN METHANE STEAM REFORMING

4.1 Introduction

Methane steam reforming is a typical heterogeneous gas- solid catalytic reaction. The diffusion of the reactants and products in the particle plays an important role in this reaction, especially for reactions taking place on highly active catalysts, such as nickel/alumina. The effectiveness factor of this reaction, a criterion characterizing the ratio of diffusion rate to intrinsic reaction rate, is often less than 0.01, or even sometimes 0.001 in industrial cases. Experimental measurements of the effective diffusivities of these gases is necessary to facilitate an understanding of the reaction kinetics of methane steam reforming.

In this chapter the steady state method is used to measure the effective diffusivities using the Wicke-Kallenbach(W-K) type diffusion apparatus, over the temperature range of 293-873 K and a pressure range of 100-1000kPa. These ranges are wider than are usually employed.

The W-K type diffusion apparatus has been used previously for diffusion measurements at elevated temperature. However, a severe leakage problem exists for high temperature measurements, caused by leakage through the space between the pellet and seal. Growcock and co-workers(1977-1978) have experimentally demonstrated the occurrence of severe leakage problems, in which the leak rate could be an order of magnitude higher than the pore diffusion rate in a graphite pellet at 773-1073 K. Yang(1982) solved the leak problem in his W-K diffusion cell by using an electroplated metal layer around the graphite sample

for the temperature range of 300-973 K. In the present work, the leakage problem in the W-K diffusion cell has been eliminated by employing a graphite "O" ring which seals the catalyst pellet. High pressure applied to the two ends of the graphite ring by compression, ensured that it was very tightly held around the catalyst pellet due to the radial expansion of the ring. No leakage was observed using this arrangement when tested at high temperature and pressure.

4.2 Experimental Measurements of the Effective Diffusivities

4.2.1 Materials used in the experiments

Gases:

The gases used were nitrogen, hydrogen, methane, carbon dioxide and helium. All gases were supplied by B.O.C Ltd. The purities of these gases were acceptable under experimental conditions used. Some physical properties of these gases and water vapour are listed in Table 4.1 below

Table 4.1 Physical properties of the gases and water vapour

	H_2	H_e	N_2	CO_2	CH_4	H_2O
Molecular weight	2.016	4.003	28.01	44.01	16.04	18.01
Thermal conductivity W/mK at 300 K	0.195	0.150	0.026	0.017	0.127	

Catalyst pellets:

The catalyst pellets were made from alumina catalyst powder supplied by I.C.I Ltd. The pellets were made by using a laboratory press (Apex Hydraulics). The powder was compressed in high tensile steel moulds of inside diameter 12.7 mm at one end with a slightly larger diameter at the other end. This was done to prevent the pellet from breaking during its ejection after compression. The diameter and height of the pellets were 12.7 mm (0.5 in.). The "green" density of the pellets was about 1.85 g/cm^3. The pore size distribution is shown in Table 4.2 and the porosity of the pellets was 0.39 (data provided by I.C.I Katalco).

Table 4.2 Pore size distribution of catalyst pellet sample

Pore Radius $\overset{0}{A}$	Mean pore radius $\overset{0}{A}$	V_{pi} cm^3/g	$f(r_p)dr_p$ %
1000000-100000	550000	.00342	2.135
100000-50000	75000	.00153	.955
50000—10000	30000	.00021	.131
10000—7500	8750	.00021	.131
7500—5000	6250	.0055	3.434
5000—2500	3750	.0249	15.546
2500—1000	1750	.1011	63.12
1000—500	750	.0099	6.181
500—250	375	.0119	7.430
250—100	175	.0010	.624
100—10	55	.0005	.312
Total pore volume cm^3/g		.1601	

4.2.2 Apparatus

Effective diffusivities were measured by the steady state flow technique as first used by Wicke and Kallenbach in their studies of ordinary diffusion in porous solids. This method was later modified by many investigators for measuring the effective diffusivities of porous particles.

A similar procedure was employed in this work for the measurement of effective diffusivities under steady state conditions through the a catalyst pellet. Fig.4.1 shows the experimental layout used in the diffusion experiments for gases. Minor modifications were made for measuring the effective diffusivities of water vapour into the other gases as illustrated in Fig.4.2. Pressure transducers were used across the chambers of the diffusion cell to monitor pressures on both sides of the pellet. A zero pressure difference is attained by adjusting the needle valves until the transducers show equal pressures on both sides of the cell. In order to study the temperature dependence of the effective diffusivities provision was made for heating the cell by enclosure in a furnace. The temperature was kept constant for each reading by means of the furnace temperature controller.

4.2.3 Analysis

To determine the amount of gas which had diffused into the carrier, a thermal conductivity detector (TCD) was employed. The TCD operates on the basis of the difference of thermal conductivities between the gas detected and the carrier gas. The deflections of the TCD output at steady state during the diffusion experiments, were recorded on a chart recorder. The amount of gas which had diffused into the carrier gas B was determined by comparing

the deflection with the relation between deflection and concentration of gas A in carrier gas B. This relation was obtained from calibrations using mixed gases of known composition of A and B which flowed through the TCD. The amount of water which diffused into the other gas stream was measured by using a relative humidity meter(RHM). In general, the relative humidity of the dry carrier gas (N_2, or other permanent gases) is close to zero. When water vapour diffused into the carrier the new value of the relative humidity was measured. The amount of water vapour in the carrier was calculated from this value. In the two cases above, the rotameters calibrated using a soap film meter were utilized to meter the flow rates of gases A and B.

4.2.4 Equation derivation

The equation for steady state diffusion of a binary gas mixure is obtained as follows: The flux for species A in the binary mixture A-B in the pellet is given by

$$N_A = -D_{AB,eff} \frac{P}{RT} \frac{dy_A}{dz} + y_A(N_A + N_B) \tag{4.1}$$

$$\frac{dN_A}{dz} = 0 \tag{4.2}$$

$$\frac{dN_B}{dz} = 0 \tag{4.3}$$

where N_A, N_B are flux of species A and B, respectively, and y_A is a molar fraction of species A in the mixture.

with boundary conditions

$$y_A = y_{A0}; \qquad z=0$$

$$y_A = y_{AZ}; \qquad z=Z$$

Upon integration of (4-1)

$$N_A = \frac{D_{AB,eff}P}{\alpha ZRT}\ln\left(\frac{1-\alpha y_{AZ}}{1-\alpha y_{A0}}\right) \tag{4.4}$$

where

$$\alpha = 1 + N_B/N_A = 1 - (M_A/M_B)^{1/2}$$

or

$$D_{AB,eff} = \frac{\alpha N_A ZRT}{P\ln[(1-\alpha y_{AZ})/(1-\alpha y_{A0})]} \tag{4.5}$$

The flux N_A, can be calculated as the product y_{AZ} and the flow rate of B, divided by the cross-sectional area of the pellet. Equation (4.5) is used for calculating effective diffusivities from the steady state experiments.

4.3 Experimental Results and Discussion

Pairs of gases (including water vapour) were used in the measurement of effective diffusivities. The gas pairs, temperature and pressure ranges are listed in Table 4.3 below.

4.3.1 Temperature dependence of the effective diffusivities

Fig.4.3 shows the effective diffusivities obtained for three gases in N_2 as a function of temperature at ambient pressure. Clearly, for all three gases (H_2, CO_2, CH_4), the effective diffusivities increased with increase in temperature. At ambient pressure, assuming that

$$D_{AB,eff} = D_{AB0,eff}(T/298)^{\rho_{AB}} \tag{4.6}$$

The values of α_{AB} for H_2/N_2, CO_2/N_2 and CH_4/N_2 were estimated by regression analysis to be 1.06, 1.138, and 1.212 respectively. The value for α_{CO_2, N_2} is in good agreement with

the result of Yang (1982), who obtained a corresponding value of 1.108 for CO_2 diffusion in N_2.

Fig.4.4 shows the experimental results obtained for CH_4 diffusion in CO_2 , and CO_2 diffusion into CH_4 respectively. The near equal values of α_{ij} are 1.086 and 1.056 respectively.

Except for α_{AB} values for water vapour diffusion into N_2 and CH_4, and for H_2 diffusion into CO_2, all values for the diffusion of gases at ambient pressure lie between 1.0 and 1.25 as shown in Table 4.4. The exponents on T for the remaining gas pairs indicate that the diffusion lies in the transition region under the present experimental conditions.

Table 4.4 also shows α_{AB} values for the temperature dependence for gaseous diffusion at different pressures. The trend that all values increase with increase in pressure is clear. this demonstrates that the diffusivity gradually moved to the ordinary bulk diffusion regime with pressure increase. This is to be expected since the mean free path (M.F.P) will decrease with increase in pressure, leading to a reduction in the Knudsen contribution to the effective diffusivity. At 1 MPa pressure, the high values of α_{AB} obtained exhibit that under these conditions diffusion basically lies in the bulk diffusion regime. Interestingly, the α_{AB} values of the temperature dependence for water vapour diffusion into N_2 and CH_4 decreased slightly when pressure is increased.

Table 4.3 The gas pairs used and ranges measured

	Temperature range K	Pressure Range 100 kPa
H_2-N_2	293-873	1 – 9
CO_2-N_2	293-873	1
CH_4-N_2	293-873	1 – 10
CH_4-CO_2	293-873	1 – 9
CO_2-CH_4	293-873	1 – 9
CO_2-H_2	293-873	1
H_2-CO_2	293-773	1 – 9
He-CO_2	293-873	1 – 10
N_2-H_2	293-873	1 – 9
Water vapour-N_2	573-873	1 – 10
Water vapour-CH_4	573-873	1 - 8.45

4.3.2 Effect of pressure on effective diffusivities

The experimental results for all gases at different pressure are shown in Figs.4.5-12. The effective diffusivities for all gases decrease monotonically with pressure, i.e. when the temperature is constant, the relation between $D_{AB,eff}$ and P is

$$D_{AB,eff} = \frac{D_{AB0,eff}}{(P/100)^{\beta_{AB}}}$$

(4.7)

By regression, the values of β_{AB} obtained for all gas pairs at different temperatures are listed in Table 4.5. Clearly variation of operating temperature within this range has only a small effect on the β_{AB} values for most gases. However, different gases have different values, for the effect of pressure on diffusion. Except for the β_{AB} value for water vapour diffusion, all values for the diffusion of gases decrease slightly with increase in temperature. The values

for water vapour basically keep constant in the temperature range of 573-873 K. It is

worthy of noting that β_{AB} is not 1 as is usually assumed.

Table 4.4 Effect of pressure on temperature dependence

of gas effective diffusivities

P (100 kPa)	1.0	4.0	7.0	10.0
	α_{AB}			
H_2 into N_2	1.060	1.108	1.195	1.544
H_2 into CO_2	0.747	0.987	1.434	1.410
CH_4 into N_2	1.212	1.220	1.548	1.740
CH_4 into CO_2	1.086	1.175	1.542	1.465
CO_2 into CH_4	1.056	1.472	1.318	1.726
He into CO_2	1.094	1.278	1.427	1.477
N_2 into H_2	1.103	1.362	1.358	1.638
H2O into CH_4	1.483	1.243	1.436	1.451
H_2O into N_2	1.793	1.743	1.710	1.620

Table 4.5 Effect of temperature on pressure dependence of

gas effective diffusivities

Temperature K	373	473	573	673	773	873
	β_{AB}					
H_2 into CO_2	0.7572	0.6369	0.5188	0.4904	0.4723	
CH_4 into N_2	0.8501	0.7475	0.6862	0.6667	0.6660	0.6640
H_2 into N_2	0.5952	0.5192	0.4788	0.4581	0.4481	0.4458
N_2 into H_2	0.5928	0.5284	0.4910	0.4590	0.4430	0.4530
CH_4 into CO_2	0.8297	0.7756	0.7314	0.7003	0.6813	0.6679
He into CO_2	0.5242	0.4733	0.4441	0.4138	0.4031	0.3963
H_2O into CH_4			0.9134	0.9303	0.9380	0.9322
H_2O into N_2			0.8715	0.8935	0.9062	0.8982

4.3.3 Estimation of tortuosity

The tortuosity of a catalyst pellet is often an important factor for predicting the effective diffusivities with some theoretical models. However, the tortuosity cannot be measured directly, but by combining the experimental data and a diffusion model, the tortuosity may be estimated approximately. Of these diffusion models the parallel path pore model (Johnson and Stewart) is probably better in comparison with other models. The basic assumption of the parallel path pore model is that all pores of the catalyst pellet are cylindrical, but have different values for the pore radius. The integral form of this model is the equation (3.28) (see it in Chapter 3):

$$N_A = \frac{\varepsilon_p D_{AB} P}{\alpha \tau R T Z} \int_{55}^{550000} \ln\left[\frac{1 - \alpha y_{AZ} + \frac{D_{AB}}{D_{KA}}}{1 - \alpha y_{A0} + \frac{D_{AB}}{D_{KA}}}\right] f(r_p) dr_p$$

Tables 4.6 and 4.7 show the results obtained from equation (3.28).

Table 4.6   Estimated tortuosity for some gas pairs

P (100 kPa)	1.0	4.0	7.0	10.0	τ_{max}/τ_{min}
	τ				
H_2-N_2	2.51	1.96	1.87	1.78	1.41
CH_4-N_2	2.29	2.25	2.03	2.00	1.15
He-CO_2	2.29	2.24	1.68	1.35	1.7

Table 4.7   Estimating tortuosity at ambient pressure

	CH_4 -N_2	CH_4 -CO_2	H_2 -N_2	H_2 -CO_2	CO_2 -H_2	CO_2 -CH_4	He-N_2 400kPa	He-CO_2 400kPa
τ	2.29	1.84	2.51	2.32	2.14	2.09	2.21	2.24

Because the tortuosity is a basic characteristic property of the catalyst pellet, it should be virtually constant under varying conditions. These results imply that application of equation (3.28) may be limited within a narrow pressure range for estimating tortuosity.

4.3.4 Calculation of mean free paths of the gases studied

Mean free path (mean distance travelled between successive collisions) of gas is an important criterion for determining the diffusion mode. The mean free paths of the individual gases were calculated from the kinetic theory of gases:

$$\lambda = 3.067 \times 10^{-21} \left(\frac{T}{P\sigma^2} \right)$$

(4-8)

where λ and σ are expressed in cm, and σ is the molecular diameter of the gas. Values of σ are listed below.

Gas	H_2	N_2	He	H_2O	CO_2	CH_2
σ (10^{-8}cm)	2.24	2.55	2.14	2.34	2.62	2.20

Values of the mean free path as a function of temperature and pressure are presented in Table 4.8. A comparison of these results with the pore size distribution given in Table 4.2 shows that for all pressures, except atmospheric the mean free paths for all gases are less than the pore diameter of 1500 $\overset{o}{A}$ and therefore the diffusion should be within the molecular diffusion range for all but 15 % of the pores.

4.4 Conclusions and Discussion

Effective diffusivities of gases and water vapour associated with methane steam reforming have been measured for catalyst pellets in a Wicke-Kallenbach type diffusion cell at

pressures up to 1MPa and temperatures ranging from 293 to 873 K. The effect of pressure on the temperature dependencies of the effective diffusivities has been studied. The experimental results demonstrate that the diffusion lies mainly in the bulk diffusion region at pressures up to 1MPa for catalyst pellets used. At ambient pressure, the temperature exponent values range from 1.0 to 1.25. this indicates that the diffusion occurs in the transition region. The relation between β_{ij} and temperature is non-linear. The pressure exponent was generally less than 1 with values lying between 0.4 and 0.85 except for gas - water vapour pairs where the exponent was close to 1. The tortuosity estimated for the catalyst pellet varied from 1.84 to 2.51 for different gases at ambient pressure, but decreased with increase in pressure.

From Table 4.5, the pressure exponents of gas effective diffusivities for hydrogen, methane and water vapour which are the main components in methane steam reforming, approach stable values as the temperature is increased to exceed 573 K. The estimated tortuosity for hydrogen, and methane in the pressure range of 400-1000kPa tends to a constant tortuosity for the catalyst pellets.

Table 4.8 Calculated values of the mean free path ($\overset{o}{A}$)

T K	Hydrogen					
	373	473	573	673	773	873
P= 100 kPa	2280	2891	3502	4414	4725	5336
400 kPa λ	570	723	876	1028	1181	1334
700 kPa	326	413	500	588	672	762
1000 kPa	228	289	350	411	472	533

Table 4.8 cont'd

T K	Nitrogen					
	373	473	573	673	773	873
P= 100 kPa	1759	2231	2701	3174	3646	4118
400kPa λ	440	558	676	794	911	1029
700 kPa	251	318	386	453	521	588
1000 kPa	176	223	270	317	365	412

T K	Helium					
	373	473	573	673	773	873
P= 100 kPa	2498	3168	3838	4507	5177	5846
400 kPa λ	624	792	959	1127	1294	1461
700 kPa	357	452	548	643	740	835
1000 kPa	250	317	384	457	517	585

T K	Water vapour					
	373	473	573	673	773	873
P= 100 kPa	2089	2649	3209	3767	4330	4890
400 kPa λ		662	802	942	1082	1223
700 kPa		378	459	539	619	700
1000 kPa		265	321	377	433	489

T K	Carbon dioxide					
	373	473	573	673	773	873
P= 100 kPa	1667	2113	2560	3007	3453	3901
400 kPa λ	417	528	640	752	863	975
700 kPa	238	302	366	430	493	557
1000 kPa	167	211	256	301	345	390

Table 4.8 cont'd

T K	Methane					
	373	473	573	673	773	873
P= 100 kPa	2363	2997	3631	4265	4898	5532
400 kPa λ	591	749	908	1066	1225	1383
700 kPa	338	428	519	609	700	790
1000 kPa	236	300	363	427	490	553
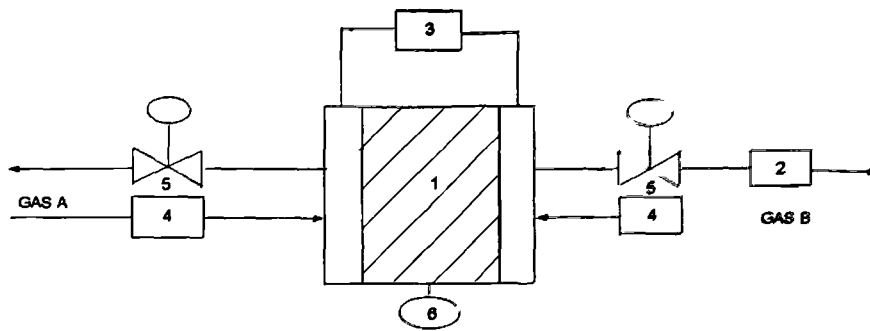
Fig.4.1 Schematic of flow system for the gas diffusion experiment

1: Catalyst pellet,   2: Thermal conductivity detector (TCD)
3: Pressure transducer,   4: Rotameters
5: Needle valves,   6: Temperature controller
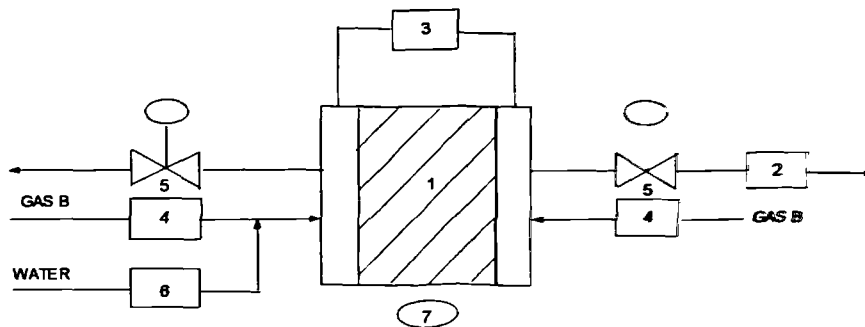
Fig.4.2 Schematic of flow system for the gas- water vapour diffusion experiment

1: Catalyst pellet,   2: Relative humidity meter (RHM)
3: Pressure transducer,   4: Rotameters
5: Needle valves,   6: Pump for transport of water
7: Temperature controller
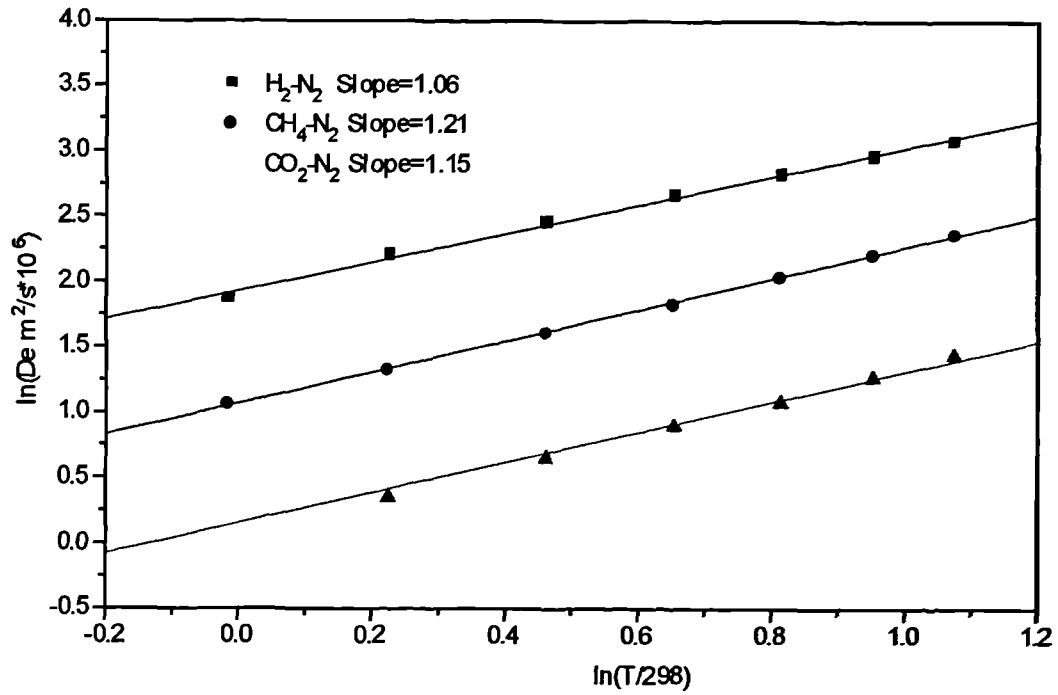
Fig.4.3 Effect of temperature on gas effective diffusivities through catalyst pellet
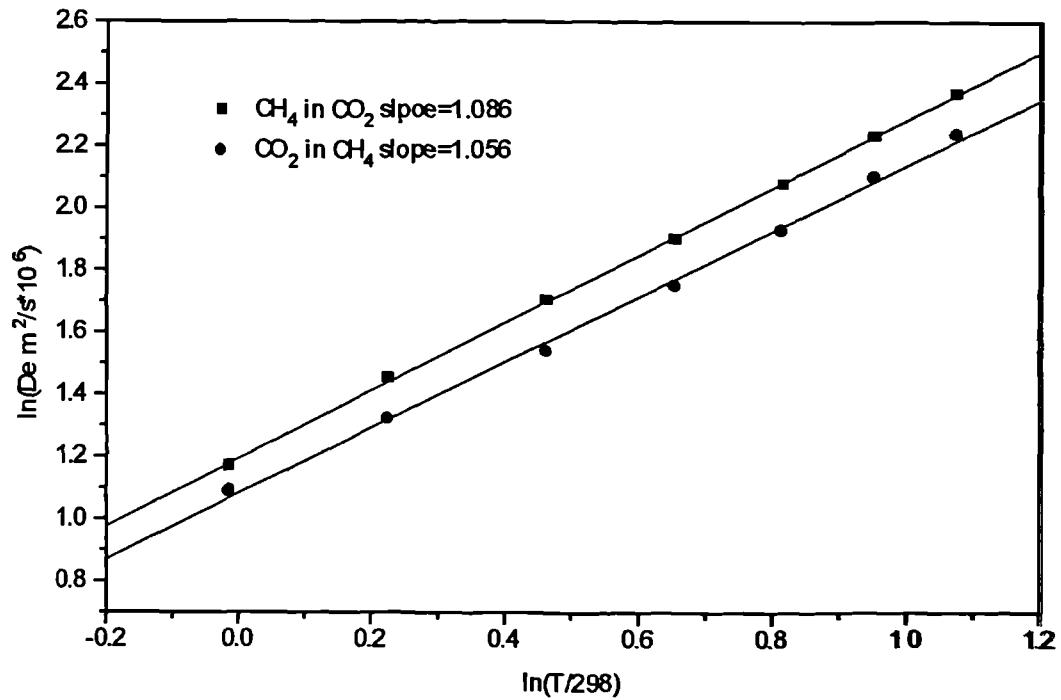
Legend (top figure):
- H_2-N_2 Slope=1.06
- CH_4-N_2 Slope=1.21
- CO_2-N_2 Slope=1.15

Axis labels: $\ln(De\ m^2/s \cdot 10^5)$ vs $\ln(T/298)$

Fig.4.4 Effect of temperature on gas effective diffusivities through catalyst pellet

Legend (bottom figure):
- CH_4 in CO_2 slope=1.086
- CO_2 in CH_4 slope=1.056

Axis labels: $\ln(De\ m^2/s \cdot 10^5)$ vs $\ln(T/298)$
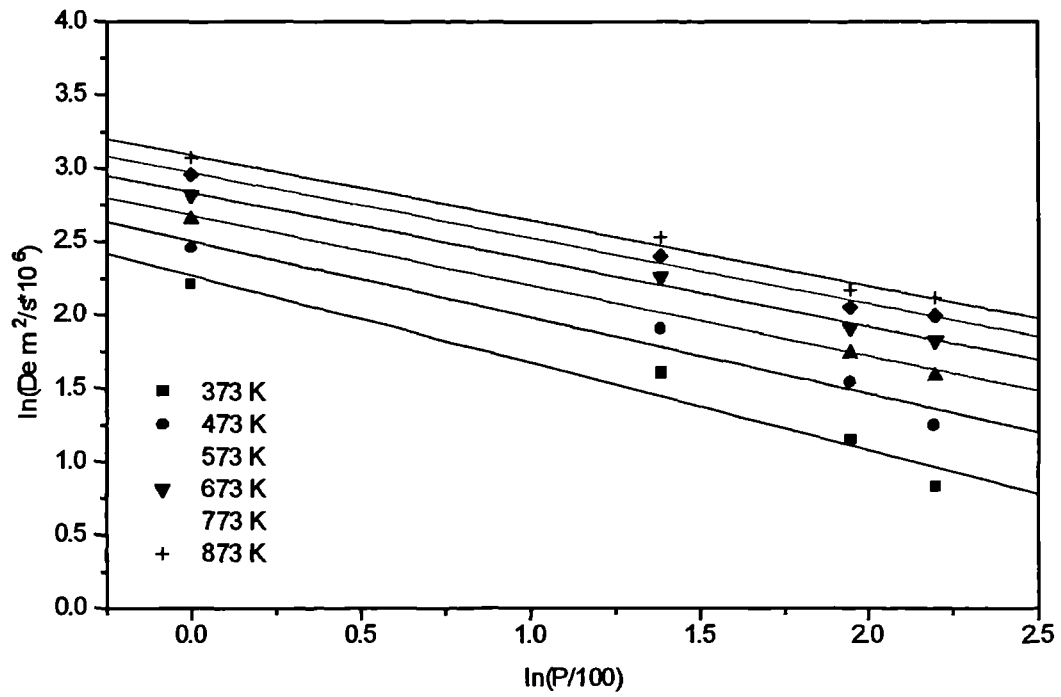
Fig.4.5 Effect of pressure on gas effective diffusivities through catalyst pellet: H_2 in N_2

Legend:
■ 373 K
● 473 K
573 K
▼ 673 K
773 K
+ 873 K
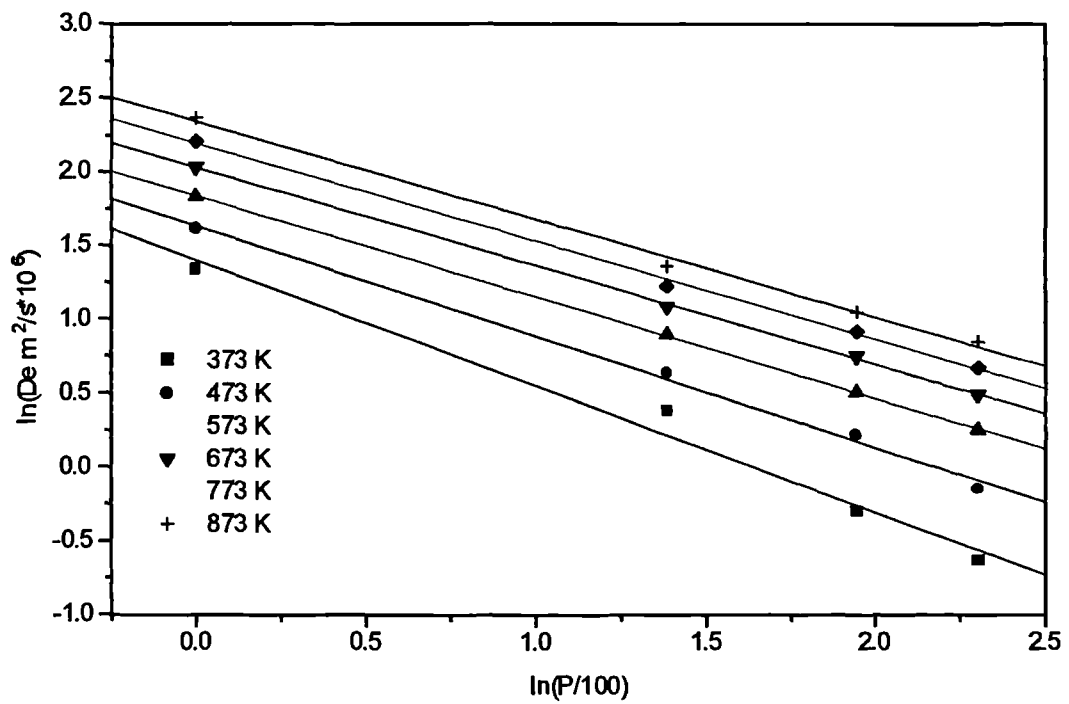
Fig.4.6 Effect of pressure on gas effective diffusivities through catalyst pellet: CH_4 in N_2

Legend:
■ 373 K
● 473 K
573 K
▼ 673 K
773 K
+ 873 K
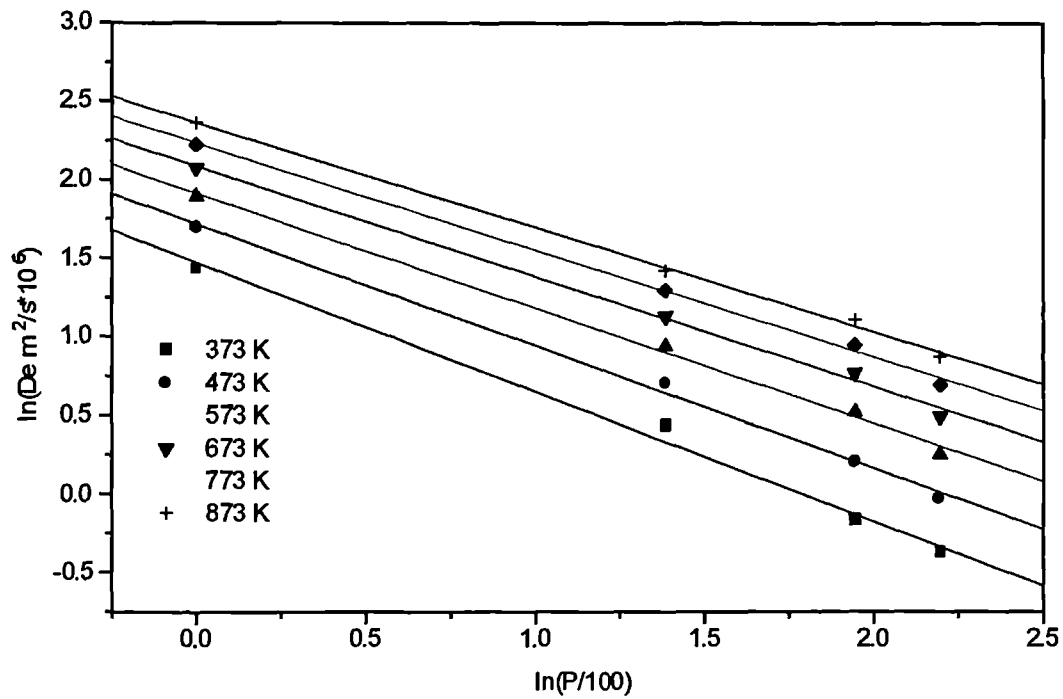
Fig.4.7 Effect of pressure on gas effective diffusivities
through catalyst pellet: CH_4 in CO_2
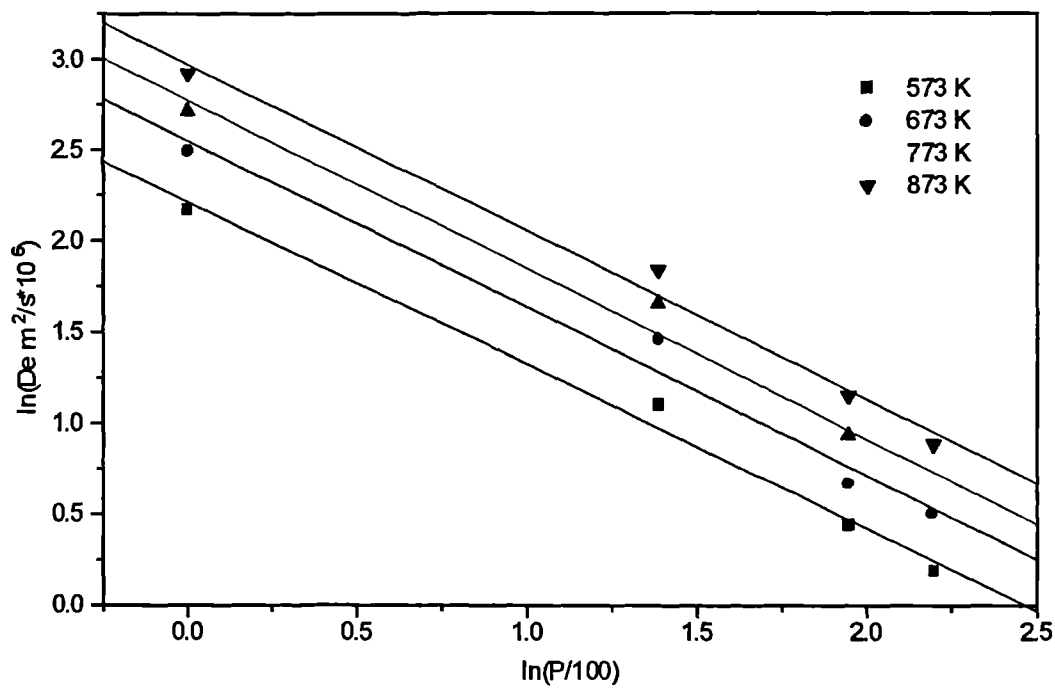
Fig.4.8 Effect of pressure on gas effective diffusivities
through catalyst pellet: water vapour in N_2
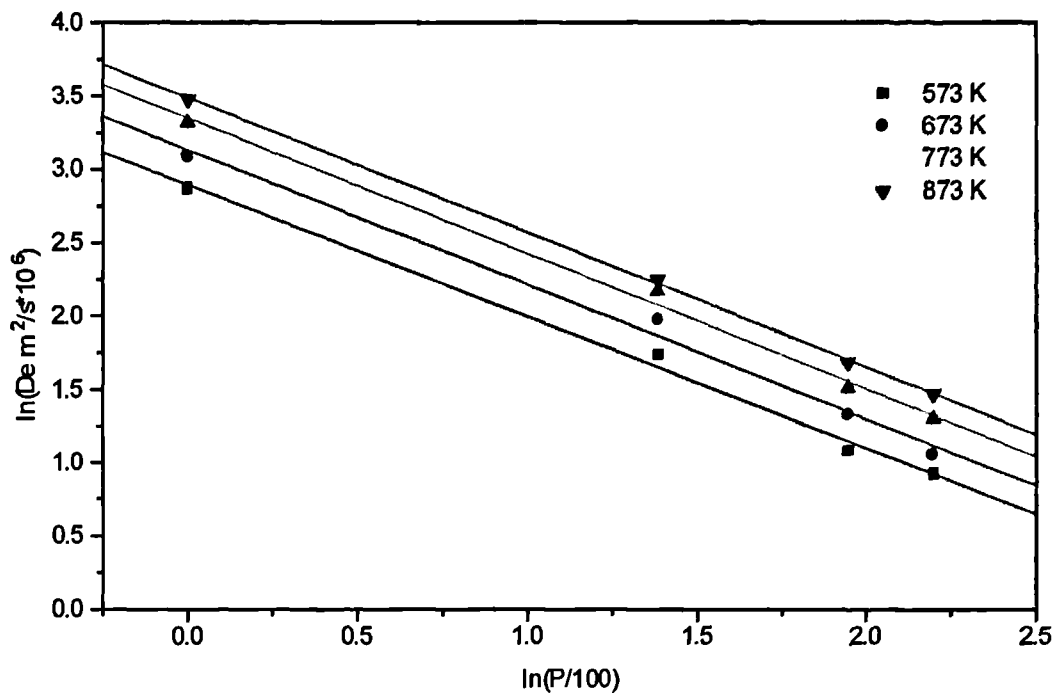
Fig.4.9 Effect of pressure on gas effective diffusivities
through catalyst pellet: water vapour in CH_4

CHAPTER 5 EXPERIMENTAL STUDY OF METHANE STEAM REFORMING ON A SINGLE PELLET REACTOR

5.1 Introduction

Flow schemes of the experimental facilities employed during the present research are shown in Figs.5.1 and 5.2. The main component of the apparatus used, is the single pellet reactor, which was modified from the W-K diffusion cell used to measure the effective diffusivities of the gases (see Chapter 4). Single pellet reactors have been used previously in poisoning studies by Petersen and co-workers (1968, 1970). The single pellet reactor employed in this work was arranged in such a manner that the equipment could couple the effect of diffusion on reaction kinetics of the methane steam reforming reaction under high intraparticle diffusion resistance. The experiments were carried out over two types of the catalyst pellets at temperatures of 853 –873 K and at ambient pressure. The molar ratios of steam to methane were 3 and 4, respectively.

5.2 Materials

Two types of Ni/α-alumina catalyst pellets either with holes or without holes were used in the experiments. The α-alumina pellets and the holes were made in the laboratory at Salford. The impregnation of the active metal component NiO was performed by ICI Katalco. Five different NiO loadings of the catalyst pellets obtained are listed below:

Catalyst pellet	C1	C2	C3	C4	C5
NiO weight (%)	20	10	5	1	0.5

B.O.C LTD supplied the methane used in the experiments. It was 100 cp grade Helium carrier,

hydrogen, carbon dioxide and nitrogen gases were purchased from B.O.C Ltd and were of a purity sufficient for experimental requirements.

5.3 Experimental System

The main parts of the rig consisted of a methane and water feed section, a preheater and evaporator section, the single pellet reactor, a condenser and dryer section and an analysis section. The latter included a gas chromatograph (GC) and an infra red gas analyser as well as a relative humidity meter (RHM). Schematic diagrams of the reaction flow systems are shown in Figs.5.1 and 5.2.

5.3.1 Feed section

The methane was obtained from a cylinder. After pressure reduction by mean of a regulator, the flow rate of methane was controlled by a mass flow controller within the range 20-70 ml(stp)/min. It then flowed into the preheater and evaporator, in which it was heated, and mixed with steam in a predetermined ratio. Liquid water was fed by a syringe pump at flow rates of 4.1, 6.5 and 9.7 ml/min, respectively. With such small flow rates, a small needle was used to connect the water pipe from the pump to the inlet of the preheater and evaporator in order that a continuous flow of steam was achieved. This homogeneous mixture of methane-steam was then passed into the reactor.

5.3.2 Preheater and evaporator section

A stainless steel tube with a heating wire coiled on its external surface was used to vaporize the water. The energy input to it was controlled by a Variac. The temperature of the evaporator ranged from 473-523 K. The stainless steel pipe that connected the exit of the evaporator and the inlet of the reaction-diffusion cell played the role of the preheater/mixer for the methane and steam.

5.3.3 The single pellet reactor

The structure of single pellet reactor was as the same of W-K type diffusion cell used before. The reactor was electrically heated. A thermocouple was employed to measure the temperature near the surface of the catalyst pellet. Since the length of catalyst pellet is only 0.0127 m, the whole pellet could be considered to be isothermal. Reaction temperature control was achieved by a temperature controller connected to the temperature indicator and the thermocouple. During an experimental run, the temperature deviation was ±2 K.

5.3.4 Condensing and drying section

This section consisted of an air-cooled copper tube condenser and two silica gel dryers. On leaving the reaction-diffusion cell, the reaction product was condensed and dried before being analysed. In the case of catalyst pellets without holes (case A), there are two streams flowing across each side of the reactor. The main stream from the feed side passed into the condenser for separation and collection of unreacted steam. This wet gas stream was then passed through the dryer to remove water vapour. The side stream from the sweep side passed first through the relative humidity meter (RHM) to measure the water vapour content. Another dry stream

was obtained after this wet gas stream flowed through another dryer. In the case of the catalyst pellet with holes (case B), the flow through stream was condensed and dried.

5.3.5 Analysis section

The analysis section consisted of a gas chromatograph (Varian 3400), an infra red gas analyser (Analytical development Co. Ltd.) and a relative humidity meter (Vaisala, Finland). The gas chromatograph (GC) was used to detect the methane, carbon monoxide, nitrogen and low concentrations of hydrogen. Carbon dioxide was measured by the infra red gas analyser and water vapour in the side stream was analysed by the relative humidity meter (RHM). The analysis methods will be described in detail below.

5.4 Analysis and Experimental Procedure

5.4.1 Analysis of reaction product

For the study of coupling of reaction and diffusion during methane steam reforming, it is necessary to know the compositions of the exit gases. In the present work, the reactants and products were methane, water vapour, hydrogen, carbon dioxide, carbon monoxide and nitrogen.

The GC (Varian 3400) with a thermal conductivity detector (TCD) was used to analyse all permanent gases except for carbon dioxide. The main operating conditions of the GC were:

Detector: TCD, temperature 413 K.

Filament: temperature 523 K, current 270 mA.

Column: 5A molecular sieve, 2-meter length, i.d 2mm.

Carrier gas: Helium, flow rate 50 ml(stp)/min.

The retention times of the gases were identified by using the standard calibration gas mixture supplied by Phase Separations Ltd. Under the operating conditions quoted above, Table 5.1 shows the retention times of each component.

Table 5.1 The retention time of gases

gas	hydrogen	oxygen	nitrogen	methane	carbon monoxide
t_r min	.30	.55	1.10	1.90	4.25

The calibration procedure was made by injection of these standard gas mixtures and gas mixtures made from high purity nitrogen and other gases at operating conditions. The calibration results are listed in Table 5.2.

By comparison of the peak area of component i in sample with its standard peak area, the mole fraction of the component was determined. Carbon dioxide was detected by the infra red gas analyser. The basic principle of operation of this instrument is a comparison of the radiation absorbed by the sample gas with that of a standard concentration. The range over which the analyser operates depends upon the length of the sample absorption chamber. (i.e. to alter the range, the infra red radiation path length is changed). In this work the analyser was operated in the two ranges of 0.0-3.0 and 0.0-15.0 percent volume, respectively. The calibration of the analyser was performed by using standard gas mixtures of nitrogen and carbon dioxide, made from high purity nitrogen and carbon dioxide in different ratios. The calibration results of the

analyser are shown in Fig.5.3.

Table 5.2 The calibration results

Component i	Relation between concentration y (%vol.) and peak area A	Concentration range y (% vol.)
CH₄	$y=6.3557 \times 10^{-5} A$	0 - 85
N₂	$y=5.3741 \times 10^{-5} A$	0 - 90
CO	$y=4.8667 \times 10^{-5} A$	0 - 10
H₂	$y=2.9499 \times 10^{-3} A$	0 - 10

5.4.2 Experimental procedure

5.4.2.1 Pretreatment of the catalyst

Before the experiments were carried out, the fresh catalyst pellet had to be reduced. The procedure used, was as follows:

1. The inlet to the sweep side of the reactor and the outlet of the feed side of the reactor were closed.

2. The catalyst pellet was heated to 673 K in nitrogen and held at this temperature for 1 hour.

3. The catalyst pellet was then held at the same temperature for 4 hours in hydrogen to reduce the nickel oxide to active metallic nickel.

4. After catalyst pellet reduction, the hydrogen gas was replaced by nitrogen to avoid air ingress into the reactor and protect the pellet against oxidation at high temperature.

5.4.2.2 Procedure for reforming experiments

After leak testing of the system with nitrogen, the reactor was heated to operating temperature in nitrogen. When the reactor temperature had attained the required level, which was maintained for at least 2 hours, the water pump was switched on at a larger flow rate than required with the nitrogen flow continued. The methane feed replaced the nitrogen when water drops appeared at the outlet of the condenser. After introduction of the methane-steam mixture at a constant ratio, the reforming reaction was allowed to continue at a constant temperature for about one hour to ensure steady state operation. Sampling started after the concentration of carbon dioxide monitored by the analyser had attained a stable value.

5.5 Experimental Results

All experimental results discussed in this section were obtained with two types of catalyst pellets of different active metal contents. The investigation considered the effects of diffusion, active metal content, "contact time", pellet type and temperature on the conversion of methane.

5.5.1 Experimental results for case A and discussion

Experiment of methane steam reforming over catalyst pellets without holes is named as case A. All experimental conditions are given in Table 5.3. The experiments for the low loading NiO of the pellets were not mentioned in this Chapter because the extent of reaction was so low that significant results were not obtained.

Table 5.3 Case A experimental conditions

Cat. pellet	C11	C21	C31
NiO % (wpu)	20.0	10.0	5.0
Cat. Weight gram	3.5134	3.1426	2.9981
H_2O/CH_4 molar ratio	3.0		
CH_4 flow rate ml /min	28.-70.		
Temperature K	853-873		
Pressure kPa.	100		

Figs.5.4-6 show the relations between the methane conversion and W/F ("contact time" i.e. catalyst pellet weight divided by the feed rate of the methane expressed as kgcat second/kmole) for the three catalyst pellets under conditions listed in Table 5.3. Under the same conditions, the equilibrium conversion of methane is 70-80 %. The very low conversion of methane, obtained from the experiments, means that only a small part of the methane feed takes part in the reaction. In other words, most of the methane feed did not diffuse into the catalyst pellet, and by-passed the catalyst. Comparing the conversions of methane from the Figs.5.4-6, there are only small differences of conversion among the different active metal contents of catalyst pellets. This suggests that the catalyst activity is not an important factor affecting the reaction under the present experimental conditions. From these Figures, it can be seen that there is only a small difference in conversion between the two reaction temperatures for the same catalyst pellet. The small effect of temperature on the conversion of methane also implies that the most significant factor controlling the reaction is that of reactant diffusion into the pellet in the

present experiments. From the analysis data of the compositions of the outlet of side streams, it is clear that most of the methane diffusing into the pellet had reacted with steam. On the other hand, based on the compositions at the two sides at outlet and the effective diffusivities of the gases measured by the diffusion experiments, the estimated amount of methane which diffused through the pellets was about 10-12 x 10^{-10} kmol/sec. This value is very close to the values of methane converted during those experiments with a high feed flow rate. However, this value is little greater than those of methane being reacted in the experiments of low feed flow rate. This may indicate that the diffusion resistance from bulk phase to the surface of the pellet was not eliminated completely in the present conditions.

In conclusion, for the methane steam reforming over the catalyst pellet without holes, the diffusion rate of methane almost totally controls the methane conversion. Under this diffusion limitation, other factors, such as the reaction temperature, the catalyst activity and the "contact time", do not show any apparent effects due to the reforming reaction.

5.5.2 Experimental results for case B and discussion

The case B, methane steam reforming experiments were carried out over the catalyst pellet with four holes. The diameter of each hole was 1.59 mm. The experimental conditions of case B are listed in Table 5.4

The relations between methane conversion vs. "contact time " are shown in Figs.5.7 and 5.8. It can be noticed that the methane conversion has now increased significantly, compared with the case A experiments. The experimental methane conversion now attained 25-60 percent of

equilibrium conversion. This suggests that the diffusion limitation to steam reforming over the catalyst pellet with holes had been lessened considerably. However, the catalyst activity still did not play an important role in affecting the reaction though its effect was greater than that in case A. Interestingly, there are two trends of the effect of reaction temperature on methane conversion with "contact time" change for the catalysts with different active metal content. For the catalyst with the higher active metal content, the difference of methane conversions between two temperatures increased with increase of "contact time", whereas a difference of methane conversion between two temperatures decreased with "contact time" increase for the lower activity catalyst. This effect could result from a change of the extent of diffusion limitation on the catalyst pellets with different activities. In other words, the effect of diffusion limitation on the catalyst pellet with higher activity is greater than on the catalyst pellet with lower activity. From these experiments, it may be concluded that the diffusion of the reactants from the external surface to the active sites of the catalyst is still the main factor controlling the reaction compared with other experimental variables for the catalyst pellet with four holes.

Table 5.4   The experimental conditions of the case B

cat. Pellet	C12	C32
NiO%(wpu)	20	5
cat. Weight gram	2.4019	2.7834
H_2O/CH_4 molar ratio	4.0	
CH_4 flowrate ml/min	20.0-50.0	
Temperature K	853-873	
Pressure kPa.	100	
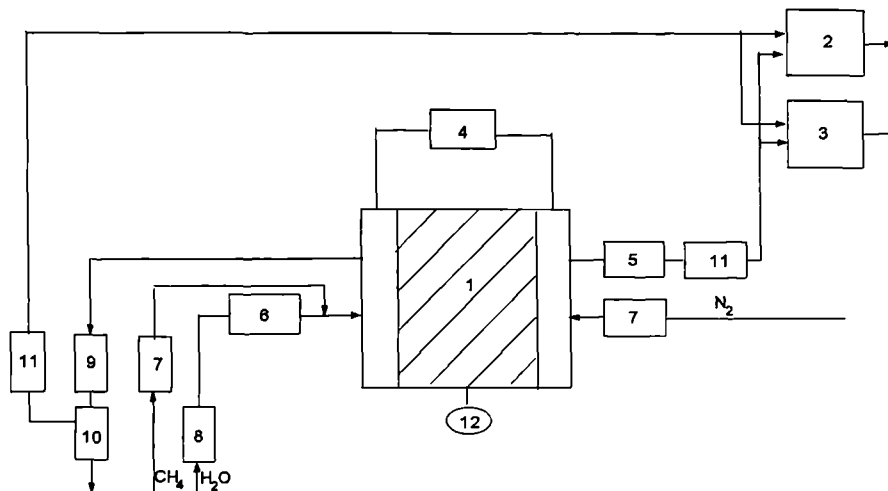
Fig.5.1 Schematic of flow system for methane steam reforming (pellet reactor, Case A)

1: Catalyst pellet,	2: Gas chromatograph,	3: CO_2 analyser
4: Pressure transducer,	5: RHM,	6: Evaporator
7: Mass flow controllers,	8: Syringe pump,	9: Condenser
10: Gas-liquid separator,	11: Dryers	12: Temperature controller
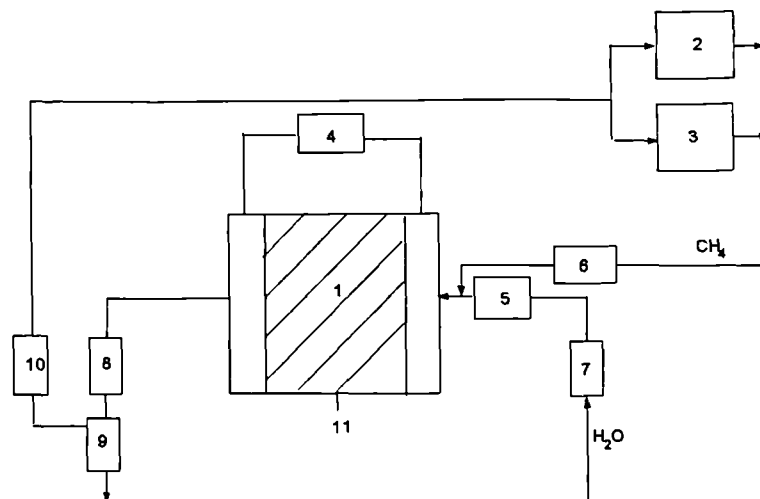
Fig.5.2 Schematic of flow system for methane steam reforming (pellet reactor, Case B)

1: Catalyst pellet,	2: Gas chromatograph,	3: CO_2 analyser
4: Pressure transducer,	5: Evaporator,	6: Mass flow controller
7: Syringe pump,	8: Condenser,	9: Gas-liquid separator
10: Dryer,	11: Temperature controller	
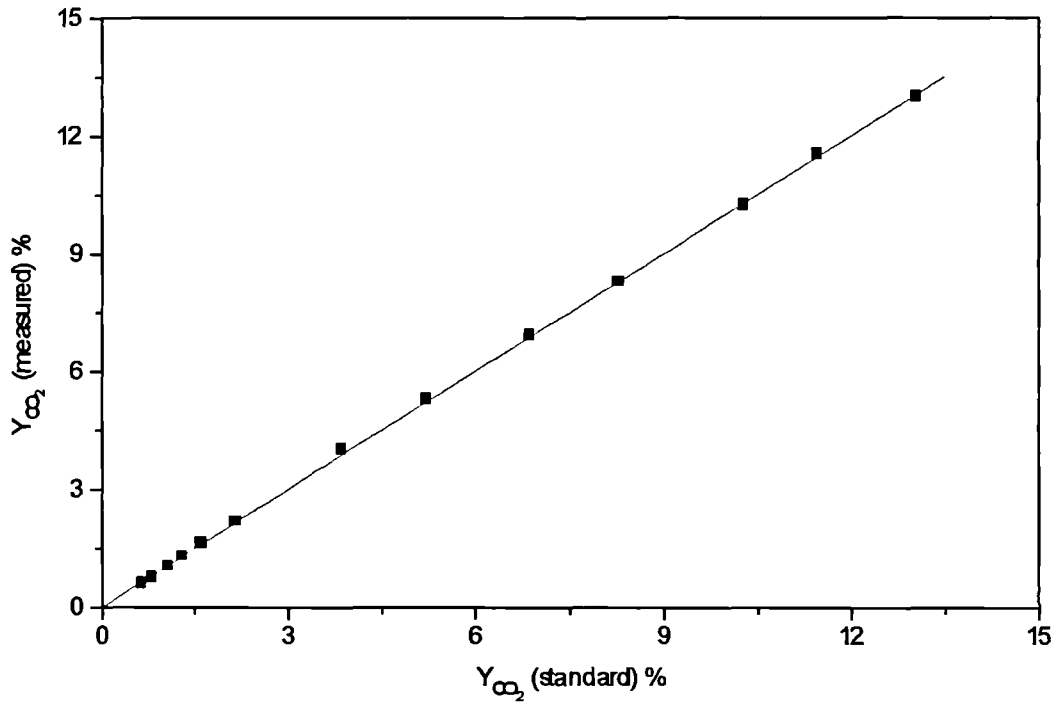
Fig.5.3 Carbon dioxide calibration
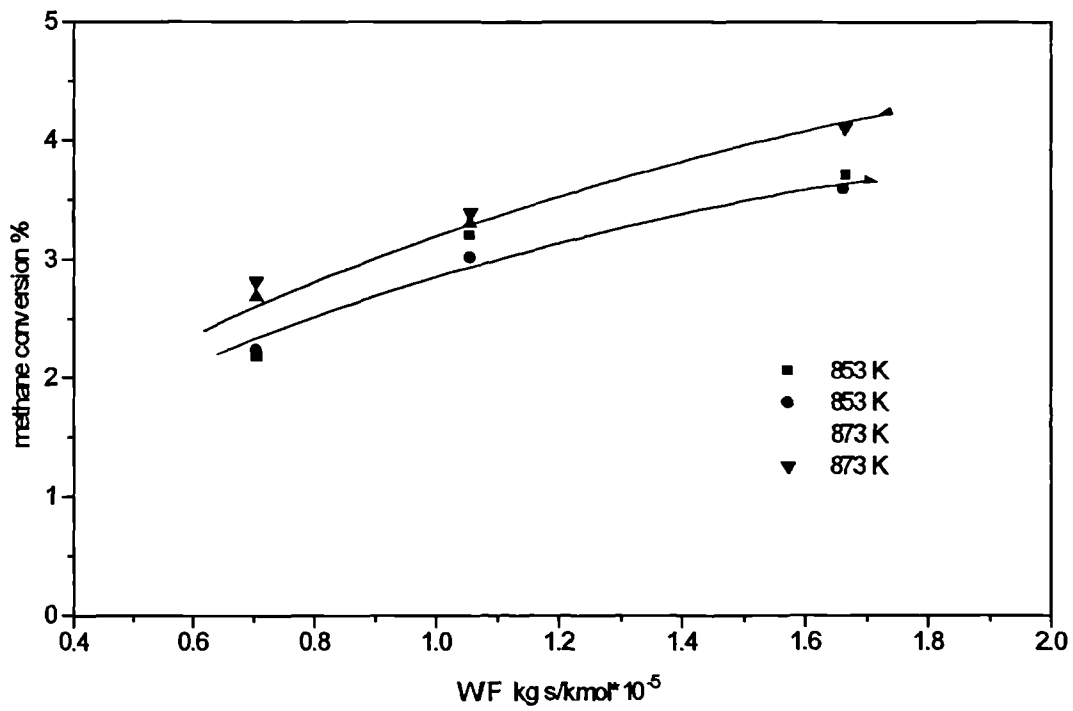
Fig.5.4 Methane conversion vs. WF (C11)
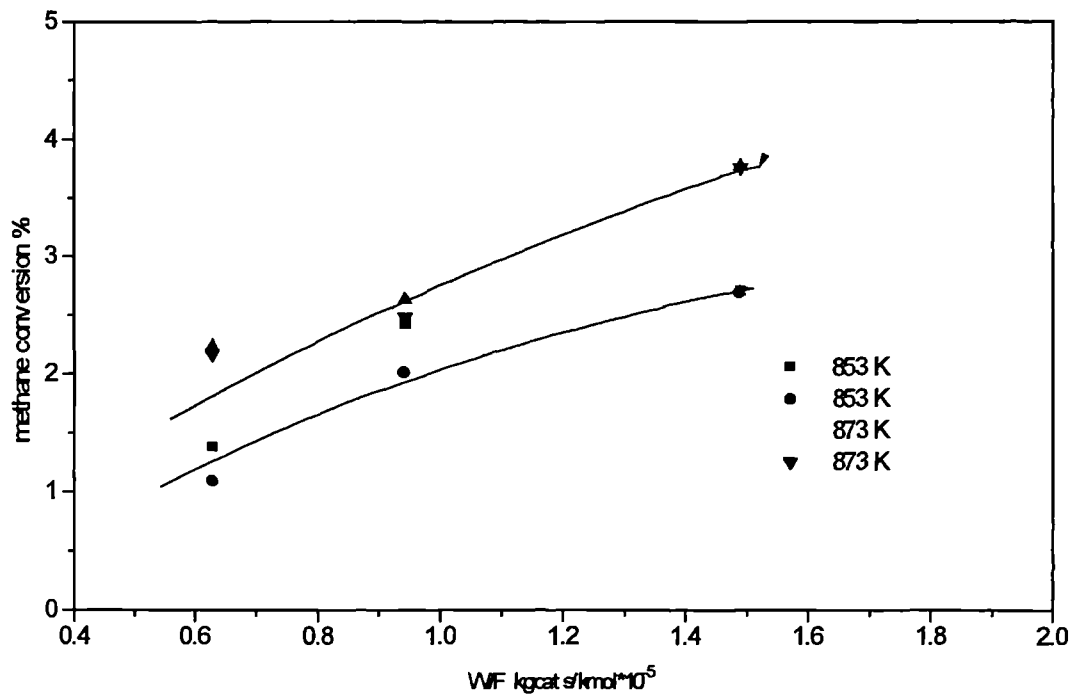
Fig.5.5   Methane conversion vs. WF (C21)
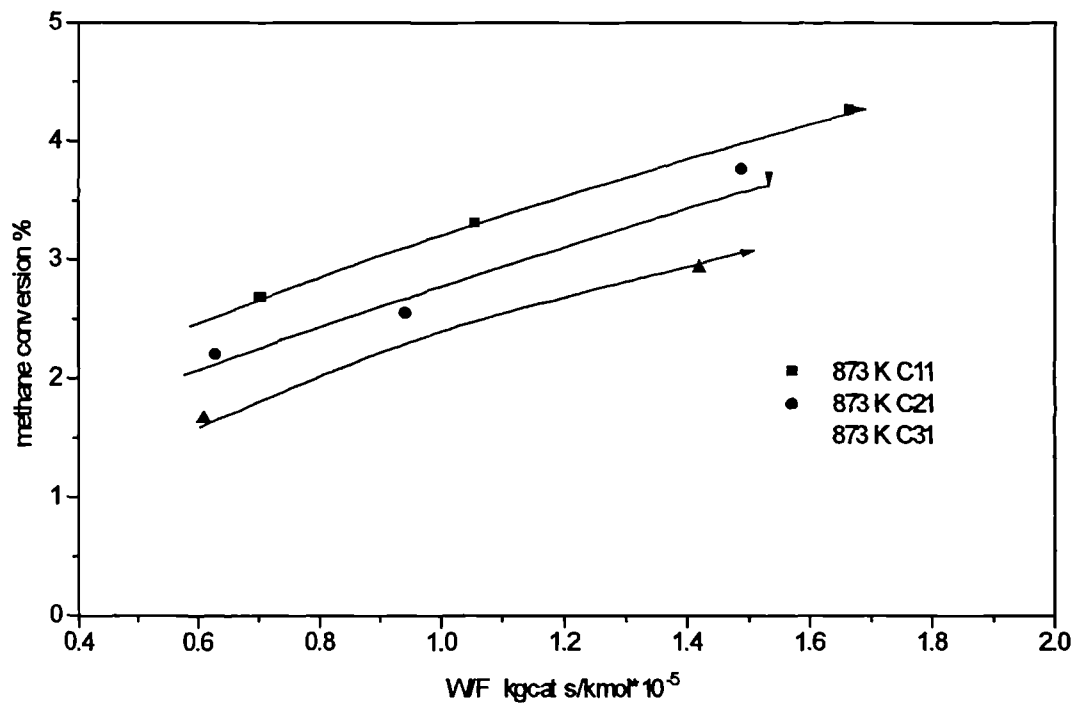
Fig.5.6   Effect of catalyst activity on methane conversion
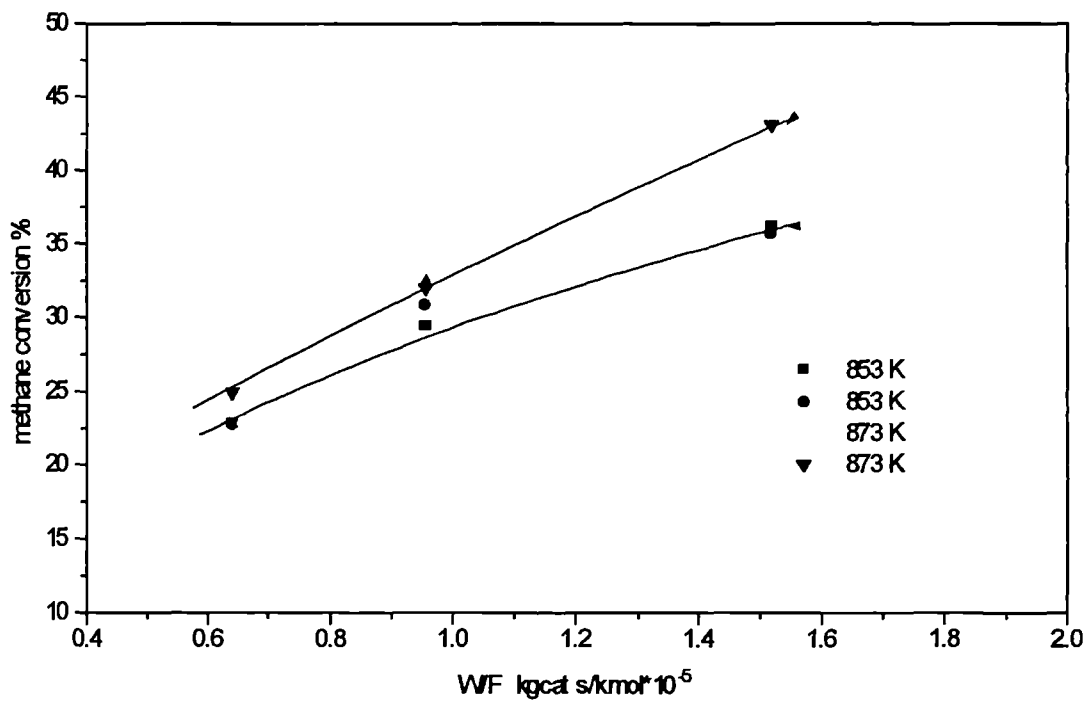
Fig.5.7   Methane conversion vs. W/F (C12)
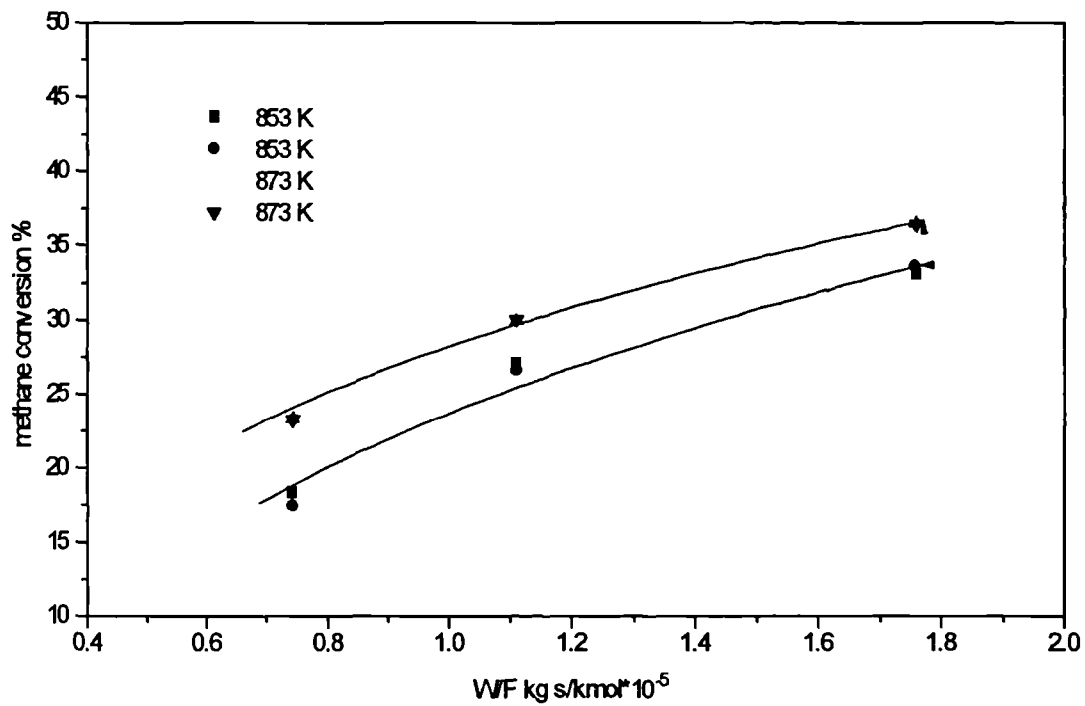
Fig.5.8   Methane conversion vs. W/F (C32)

CHAPTER 6 EXPERIMENTAL MEASUREMENTS OF METHANE STEAM REFORMING AND THE REVERSE WATER GAS SHIFT REACTION IN AN INTEGRAL REACTOR

6.1 Introduction

Methane steam reforming on a porous catalyst is a complex process. It not only involves the transfer and diffusion of reactants and products between the bulk phase and catalyst surface as well as within the catalyst, but also involves several reactions simultaneously in parallel or in series. To investigate the intrinsic kinetics of methane steam reforming, it is important to choose a suitable type of laboratory reactor. Generally, laboratory reactors for heterogeneous reactions can be grouped into four types: differential, integral, gradientless and single pellet reactors. There is no major difference between differential reactors and integral reactors in construction. Single pellet reactors are mostly used for studying catalyst poisoning and the influence of diffusion so that this type of reactor is not usually chosen for a study of intrinsic kinetics. To deal with and interpret the experimental data, differential or gradientless reactors are often preferred for an intrinsic kinetic study of simple reactions in the laboratory. However, a high accuracy of composition analysis and flow rate measurement is vital in using these two types of reactors. In view of the complexity of methane steam reforming and the limitations of analytical equipment, an integral reactor was chosen for the present experimental study of the intrinsic kinetics of methane steam reforming.

The present experimental study can be classified into three groups according to their purpose, i.e. (1) experiments to examine catalyst deactivation and to find a way to keep the catalyst stability, and to eliminate the limitations of intraparticle diffusion; (2) experiments

to obtain the methane conversion and product distribution of methane steam reforming at different experimental conditions; (3) experiments to examine the carbon dioxide conversion and product distribution of the reverse water gas shift reaction as a subsidiary process in methane steam reforming experiments. For each group, the effects of mass transfer and temperature difference between fluid phase and solid phase should be determined or minimised.

6.2 Experimental Set up

6.2.1 Materials

The feed gases used were methane, hydrogen, carbon dioxide; the carrier gas for the gas chromatograph (Varian 3400) used was helium. All gases are as the same purity and supplier as for the diffusion experiments. Deionised water was used for production of steam. A nickel/alumina catalyst (ICI steam reforming catalyst 57-4) of cylindrical type with four axial holes was provided by ICI Katalco. The main properties of the catalyst are listed in Table 6.1, and the pore size profile is shown in Fig.6.1. The original catalyst was crushed into particles of average diameter 0.15mm. The amounts of catalyst loaded were 0.3 and 0.1 gram for the formal methane steam reforming reaction and the reverse water gas shift reaction experiments, respectively.

Table 6.1   the catalyst properties

NiO content	%	15-17
Surface area	m^2/g	14.30(average value)
Skeletal (He) density	g/cm^3	3.204
Geometric (Hg) density	g/cm^3	1.792
Total pore volume	cm^3/g	0.246
Porosity		0.44

6.2.2 Experimental system

A schematic diagram of the experimental facilities used is given in Fig.6.2. Most components were the same as used in experiments for the single pellet reactor. The different components are described as below.

The integral reactor and evaporator used in present study are made from stainless tubes 1 cm inner diameter and formed into a Y shape and was covered by heating wires. A sectional view is shown in Fig.6.3. The straight section 33.8 cm long served as the reactor, while the side arm section, 21.5 cm long, was used as the evaporator/preheater. A thermocouple was placed in the thermocouple well which was of 0.2 cm outer diameter and was located at the centre/axis of the reactor. The thermocouple connected to a temperature indicator and a temperature controller to monitor and control the reaction temperature. Another thermocouple was located adjacent to the heating wire surrounding the evaporator to measure and control the evaporator temperature.

A piston pump (Gilson Model 305) was used to transport deionised water to the evaporator. Compared with the syringe pump used before, the piston pump can provide water at any arbitrary flow rate required.

The analysis section contains the gas chromatograph (Varian 3400) and the infra red gas analyser as used previously for the single pellet studies. The gas chromatograph (GC) was used to analyse the methane and carbon monoxide only, and the infra red gas analyser was used to detect the carbon dioxide. The concentration of hydrogen in the dry gases was determined by a hydrogen balance since the GC with carrier gas helium and 5A molecular

sieve column cannot detect high concentrations of hydrogen. The amount of steam consumed was calculated by an oxygen balance.

6.2.3 Experimental procedure

6.2.3.1 Leakage testing

The fresh catalyst was loaded to a fixed position for each experimental run for methane steam reforming. The space remaining between the steel mesh support and the outlet was packed with inert α-alumina particles. Catalyst and α-alumina removal from the reactor were prevented by a layer of glass wool at the outlet of reactor.

After catalyst loading, leak testing of the experimental system was carried out as follows: (1) the system was pressurised with nitrogen to a pressure higher than the experimental pressure desired; (2) the back pressure valve was closed; (3) when the system pressure was equal to the nitrogen pressure, if the nitrogen flow rate decreased to or was very near a zero value, the leak testing was finished.

6.2.3.2 Reduction of the catalyst

When the leak testing had been completed, the catalyst was reduced by the following procedures: (1) the reactor was heated to 673 K at 3 K/min in nitrogen and maintained at this temperature for one hour; (2) the catalyst was sustained at the same temperature for 2 hours in hydrogen, and then the catalyst was heated to 873 K at 2.5 K/min in hydrogen; (3) the catalyst was kept at 873 K for one hour in hydrogen; (4) the temperature was deceased to the required temperature in hydrogen. The catalyst was then ready for the reaction experiments.

6.2.3.3 Procedure for kinetic experiments

At the reference temperature, hydrogen and water were set at their reference flow rates. Methane was fed into the evaporator at desired flow rate until water drops collected in the gas/liquid separator. A sample analysis was done at 20 minutes for monitoring the variation of the catalyst activity, since the experiment was run at reference conditions. When near constant values for the sample analysis had been obtained (c.a. 4.5 hours from the time of the methane was initially fed in), the operating conditions were changed to the formal experimental conditions. During each experimental run, if the total feed flow rate was increased, the order in which each feed flow rate was increased was: (1) hydrogen, (2) water and (3) methane. Similarly if the total feed flow rate was decreased, the order was reversed. By such means, the risk of carbon formation due to lack of steam in the feed could be avoided.

6.3 Determination of Physical and Catalyst Deactivation Influences
   on Methane Steam Reforming

In experimental studies of heterogeneously catalysed reactions, one of the objectives should be to determine whether the investigation is concerned with catalytic kinetics or with interactions between the kinetics and transport phenomena. The intrusion of temperature and concentration gradients as well as catalyst deactivation (except for deactivation studies) can lead to severe deviations in the catalyst performance, in many cases completely disguising the true kinetics of the reaction. To ensure that the kinetic data obtained in an experimental reactor reflect only chemical events, any physical resistances must be minimised or eliminated.

Four aspects need to be assessed i.e.:

1) Intraparticle diffusion within the catalyst particles.

2) Interphase mass transfer between bulk bulk phase and the outer surface of the particles.

3) Temperature gradients within the particles and between the bulk phase and the solid phase.

4) Catalyst deactivation.

For any gas-solid heterogeneous reaction in which the gaseous reactants pass through a bed of solid catalyst particles, several physical and chemical steps are involved between the gaseous reactants and the porous catalyst particles. In general, the sequence of these steps is as follows:

1. Transfer of reactants from the bulk phase to the catalyst surface.

2. Diffusion of the reactants into the interior of the catalyst particle.

3. Adsorption of the reactants at interior sites of the catalyst.

4. Chemical reaction of adsorbed reactants to adsorbed products.

5. Desorption of adsorbed products.

6. Diffusion of products back to the exterior surface of the catalyst particle.

7. Transfer of the products from the exterior surface to the bulk phase.

Physical steps 1 and 7, 2 and 6 are termed as interphase mass transfer and intraparticle diffusion respectively. As a rule of thumb, it can be concluded that the effects of steps 6 and 7 on the reactions are quite small, compared with steps 1 and 2. However, the effects of the steps 1 and 2 on the reactions are sometime so significant that misunderstandings of reaction kinetics are obtained from experiments. The chemical steps 3, 4 and 5 involve activated adsorption of the reactants, surface reactions on active sites and desorption of the products.

In order to simplify the interpretation of the experimental data, it is desirable to minimise the effects offered by each of these physical steps (1, 2, 6 and 7) and thus to study only the intrinsic kinetics of the reactions.

For highly endothermic reactions or highly exothermic reactions, if the reactions are fast, the catalyst particles are relatively big and transfer of heat between the bulk phase and catalyst particles is insufficient, a temperature difference may be built up between the bulk phase and the interior of catalyst particles, which often leads to inaccurate results obtained from experiments due to the temperature in the interior of catalyst particles being different from the bulk phase. It is necessary to minimise or account for any effect of temperature difference on the experimental results.

Another key factor affecting the quality of the experimental data is catalyst deactivation resulted from coking, poisoning and ageing.

It is evident that an experimental study of all these possible effects simultaneously is not realisable because of their complexity. For the investigation of the intrinsic kinetics of the reactions, it is necessary, therefore, that experiments are arranged to determine or eliminate these different effects separately. Resistance to interphase mass transfer can be minimised by operating at sufficiently high mass flow velocities to make the partial pressure differences across the gas film negligible. The effects of intraparticle diffusion can be eliminated by using catalyst particles of small size. Elimination of the effect of temperature also can be achieved by using small catalyst particles. Changes in the catalyst activity due to deactivation by coke deposition, poisoning and ageing can be avoided by employing fresh catalyst for each run.

6.3.1 Experiments to determine catalyst stability

The catalyst may be deactivated by coking (also termed as carbon formation) from some reactions, poisoning from impurities and ageing. Even without coking and poisoning, it is inevitable that the catalyst is slowly deactivated by ageing effects, such as sintering and loss of active metal. To obtain more reliable result from experiments, the effects of coking and poisoning on the catalyst activity have to be eliminated or minimised to an extent that can be tolerated for the experimental requirements. In the present experiments, as the methane was of purity cp. and deionized water was used as feed, it was unlikely that the catalyst was poisoned by impurities. If catalyst deactivation does take place, the main cause is likely to be coking.

Fig. 6.4 shows the variation of catalyst activity with time at p_t=120 kPa, T=823 K, H_2O/CH_4 molar ratio = 3 and W/F_{CH_4} = 1.336×10^4 kgcat s/kmol. It is clear that the catalyst activity drops very fast. In such a case, the quality of the experimental data is unacceptable. At the experimental conditions used above, the rate of carbon formation on the catalyst should be quite slow. However, it was confirmed experimentally that small sized catalyst particles are quickly deactivated by coking because reactions leading to carbon formation can occur in the interior of the catalyst particles (Blue, et al., 1952). Hence the fast deactivation might be due to the use of a small size catalyst which had been selected to minimise the effect of intraparticle diffusion.

Based on a thermodynamics analysis of possible carbon formation reactions, it was found that methane decomposition is the main carbon formation reaction. To inhibit the methane

decomposition, hydrogen, one of products of this reaction, may be added to the feed. By increasing the hydrogen/methane molar ratio in the feed by small steps, an acceptable equimolar ratio of hydrogen to methane was determined. At this ratio, other reaction conditions, such as temperature, pressure and the steam/methane molar ratio could vary over wider ranges.

Fig.6.5 shows the variation of catalyst activity with time at p_t=120 kPa, $H_2O/CH_4/H_2$ molar ratio = 5.5/1/1, W/F_{CH_4} = 1.336×10^4 kgcat s/kmol and T=798, 823 K respectively. The activity of the catalyst still drops rapidly during the first 200 minutes, but then more slowly. After 250 minutes, the deactivation has become so slow that only minor corrections, as explained in section 6.4, are sufficient to account for it. Deactivation for this period is probably caused by ageing. The experimental data, for the kinetics study under specific conditions, were collected during times from 270 to 450 minutes on stream.

The variation of catalyst activity with time for the reverse of the water gas shift reaction at p_t = 120 kPa, H_2/CO_2=0.75, W/F_{co2} =1800 kgcat s/kmol and 673 K is presented in Fig.6.6. At the low temperature used with less risk of carbon formation from this reaction, the stabilised activities of fresh catalyst and used catalyst were obtained. The data for the reverse of water gas shift experiments were collected at 200-400 minutes on stream.

6.3.2 The effects of interphase mass transfer

For the catalyst to be effective, the catalyst must be brought into contact with reactants at rates which are comparable with the rates at which reactants transfer from the bulk phase

to the catalyst. Otherwise, the conversion will be controlled by mass transfer variables rather than by the catalyst activity.

In a commercial reactor, there is almost no resistance to interphase mass transfer as a high gas velocity is used which increases turbulence, which in turn promotes mass transfer from the bulk phase to the catalyst surface. Taking account of the limitations of laboratory equipment, the gas velocity used is as high as possible to minimise or eliminate the effect of interphase mass transfer.

The resistance of interphase mass transfer can be determined by two ways. One is by experimental methods, and another combines experiment and theoretical calculation.

The experimental method is to increase the gas velocity and catalyst amount in proportion in order to keep the contact time constant. When the conversions reach a constant level the bulk mass transfer resistance is eliminated. An example is seen in the results of a study of the water-gas shift reaction on 9.4 mm diameter iron oxide pellets as reported by Hulburt and Srini Vasan (1961). For this method to be reliable, it should be carried out carefully in order to obtain conversions far from the thermodynamic limitation for reversible reactions, otherwise, the thermodynamic limitation will mask the effect of bulk mass transfer on the reaction.

The method of combining experiment and theoretical calculation used in this section is described in detail below. In order to determine the effect of resistance due to interphase mass transfer, consider the reversible methane steam reforming reactions.

$$CH_4 + H_2O = CO + 3H_2$$

or $\qquad\qquad$ $CH_4 + 2\,H_2O = CO_2 + 4\,H_2$

At steady state the disappearance of methane, expressed in per unit mass of catalyst, may

be written either in terms of the mass transfer from the bulk phase to the surface or in terms

of the reaction rate on the catalyst,

$$r = k_C\,a_m\,(C_{Ab} - C_{As})$$ (6.1)

$$r = \frac{F_{CH_4}\,X_{CH_4}}{W_{cat}}.$$ (6.2)

where C_{Ab} and C_{As} are the concentrations of methane in the bulk phase and at the catalyst

surface respectively, a_m is outer surface area per unit mass of the catalyst, F_{CH4} is a flow

rate of methane, X_{CH4} is a methane conversion and W_{cat} is the catalyst amount used and k_C

is the mass transfer coefficient between the bulk phase and catalyst surface. k_C can be

correlated in terms of dimensionless groups that describe the flow conditions. For mass

transfer, the k_C is a function of the Reynolds number d_pG/μ and Schmidt number $\mu/\rho D_{Am}$.

Their different relationships can be found in the literature (Satterfield, 1970 and 1980;

Wakao et al. 1974; Froment et al. 1979 and Li Shaofen, 1986). By comparing the ranges

for these relationships being applied and the present experimental conditions as well as

comparing differences between k_C calculated from these relationships, the following

relationship (Li Shaofen,1986) was chosen for the determination of interphase mass

transfer:

$$\frac{k_C\rho}{G}(Sc)^{2\,/\,3} = \frac{0.725}{(Re_p)^{0.41} - 0.15}$$ (6.3)

where:

d_p = Diameter of a particle.

D_{Am} = molecular diffusivity of the component A being transferred in

$\qquad$ the mixed gases.

μ = viscosity of fluid.

G = mass velocity based on total cross-sectional area of reactor.

ρ = density of fluid.

Combining equations (6.1), (6.2) and (6.3) at steady state, we obtain:

$$\frac{C_{Ab} - C_{As}}{C_{Ab}} = \frac{F_{CH_4} X_{CH_4}}{W_{cat} k_C a_m C_{Ab}} \tag{6.4}$$

If the rate of the reaction becomes entirely chemical rate-controlling the value of C_{Ab} should approach C_{As} and $(C_{Ab} - C_{As})/C_{Ab}$ should be very small; under these conditions the resistance to external mass transfer can be neglected. The values of $(C_{Ab} - C_{As})/C_{As}$ in Table 6.1 were calculated directly from equation (6.4) by using the experimental data for methane steam reforming at the reaction temperature of 823 K. The detailed calculation procedure is given in Appendix B. It should be pointed out that equation (6.4) is strictly valid for experimental data collected using a differential reactor. In the present experiments, both reaction rates calculated from the equation (6.2) and C_{Ab} are average values for the reaction over the total reactor so equation (6.4) is only roughly valid for the present case. From Table 6.2 it can be seen that the values of $(C_{Ab} - C_{As})/C_{Ab}$ are extremely small. This indicates that the interphase mass transfer effects should be negligible under the present experimental conditions.

Table 6.2 Determination of the effect of interphase mass transfer

Temperature K	W_{cat}/F_{CH4} kgcat. s /kmol	$r_{CH4} \cdot 10^5$ kmol/ kgcat.s	$(C_{Ab} - C_{As})/C_{Ab}$ $\times 10^3$
823*	13356	3.13	2.34
	10872	3.27	2.16
	8712	3.37	1.94
	6516	3.41	1.64
	4320	3.55	1.34
	2880	3.67	1.10
823**	13356	3.35	2.40
	10872	3.78	2.48
	8712	4.04	2.32
	6516	4.57	2.25
	4320	5.12	1.99
	2160	5.92	1.55

* $H_2O/CH_4/H_2 = 5.5/1/1$, $p_t = 120$ kPa

** $H_2O/CH_4/H_2 = 4.0/1/1$, $p_t = 120$ kPa

6.3.3 The Effects of intraparticle diffusion

When the catalyst particles are large, the resistance of intraparticle diffusion will reduce the reactant concentration within the particles. Hence, the average reaction rate will be less than what it would be if there were no internal concentration gradients. Under such severe limitation of the intraparticle diffusion, incorrect experimental results, for the reaction mechanism, activation energies and rate constants, will be obtained.

Intraparticle transport has been analysed for a wide variety of reaction kinetics and particle geometries. Generally the objective has been to calculate an effectiveness factor, η, defined

as the ratio of the observed rate to the rate would occur if the temperature and concentration were constant throughout the catalyst particle. Solutions for the effective factor show that η becomes inversely proportional to the characteristic dimension of the particle in the regime of strong diffusion influence. Unfortunately, direct application of such solutions requires knowledge of the true kinetic behaviour and the intrinsic rate constant.

Some analytical criteria for the absence of significant diffusion effects which are independent of the rate constant have been reviewed by Mears (1971). Because these criteria were derived by means of linear approximation of the concentration gradient at the surface or using a perturbation method for simple nth order irreversible kinetics, these can fail for complicated reaction kinetics. In addition, the accuracy of these criteria is also limited by the accuracy with which diffusivities and physical properties can be predicted.

To determine the effects of intraparticle diffusion reliably, an experimental method is preferentially employed. The influence of intraparticle diffusion can be minimised by decreasing the size of particle. By keeping other conditions constant and decreasing the size of the particles gradually, the attainment of a constant conversion indicates that intraparticle effects are totally eliminated for such sizes of particles.

The effects of particle size on methane steam reforming was examined using five different average sizes of particles (0.608 mm, 0.440 mm, 0.253 mm, 0.150 mm, 0.105mm). Fig.6.7 shows methane conversions obtained on five sizes of particle at p_t= 120 kPa, H_2O CH_4/H_2 =4/1/1, W_{cat}/F_{CH4}=2.225$\times10^4$ kgcat.s/kmol and temperatures ranging from 748 to 823 K. It can be noticed that there are no significant changes in values of the methane conversion for

the last two particle sizes, while conversion changes are appreciable for the three larger sizes (particularly at high temperature). This result shows that the intraparticle diffusion limitation can be negligible for small size particles within the present temperature range. The decrease in conversion in the larger particles is evidence of diffusion limitations. At the lower temperature of 748 K, the conversions reached a constant value with decreasing sizes of particle much earlier, whereas at high temperature, a smaller size of particle is required to eliminate the limitation of intraparticle diffusion. This is because the influence of temperature on the reaction rate is stronger than the diffusion rate. In this study small catalyst particles of 60-90 mesh size (average d_p 0.150 mm) were used in order to minimise the effects of diffusion in the interior of the catalyst particles.

6.3.4 Estimation of temperature difference between catalyst surface and bulk phase

For the highly endothermic reactions of methane steam reforming, there may be a temperature difference between bulk phase and catalyst surface. At steady state conditions, the disappearing rate of methane within the catalyst multiplied by the heat of reaction per mole of methane must equal the rate of heat transfer from the fluid towards to the solid. Hence

$$r\,(\Delta H\,) = h\,a_m\,(T_b - T_s\,) \tag{6.5}$$

Rearranging equation (6.5),

$$T_s - T_b = r\,(-\Delta H)\,/h\,a_m \tag{6.6}$$

where

$$h = \frac{1.10\,G C_{pm}}{Pr^{0.67}\left(Re_p^{0.41} - 0.15\right)} \quad \text{(Li Shaofen, 1986)} \tag{6.7}$$

and

$$Pr = C_{pm}\,\mu\,/\,\lambda_f \tag{6.8}$$

here T_b and T_s are the fluid and solid temperatures respectively, ΔH is the heat of reaction per kmol methane, h is the heat transfer coefficient, C_{pm} is the heat capacity per unit mass of fluid, Pr is the Prandtl number, and λ_f is the thermal conductivity of the fluid. From the analogy between the mass transfer and the heat transfer and applying j_d and j_h functions, another equation for estimation of the temperature difference has been given by Satterfield (1980) as follows

$$T_s - T_b = \frac{j_d}{j_h}\left(\frac{\text{Pr}}{S_c}\right)^{2/3}\frac{\left(-\Delta H\right)\left(C_{Ab} - C_{As}\right)}{\rho C_{pm}} \tag{6.9}$$

From equations (6.6) and (6.9), the temperature difference is seen to been directly proportional to the reaction heat per kmol reacting component. Equation (6.9) emphasises the fact that, if the heat of reaction is large, even though mass transfer limitations may be small, heat transfer can still cause significant effects.

The temperature differences in Table 6.3 were calculated directly by using equations (6.6) and (6.9) with the experimental data for methane steam reforming at a reaction temperature of 823 K. The small temperature difference obtained is compared to the reaction temperature used. This indicates that the resistance to heat transfer is very small and the effects of temperature difference could be neglected in the present study. In addition, the temperature gradient within the catalyst particle can be neglected because of the small size of particles employed in the study.

Table 6.3 Temperature difference between the catalyst surface and bulk phase

Temperature K	W_{cat}/F_{CH4} Kgcat s /kmol	ΔT K eqn. (6.6)	ΔT K eqn. (6.9)
823*	13356	-0.84	-0.90
	10872	-0.81	-0.86
	8712	-0.77	-0.81
	6576	-0.69	-0.73
	4320	-0.59	-0.63
	2880	-0.50	-0.53
823**	13356	-.0.97	-1.03
	10872	-1.03	-1.09
	8712	-1.00	-1.06
	6576	-1.06	-1.07
	4320	-0.93	-0.99
	2160	-0.78	-0.83

* $H_2O/CH_4/H_2 = 5.5/1/1$, $p_t = 120kPa$

** $H_2O/CH_4/H_2 = 4.0/1/1$, $p_t = 120kPa$

6.4 Methane Steam Reforming Experimental Results and Discussion

6.4.1 Experimental mode and correction of experimental results

The thermodynamic relationships for methane steam reforming limits any kinetic study to a rather narrow temperature range. Also reaction pressure and total flow rate are limited by the equipment. The conditions chosen for the experiments are listed in Table 6.4. For steam reforming, the temperature range was well below that practised industrially.

However, the temperature had to be limited to such a range to avoid measuring only equilibrium conversions.

Based on the catalyst stability experiments for methane steam reforming, a mode of operation enabling runs to be completed within one day was chosen, but using fresh catalyst due to its slow deactivation

After the catalyst had been reduced, standard experimental conditions were set as follows

Temperature = 798 K

Pressure   = 120kPa

$H_2O/CH_4/H_2$ =5.5/1/1

$W_{cat.}/F_{CH4}$ = 13356 kgcat s /kmol

The above conditions are considered to be the reference conditions for methane steam reforming.

Tests under reference conditions were carried out for each experiment, prior to runs at other conditions. The contact time of the test was assigned a $(W_{cat}/F_{CH4})_1$ value at the beginning of each set of experiments. When the data collection was finished, the contact time $(W_{cat}/F_{CH4})_2$ for obtaining the same conversion as at the beginning was determined. The correction factor for contact time due to the catalyst deactivation is given by

$$f_c = 1 - \frac{t}{t_{1-2}} \left[1 - \frac{\left(\dfrac{W_{cat}}{F_{CH_4}} \right)_1}{\left(\dfrac{W_{cat}}{F_{CH_4}} \right)_2} \right]$$

(6.10)

Where t is time for collecting data from the beginning of the test, and t_{1-2} is the time duration from the beginning of the test to the end of the test. The correct contact time is then

$$\left(\frac{W_{cat}}{F_{CH_4}}\right)_c = f_c \frac{W_{cat}}{F_{CH_4}} \qquad (6.11)$$

For convenience, the corrected contact time is still termed the contact time, and it is expressed as W_{cat}/F_{CH4} in the all following descriptions. Details of the experimental results of methane steam reforming are listed in Table 1-5 in Appendix A. Each point is an average of the analysis of three to five samples taken. Any obvious error detected by a carbon balance was discarded.

Table 6.4 Experimental conditions for methane steam reforming

Pressure kPa	$H_2O/CH_4/H_2$	Temperature K
120	4/1/1	748, 773, 798, 823
120	5.5/1/1	748, 773, 798, 823
300	5.5/1/1	748, 773, 798, 823
450	5.5/1/1	798, 823
600	5.5/1/1	748, 773, 798, 823
120	7/1/1	748, 773, 798, 823

.6.4 2 The effects of temperature, pressure and ratio of steam/methane on methane conversion

Typical methane conversions vs. contact time are shown in Figs.6.8-10. Except for the positive effect of temperature on methane conversion found, two other main observations may be noted from the conversion-contact time data. First, the temperature effect is

augmented as temperature increases. In other words, the effect of temperature on methane conversion is non-linear due to a non-linear relationship between reaction rate constants and temperature. Secondly, when methane conversion is low, methane conversion is almost proportional to contact time at a constant ratio of steam/methane. Comparing the figures, it is also found that this proportional trend is enhanced by an increase in the H_2O/CH_4 ratios. This indicates that the rate of methane disappearance is proportional to the partial pressure of methane at low product concentrations, due to insignificant back reaction.

Methane steam reforming is sensitive to reaction pressure. High pressure not only enhances the forward reaction rates but also greatly enhances the backward reaction rates. Thus a high applied pressure will not benefit methane steam reforming with regard to methane conversion. Figs. 6.11 and 6.12 show the effects of pressure on methane conversion. Under the present conditions, a positive effect of pressure on methane conversion is showed in Figs. 6.11, 6.12. This is due to the low temperature used and the low product concentrations obtained in the experiments, and also because the enhancement of the forward reaction rate with pressure increase is larger than that of the backward reaction rate. Variations of these effects are presented in Fig.6.13, indicting the decreased significance of these effects with temperature and contact time increase. This is consistent with the thermodynamics and kinetics of methane steam reforming.

From the main reactions of methane steam reforming, the maximal stoichiometric ratio of steam/methane is 2. However, high ratios of 3 to 5 used are preferred to minimise carbon formation in a commercial reformer. To examine the effects of the ratio on steam reforming, three different ratios were used in present investigation. The dependence

between methane conversion and the H_2O/CH_4 ratio are shown in Figs.6.14-15. It can be seen that the conversions decline as the ratios increase. Reasons for this are twofold: (1) at a high ratio of steam/methane, the low methane concentration may result in decrease of the fractional methane coverage fractional on the catalyst, and a high proportion of the steam molecules would occupy the more active sites of the catalyst, which in turn obstructs the adsorption of methane, (2) a high ratio of steam/methane used would decrease the actual residence time with increase in steam flow rate.

6.4.3 The effects of temperature, pressure and the ratio of steam/methane on product distribution

Many reactions are involved in methane steam reforming. Thus the operating conditions, such as temperature, pressure and the steam/methane ratio will affect the product composition. In practice, for the manufacture of synthesis gases and hydrogen, operation with surplus steam is preferred, whereas for other applications a minimum steam surplus is required, (for example for the manufacture of reducing gas for direct reduction of iron ore). Another trend has been the wish to operate at low steam/methane ratios to achieve the optimum carbon monoxide/hydrogen ratio for alcohol synthesis or oxosynthesis. In most industrial cases, the product composition approaches the equilibrium composition which depends on the temperature and pressure at the exit of reformer as well as on the feed composition. For such cases, the influence of these operational parameters on the product composition, i.e. product distribution, depend on the thermodynamics of the reactions. The product distribution far from the equilibrium conversion is of benefit in study of the kinetics of the various reactions.

Figs. 6.16-18 show the variations of carbon dioxide selectivity, as a function of temperature and methane conversion at different steam/methane ratios from which the product distribution can be determined. An almost linear decrease of the selectivity with conversion increase was obtained at constant temperature and constant steam/methane ratio is observed from these figures. A possible reason for this decrease is that carbon dioxide is converted to carbon monoxide via the reverse water gas shift reaction. High values of the selectivity obtained at low methane conversions suggest that the main primary product is carbon dioxide. However, with the selectivities being less than 1 at low conversions, this also means that carbon monoxide is one primary product of the reactions. It is also found that the selectivity continuously drops as temperatures increase. This may result from the different effect of temperature on those reactions which produce carbon dioxide, and those which produce carbon monoxide. Based on the decreased trend of selectivity with temperature increase, it can be expected that both carbon dioxide and carbon monoxide will be the main primary products at high temperature.

An increase of the steam/methane ratio causes a considerable selectivity increase as shown in Figs.6.19-20. Comparing Fig.6.19 with Fig.6.20, the larger increase of selectivity is found at the higher temperature. High concentrations of steam are favourable to reactions which produce carbon dioxide from methane directly, and inhibit the reverse water gas shift reaction that consumes carbon dioxide. This is one of the considerations that justify the use of surplus steam for manufacture of hydrogen and synthesis gas.

No noticeable effects of pressure on the selectivity are found from Figs. 6.21-22. This may be because methane steam reforming is first order with respect to the partial pressure of

methane, and surplus steam is used, as well as the fact that experiments were carried out at low methane conversions in the present investigation.

6.5 Experimental Measurement of the Reverse Water Gas Shift Reactions and Discussion

6.5.1 Experimental results

As the water gas shift is essentially at thermodynamic equilibrium during methane steam reforming (details of the analysis are given in section 3 of Chapter 7), it was necessary to do the shift reaction on the same catalyst at a low temperature for determining the kinetic parameters of the reaction.

For the shift reaction, reference experimental conditions were chosen to measure the change in the catalyst activity throughout these experiments. The reference experiment was carried out at:

Temperature = 673 K

Pressure = 120 kPa

$H_2/CO_2 = 0.75$

$W_{cat}/F_{CO2} = 1800$ kgcat. s/kmol

Two different feed compositions were used to the reaction, each was run at four different temperatures. The experimental data for each feed composition were collected at one catalyst loading since the activity of the catalyst used was restored by hydrogen re-reduction. Minor corrections of experimental data due to slow catalyst deactivation were taken into account in the same way as for methane steam reforming described above. The

experimental conditions are listed in Table 6.5. Full details of the results obtained are presented in Tables 6 and 7 in Appendix A.

Table 6.5 Experimental conditions for the reverse water gas shift reaction

Pressure KPa	H_2/CO_2	Temperature K
120	0.75	598, 623, 648, 673
120	0.50	598, 623, 648, 673

6.5.2 Preliminary analysis and discussion of experimental results

Typical carbon dioxide conversions, conversions of carbon dioxide into methane and carbon monoxide vs. contact time are shown in Figs. 6.23-25 at p_t=120 kPa and H_2/CO_2= 0.75 with different temperature. The monotonic increase of conversion X_{CH4} of carbon dioxide into methane with contact time is exhibited in Fig.6.25. This is because methane either could be produced from reaction with carbon dioxide and hydrogen directly or could be produced from reaction with carbon monoxide and hydrogen indirectly, and the concentration of steam produced was so low that methane steam reforming reaction is unimportant, compared with reactions which produced methane. As carbon monoxide is not only a product of reverse water gas shift reaction, but also is a reactant to produce methane, a non-monotonic change of the conversion X_{CO} of carbon dioxide into carbon monoxide is expected at high conversions of carbon dioxide and high reaction temperatures as shown in Figs.6.26.

Fig. 6.27 shows the effects of the ratio of hydrogen/carbon dioxide on the conversion of carbon dioxide. Increase of this ratio promoted carbon dioxide conversion though a high

hydrogen flow rate decreases the actual residence time of feed throughout the reactor. According to the stoichiometry of the reactions, hydrogen is a limiting reactant under the present feed compositions. Thus, increase of this ratio should enhance the reactions to convert carbon dioxide into carbon monoxide or methane.
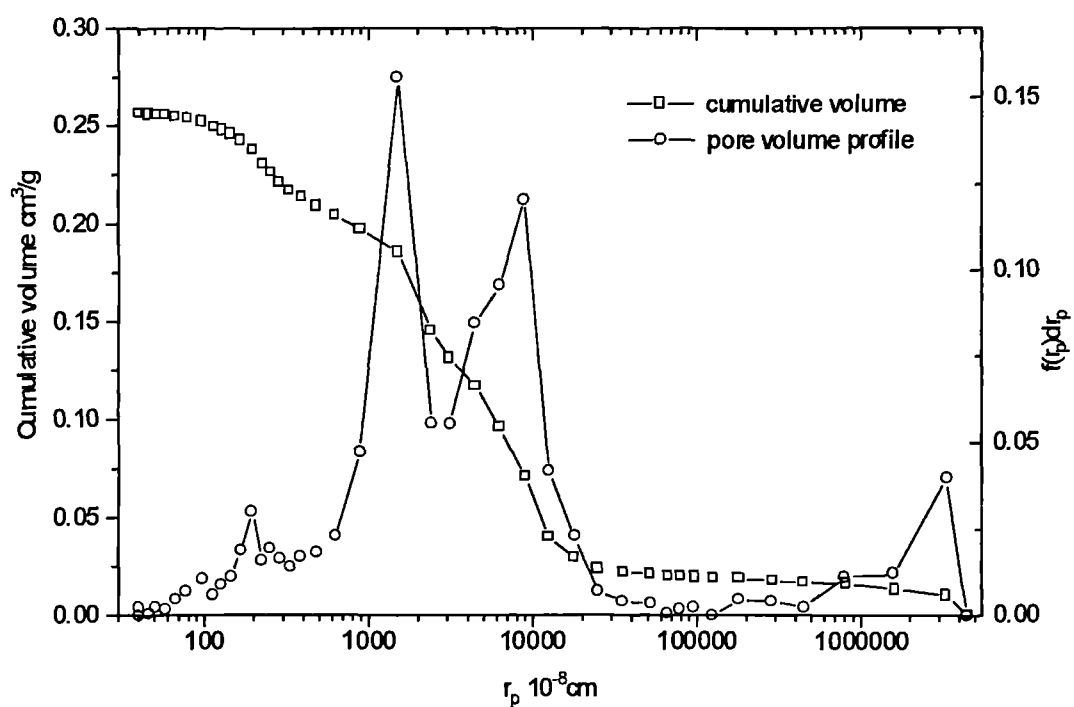
Fig.6.1 Pore cumulative volume and pore volume profile of the catalyst
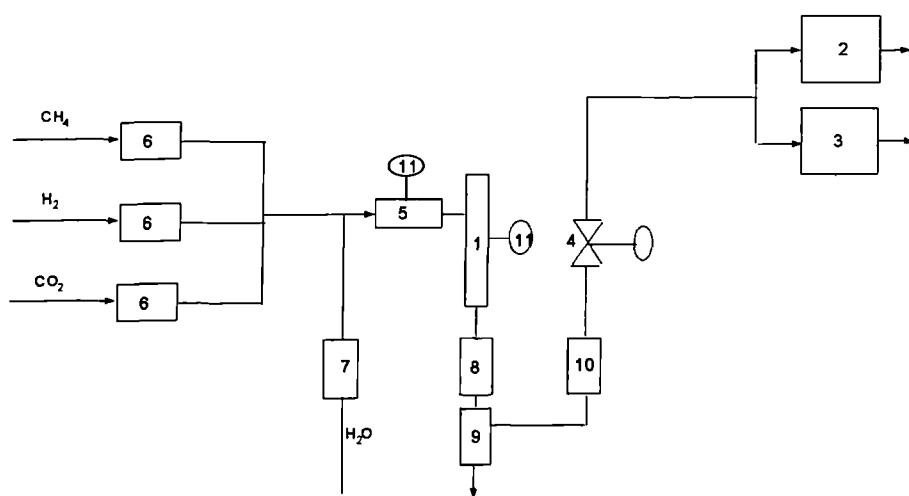
Fig.6.2 Schematic of flow system for methane steam reforming (integral reactor)

1: Reactor,   2: Gas chromatograph,   3: CO_2 analyser
4: Back pressure valve,   5: Evaporator,   6: Mass flow controller
7: Piston pump,   8: Condenser,   9: Gas-liquid separator
10: Dryer,   11:Temperature controllers

inlet

evaporator

a well of thermocouple

steel sieve

a position of
catalyst placed

reactor

outlet
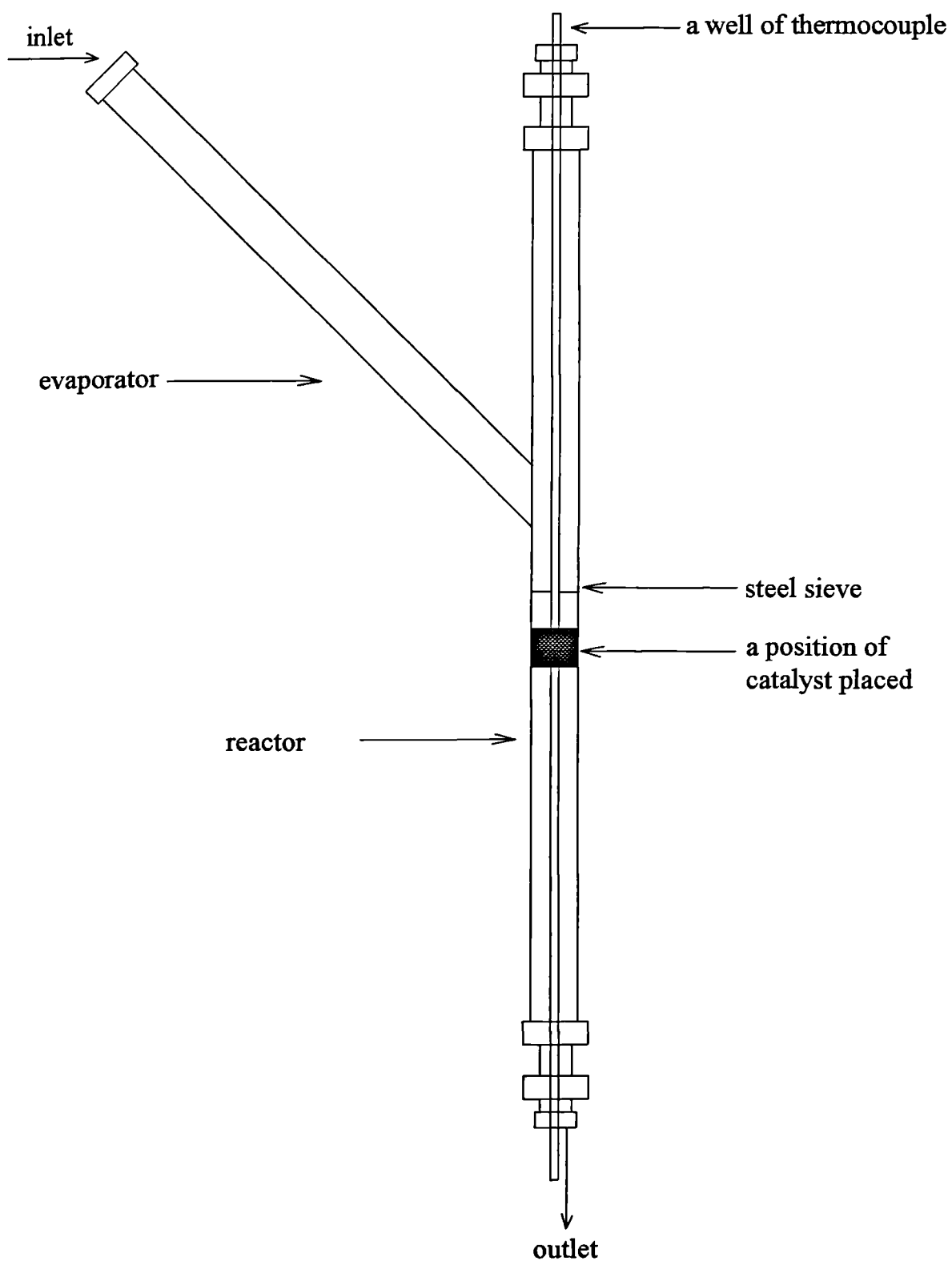
Fig. 6.3 An integral reactor and evaporator
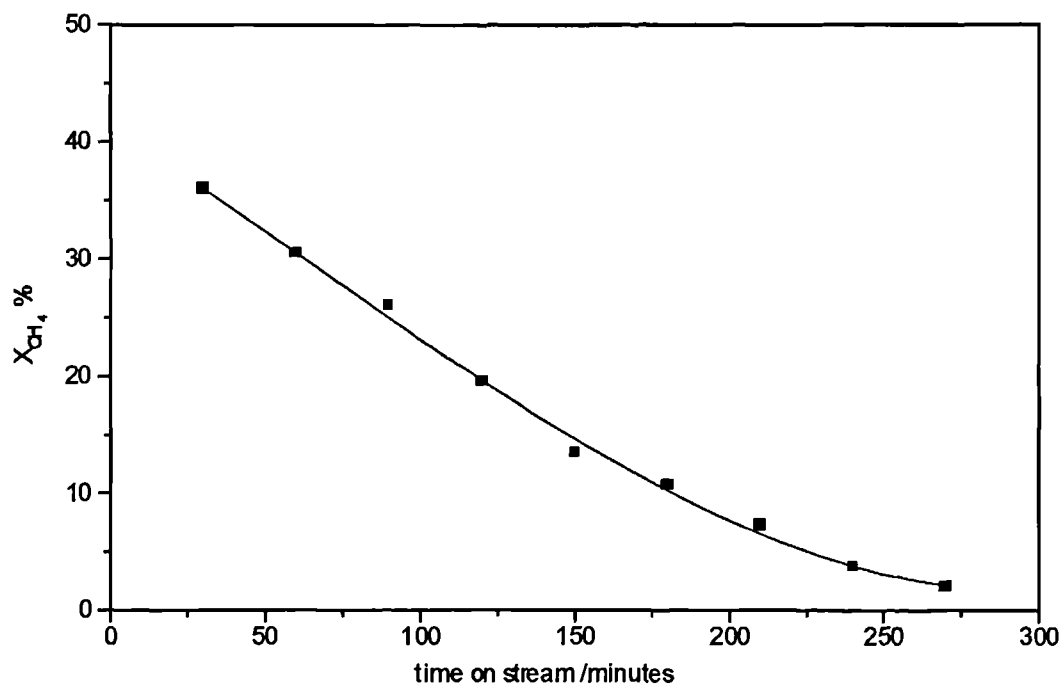
Fig.6.4 Variation of catalyst activity with time (57-4, 40-50 mesh)
P_t=120 kPa, H_2O/CH_4=3/1, WF_{CH_4}=13356 kgcat s/kmol, 823 K

■ 798 K,run s3
● 798 K, run s5
▲ 823 K, run s4
▼ 823 K, run s7
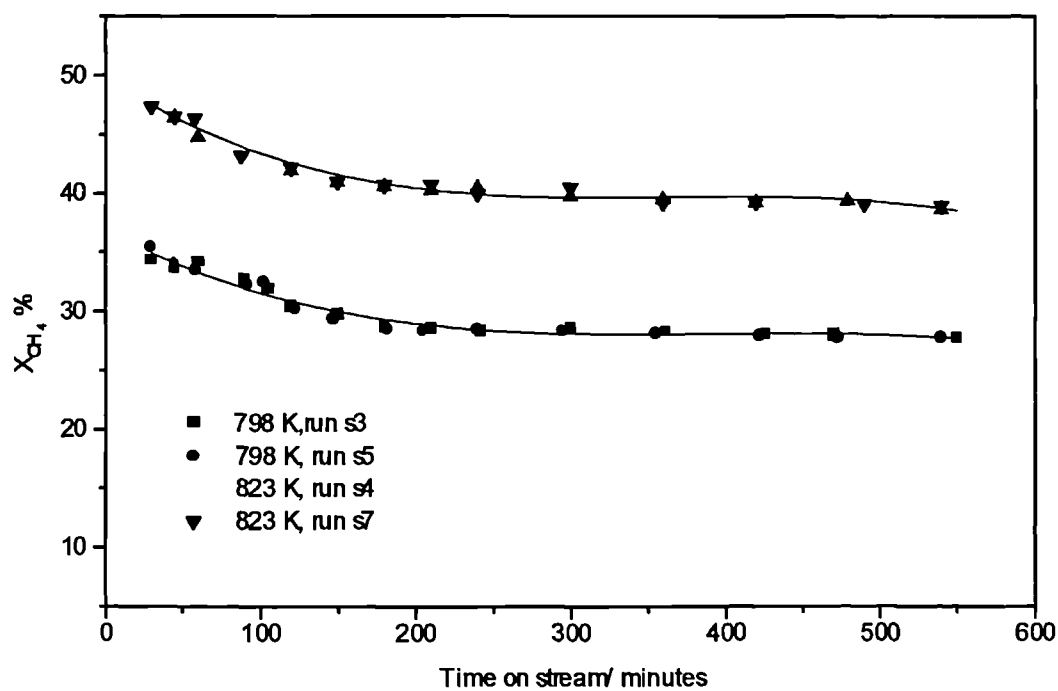
Fig.6.5 Variation of catalyst activity with time (57-4, 60-90 mesh),
P_t=120 kPa, $H_2O/CH_4/H_2$=5.5/1/1, WF_{CH_4}=13356 kgcat s/kmol
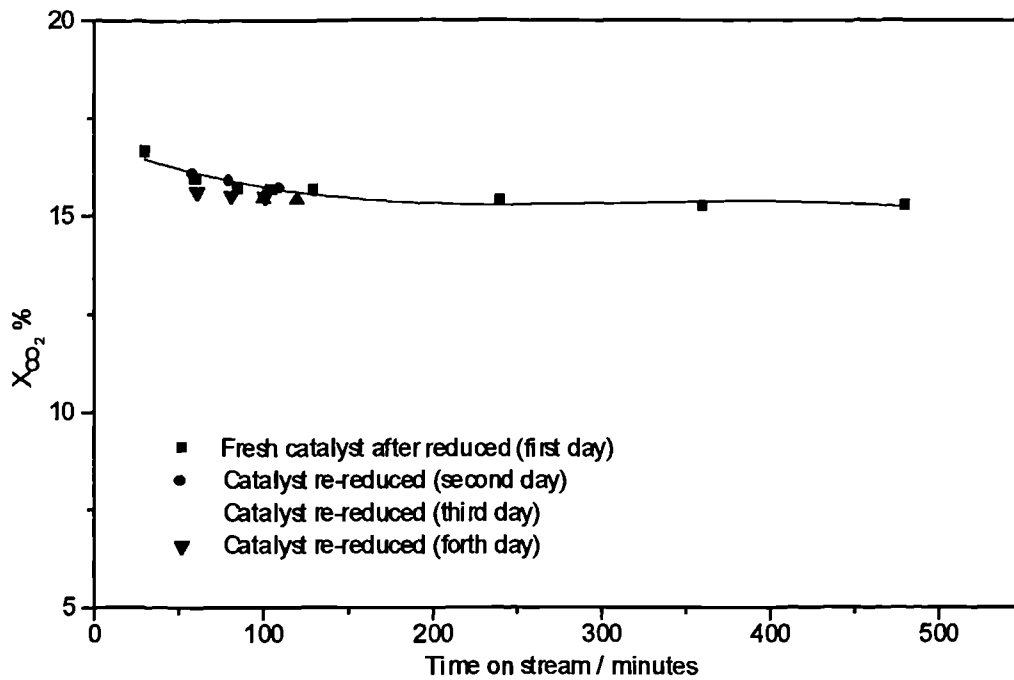
Fig.6.6 Variation of catalyst activity with time (57-4, 60-90 mesh), 673 K, P_t=120 kPa, H_2/CO_2=0.75, WF_{CO_2}= 1800 kgcat s/kmol (reverse reaction of water gas shift)
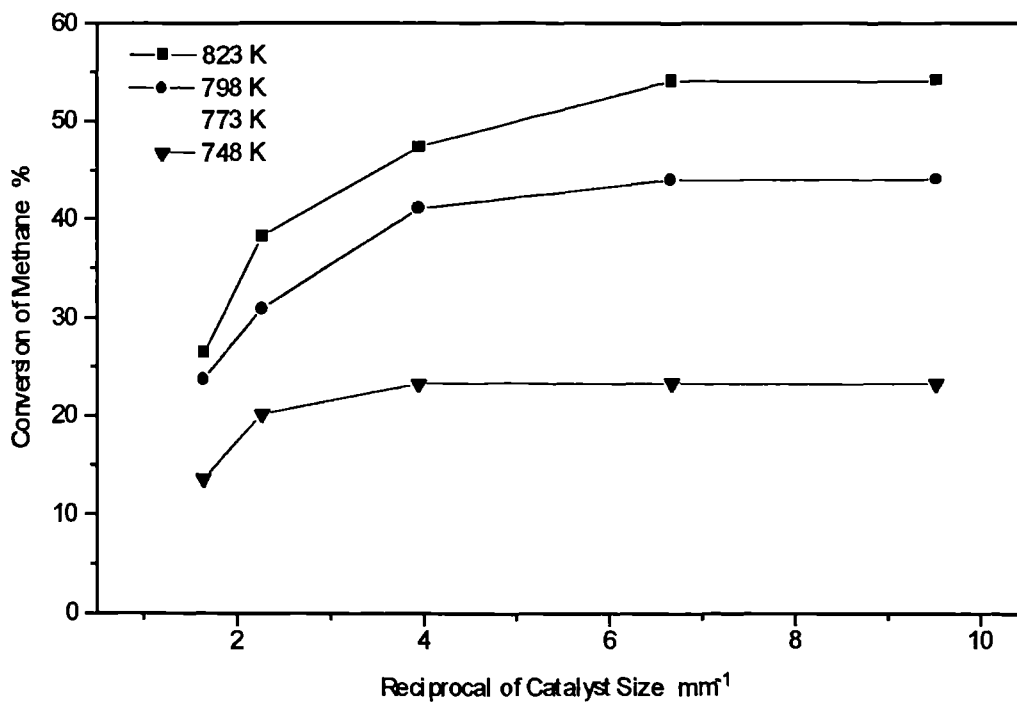
Fig.6.7 Experimental determination of intraparticle diffusion limitation
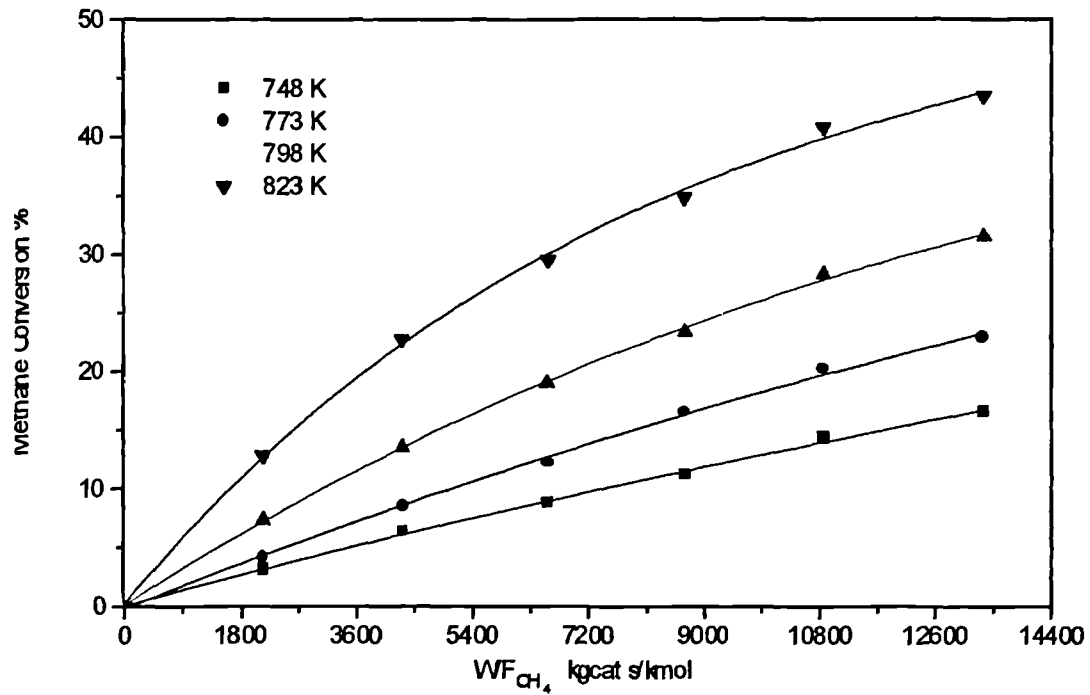
Fig.6.8 Methane conversion % vs. contact time: WF_{CH_4}, P_t=120 kPa, steam/methane/hydrogen=4:1:1
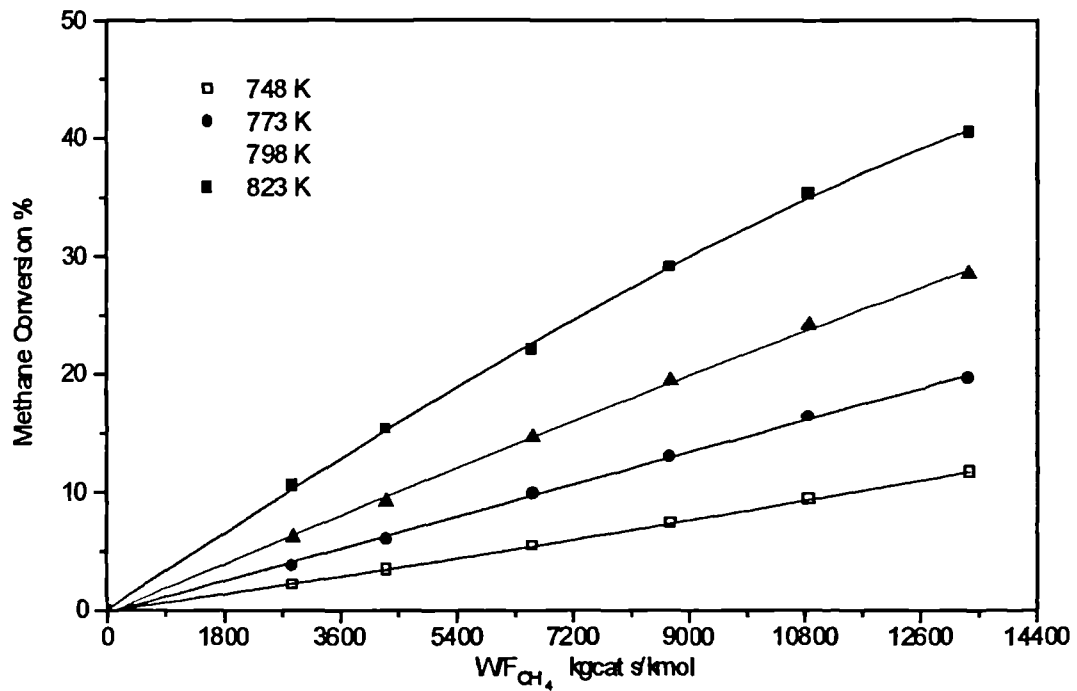
Fig.6.9 Methane conversion % vs. contact time: WF_{CH_4}, P_t=120 kPa, steam/methane/hydrogen=5.5:1:1
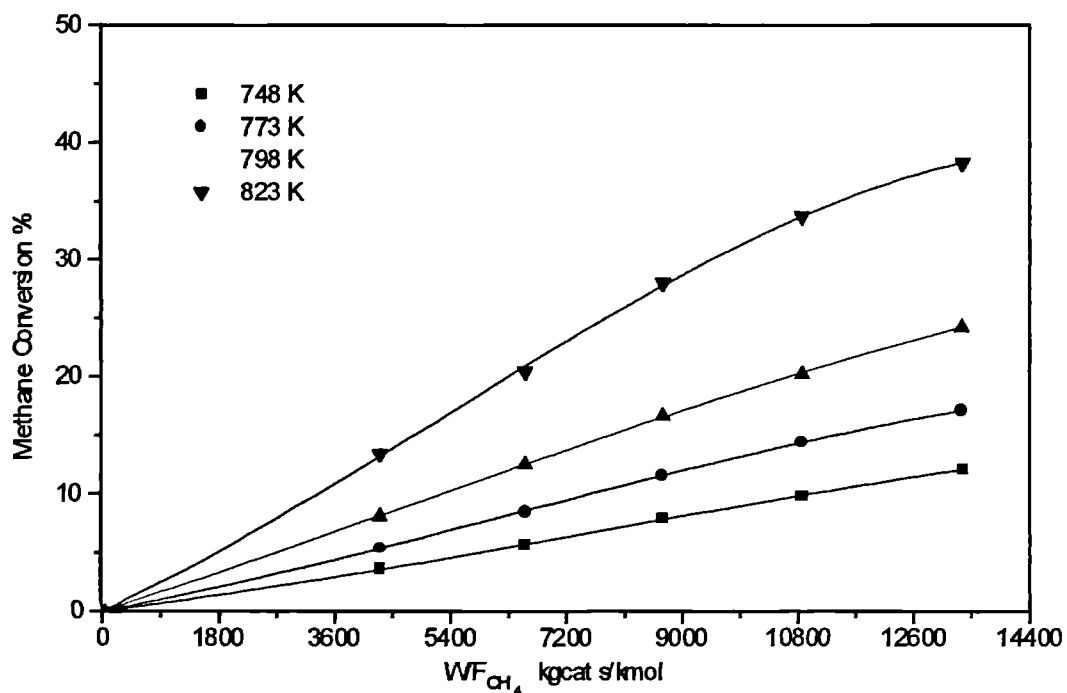
Fig.6.10 Methane conversion % vs. contact time: WF$_{CH_4}$, P$_t$=120 kPa, steam/methane/hydrogen=7.0:1:1
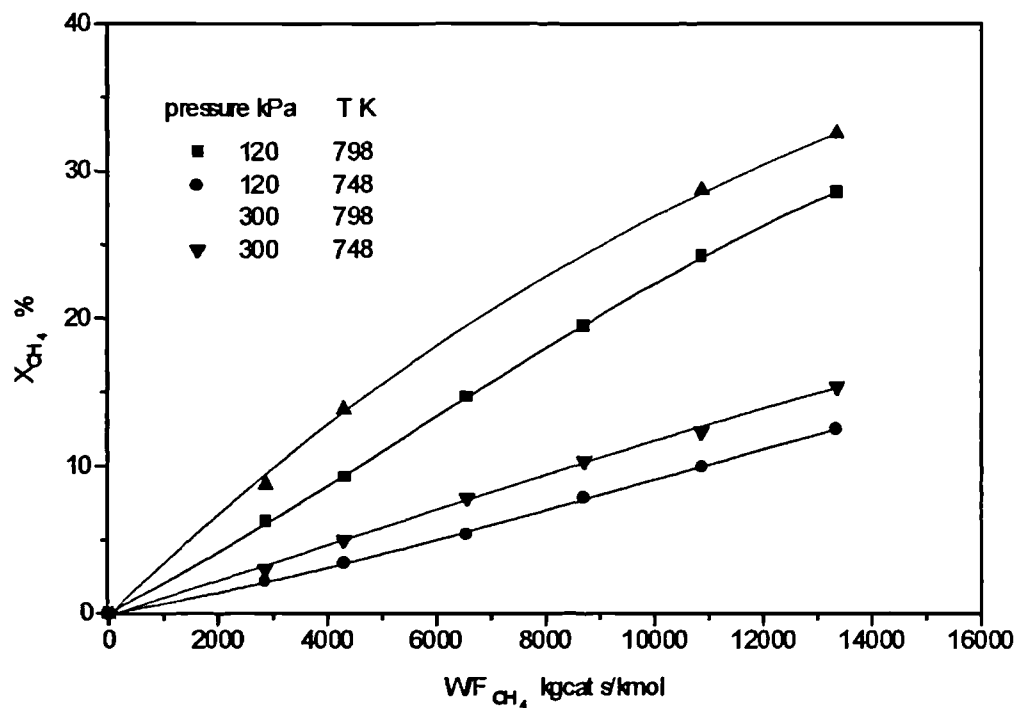
Fig.6.11 The effects of reaction pressure on methane conversion,H$_2$O/CH$_4$/H$_2$=5.5/1/1
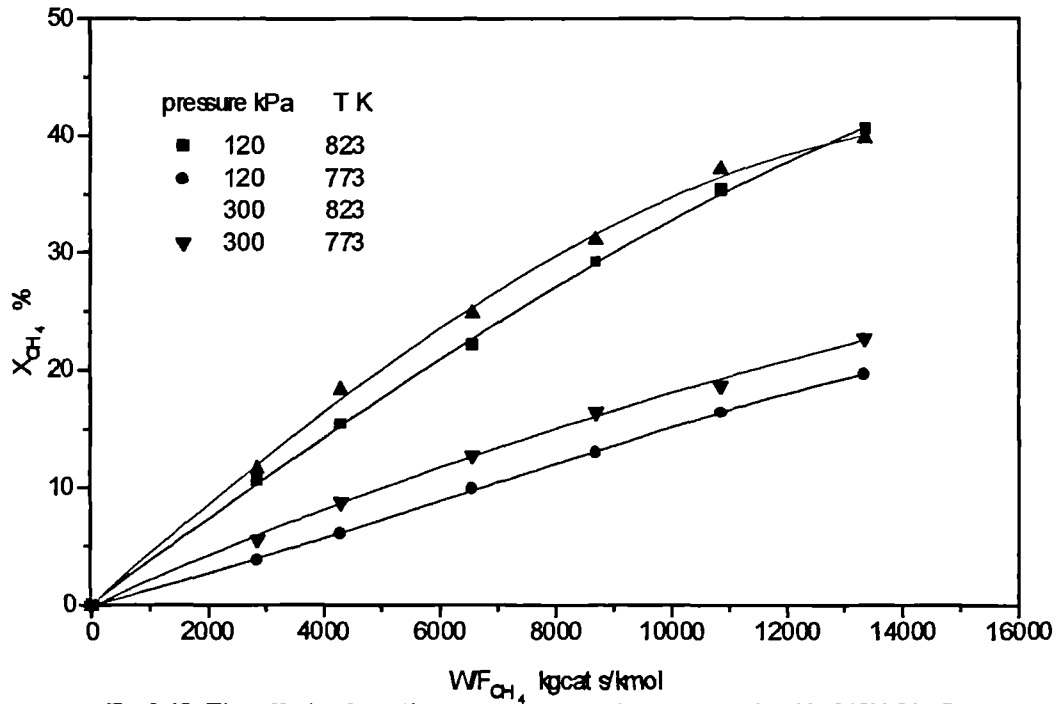
Fig.6.12 The effects of reaction pressure on methane conversion,$H_2O/CH_4/H_2$=5.5/1/1
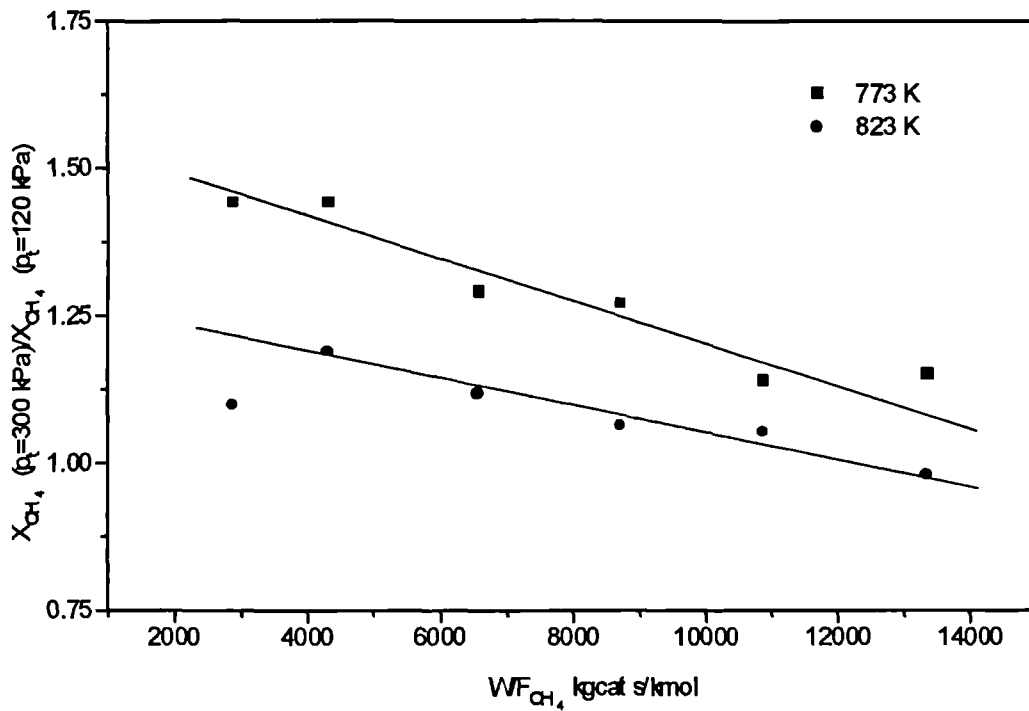
Fig.6.13 The variation of the effect of pressure on methane conversion, $H_2O/CH_4/H_2$= 5.5/1/1
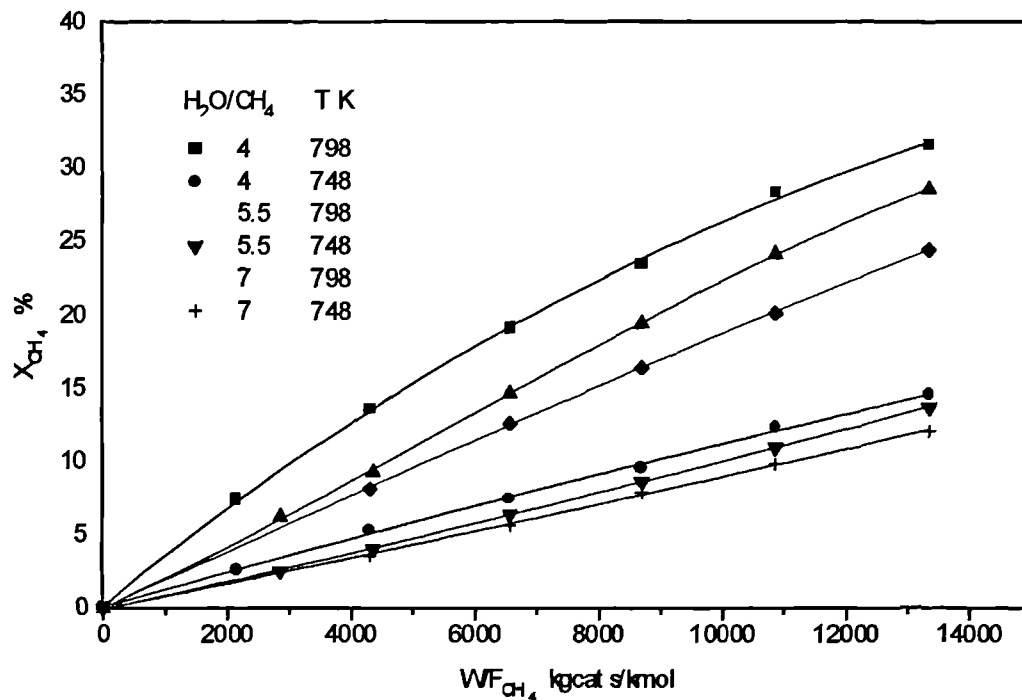
Fig.6.14 The effect of the steam/methane ratio on methane conversion, p_t = 120 kPa
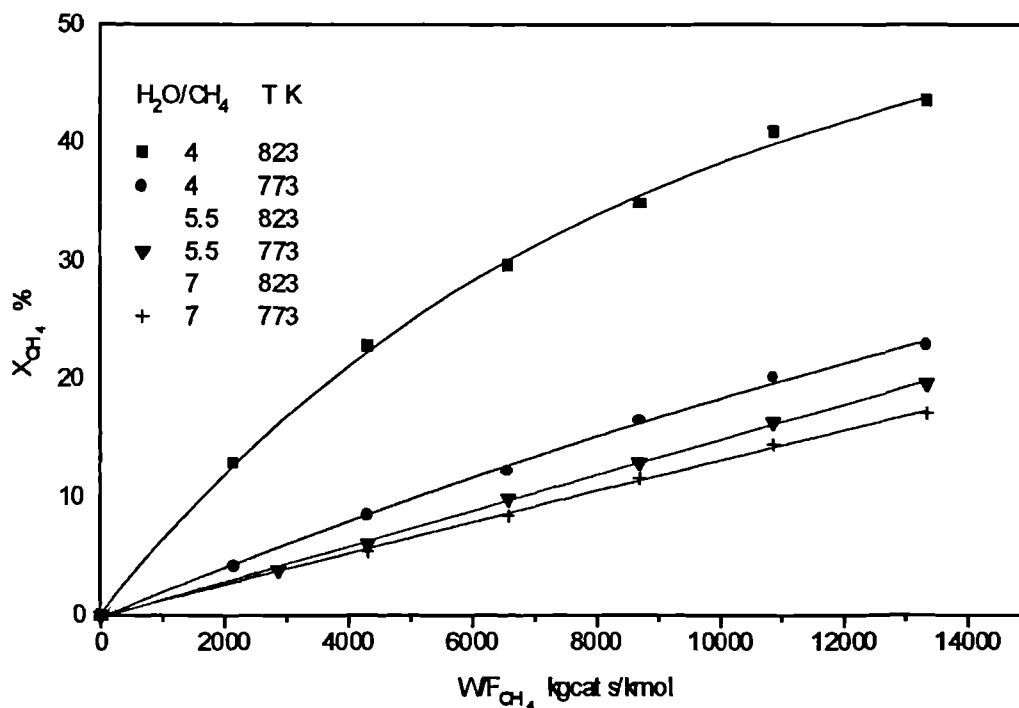
Fig.6.15 The effect of the steam/methane ratio on methane conversion, p_t = 120 kPa
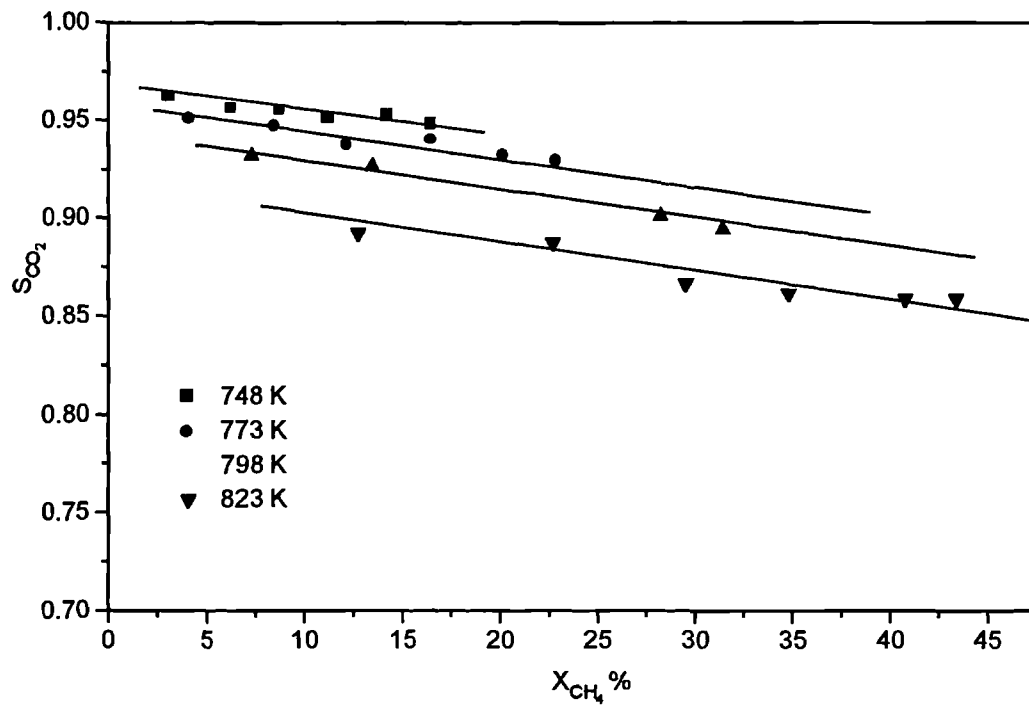
Fig.6.16 Selectivity of carbon dioxide vs. methane conversion
steam/methane/hydrogen=4:1:1, Pt=120 kPa
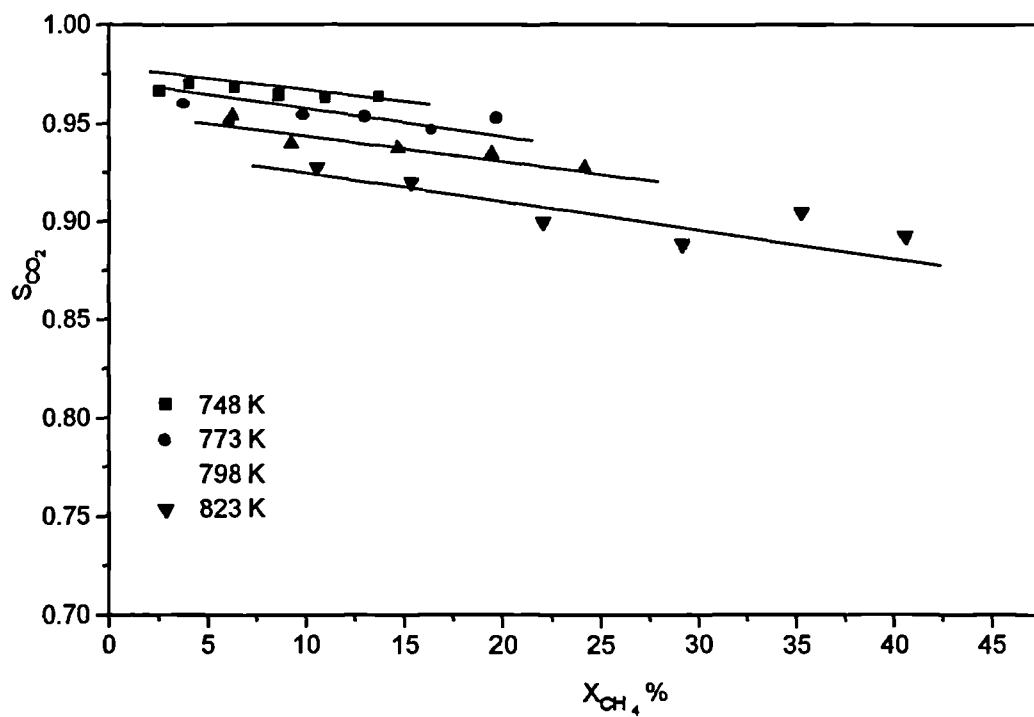
Fig.6.17 Selectivity of carbon dioxide vs. methane conversion
steam/methane/hydrogen=5.5:1:1, Pt=120 kPa
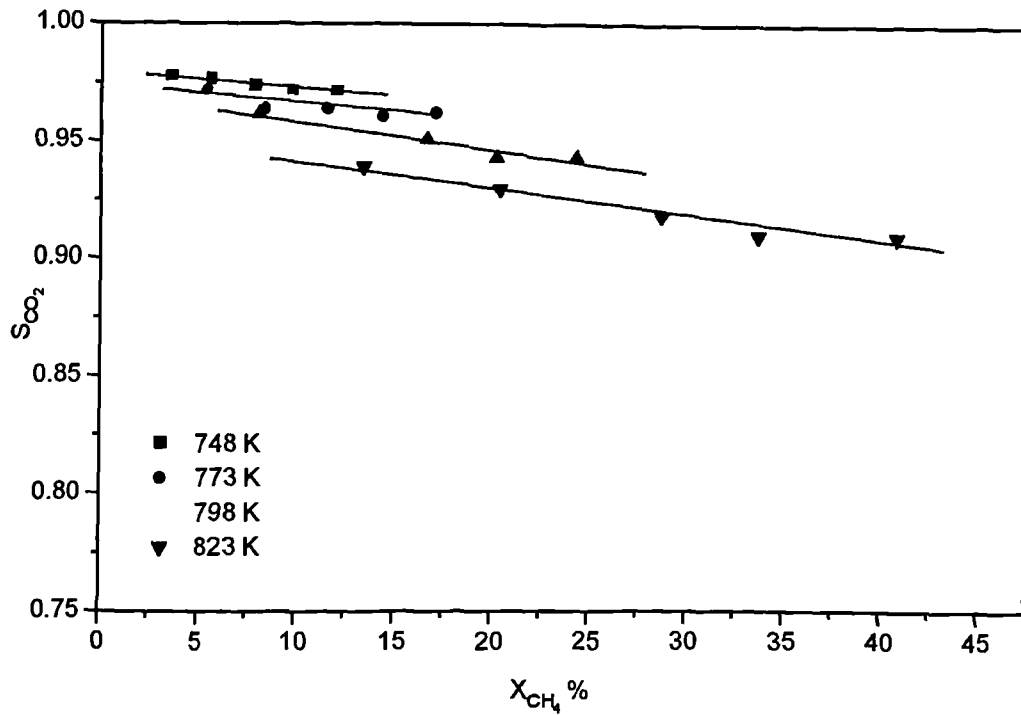
Fig.6.18 Selectivity of carbon dioxide vs. methane conversion
steam/methane/hydrogen=7:1:1, Pt=120 kPa.
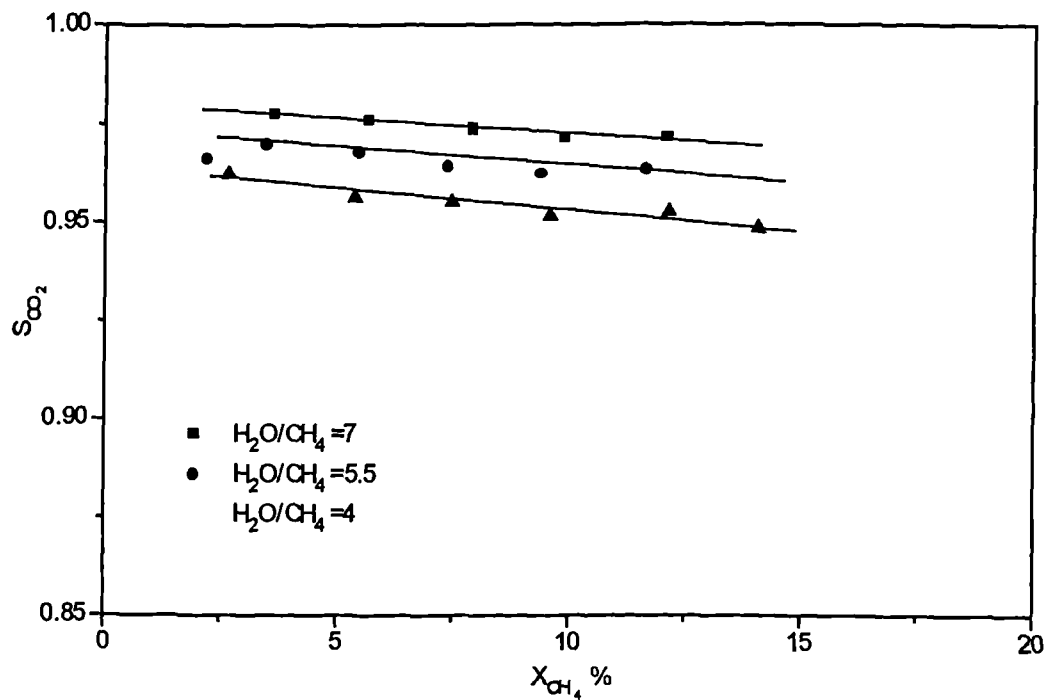
Fig.6.19 The effect of the steam/methane ratio on selectivity of carbon dioxide
P_t = 120 kPa, T = 748 K
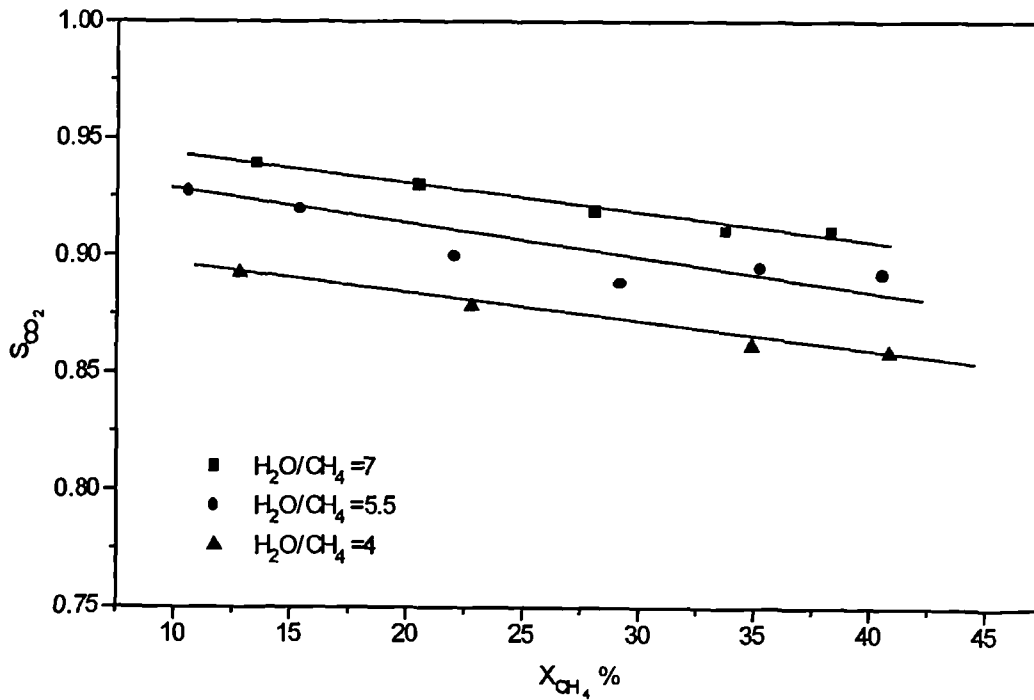
Fig.6.20 The effect of the steam/methane ratio on selectivity of carbon dioxide
P_t = 120 kPa, T = 823 K
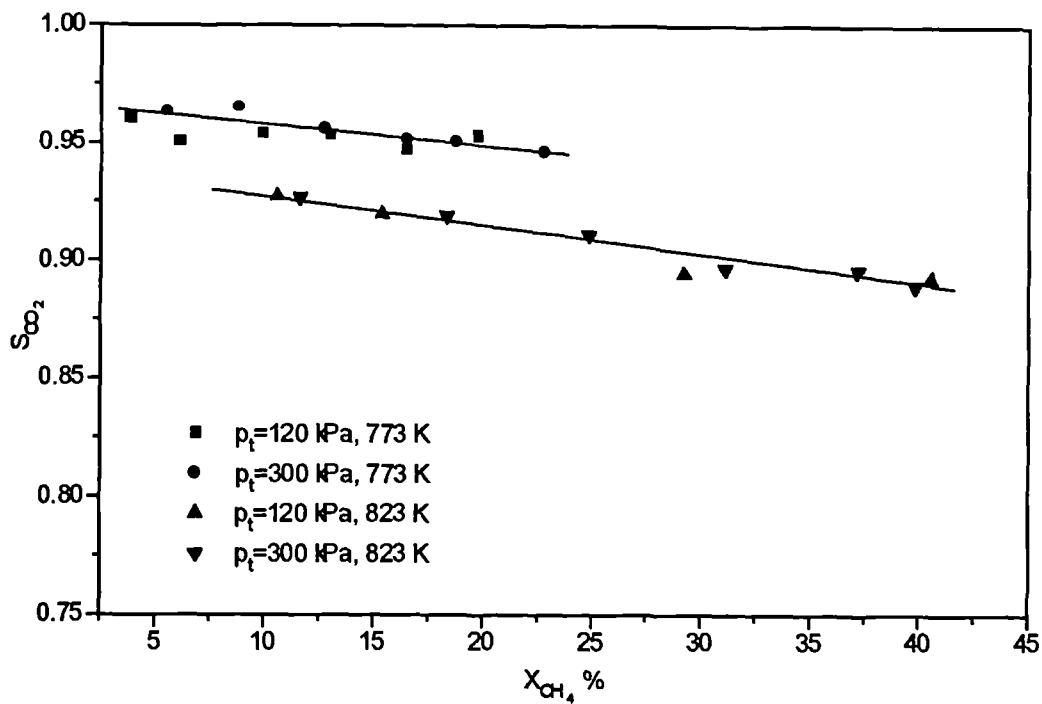
Fig.6.21 The effects of reaction pressure on selectivity of carbon dioxide, $H_2O/CH_4/H_2$= 5.5/1/1
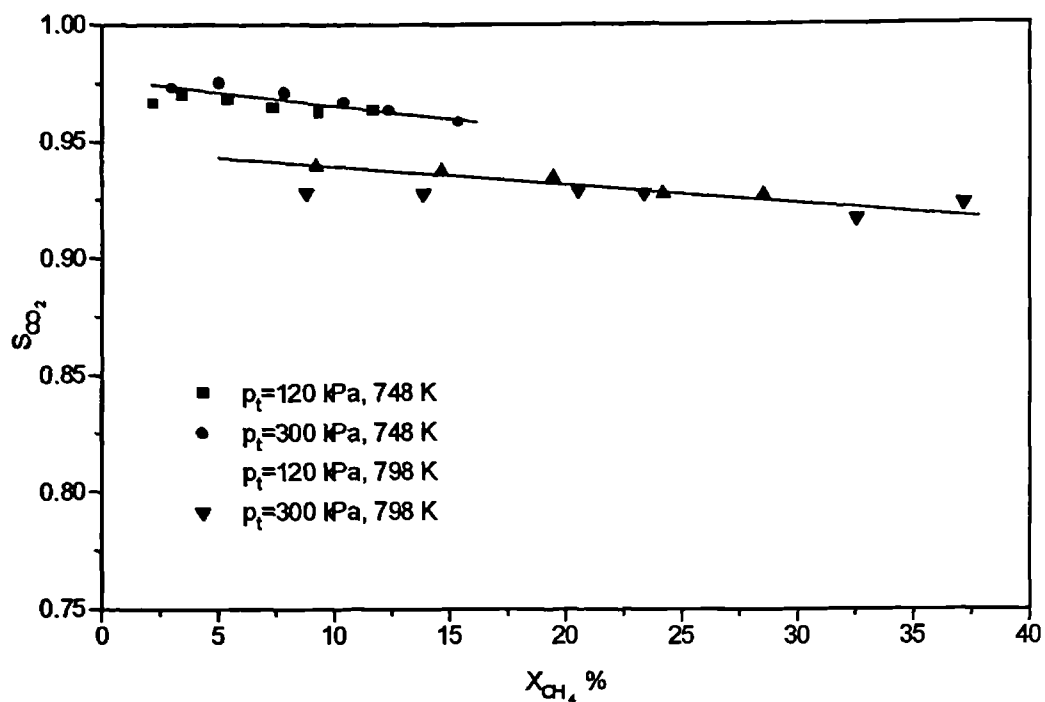
Fig.6.22 The effect of reaction pressure on selectivity of carbon dioxide, $H_2O/CH_4/H_2 = 5.5/1/1$
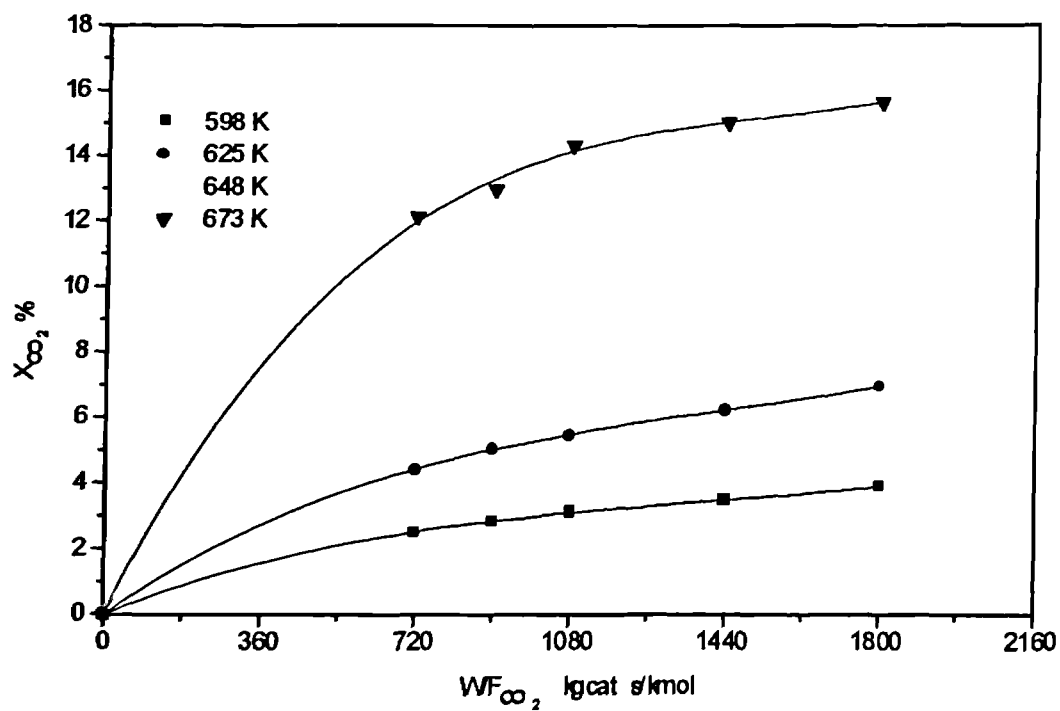
Fig.6.23 Conversion of CO_2 vs contact time WF_{CO_2}, Pt=120 kPa, $H_2/CO_2 = .75$
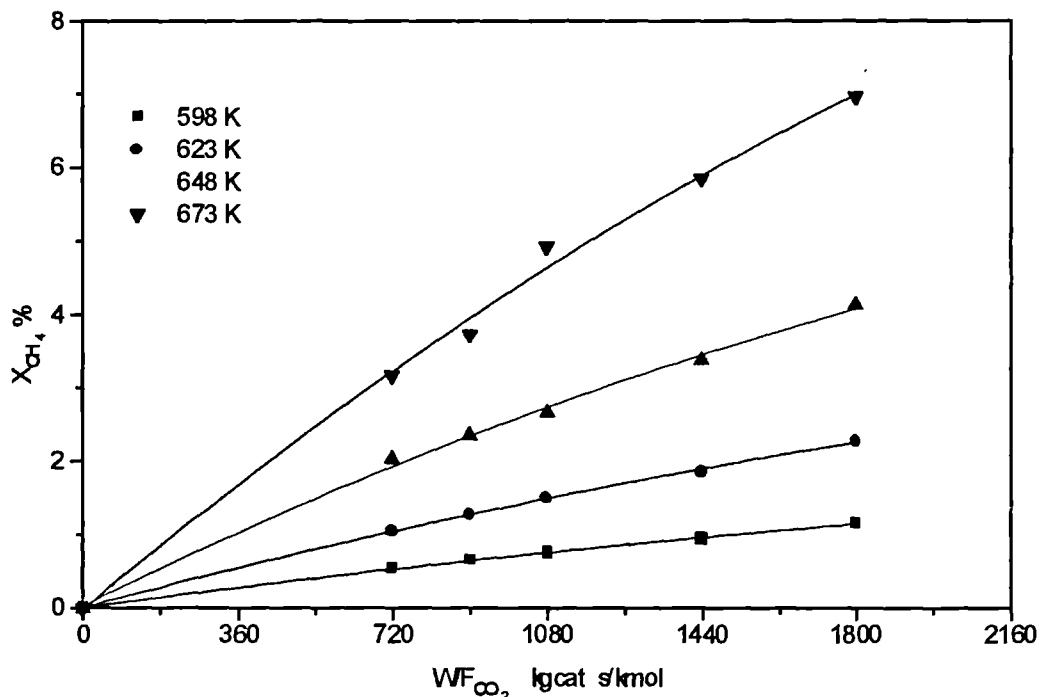
Fig.6.24   Conversion of CO_2 into methane vs contact time WF_{CO_2},
P_t=120 kPa, H_2/CO_2=.75
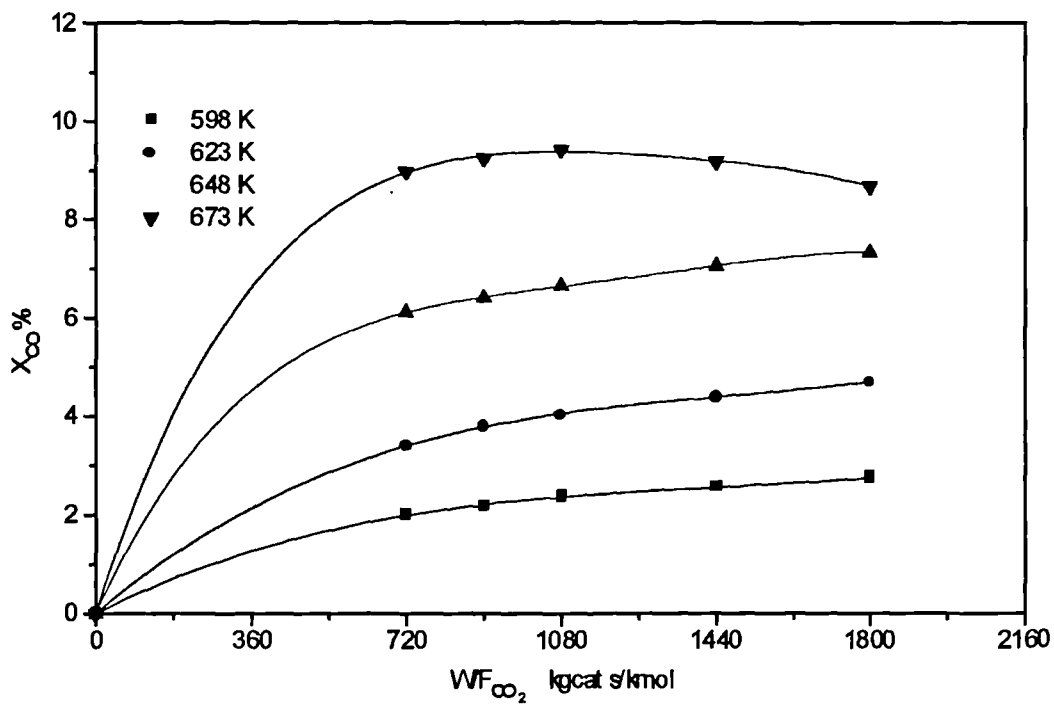
Fig.6.25 Conversion of CO_2 into CO vs contact time WF_{CO_2}, P_t=120 kPa, H_2/CO_2=.75
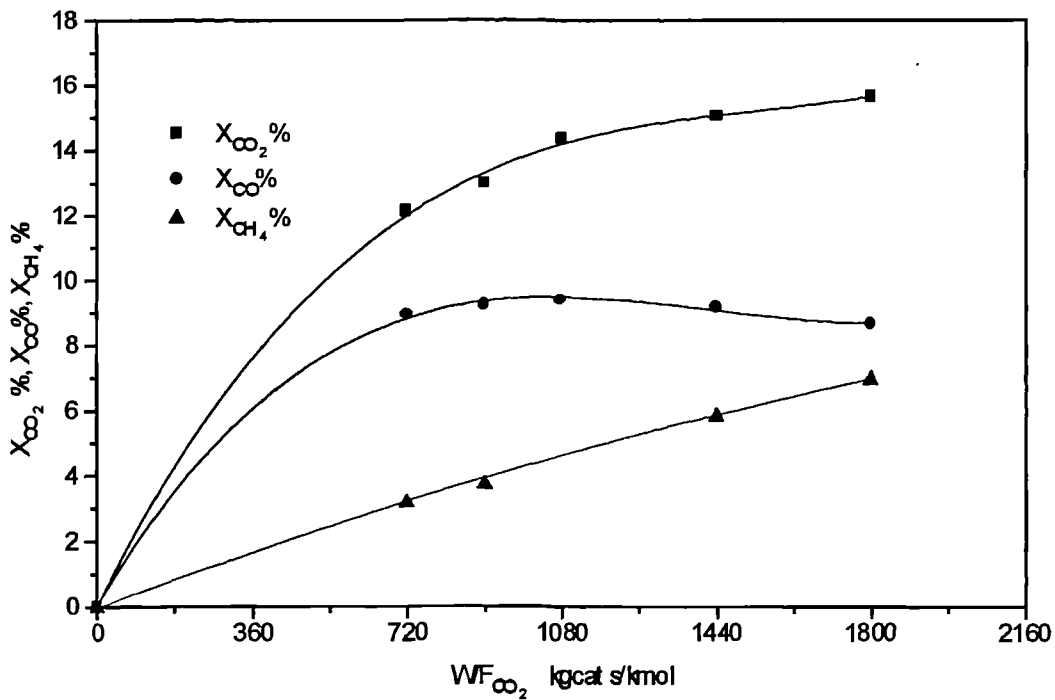
Fig.6.26 Distribution of X_{CO_2}%, X_{CO}%, X_{CH_4}%, P_t=120 kPa, H_2/CO_2=.75, 673 K
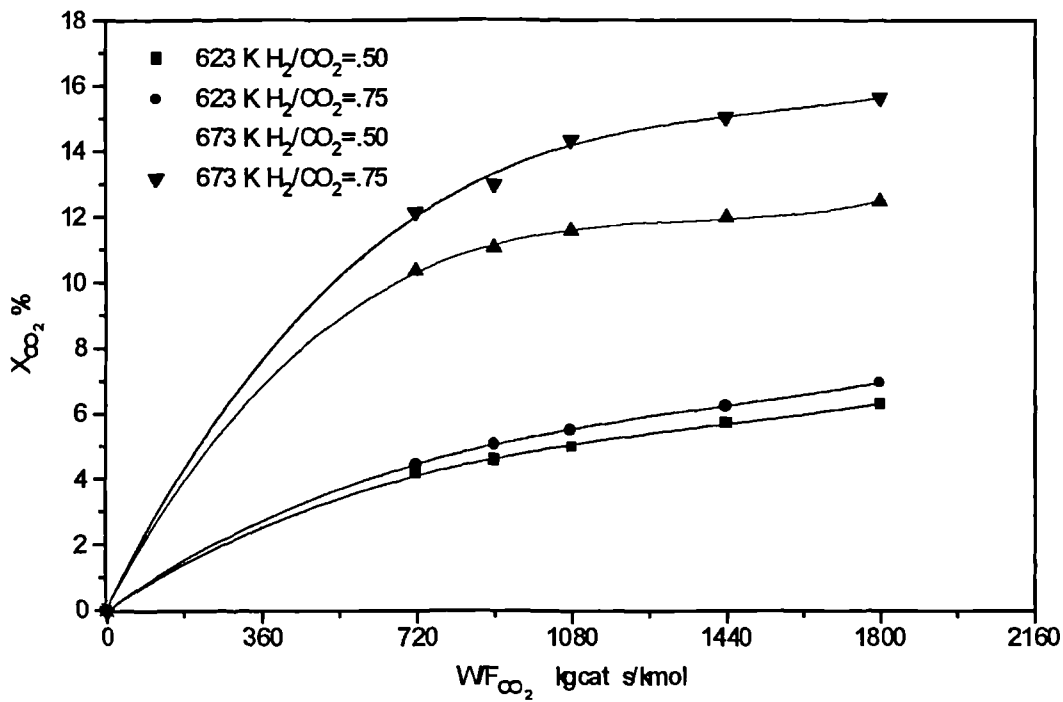
Fig.6.27 Effect of H_2/CO_2 on conversion of CO_2, P_t=120 kPa

CHAPTER 7 INTRINSIC KINETICS AND PARAMETER ESTIMATION
OF METHANE STEAM REFORMING

7.1 Introduction

Further analysis of the experimental results from Chapter 6 is done in this chapter. First of all, the main reactions involved in methane steam reforming were analysed thermodynamically and the effects of pressure and steam/methane ratio on the initial reaction rate were studied. A possible reaction mechanism of methane steam reforming is proposed, with the intrinsic rate equations derived by using the Langmuri-Hinshelwood-Hougen-Watson (LH-HW) approach and Freundlich's non-ideal adsorption concept. Parameter estimation was based on the minimisation of the sum of residual squares of the reaction rates obtained by the experiments and predicted by the models. Model discrimination was carried out by the physical characterisation of parameters and comparison with the sums of the residual squares. The verification of the intrinsic kinetics was achieved by comparing the calculated and experimental conversions.

7.2 Thermodynamic Analysis of Methane Steam Reforming

7.2.1 Wet gas composition

For thermodynamic analysis, the wet gas composition was determined first. For methane steam reforming experiments, the feed flowing in the reactor contained only methane, steam and hydrogen and the exit effluent comprised methane, steam, hydrogen, carbon dioxide and carbon monoxide.

From the carbon, oxygen and hydrogen element balances respectively, the following equations were obtained:

$$n^o_{CH_4} = n^i_{CH_4}\left(1 - X_{CH_4}\right) \tag{7.1}$$

$$n^o_{CO_2} = n^i_{CH_4} X_{CO_2} \tag{7.2}$$

$$n^o_{CO} = n^i_{CH_4} - n^o_{CH_4} - n^o_{CO_2} \tag{7.3}$$

$$n^o_{H_2O} = \left(m_1 - 1\right) n^i_{CH_4} + n^0_{CH_4} - n^0_{CO_2} \tag{7.4}$$

$$n^o_{H_2} = \left(m_2 + 3\right) n^i_{CH_4} - 3 n^o_{CH_4} + n^o_{CO_2} \tag{7.5}$$

$$n^0_{total} = \left(m_1 + m_2 + 1\right) n^i_{CH_4} + 2\left(n^i_{CH_4} - n^o_{CH_4}\right) \tag{7.6}$$

Where m_1, and m_2 are molar ratios of steam/methane and hydrogen/methane respectively, n^i_j and n^o_j are molar flow rates of component j at inlet and outlet of the reactor respectively, and n^o_{total} is a total molar flow rate at outlet of the reactor.

Combining the above equations and the definitions of X_{CH_4} and X_{CO_2} for methane steam reforming experiments, molar fractions of all components were derived as follows:

$$y_{CH_4} = \frac{1 - X_{CH_4}}{dem} \tag{7.7}$$

$$y_{H_2O} = \frac{m_1 - X_{CH_4} - X_{CO_2}}{dem} \tag{7.8}$$

$$y_{CO} = \frac{X_{CH_4} - X_{CO_2}}{dem} \tag{7.9}$$

$$y_{CO_2} = \frac{X_{CO_2}}{dem} \tag{7.10}$$

$$y_{H_2} = \frac{m_2 + 3 X_{CH_4} + X_{CO_2}}{dem} \tag{7.11}$$

where $\qquad dem = 1 + m_1 + m_2 + X_{CH_4}$

For the reverse water gas shift experiments, the feed flowing in the reactor contained only hydrogen and carbon dioxide, whereas the effluent contained all five components present in methane steam reforming. In a similar manner, with the definitions of X_{CH_4} and X_{CO_2} for the reverse water gas shift reaction, the mole fractions of all components could be calculated by:

$$y_{CH_4} = \frac{X_{CH_4}}{des} \qquad (7.12)$$

$$y_{H_2O} = \frac{X_{CO_2} + X_{CH_4}}{des} \qquad (7.13)$$

$$y_{CO} = \frac{X_{CO_2} - X_{CH_4}}{des} \qquad (7.14)$$

$$y_{CO_2} = \frac{1 - X_{CO_2}}{des} \qquad (7.15)$$

$$y_{H_2} = \frac{m_3 - X_{CO_2} - 3X_{CH_4}}{des} \qquad (7.16)$$

where m₃ is molar ratio of hydrogen/carbon dioxide, and

$$des = 1 + m_3 - 2X_{CH_4}$$

The equations obtained above may be used for calculation of the wet gas composition at any arbitrary reaction extent if the corresponding X_{CH_4} and X_{CO_2} are given, even though the equations were derived by mass balances from the inlet to the outlet of the reactor.

7.2.2 Thermodynamic analysis

7.2.2 Thermodynamic analysis

The overall reaction of methane and steam to form carbon, carbon monoxide, carbon dioxide and hydrogen may be presented by the following 11 equations (Dirksen, et al, 1953; Akers, et al, 1955; Xu and Froment, 1989):

$$CH_4 + H_2O = CO + 3H_2 \tag{1}$$

$$CO + H_2O = CO_2 + H_2 \tag{2}$$

$$CH_4 + 2H_2O = CO_2 + 4H_2 \tag{3}$$

$$CH_4 + CO_2 = 2CO + 2H_2 \tag{4}$$

$$CH_4 + 3CO_2 = 4CO + 2H_2O \tag{5}$$

$$CH_4 = C + 2H_2 \tag{6}$$

$$2CO = C + CO_2 \tag{7}$$

$$CO + H_2 = C + H_2O \tag{8}$$

$$CO_2 + H_2 = C + 2H_2O \tag{9}$$

$$CH_4 + 2CO = 3C + 2H_2O \tag{10}$$

$$CH_4 + CO_2 = 2C + 2H_2O \tag{11}$$
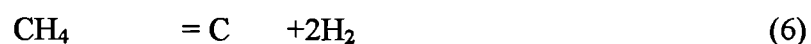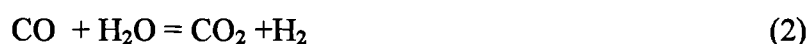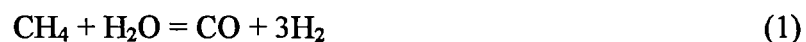
The equilibrium constants of reactions (1-5) in the experimental temperature range can be calculated from the Gibbs free energies of the reactions, while those of reactions (6-7) were obtained from the literature (Reitmeier, et al, 1948). The other reaction equilibria can be calculated from combining with reactions (1-7). The equilibrium constants of the reactions are listed in Table 7.1

From the standpoint of the thermodynamics of a reaction system, the ratios of

$$\frac{\left(\prod_j p_j^{v_j}\right)_i}{K_{pi}} \tag{7.17}$$

represented by Vi, were calculated from the experimental results. If Vi is less than 1, reaction i is proceeding to the right, otherwise, the reaction has a tendency to go to the left. In other words, the possible direction of the eleven reactions can be determined by the values of their V_i. Figs.7.1-4 show the distributions of Vi with reaction extent at $P_t=120$ kPa, $T=823$ K, and at a steam/methane/hydrogen=5.5/1/1. Similar results were obtained from experiments on methane steam reforming at other conditions. From Fig. 7.1, it can be

Table 7.1   Equilibrium constants

I	K_{pi}	Dimensions
1	$1.198 \ 10^{17} \exp(-26830/T)$	$(kPa)^2$
2	$1.767 \ 10^{-2} \exp(4400/T)$	$(kPa)^0$
3	$2.117 \ 10^{15} \exp(-22430/T)$	$(kPa)^2$
4	$6.780 \ 10^{18} \exp(-31230/T)$	$(kPa)^2$
5	$2.170 \ 10^{22} \exp(-40030/T)$	$(kPa)^2$
6	$4.161 \ 10^{7} \exp(-10614/T)$	kPa
7	$5.744 \ 10^{-12} \exp(20634/T)$	$(kPa)^{-1}$
8	$3.173 \ 10^{-10} \exp(16318/T)$	$(kPa)^{-1}$
9	$1.753 \ 10^{-8} \exp(12002/T)$	$(kPa)^{-1}$
10	$4.190 \ 10^{-12} \exp(22022/T)$	$(kPa)^{-1}$
11	$0.730 \ \exp(1388/T)$	$(kPa)^0$

seen that V_1 of reactions (1), and (3), (4)and (5) increase monotonically with reaction extent and are always smaller than one. This indicates that these reactions should proceed to the right in terms of thermodynamics. Since the observed methane disappearance rate decreased as methane conversion increased and therefore the carbon dioxide concentration increased, in contrast with the V_4 and V_5 values, the rates of reactions (4) and (5) could be quite slow. Thus reactions (4) and (5) were not considered to occur from the viewpoint of kinetic analysis The V_2 and V_6 distributions with reaction extent are presented in Fig. 7.2. The V_2 distribution suggests that the reaction (2) should proceed to the right initially for

low extent of reaction, and then reverse to the left as the reaction extent increased. This means that the part carbon monoxide was produced from the reaction (2) at high reaction extent. It may be a proof of the possible carbon formation caused by the methane decomposition reaction (6) that V_6 is less than 1 at low extents of reaction as shown in Fig.7.2. The quite large values of V_i for reactions (7-11) obtained are shown in Figs.7.3-4. This attests that no carbon formation resulted from these reactions. If these reactions were involved in methane steam reforming, they would progress to the left according to thermodynamics under the present experimental conditions.

A similar analysis applied to the data on the reverse water gas shift experiments. The V_i values exceeded one for reactions (1-5) suggesting that these reactions tend to go the left. Since the carbon dioxide concentration decreased monotonically as contact time increased, the effects of reactions (4-5) proceeding to the left on the process mass balance would not be meaningful. Among the six reactions involving carbon, five reactions (7-11) proceed to the right and could yield carbon, as their V_i values were much smaller than one, whereas reaction (6) displayed a tendency to the left, which might play a role in decoking to some extent. During the reverse water gas shift experiments, it was found that there was noticeable carbon formation on the catalyst, hence this would not significantly affect the mass balance for the kinetics consideration. Based on this study of thermodynamic analysis supplemented by a kinetics analysis, the process of methane steam reforming, and the reverse water gas shift can be described on the basis of reactions (1-3) for the study of the intrinsic kinetics.

7.3 The Possible Rate Controlling Steps (r.c.s) of Methane Steam Reforming

Methane steam reforming consists of a series steps: reactants are adsorbed on the catalyst surface with or without dissociation, surface reactions occur between reactants adsorbed or between reactants adsorbed and reactants in the gas phase, and finally desorption of products occurs. These steps may have nearly the same rates. However, in most cases of gas-solid heterogeneous catalytic reactions, there are one or more slowest steps, which control the total reaction rate and are termed as rate controlling steps. The determination of the rate controlling step(s) is very useful in postulating a kinetic mechanism and in deriving the rate equations. When the effects of heat and mass transfer, intraparticle diffusion and deactivation have been minimised or eliminated, an analysis of the effects of operating conditions on the initial reaction rate can provide some meaningful clues for guessing the rate controlling steps. For instance, the effect of total pressure or partial pressure, (i.e. concentration), on initial reaction rate has been used for determining the rate controlling steps for several types of reaction (Yang, and Hougen, 1950)

7.3.1 Reaction rates derived from data on the integral reactor

Measurements of concentration and flow rate lead to kinetic data in terms of reaction rates for differential, CSTR, and recycle reactors. On the other hand, integral kinetic data are obtained in integral reactor. However, the integral kinetic data can give reaction rates by mathematical manipulation. In this section, second or third degree polynomial regression were used for correlating relationships between methane conversion and contact time, and between conversion of methane into carbon dioxide and contact time respectively; numerical differentiation was used for deriving the reaction rates from the relationships.

Applying polynomial regression to the experimental data for methane steam reforming, the relationships for a fixed temperature, pressure and the ratio of water/methane/hydrogen were obtained as follows:

$$X_{CH_4} = a_0 + a_1 \left(\frac{W}{F_{CH_4}} \right) + a_2 \left(\frac{W}{F_{CH_4}} \right)^2 + a_3 \left(\frac{W}{F_{CH_4}} \right)^3 \qquad (7.18)$$

$$X_{CO_2} = b_0 + b_1 \left(\frac{W}{F_{CH_4}} \right) + b_2 \left(\frac{W}{F_{CH_4}} \right)^2 + b_3 \left(\frac{W}{F_{CH_4}} \right)^3 \qquad (7.19)$$

Some of the a_i and b_i constants are listed in Table 7.2.

By differentiating equations (7.18) and (7.19), the methane disappearance rate and carbon dioxide formation rate can be given respectively as

$$r_{CH_4} = \frac{dX_{CH_4}}{d\left(\dfrac{W}{F_{CH_4}} \right)} = a_1 + 2a_2 \left(\frac{W}{F_{CH_4}} \right) + 3a_3 \left(\frac{W}{F_{CH_4}} \right)^2 \qquad (7.20)$$

$$r_{CO_2} = \frac{dX_{CO_2}}{d\left(\dfrac{W}{F_{CH_4}} \right)} = b_1 + 2b_2 \left(\frac{W}{F_{CH_4}} \right) + 3b_3 \left(\frac{W}{F_{CH_4}} \right)^2 \qquad (7.21)$$

Similarly, applying the procedures above to the reverse water gas shift experiments, the carbon dioxide disappearance rate and methane formation rate can be obtained from

$$r_{CO_2}^{\bullet} = \frac{dX_{CO_2}^{\bullet}}{d\left(\dfrac{W}{F_{CO_2}} \right)} = a_1^{\bullet} + 2a_2^{\bullet} \left(\frac{W}{F_{CO_2}} \right) + 3a_3^{\bullet} \left(\frac{W}{F_{CO_2}} \right)^2 \qquad (7.22$$

$$r^\bullet_{CH_4} = \frac{dX^\bullet_{CH_4}}{d\left(\dfrac{W}{F_{CO_2}}\right)} = b_1^\bullet + 2b_2^\bullet\left(\frac{W}{F_{CO_2}}\right) + 3b_3^\bullet\left(\frac{W}{F_{CO_2}}\right)^2 \tag{7.23}$$

Table 7.2 Correlation of conversion data

		$a_0\ (b_0)\times10^2$	$a_1(b_1)\times10^5$	$a_2(b_2)\times10^9$	$a_3(b_3)\times10^{13}$
	748 K	0.03690	1.2471	-0.1444	
X_{CH4}	773 K	-0.02036	2.1734	-0.3102	
P_t=120kPa	798 K	0.1332	3.4292	-0.8011	
$H_2O/CH_4/H_2$	823 K	0.6764	5.7203	-1.8931	
=4/1/1	748 K	0.01887	1.2009	-0.1499	
X_{CO2}	773 K	-0.1745	2.0620	-0.3210	
	798 K	0.1886	3.1553	-0.7882	
	823 K	0.7589	4.9861	-1.6971	
	748 K	-0.05345	0.7894	-0.06790	
X_{CH4}	773 K	-0.2194	1.5294	-0.01696	
P_t=120kPa	798 K	-0.2591	2.4181	-0.1373	
$H_2O/CH_4/H_2$	823 K	0.8996	3.6050	-0.08804	-0.2510
=5.5/1/1	748 K	-0.04759	0.7639	-0.06102	
X_{CO2}	773 K	-0.1881	1.4465	-0.01090	
	798 K	-0.2170	2.2337	-0.1627	
	823 K	0.1230	3.3117	-0.1341	-0.2330
	748 K	-0.04810	0.7697	-0.04120	
X_{CH4}	773 K	-0.1045	1.3687	-0.04445	
P_t=120kPa	798 K	-0.1006	2.0453	-0.1580	
$H_2O/CH_4/H_2$	823 K	0.02009	2.5509	1.6934	-1.0892
=7.0/1/1	748 K	-0.04776	0.7618	-0.02877	
X_{CO2}	773 K	-0.09124	1.3228	-0.04865	
	798 K	-0.08179	1.9766	-0.1863	
	823 K	0.1161	2.5386	1.2192	-0.8730

7.3.2   Effects of experimental conditions on initial reaction rates

Letting $\dfrac{W}{F_{CH_4}} = 0$, the initial methane disappearance rate can be derived from equation

(7.20). Fig.7.5 shows initial methane disappearance rates were obtained at $P_t=120kPa$, for

different temperatures and steam/methane/hydrogen ratios. From this Figure, two

conclusions can be obtained. First, the initial methane disappearance rate decreased as the

steam concentration increased, even though steam served as a reactant in methane steam

reforming. Secondly, the effect of steam concentration on initial methane disappearance

rate increased with temperature increase. The reasons for this behaviour are twofold: (1)

the increase of steam concentration actually decreased the methane concentration in the

system for a given total constant pressure and the methane disappearance rate is first order

with respect to methane as confirmed by most investigators (Akers and Camp, 1955,

Bodrov et al, 1967, Ross and Steel, 1973, Kopsel et al, 1980, Xu and Froment, 1989), (2)

the high steam concentration hinders methane from adsorbing on the catalyst surface,

particularly at high temperatures as high temperature is favourable to water vapour

adsorption with dissociation on the catalyst surface.

The effects of total pressure on initial methane disappearance rates are presented in Fig.7.6

at ratios of steam/methane/hydrogen=5.5/1/1 and for different temperatures It is clear that

the initial methane disappearance rates increased slightly as pressure increased. Based on

this fact, desorption of products is not the rate controlling step of steam reforming.

Comparing this Figure with the Figures for the determination of rate controlling steps

presented by Yang and Hougen (1950), it suggests that the surface reactions are rate

controlling during methane steam reforming

7.4 Model Development

From the literature survey presented in Chapter 2, the following possibilities regarding the mechanism of steam reforming on different catalyst at different conditions have been reported by some investigators.

Steam: (a1) steam is adsorbed on the catalyst:

$$H_2O + s = H_2O(s)$$
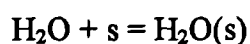
(a2) steam is adsorbed on the catalyst with dissociation:

$$H_2O + s = H_2 + O(s)$$

Methane: (b1) methane is adsorbed on the catalyst:

$$CH_4 + s = CH_4(s)$$
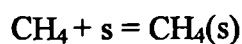
(b2) methane is adsorbed on the catalyst with dissociation into H_2 and CH_2:

$$CH_4 + \quad s = CH_2(s) + H_2$$
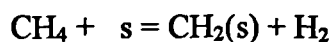
or $CH_4 + 3s = CH_2(s) + 2H(s)$

(b3) methane is adsorbed on the catalyst with dissociation into H_2 and C:

$$CH_4 + s \quad = C(s) + 2H_2$$
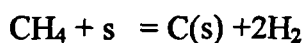
or $CH_4 + 5s = C(s) + 4H(s)$

where s is a active site of the catalyst

7.4.1 Kinetic mechanisms

By different combinations of the possibilities for steam and methane above, at least six kinetic mechanisms can be postulated. The way in which they are combined and the descriptions of the process are listed in Table 7.3.

Table 7.3 Descriptions of the kinetic mechanisms and combinations

Kinetic mechanism	Combination	Description
1	(a1) and (b1)	Steam and methane adsorbed on the catalyst respectively.
2	(a1) and (b2)	Steam adsorbed on the catalyst and methane absorbed on the catalyst with dissociation into CH_2 and H_2 or adsorbed H
3	(a1) and (b3)	Steam absorbed on the catalyst and methane absorbed on the catalyst with dissociation into C and H_2 or absorbed H
4	(a2) and (b1)	Methane absorbed on the catalyst and steam adsorbed on the catalyst with dissociation into H_2 and adsorbed O
5	(a2) and (b2)	Both methane and steam adsorbed on the catalyst with dissociation; methane dissociated into CH_2 and H_2 or adsorbed H
6	(a2) and (b3)	Both methane and steam adsorbed on the catalyst with dissociation, but methane dissociated into C and H_2 or adsorbed H

In order to develop these kinetic mechanisms in detail, some assumptions are applied to the different kinetic mechanisms, based on information which is well accepted in the literature. The surface reactions producing CO and CO_2 are chosen as the rate controlling steps (r.c.s) from the analysis made in section 7.3.2. Among the six possible kinetic mechanisms, the kinetic mechanism 5 is remained only to the end of the model discrimination. Criteria used

in the model discrimination will be given in the Section 7.5. To shorten the content of this Chapter, the three possible kinetic mechanisms, which include the kinetic mechanism 5, to be selected are described in detail below.

Kinetic mechanism 2:

Basic assumptions:

1) Steam adsorbs on the surface nickel atoms.

2) Methane reacts with surface nickel atoms, yielding the adsorbed radical CH_2 and adsorbed H.

3) The adsorbed steam and adsorbed CH_2 react to form CH_2O which dissociates into absorbed CHO and adsorbed H.

4) The adsorbed CHO either dissociates into adsorbed CO and H, or reacts with adsorbed steam, yielding adsorbed CO_2 and H.

5) Adsorbed CO reacts with adsorbed steam to form CO_2, or desorbs into the gas phase.

Under these assumptions, the following kinetic scheme may be suggested:

$$H_2O + s = H_2O(s) \tag{m2.1}$$

$$CH_4 + 3s = CH_2(s) + 2H(s) \tag{m2 2}$$

$$CH_2(s) + H_2O(s) + s = CH_2O(s) + 2H(s) \tag{m2.3}$$

$$CH_2O(s) + s = CHO(s) + H(s) \tag{m2.4}$$

r.c.s 1 $$CHO(s) + s = CO(s) + H(s) \tag{m2.5}$$

r.c.s 2 $$CO(s) + H_2O(s) + s = CO_2(s) + 2H(s) \tag{m2.6}$$

r.c.s 3 $$CHO(s) + H_2O(s) + 2s = CO_2(s) + 3H(s) \tag{m2.7}$$

$$CO(s) = CO + s \tag{m2.8}$$

$$CO_2(s) = CO_2 + s \tag{m2.9}$$

$$2H(s) = H_2 + 2s \tag{m2.10}$$
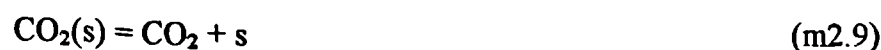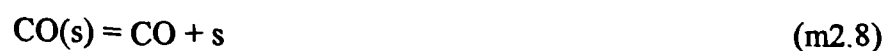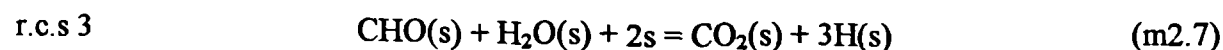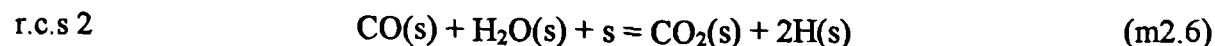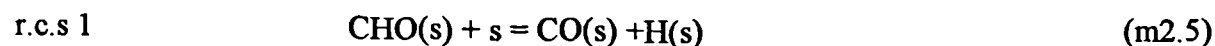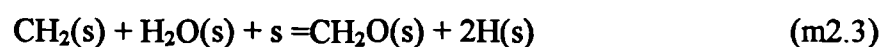
Kinetic mechanism 4:

Basic assumptions:

1) H_2O reacts with surface nickel atoms, yielding adsorbed oxygen and gaseous hydrogen.

2) Methane adsorbs on surface nickel atoms.

3) Adsorbed methane and adsorbed oxygen react to yield adsorbed CH_2O which dissociates into adsorbed CHO and adsorbed hydrogen.

4) Adsorbed CHO dissociates into adsorbed CO and H, or reacts with adsorbed oxygen, yielding adsorbed CO_2 and H in parallel.

5) Adsorbed CO reacts with adsorbed oxygen to form CO_2, or desorbs into gas phase.

The following kinetic scheme can be postulated, based on the above assumptions

$$H_2O + s = H_2 + O(s) \tag{m4.1}$$

$$CH_4 + s = CH_4(s) \tag{m4.2}$$

$$CH_4(s) + O(s) + s = CH_2O(s) + 2H(s) \tag{m4.3}$$

$$CH_2O(s) + s = CHO(s) + H(s) \tag{m4.4}$$

r.c.s 1 $$CHO(s) + s = CO(s) + H(s) \tag{m4.5}$$

r.c.s 2 $$CO(s) + O(s) = CO_2(s) + s \tag{m4.6}$$

r.c.s 3 $$CHO(s) + O(s) = CO_2(s) + H(s) \tag{m4.7}$$

$$CO(s) = CO + s \tag{m4.8}$$

$$CO_2(s) = CO_2 + s \tag{m4.9}$$

$$2H(s) = H_2 + 2s \tag{m4.10}$$
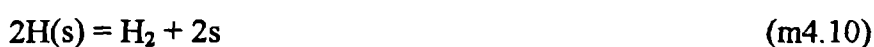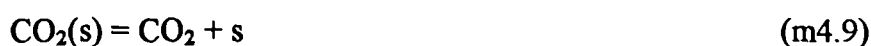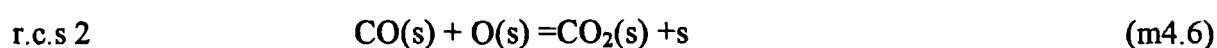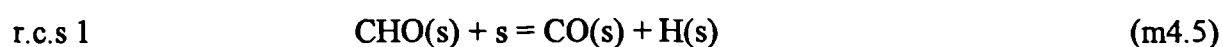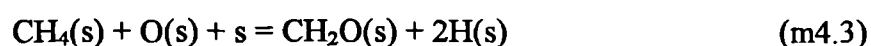
Kinetic mechanism 5

The basic assumptions made for this kinetic mechanism are as follows:

1) H₂O reacts with surface nickel atoms, yielding adsorbed oxygen and gaseous hydrogen

2) Methane reacts with surface nickel atoms, yielding adsorbed CH_2 radicals and adsorbed H.

3) The adsorbed radicals CH_2 and adsorbed oxygen react to yield adsorbed CHO and adsorbed hydrogen.

4) Adsorbed CHO dissociates to adsorbed CO and H, or reacts with adsorbed oxygen, yielding adsorbed CO_2 and H in parallel.

5) Adsorbed CO reacts with adsorbed oxygen to form CO_2, or desorbs into the gas phase.

Based on these assumptions, the kinetic mechanism 5 can be described by

$$H_2O + s = H_2 + O(s) \tag{m5.1}$$

$$CH_4 + 3s = CH_2(s) + 2H(s) \tag{m5.2}$$

$$CH_2(s) + O(s) = CHO(s) + H(s) \tag{m5.3}$$

r.c.s 1
$$CHO(s) + s = CO(s) + H(s) \tag{m5.4}$$

r.c.s 2
$$CO(s) + O(s) = CO_2(s) + s \tag{m5.5}$$

r.c.s 3
$$CHO(s) + O(s) = CO_2(s) + H(s) \tag{m5.6}$$

$$CO(s) = CO + s \tag{m5.7}$$

$$CO_2(s) = CO_2 + s \tag{m5.8}$$

$$2H(s) = H_2 + 2s \tag{m5.9}$$
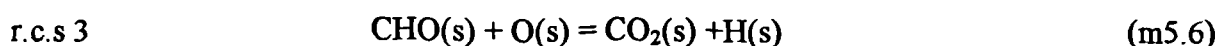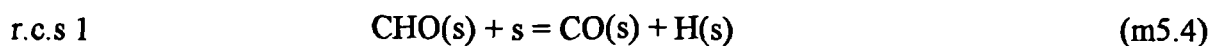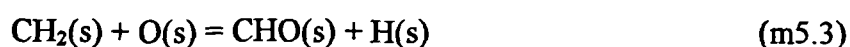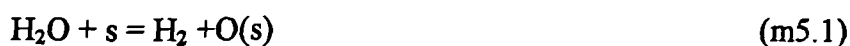
7.4.2 Rate equations

Applying the LH-HW approach to the six different the kinetic mechanisms postulated above, different rate equations can be derived. Because other five kinetic mechanisms are rejected by the model discrimination done in the following Section 7 5, only one set of rate

equations developed for the kinetic mechanism 5, which remained to the end of the model

discrimination, is given as follows

For reaction (1):

$$r_1 = k_1 \frac{P_{CH_4} P_{H_2O}}{P_{H_2}^{2.5}} \left(1 - \frac{P_{CO} P_{H_2}^3}{K_{P1} P_{CH_4} P_{H_2O}} \right) /(den)^2 \tag{7.24}$$

For reaction (2):

$$r_2 = k_2 \frac{P_{CO} P_{H_2O}}{P_{H_2}} \left(1 - \frac{P_{CO_2} P_{H_2}}{K_{P2} P_{CO} P_{H_2O}} \right) /(den)^2 \tag{7.25}$$

For reaction (3)

$$r_3 = k_3 \frac{P_{CH_4} P_{H_2O}^2}{P_{H_2}^{3.5}} \left(1 - \frac{P_{CO_2} P_{H_2}^4}{K_{P3} P_{CH_4} P_{H_2O}^2} \right) /(den)^2 \tag{7.26}$$

and

$$den = 1 + K_{CO} P_{CO} + K_{CO_2} P_{CO_2} + K_H P_H^{0.5} + K_{H_2O} \frac{P_{H_2O}}{P_{H_2}} + K_{CH_4} \frac{P_{CH_4}}{P_{H_2}} + K_{CHO} \frac{P_{CH_4} P_{H_2O}}{P_{H_2}^{2.5}}$$

Where K_{Pi} is a equilibrium constant of reaction (i), and K_i is a adsorption constant of

component i.

The rate equations developed above are based on the Langmuir's ideal surface adsorption

concept. Accounting for the non-uniform characteristic of the catalyst surface, the concept

of Freundlich's non-ideal adsorption is introduced to adjust the powers of steam and

hydrogen in the rate equations, which are the main adsorbed components in the system

(Numaguchi et al, 1988). To do this, equations (7.24-26) are changed into

$$r_1 = k_1 \frac{P_{CH_4} P_{H_2O}^{\alpha_{11}}}{P_{H_2}^{\alpha_{12}}} \left(1 - \frac{P_{CO} P_{H_2}^3}{K_{P1} P_{CH_4} P_{H_2O}} \right) /(den)^2 \tag{7.27}$$

$$r_2 = k_2 \frac{P_{CO} P_{H_2O}^{\alpha_{21}}}{P_{H_2}^{\alpha_{22}}} \left(1 - \frac{P_{CO_2} P_{H_2}}{K_{P2} P_{CO} P_{H_2O}} \right) / (den)^2 \qquad (7.28)$$

$$r_3 = k_3 \frac{P_{CH_4} P_{H_2O}^{\alpha_{31}}}{P_{H_2}^{\alpha_{32}}} \left(1 - \frac{P_{CO_2} P_{H_2}^4}{K_{P3} P_{CH_4} P_{H_2O}^2} \right) / (den)^2 \qquad (7.29)$$

Where α_{ij} is a adjustable parameter to be determined simultaneously with other parameter estimations for obtaining a suitable model that is statistically and thermodynamically consistent. The same measurements were applied to the other five sets of rate equations.

7.5 Model Discrimination and Parameter Estimation

Since the experiments were carried out in the integral mode, a non-linear least square analysis was employed for the parameter estimation based on the minimisation of the sum of residual squares of the reaction rates obtained by experiments and predicted by the models. The models were discriminated by the combination of the comparison among the sums of residual squares and the physical characteristics of the parameters. A linearisation method was used to solve the problem of non-linear least square analysis.

7.5.1 Linearisation method for the non-linear least square

A linearisation method is a basic method for solving the problem of non-linear least square analysis (Draper et al, 1981). Its main idea is that the non-linear model functions are linearised by first order Taylor series within a local range. Thus the non-linear problem is transformed into a linear problem to be solved by the Gauss-Newton method. By successive iterations to be described below, the best values of the parameters can be obtained

An objective function for the non-linear least squares for parameter estimation is defined as follows

$$S(K) = \sum_{J}^{M} [Y_J - F(X_J, K)]^T Q_J [Y_J - F(X_J, K)]$$

(7.30)

Where $Y_j = (Y_{1j}, Y_{2j}, \ldots \ldots Y_{nj})$, jth experimental values, dependent variables,

$X_j = (X_{1j}, X_{2j}, \ldots \ldots X_{mj})$, jth experimental measured values, independent variables,

$F(X_j, K) = (f_1(X_j, K), f_2(X_j, K), \ldots \ldots f_n(X_j, K)$, non-linear model functions,

$K = (k_1, k_2, \ldots \ldots k_q)$, parameters to be estimated,

Q_j is a n×n weighing matrix of jth experiment.

Guessing initial values K as $K^{(0)}$, the $F(X_j, K)$ linearised by the first order Taylor series at $K^{(0)}$ are given by

$$F(X_j, K) \approx F(X_j, K^{(0)}) + \left(\frac{\partial F}{\partial K}\right)_{K^{(0)}} \Delta K$$

(7.31)

Substituting equation (7.31) into equation (7.30), the following equation can be obtained:

$$S(\Delta K) \approx \sum_{J}^{M} \left[Y_J - F(X_J, K^{(0)}) - \left(\frac{\partial F}{\partial K}\right)_{K^{(0)}} \Delta K\right]^T Q_J \left[Y_J - F(X_J, K^{(0)}) - \left(\frac{\partial F}{\partial K}\right)_{K^{(0)}} \Delta K\right]$$

(7.32)

Since $K^{(0)}$ guessed, $F(X_j, K^{(0)})$ and $\left(\frac{\partial F}{\partial K}\right)_{K^{(0)}}$ are all assigned to values at a given X_j; then

$S(\Delta K)$ is a linear function related to ΔK, which can be solved by the Gauss-Newton method.

Letting $\dfrac{\partial S(\Delta K)}{\partial \Delta K} = 0$, we get

$$Z^{(0)}\Delta K = 2\sum_{J}^{M}\left(\frac{\partial F}{\partial K}\right)_{K^{(0)}}^{T} Q_{J}\left[Y_{J} - F(X_{J},K^{(0)})\right] \tag{7.32}$$

and

$$Z^{(0)} = 2\sum_{J}^{M}\left(\frac{\partial F}{\partial K}\right)_{K^{(0)}}^{T} Q_{J}\left(\frac{\partial F}{\partial K}\right)_{K^{(0)}} \tag{7.33}$$

$Z^{(0)}$ is a matrix with q×q dimensions, and equation (7.32) is a set of linear algebraic equations containing unknown variables ΔK. Solving equation (7.32), ΔK, which can lead $S(\Delta K)$ to minimisation, can be given as follows:

$$\Delta K = \left(Z^{(0)}\right)^{-1}2\sum_{J}^{M}\left(\frac{\partial F}{\partial K}\right)_{K^{(0)}}^{T} Q_{J}\left[Y_{J} - F(X_{J},K^{(0)})\right] \tag{7.34}$$

Therefore for the ith iteration, the iteration equation is

$$K^{(i)} = K^{(i-1)} + \left(Z^{(i-1)}\right)^{-1}2\sum_{J}^{M}\left(\frac{\partial F}{\partial K}\right)_{K^{(i-1)}}^{T} Q_{J}\left[Y_{J} - F(X_{J},K^{(i-1)})\right] \tag{7.35}$$

By repeated iteration of equation (7.33) through (7.35), the best K values can be obtained until the solution converges, that is, until the iteration ith, (i-1)th,

$$\left|S\left(K^{(i)}\right) - S(K^{(i-1)})\right| \le \delta_1 \qquad \text{or} \qquad \left\|\Delta K^{(i)}\right\| \le \delta_2 \tag{7.36}$$

where δ_1 and δ_2 are some prespecified amounts (e.g., 0.000001).

The linearisation method has possible drawbacks for some problems in that

1) It may converge very slowly; that is, a very large number of iterations may be required before the solution stabilises even though the sum of squares $S(K^{(i)})$ may decrease consistently as i increases.

2) It may oscillate widely, continually reversing direction, and often increasing, as well as decreasing the sum of squares. Nevertheless the solution should eventually converge.

3) It may not converge at all, and even diverge, so that the sum of squares increases for iteration after iteration without bound.

To combat these deficiencies, a very careful guess must first be made of the initial K values (they may be values suggested by information found in literature or suggested as "about right" by the experimenter's experience and knowledge). Secondly, some modifications are required to be applied to the method. In this section, a dumping factor being similar to one suggested by Marquardt (1963) was employed for improving the stabilisation of the method.

7.5.2 Parameter estimation and model discrimination for the experiments

Reaction rates for the formation of CO and CO_2 and for the disappearance of methane in steam reforming are predicted from

$$r_{CO}^{\circ} = r_1 - r_2$$

$$r_{CO_2}^{\circ} = r_2 + r_3$$

$$r_{CH_4}^{\circ} = r_1 + r_3 \tag{7.37}$$

Two of these rate equations are independent.

Reaction rates for the disappearance of CO_2 and for the formation of CO and methane in the reverse water gas shift are predicted from

$$r_{CO}^{\bullet\bullet} = r_1 - r_2$$

$$r_{CO_2}^{\bullet\bullet} = -(r_2 + r_3)$$

$$r_{CH_4}^{\bullet\bullet} = -(r_1 + r_3)$$ (7.38)

Similarly, two of these rate equations are independent.

Applying the linearisation method described above, an objective function for the parameter estimation is given by equation (7.30)

$$S(K) = \sum_{j}^{M} \left[Y_j - F(X_j, K)\right]^T Q_j \left[Y_j - F(X_j, K)\right]$$

Where

$Y_j = (Y_{1j}, Y_{2j}) = (r_{CH_4,j}, r_{CO_2,j})$, or $= (r_{CH_4,j}^{\bullet}, r_{CO_2,j}^{\bullet})$ for steam reforming and the reverse water gas shift reactions, respectively, values of which can be calculated from equations (7.20-21) and (7.22-23), respectively;

$X_j = (X_{1j}, X_{2j}, \ldots\ldots\ldots, X_{5j}) = (P_{CH_4,j}, P_{H_2O,j}, P_{CO,j}, P_{CO_2,j}, P_{H_2,j})$, which values can be obtained from equations (7.7-11) or (7.12-16);

$K = (k_1, k_2, k_3, K_{CO}, K_{H_2O}, \ldots\ldots\ldots K_{CH_4})$, are reaction rate constants and adsorption coefficients to be estimated;

$F(X_j, K) = (f_{1j}, f_{2j}) = (r_{CH_4,j}^{\bullet}, r_{CO_2,j}^{\bullet})$, or $= (r_{CH_4,j}^{\bullet\bullet}, r_{CO_2,j}^{\bullet\bullet})$ for the steam reforming and reverse water gas shift reactions, respectively, values of which can be predicted by equations (7.37) and (7.38) respectively.

Q_j is a 2×2 unit matrix, this means that an equal weighting factor is applied to all experimental data.

For each experimental temperature, applying the method above, the stabilised parameters values were obtained by the following procedure using a program written in FROTRAN77 for parameter estimation given in Appendix C.

1) Guess initial K values as $K^{(0)}$,

2) Linearise the objective function by first order Taylor series; the non-linear objective function S(K) is transformed into a linear objective function S(ΔK).

3) $\left(\dfrac{\partial F}{\partial K}\right)_{K^{(0)}}$ and $Z^{(0)}$ are calculated

4) Solve equations (7.33), and obtain $\Delta K^{(0)}$ and new $K^{(1)}$ values through equations (7.34) and (7.35).

5) Repeat the procedures 3) and 4); if equation (7.36) is valid, the iteration is finished and the last $K^{(n)}$ are obtained.

It should be pointed out that the $K^{(0)}$ guessed and δ_1 or δ_2 specified have to be adjusted by a trial and error method according to the progress of the iteration for obtaining the stabilised K values

The models were discriminated by the physical characterisation of the parameters and by comparison among the sums of the residual squares in two steps. First, if one of the main parameters of the model was found to have a negative value, e.g., k_1 or k_3 which should be positive, the model could be rejected. The remaining models were then checked by the sum of the residual squares.

The t value of a parameter estimate is the ratio of the parameter estimate minus zero and the standard derivation of that parameter. If a parameter is found to have a very small t value or to conflict with its physical characterisation, it is considered to have no significant contribution to the models. Consequently, it may be deleted from the latter.

7.5.3 Results

During the experiments of methane steam reforming, reaction (2) was very close to equilibrium, the partial pressure of CO was low and the adsorption coefficient of H_2 was very small due to a high temperature used. Thus the rate constant k_2 and adsorption coefficients of K_{CO}, K_H and K_{H2} could not be estimated significantly from these experiments. In the reverse water gas shift experiments, the partial pressures of CH_4 and H_2O were low so that their adsorption coefficients were determined from the steam reforming data.

The deletion of some adsorption terms in the denominator of the models and the first step of the model discrimination were carried out simultaneously by trial and error. This task was continued until the parameters in the models remaining were found to have correct values corresponding to their physical meanings.

Only the model 5, which has a minimal sum of the residual squares, remained at the end of model discrimination. K_{CO_2}, K_{CH_4} and K_{CHO} did not appear in the model 5 at the end because they were found to have no significant contributions to the model or to have wrong physical characterisations. This may be due to very weak adsorption of CO_2 and CH_4 on the catalyst or to very low concentrations of intermediates CH_2O and CHO.

The final kinetic model based on kinetic mechanism 5 after discrimination is given by:

For reaction (1):

$$r_1 = k_1 \frac{P_{CH_4} P_{H_2O}^{0.5}}{P_{H_2}^{1.25}} \left(1 - \frac{P_{CO} P_{H_2}^3}{K_{P1} P_{CH_4} P_{H_2O}} \right) / (den)^2 \qquad (7.39)$$

For reaction (2):

$$r_2 = k_2 \frac{P_{CO}P_{H_2O}^{0.5}}{P_{H_2}^{0.5}}\left(1 - \frac{P_{CO_2}P_{H_2}}{K_{P2}P_{CO}P_{H_2O}}\right)/(den)^2 \tag{7.40}$$

For reaction (3)

$$r_3 = k_3 \frac{P_{CH_4}P_{H_2O}}{P_{H_2}^{1.75}}\left(1 - \frac{P_{CO_2}P_{H_2}^4}{K_{P3}P_{CH_4}P_{H_2O}^2}\right)/(den)^2 \tag{7.41}$$

and

$$den = 1 + K_{CO}P_{CO} + K_H P_H^{0.5} + K_{H_2O}\frac{P_{H_2O}}{P_{H_2}}$$

The parameters estimated and standard derivations at each temperature in the model are listed in Table 7.4.

Applying the Arrhenius equation and van't Hoff equation to these parameters for all temperatures:

$$k_i = A_i \exp(-\frac{E_i}{RT})$$

$$K_i = A(K_i)\exp(-\frac{\Delta H_{i,a}}{RT})$$

the reaction activation energy E_i and the adsorption enthalpy ΔH_i (heat of chemisorption) of components and the preexponential factors A_i and $A(K_i)$ have been determined, and are shown in Figs 7.7 and 7.8, and listed in Table 7.5.

Table 7.4 Parameter estimates of the final model

dimension	$k_1 \times 10^7$ kmol/kgcat s $(kPa)^{0.25}$	$k_2 \times 10^5$ kmol/kgcat s kPa	$k_3 \times 10^6$ kmol/kgcat s $(kPa)^{0.25}$	$K_{CO} \times 10^2$ $(kPa)^{-1}$	$K_H \times 10^2$ $(kPa)^{-0.5}$	K_{H_2O}
Reverse water gas shift						
598 K	2.880×10^{-3}	2.708	0.3041	84.91	7.800	
$\sigma_i(k)$	2.775×10^{-3}	0.3764	0.1116	5.393	1.190	
623 K	1.889×10^{-2}	3.125	0.7675	29.05	4.010	
$\sigma_i(k)$	1.203×10^{-2}	0.3278	0.2415	2.274	0.740	
648 K	8.081×10^{-2}	3.364	1.713	9.500	1.972	
$\sigma_i(k)$	6.667×10^{-2}	0.3389	0.3083	1.062	0.611	
673 K	0.3161	3.845	3.469	4.013	1.000	
$\sigma_i(k)$	0.1528	0.3194	0.8611	0.6700	0.330	
Methane steam reforming						
748 K	14.13		24.46			0.7158
$\sigma_i(k)$	9.117		3.672			0.0721
773 K	41.75		45.61			0.7681
$\sigma_i(k)$	11.17		4.627			0.0517
798 K	119.9		74.08			0.8369
$\sigma_i(k)$	12.97		0.2636			2.04×10^{-5}
823 K	310.8		123.0			0.9014
$\sigma_i(k)$	24.33		8.064			4.16×10^{-4}

Table 7.5 Activation energies, adsorption enthalpies and

preexponential factors for the final model

	E_1	E_2	E_3	$\Delta H_{CO,a}$	$\Delta H_{H,a}$	$\Delta H_{H_2O,a}$
				(kJ/mol)		
	209.2	15.4	109.4	-140.0	-93.4	15.9
t value	(82.4)	(8.32)	(55.0)	(63.6)	(25.2)	(11.4)
UL*	214.2	19.0	111.8	-135.7	-86.1	18.6
LL*	204.2	11.8	107.0	-144.3	-100.7	13.2
	A_1	A_2	A_3	$A(K_{CO})$	$A(K_H)$	$A(K_{H_2O})$
	5.922×10^8	6.028×10^{-4}	1.093×10^3	5.127×10^{-13}	5.68×10^{-10}	9.251

* UL=upper limit, LL= lower limit of approximate 95% confidence interval.

7.5.4 Thermodynamic consistency of the parameters estimated

When the parameters were determined from experimental data, which were based on the chemisorption on an ideal surface or a non-ideal surface or hybrids of the two, the adsorption constants have to satisfy a number of thermodynamic rules (Lee, 1985). For the convenience of using the rules reported in literature, the units of the adsorption constants are expressed in bar, so that

$$A(K_{CO}) = 5.127 \times 10^{-13} \text{ (kPa)}^{-1} = 5.127 \times 10^{-11} \text{(bar)}^{-1}$$

$$A(K_H) = 5.68 \times 10^{-10} \text{(kPa)}^{-0.5} = 5.68 \times 10^{-9} \text{(bar)}^{-0.5}$$

$$A(K_{H_2O}) = 9.251$$

1) The first rule (Butt, 1980) is

$$\Delta S_{j,a}^0 < -41.84 \quad \text{or} \quad \exp(\Delta S_{j,a}^0 / R) = A(K_j) < 6.62 \times 10^{-3} \quad (7.42)$$

The preexponential factors of the adsorption constants, $A(K_j)$ values, satisfying this rule are:

$$A(K_{CO}) = 5.127 \times 10^{-11} < 6.62 \times 10^{-3}$$

$$A(K_H) = 5.68 \times 10^{-9} < 6.62 \times 10^{-3}$$

2) The second rule (Butt, 1980) is

$$\Delta S^0_{j,a} > 1.4 \, \Delta H_{j,a} - 51.04 \tag{7.43a}$$

or

$$A(K_j) = \exp\left(\frac{\Delta S^0_{j,a}}{R}\right) > \exp\left(\frac{1.4\Delta H_{j,a} - 51.04}{R}\right) \tag{7.43b}$$

Since

$$\exp\left(\frac{1.4\Delta H_{CO,a} - 51.04}{R}\right) = 1.246 \times 10^{-13}$$

and

$$\exp\left(\frac{1.4\Delta H_{H,a} - 51.04}{R}\right) = 3.187 \times 10^{-10}$$

the parameters estimated also satisfy this rule.

3) For nondissociative adsorption, the following criterion should be satisfied (Lee, 1985):

$$\Delta S^0_{j,a} > - \Delta S^0_{j,g} \tag{7.44}$$

For CO and H_2, the $\Delta S^0_{j,g}$ values at 298 K are 197.5 and 130.5 J/mol K, respectively. The criterion thus becomes:

$$\exp\left(\frac{\Delta S^0_{CO,a}}{R}\right) = A(K_{CO}) > \exp\left(\frac{-\Delta S^0_{CO,g}}{R}\right) = 4.791 \times 10^{-11}$$

$$\exp\left(\frac{\Delta S^0_{H,a}}{R}\right) = A(K_H) > \exp\left(\frac{-\Delta S^0_{H_2,g}}{R}\right) = 1.510 \times 10^{-7}$$

With the $A(K_{CO})$ and $A(K_H)$ values given above, this criterion value is roughly satisfied for CO adsorption. The $A(K_H)$ value is smaller than 1.510×10^{-7}. This might be due to the dissociative adsorption of hydrogen on the catalyst.

For H_2O adsorption, from the results reported elsewhere and reviewed by Rostrup-Nielsen (1984) it was concluded that catalyst support plays a very important role in its adsorption. Thus the step written

$$H_2O + s = O(s) + H_2 \qquad (s1)$$

consists of the following steps:

$$H_2O + support = H_2O - support \qquad (s2)$$

$$H_2O - support + s = O(s) + H_2 + support \qquad (s3)$$
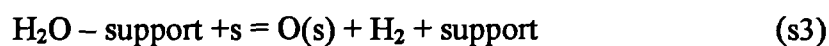
The support enhances adsorption of steam which is then adsorbed on the nickel surface. Since steam is also adsorbed directly on the nickel surface as in step (s1), the K_{H_2O}, which appears in the model that have been taken into consideration steam adsorption, cannot be considered a true equilibrium constant. In fact, it only reflects a steady-state condition reached by the steps involved in s1-s3. Thus K_{H_2O} can be written as

$$K_{H_2O} = K_{s2} \frac{k_{s3}}{k_{-s1}}$$

where K_{s2}=equilibrium constant of step s2, k_{s3} = direct kinetic constant of step s3, k_{s1}=reverse kinetic constant of step s1. As stated above, K_{H_2O} cannot be considered a real equilibrium constant and in consequence does not follow the rule discussed above.

7.6 Model Verification

The model verification was carried out in an integral mode. In order to derive the model that describes the experimental reactor, the following assumptions have been made:

(1) Steady state operation.

(2) Isothermal conditions prevail.

(3) Negligible pressure drop.

(4) Plug flow in the reactor.

(5) No interphase and intraparticle mass transfer limitations.

Assumption (5) was confirmed by the experiments of size variation of the catalyst particle and the theoretical calculation done in Chapter 6. Assumption (2) also holds due to the very small amount and very small size of the catalyst used. Also a maximum pressure drop of 20 Pa was obtained throughout the whole reactor at the maximum flow rate during the experiments. Since the length of catalyst loaded (0.25-0.4 cm) is very small, compared with the reactor length (20.5 cm), the neglect of pressure drop through the catalyst bed is reasonable. Assumption (4) could be accepted under the conditions of high temperatures and low pressures used.

Based on these assumptions, a mathematical model can be written for all components as follows:

$$\frac{dn_i}{dl} = \Omega \rho_B \sum_{j=1}^{3} v_{ij} r_j \qquad (7.45)$$

where i=1, 2, 3, 4 and 5 for CH_4, H_2O, CO, CO_2 and H_2, respectively, and v_{ij} is the stoichiometric coefficient of component i in reaction j Ω is the cross-sectional area of the catalyst bed.

The initial conditions for the model are

$$L = 0 \qquad n_i = n_i^o \qquad (7.46)$$

The model is solved by the fourth Runge-Kutta method.

Figs.7.9-10 show that the comparison between the CO_2 conversion and CO_2 conversion into CO obtained from reverse water gas shift experiments and values predicted by the model at H_2/CO_2=0.75, 120kPa and temperatures ranging from 598-673 K. It is clear that the values predicted and values measured experimentally are in good agreement. The comparison between the values predicted and the measured experimentally for steam reforming are presented in Figs.7.11-14 at different conditions. Good agreement between the two kinds of values can be seen from these Figures. Based on this, one can conclude that the intrinsic kinetic model developed in this Chapter describes the methane steam reforming on the catalyst used very satisfactorily.
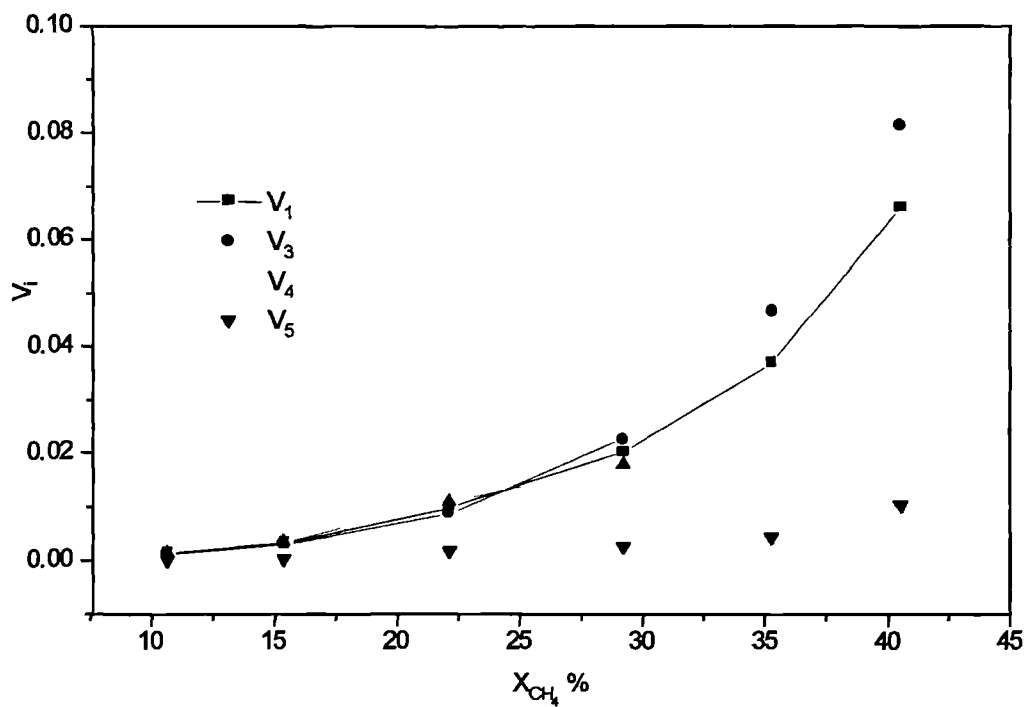
Fig 7.1 V_i distribution with reaction extent
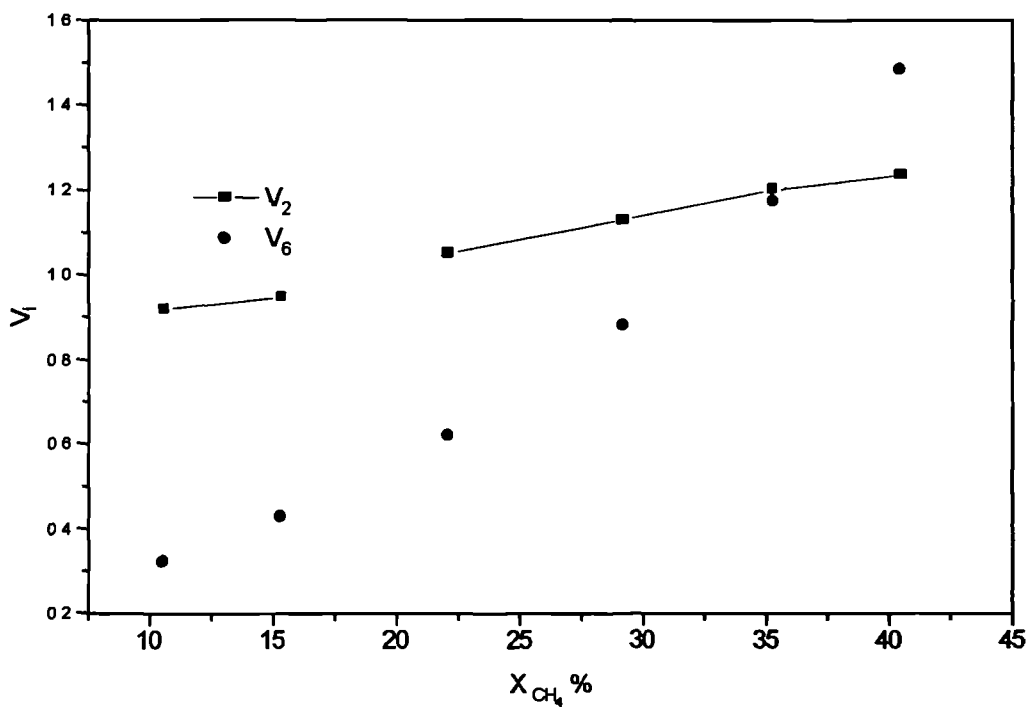
Fig 7.2 V_i distribution with reaction extent
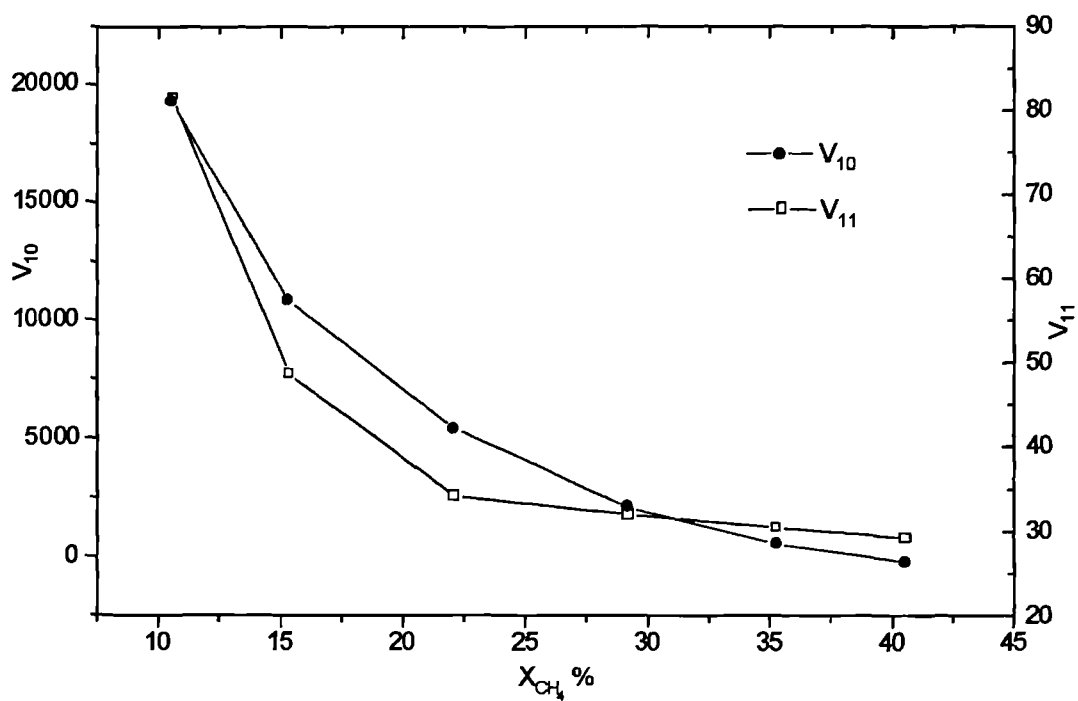
Fig. 7.3 V_i distribution with reaction extent
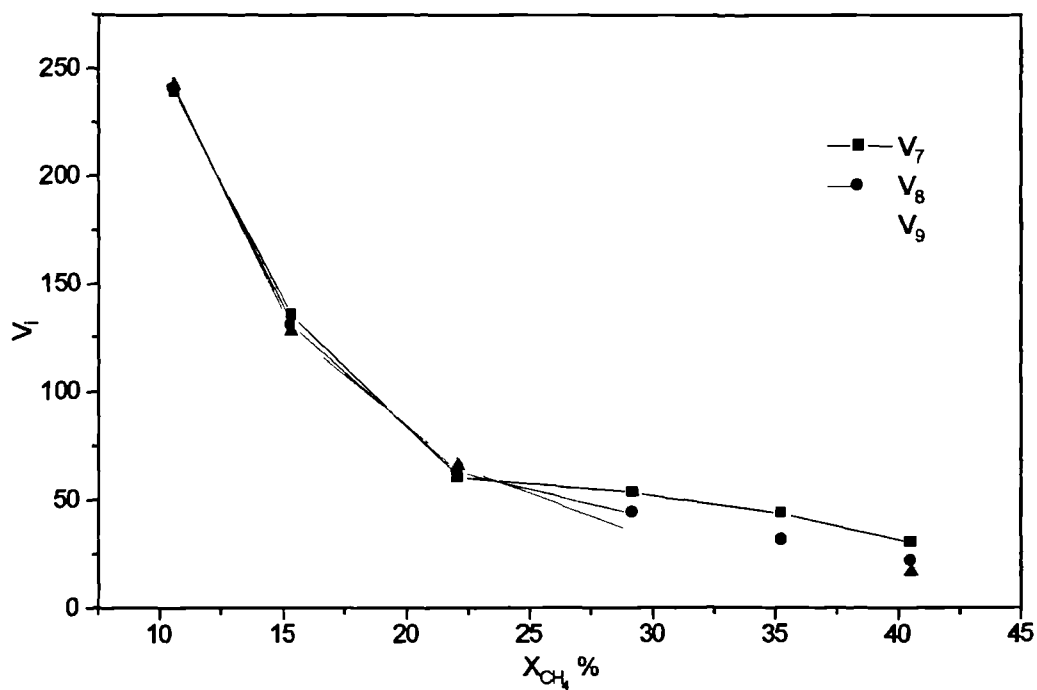
Fig 7.4 V_i distribution with reaction extent
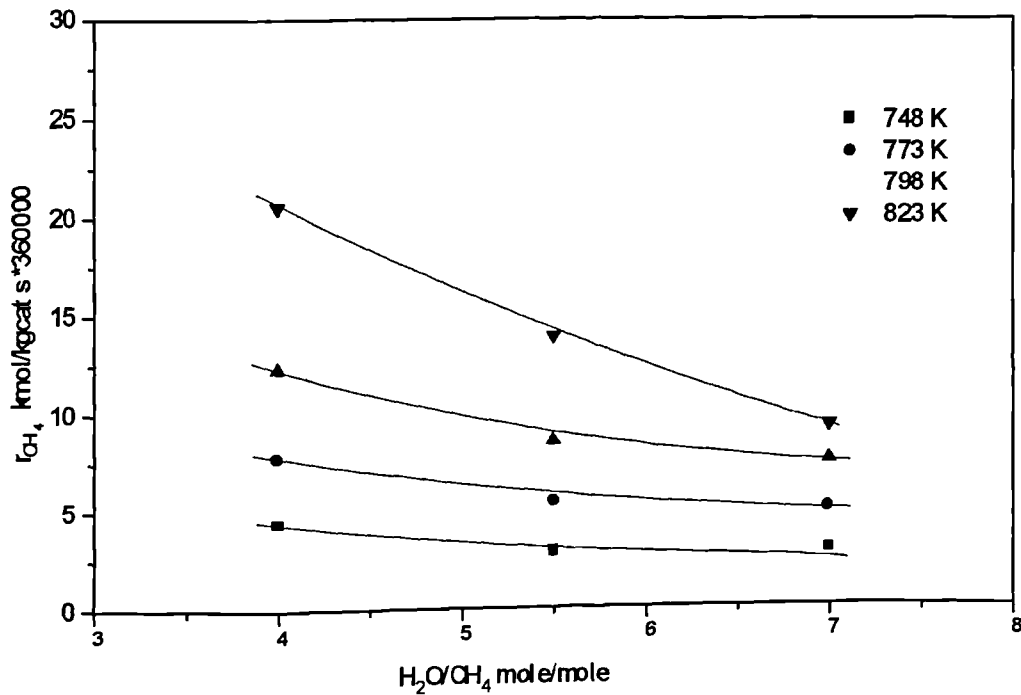
Fig.7.5 Effect of ratio of steam/methane on initial methane disappearance rate
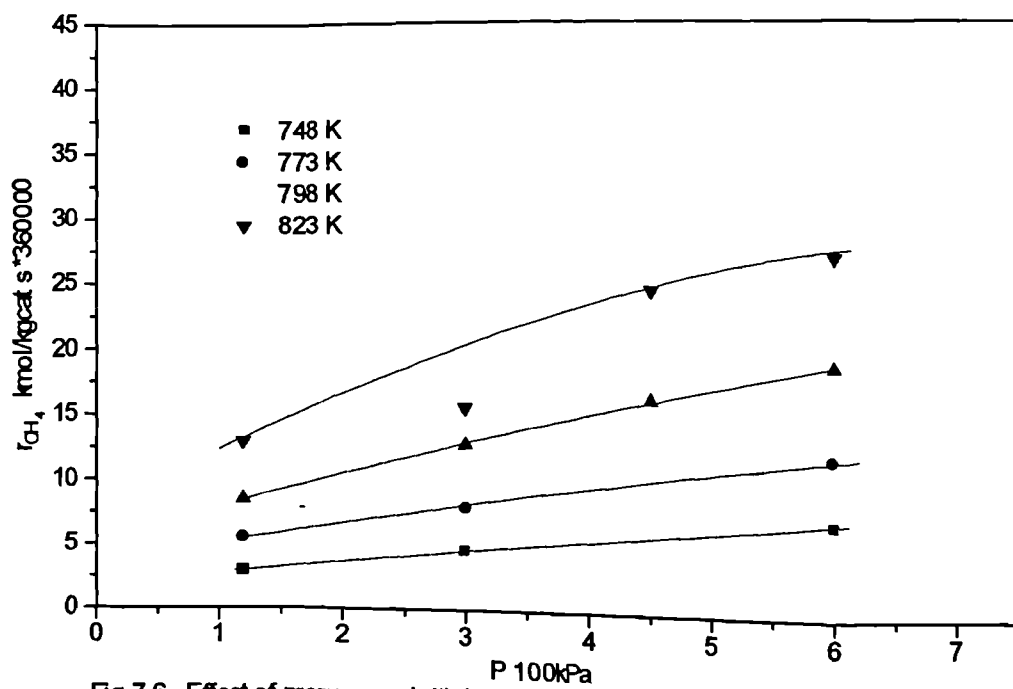
Fig.7.6 Effect of pressure on initial methane disappearance rate, $H_2O/CH_4/H_2$=5.5/1/1
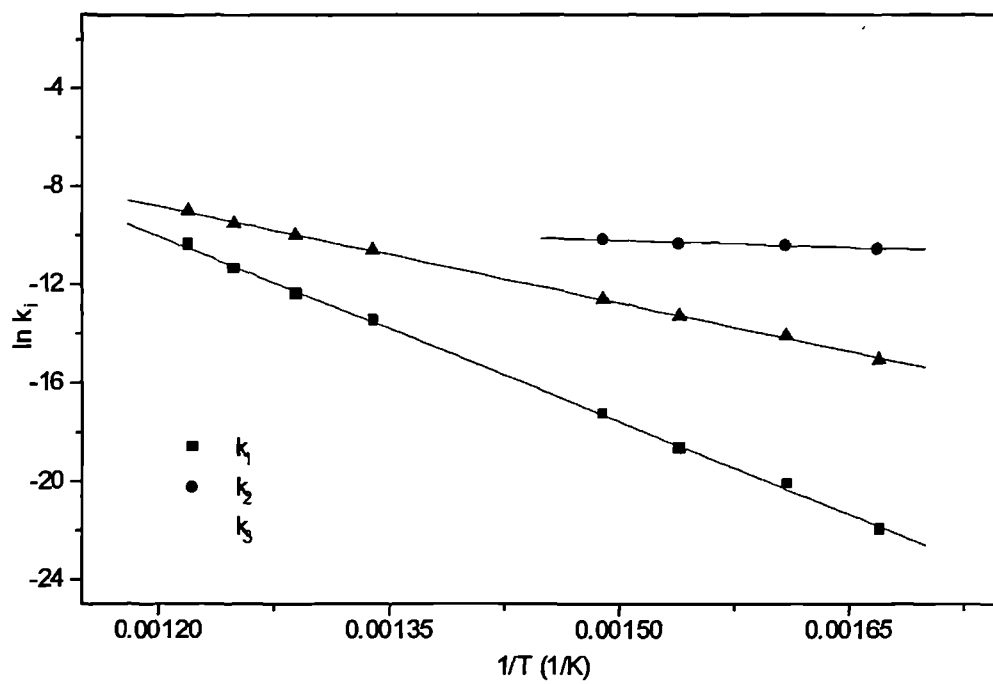
Fig.7.7 Temperature dependence of rate constants
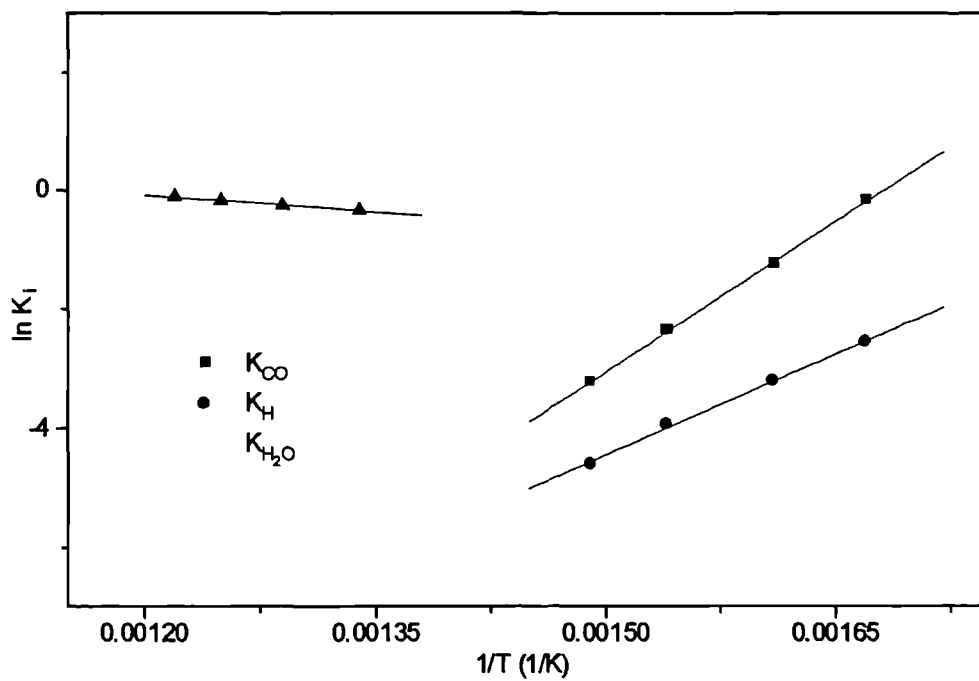
Fig.7.8 Temperature dependence of adsorption parameters
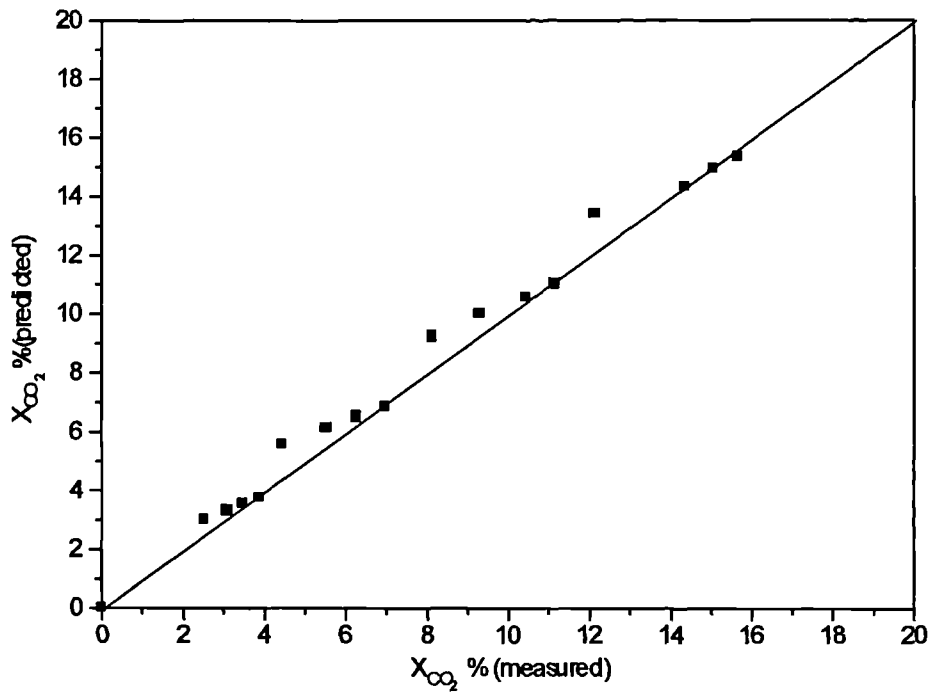
Fig.7.9 comparison between X_{CO_2}(measured) and X_{CO_2} (predicted)
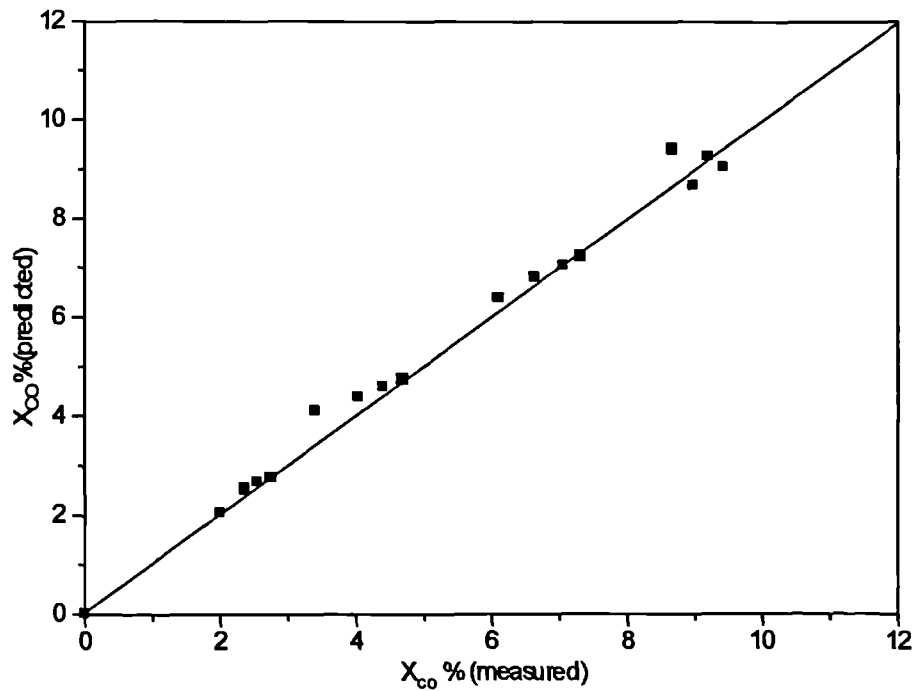
Fig.7.10 Comparison between X_{CO}(measured) and X_{CO}(predicted)
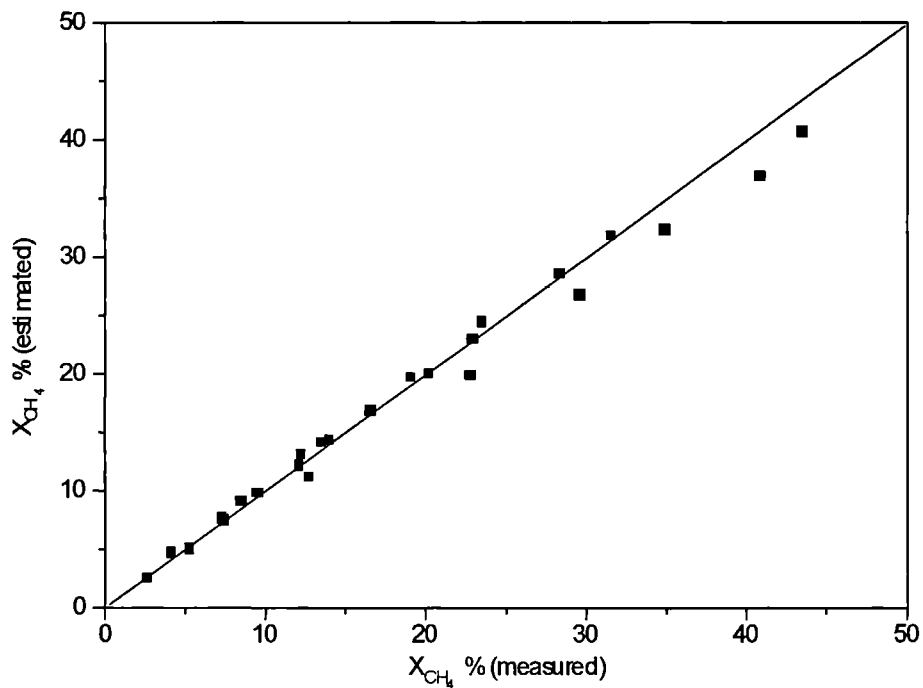
Fig.7.11 Comparison between X_{CH_4} (measured) and

X_{CH_4} (estimated), p_t = 120kPa, $H_2O/CH_4/H_2$ =4/1/1
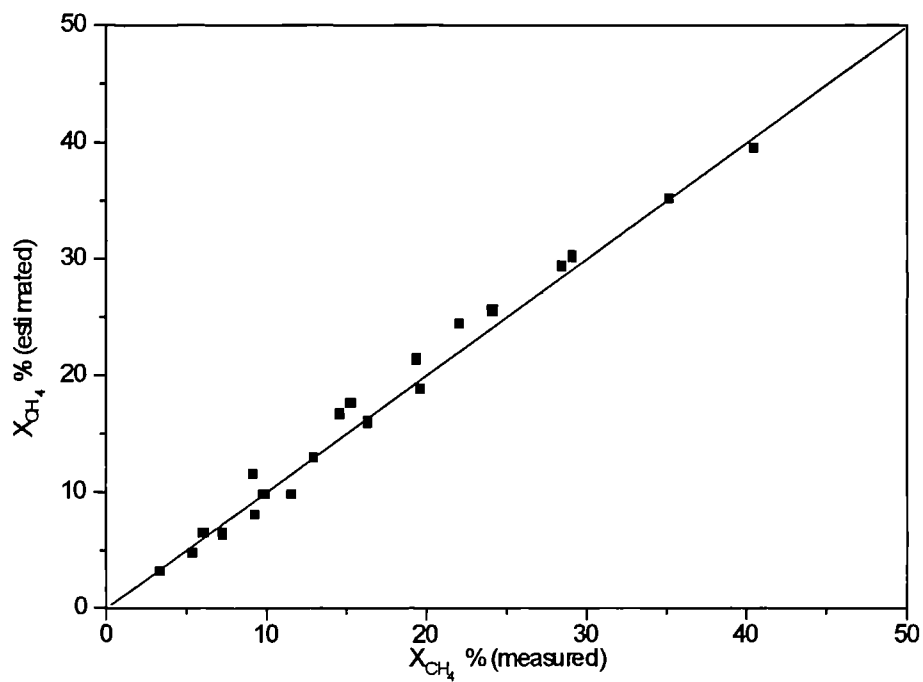
Fig.7.12 Comparison between X_{CH_4} (measured) and

X_{CH_4} (estimated), p_t= 120kPa, $H_2O/CH_4/H_2$= 5.5/1/1
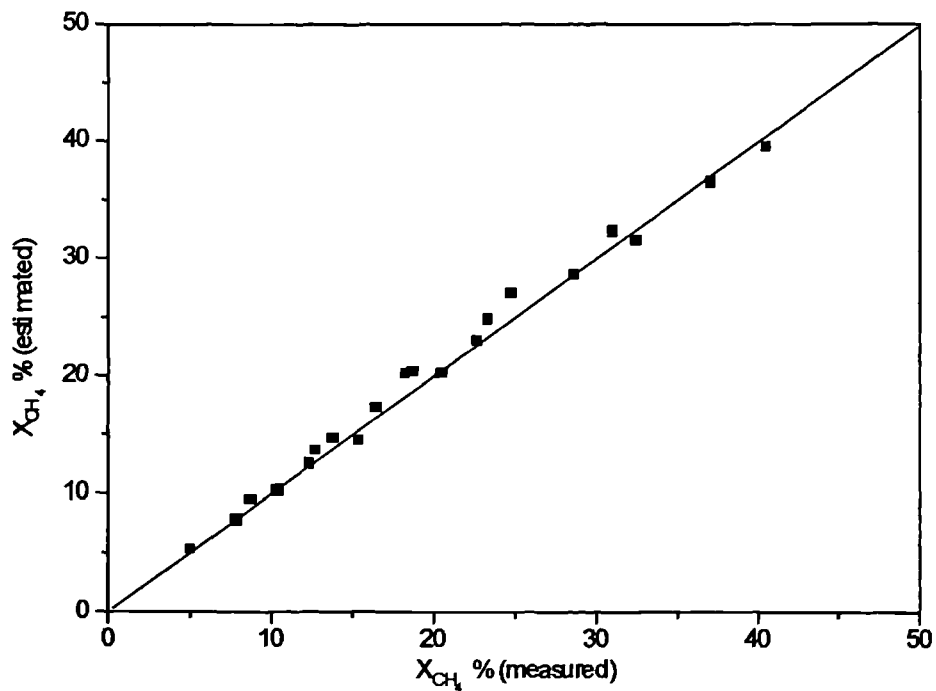
Fig.7.13 Comparison between X_{CH_4} (measured) and

X_{CH_4} (estimated), p_t=300kPa, $H_2O/CH_4/H_2$=5.5/1/1
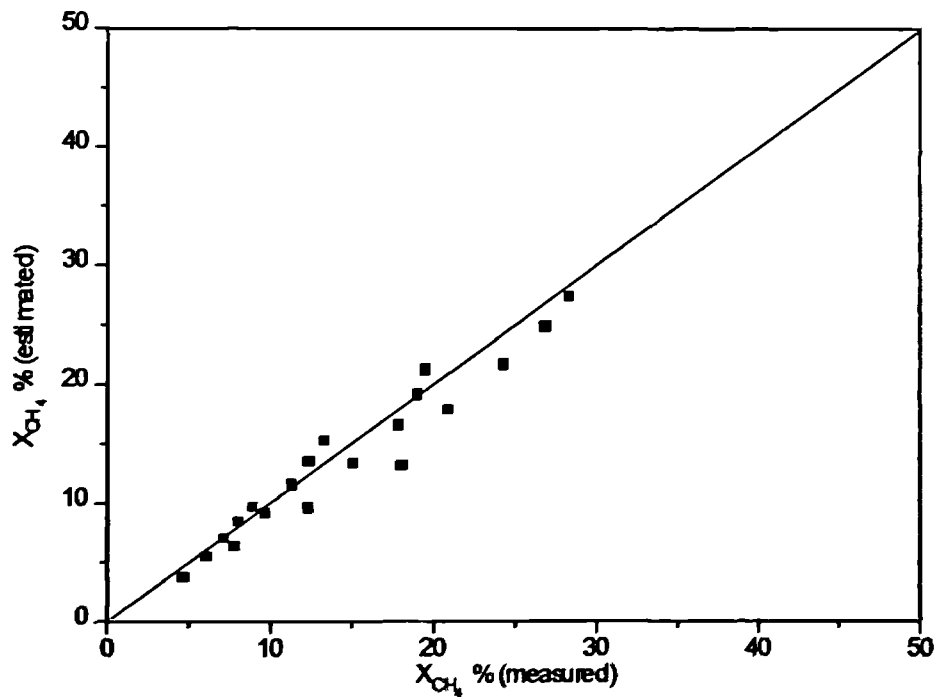
Fig.7.14 Comparison between X_{CH_4} (measured) and

X_{CH_4} (estimated), p_t = 600kPa, $H_2O/CH_4/H_2$=5.5/1/1

CHAPTER 8

THE EFFECT OF HYDROGEN REMOVAL ON THE PERFOMANCE OF A MEMBRANE REACTOR FOR METHANE STEAM REFORMING

8.1 Introduction

With the abundance of natural gas there is continuing interest in conversion of methane to more useful products such as methanol and hydrogen. Of the various processes by which this may be achieved the predominant one in synthesis gas production by means of steam reforming (Rostrup-Nielsen, 1983).

In methane steam reforming the following reversible reactions occur:

reaction (1) $CH_4 + H_2O = CO + 3H_2$

reaction (2) $CO + H_2O = CO_2 + H_2$

reaction (3) $CH_4 + 2H_2O = CO_2 + 4H_2$

reactions (1) and (3) are endothermic whereas reaction (2) is exothermic. The conversion of methane is limited by thermodynamic equilibria and is favoured by high temperature and low pressure. However, high pressure is required in the associated ammonia and methanol plants and to compensate for this high-applied pressure an increase in temperature is required. Consequently, the energy consumption for steam reforming is relatively high

An attractive technique for breaking the equilibrium limitation is the use of selective membranes to remove the hydrogen product from the reaction mixture (Uemiya et al., 1991; Adris et al.,1991; Chai et al., 1993; Shu et al., 1994; Barbieri et al., 1997). However, any disadvantages resulting from the removal of hydrogen from reaction in which steam reforming

is being carried out has received only limited attention to date (Laegsgaard Jorgensen, S., et al., 1995). Removal of hydrogen from product could limit the influences of hydrogen which inhibits carbon formation and in its effect on poisoning of the nickel catalyst by sulphur compounds. It has been pointed out by Rostrup-Nislsen (1968, 1984) and Bartholomew (1979) that the adsorption of hydrogen sulphide on nickel catalysts is very strong at low temperature and the fractional surface coverage depends on the value of p_{h2s}/p_{h2} while the tendency for methane decomposition to give carbon is determined by the ratio $(p_{H2})^2/p_{CH4}$ Removal of product hydrogen will favour the adsorption of hydrogen sulphide and the methane decomposition reaction, so that the catalyst activity and stability will be affected and may well restrict any advantages arising from the use of a membrane reactor for methane steam reforming.

The objective of this chapter is to use a mathematical model to analyses the effects of hydrogen removal on the performance of a membrane reactor for methane steam reforming in the presence of hydrogen sulphide and on the performance when carbon deposition occurs from the decomposition of methane.

8.2 Catalyst Deactivation by Sulphur Poisoning and by Carbon Formation from Methane Decomposition

8 2.1 Catalyst deactivation by sulphur poisoning

Normally, sulphur will be present in natural gas which can be purified effectively to a tolerable level preceding steam reforming Because sulphur adsorbs so strongly on nickel its presence on a catalyst surface usually causes substantial loss of activity in many important reactions,

particularly in methane steam reforming. The reasons for this are twofold: (1) sulphur adsorption on the nickel surface prevents the further adsorptions of reactant molecules, and (2) the reconstruction of Ni surface may modify or decrease the adsorption rates of reactant gases.

Adsorption of H_2S on nickel is very rapid; this high adsorption rate suggests that no barrier to adsorption and dissociation occur until saturation of the surface is approached. Accordingly, sulphur poisoning of nickel is not likely to be limited by rates of adsorption and reaction on the surface. Thus, surface coverages of sulphur can be predicted by equilibrium thermodynamics and by mass balance and mass transfer considerations under conditions of interest. At steady state, the concentration difference between H_2S in bulk phase and in the catalyst pellet may be very small, thus sulphur poisoning effects can be correlated with the H_2S concentration in bulk phase, which, is the important parameter in practical operation.

Most previous investigators (Rostrup-Nielsen, 1968; Oliphant, et al, 1978; Ng,, et al, 1978; Fowler, et al , 1979) agree that H_2S completely dissociates on nickel surface even below room temperature, but there is disagreement regarding the number of nickel atoms per sulphur atom involved. Rostrup-Nielsen (1968) suggested a one-site mechanism in high temperatures (825-925 K),

$$H_2S(gas) + Ni = Ni\text{-}S + H_2(gas) \tag{8.1}$$

based on the value of one obtained for the power , n, in the langmuir expression

$$\theta_s = \frac{A\left(P_{H_2S} / P_{H_2}\right)^n}{1 + B\left(P_{H_2S} / P_{H_2}\right)^n} \tag{8.2}$$

fitted to his data He also found that the sulphur uptake is a function of the ratio p_{H2S}/p_{H2}, a saturation layer developed at ratios above $5 \cdot 10^{-6}$ and at ratio 10^{-3} bulk sulphide (Ni_2S_3) was formed Oliphant et al (1978), on the other hand, obtained Langmuir exponents of 2.9 and 2 7 for Ni power and 3% Ni/Al_2O_3 respectively at 725 K, consistent with a three-site mechanism

Simulations of sulphur poisoning in the steam reforming process have been given by Christiansen and co-workers (1980) and Rostrup-Nielsen (1982). Their analysis indicates rapid break-through of sulphur for different inlet concentrations of sulphur and a slow approach to equilibrium on the catalyst. The transient profiles of sulphur poisoning were calculated with fixed conversion and fixed axial temperature profile. Based on their simulations, the sulphur coverage fractional on the catalyst is always greater than 0.5 along the reformer tube even for H_2S concentration in feed of less than 0.02 ppm. This decrease in catalyst activity caused by the sulphur poisoning must be compensated by increasing the reaction temperature in order to keep the outlet conditions fixed.

8 2 2 Catalyst deactivation by carbon formation from methane decomposition

Deactivation of supported metal catalyst by carbon formation is a very serious problem in steam reforming. Its causes are generally threefold: (1) fouling of the metal surface, (2) blockage of catalyst pore and voids and (3) break-up of the catalyst support material. Carbon may be formed via different routes, each influencing the morphology of the carbon. According to Rostrup Nielsen (1984) three different kinds of carbon species are produced during steam reforming (1) whisker like carbon, (2) encapsulating carbon and (3) pyrolytic carbon.

In methane steam reforming, carbon may be deposited by CO disproportionation

$$2CO = C + CO_2 \qquad (8.3)$$

and methane decomposition

$$CH_4 = C + 2H_2 \qquad (8.4)$$

Based on methane steam experiments on the ICI catalyst 57-4 at low temperature (748-823 K), it is found that probability to form carbon from CO disproportionation will be very small due to a relative low yield of CO obtained compared to CO_2. Wagner and Froment (1992) studied carbon formation and gasfication under steam reforming conditions in an electrobalance reactor. From their experiments they derived threshold constant K_M (K_M=exp(-9573/T+11.62) bar) for methane decomposition and defined a criterion V_{CH4}

$$V_{CH_4} = \frac{\dfrac{p_{H_2}^2}{p_{CH_4}}}{K_M} \qquad (8.5)$$

The definition of V_{CH4} is such that carbon formation will occur when its value is lower than 1. This is an experimental limit, not a thermodynamic one. Methane decomposition is endothermic and leads to an increase in the total number of moles. Therefore, it is favoured by high temperatures and low pressures. Methane decomposition will most likely occur near the reactor inlet, where the concentration of methane is high and hydrogen's very low. The value of V_{CH4} will be lessened by the removal of part of hydrogen produced in a membrane reactor, compared with a conventional fixed reactor, i.e., hydrogen removal will increase the risk of carbon formation from methane decomposition in membrane reactors for methane steam reforming.

8.3 Model Development

8.3.1 Intrinsic reaction kinetics

There is a large number of literature that deals with reaction kinetics of methane steam reforming (Akers and Camp, 1955; Bordow et al., 1967; Ross and Steel, 1972; De Deken et al., 1982; Xu and Froment, 1989) Here we use the intrinsic kinetics data obtained experimentally on ICI catalyst 57-4 from laboratory studies in present work. The intrinsic kinetics rate expressions determined for reaction (1), (2) and (3) are given in Chapter 7, respectively, by

$$r_1 = k_1 p_{CH_4} p_{H_2O}^{0.5} p_{H_2}^{-1.25}\left(1 - \frac{p_{CO} p_{H_2}^3}{p_{CH_4} p_{H_2O} K_{p1}}\right)/den^2 \tag{7.39}$$

$$r_2 = k_2 p_{CO}\, p_{H_2O}^{0.5} p_{H_2}^{-0.5}\left(1 - \frac{p_{CO_2} p_{H_2}}{p_{CO}\, p_{H_2O} K_{p2}}\right)/den^2 \tag{7.40}$$

$$r_3 = k_3 p_{CH_4} p_{H_2O} p_{H_2}^{-1.75}\left(1 - \frac{p_{CO_2} p_{H_2}^4}{p_{CH_4} p_{H_2O}^2 K_{p3}}\right)/den^2 \tag{7.41}$$

where,

$$den = 1 + K_{CO} p_{CO} + K_H p_{H_2}^{0.5} + K_W \frac{p_{H_2O}}{p_{H_2}} + K_{H_2S}\frac{p_{H_2S}}{p_{H_2}}$$

The intrinsic kinetic parameters except for K_{H_2S} for these rate expressions are obtained from the experiments and are listed in Table 7.5, and K_{H_2S} = 55exp(10720/T) (Christiansen, et al., 1980)

8.3.2 Mass balance equations for a membrane reactor

A dense Pd/Ag composite membrane reactor with a jacket for the removal of hydrogen is used in this investigation. The catalyst (57-4) is loaded in tubeside of the reactor Reactants enter into the tubeside and sweep gas enters the shellside in co-current with reactants The dense Pd/Ag composite membrane is permeable only to hydrogen.

In order to derive the equations presenting this type of reactor, the following assumptions have been made:

(1) Steady state operation.

(2) Isothermal conditions prevail.

(3) Negligible pressure drop

(4) Plug flow on both tubeside and shellside.

(5) Hydrogen permeability is the same as the pure gas value.

(6) No interphase and intraparticle mass transfer limitations

From these assumptions, mass balance equations can be written for all components as follows

In the tubeside,

$$\frac{dn_{it}}{dl} = \Omega \rho_B \sum_{j=1}^{3} v_{ij} r_j \tag{8 5}$$

$$i=1, 2, 3, 4$$

$$\frac{dn_{5t}}{dl} = \Omega \rho_B \sum_{j=1}^{3} v_{ij} r_j - 2\pi R_2 f_{H_2} \left[\left(\frac{n_{5t}}{\sum_{i=1}^{5} n_{it}} P_t \right)^{0.5} - \left(\frac{n_{5s}}{\sum_{i=1}^{5} n_{is}} P_s \right)^{0.5} \right] \tag{8 6}$$

where i=1, 2, 3, 4 and 5 for CH_4, H_2O, CO, CO_2 and H_2 respectively, and v_{ij} is the stoichiometric coefficient of component i in reaction j f_{H_2} is the permeability of hydrogen ,

and it is confirmed that the half-power law for hydrogen permeation through the membrane used (Gobina and Hughes, 1994) is valid.

In the shellside, only one mass balance equation for hydrogen is needed i.e.

$$\frac{dn_{5s}}{dl} = 2\pi R_2 f_{H_2} \left[\left(\frac{n_{5t}}{\sum\limits_{i=1}^{5} n_{it}} P_t \right)^{0.5} - \left(\frac{n_{5s}}{\sum\limits_{i=1}^{5} n_{is}} P_s \right)^{0.5} \right]$$

(8.7)

The initial conditions for equation (8.5-7) are

$$l=0, \quad n_{it}=n_{it}^{i} \quad \text{and} \quad n_{is}=n_{is}^{i}$$

(8.8)

The equations are solved by using the fourth order Runge-Kutta method.

8.4   Results and Discussion

In this simulation study, the effects of the removal of hydrogen produced on the catalyst poisoning by H_2S, the performance of the membrane reactor and the tendency of carbon formation from methane decomposition have been investigated. It should be pointed out that the amount of carbon formation on the catalyst could not determined from its tendency to deposit and thus the effect of carbon formation on the catalyst activity is not included. Table 8.1 shows the basic data used for this investigation

Table 8.1 Input basic data for the simulation study

Contact time W/F_{CH_4}, kgcat s/kmol	133560	Feed composition	$CH_4 > 99.9\%(Vol)$ balanced by H_2S
Membrane area / reactor volume, m^{-1}	400	Shellside pressure, kPa	100
Thickness of the palladium layer, μm	50	Tubeside pressure, kPa	120
Steam /Methane ratio	3	Temperature range, K	773-873

8.4.1 The effects of hydrogen removal on the catalyst activity and the performances of the membrane reactor

For comparing the membrane reactor with a fixed bed reactor, the f_{H_2} is set to zero for without hydrogen removal in order to simulate the performance of the fixed bed reactor but keeping other conditions the same as in the membrane reactor. In all cases for the membrane reactor, the sweep gas flows co-current to the reacting gas. From the langmuir absorption, the H_2S coverage on the catalyst is given by

$$\vartheta_S = \frac{K_{H_2S}\dfrac{p_{H_2S}}{p_{H_2}}}{1 + K_{CO}p_{CO} + K_H p_{H_2}^{0.5} + K_W \dfrac{p_{H_2O}}{p_{H_2}} + K_{H_2S}\dfrac{p_{H_2S}}{p_{H_2}}}$$

(8.9)

Fig 8.1 shows the axial profiles of H_2S coverages on the catalyst at different temperature for the fixed bed reactor, i.e. without hydrogen removal. It is clear that H_2S coverage θ_S drops after a slight decrease near the inlet, keeps an almost constant value to the exit. However, the

effect of temperature on θ_S is so significant that the θ_S is halved by a temperature rise of 100 K.

Fig.8.2 and 8.3 show the effects of H_2S concentration in the feed on θ_S at temperature 823 and 773 K respectively. At high temperature of 823 K, an increase in H_2S concentration from 0.05 ppm to 0.50 ppm, 10 times of original value, causes to θ_S increases to 4 times the original value. However, at low temperature 773 K, , an increase in H_2S concentration to 4 times the original value only, leads to an increase of θ_S from 0.3 to 0.7. consequently the effect of H_2S concentration on catalyst poisoning is more sensitive at low temperature.

The effects of the extent of hydrogen removal on the catalyst poisoning are presented in Figs.8.4 and 8.5. It can be seen from these figs. that the H_2S coverage drops continuously along the reformer tube for cases where no hydrogen removed (i.e. fixed bed reactor) and for low degrees of hydrogen removal; however, at the 80 % of hydrogen removal the H_2S coverage increase along the tube length. Consequently, at high level of H_2 removal the catalyst poisoning by H_2S is more serious than at low percentage of hydrogen removal due to the increased value of p_{H_2S}/p_{H_2} . Under conditions studied, the limitations of different H_2S contents range from 0.04 to 0.4 ppm for the cases without hydrogen removal as shown in Fig.8.6. As can be seen, higher reaction temperatures can tolerate higher H_2S concentrations in methane.

Defining X_{CH4max} as a maximum conversion of methane which can result at given temperatures and pressures when H_2S poisoning is absent, the amount of H_2S which can be tolerated to give 95% of X_{CH4max} for different extent of hydrogen removal may be estimated. Fig.8.7.

shows a plot of this H_2S tolerance level for 95%X_{CH4max} versus temperature. From this figure it can be seen that H_2S tolerance increases with increasing temperature and the H_2S tolerance also increases when hydrogen removal is less.

Because catalyst poisoning by H_2S is sensitive to the ratio p_{H_2S}/p_{H_2}, hydrogen removal may result in a decrease in methane conversions using a membrane reactor compared with a fixed bed reactor at higher H_2S concentrations. Figs.8.8 and 8.9 show the variations of the methane conversions with different percentages of hydrogen removal and different H_2S contents for operating temperatures of 773 and 823 K, respectively. At higher H_2S contents, there is no advantage in employing a membrane reactor due to the hydrogen removal resulting in more serious catalyst poisoning. To obtain benefit from the membrane reactor, the H_2S Content has to be decreased to a limiting value depended on conditions of operation. Based on Fig.8.8 and 8.9, in general, the limiting value will decrease with increase of proportion of hydrogen removal and increase with reaction temperature increase.

8.4.2 The tendency to form carbon from methane decomposition

The influences of hydrogen removal on the axial profiles of carbon formation tendency are illustrated in Figs.8.10 and 8.11. in which V_{CH4} is calculated from the values of the partial pressures of hydrogen and methane and K_M is estimated from Wagner and Froment's relation (1992) given in the introduction. From these figures it can seen that the risk of carbon formation is promoted by the hydrogen removal and this increases with increasing extents of hydrogen removal and resulting reduced hydrogen partial pressure in the reactor. Even if no hydrogen removal, the V_{CH_4} is lower than 1 from the inlet to about half way point of the

reactor, which indicates that there may be a possibility of the carbon formation in this region of the reactor from methane decomposition. It is also clear that there is a risk of carbon formation throughout the reactor for cases with higher proportion of hydrogen removal. So considerable care is then necessary in order that catalyst deactivation from the carbon formation can be efficiently inhibited by other means.

Methane decomposition is restrained by a high pressure applied, because the tendency to carbon formation is sensitive to pressure. The effects of pressures on the profiles of carbon formation tendency are presented in Fig.8.12 and 8.13 for 50 % percent of hydrogen removal and without hydrogen removal at 773 K, respectively. The increased of V_{CH_4} with pressure increase for both cases is obvious. Comparing the Fig.8.12 with Fig.8.13, it is also noted that there is a small difference between the tendencies of carbon formation of two cases at 600 kPa of pressures employed.

8.5 Conclusions

Simulation of the steam reforming of methane in a catalytic membrane reactor have been made in order to assess the effect of poisoning by small amounts of hydrogen sulphide and to estimate the extent of potential carbon deposition on the catalyst. The results have been compared with fixed bed operation. In general, the removal of hydrogen by means of the selective hydrogen permeable membrane increases the tendency to poisoning by H_2S and to carbon deposition. These effects can be minimised to some extent by operating at higher temperatures in the case of H_2S poisoning and by operating at higher pressures to minimise the extent of carbon formation. For successful catalytic membrane reactor performance for

methane steam reforming, a high degree of sulphur removal from the feed stream would appear to be necessary.
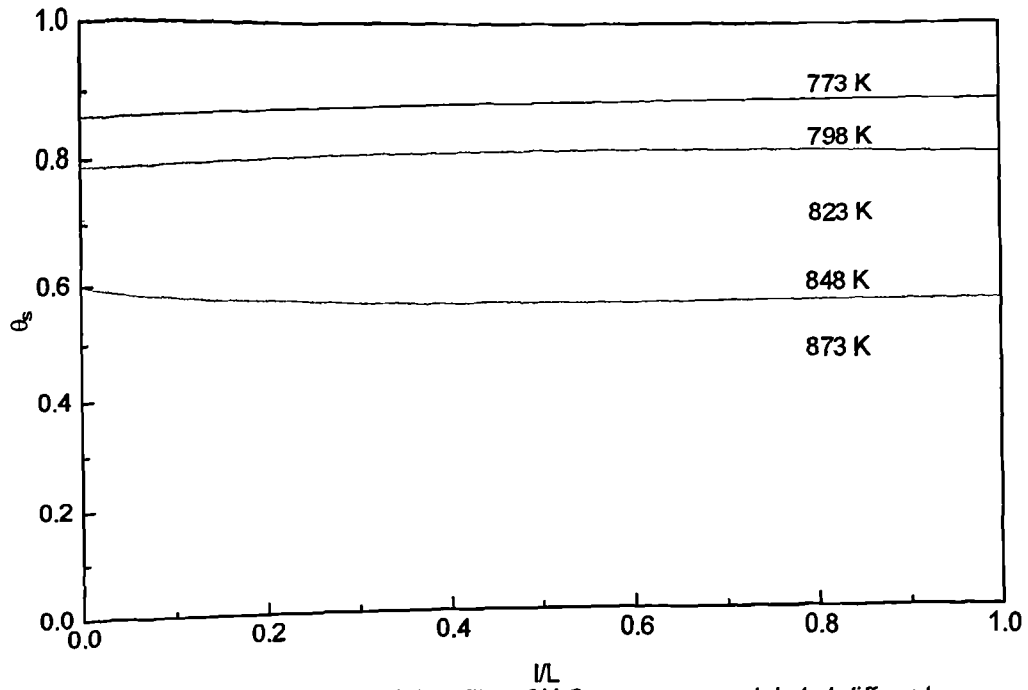
Fig. 8.1 Comparison of axial profiles of H_2S coverage on catalyst at different temperature, H_2S=0.25 ppm, P_t=120 kPa, H_2O/CH_4=3, WF_{CH4}=133560 kg s/kmol
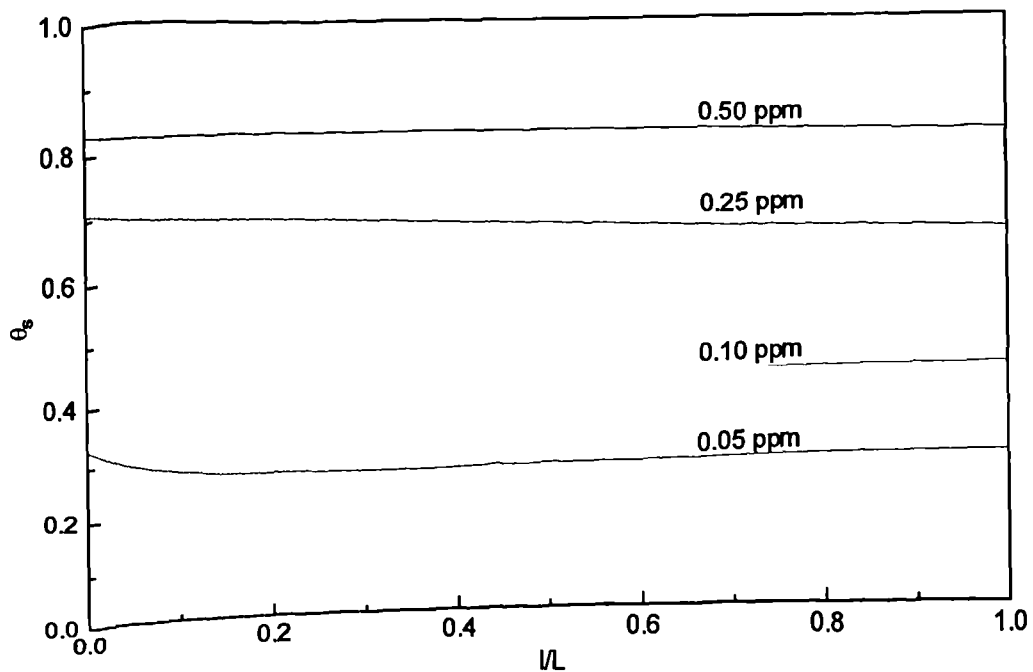
Fig. 8.2 Comparison of axial profiles of H_2S coverage on catalyst at different H_2S level, T=823 K, P_t=120 kPa, H_2O/CH_4=3, WF_{CH4}=133560 kg s/kmol
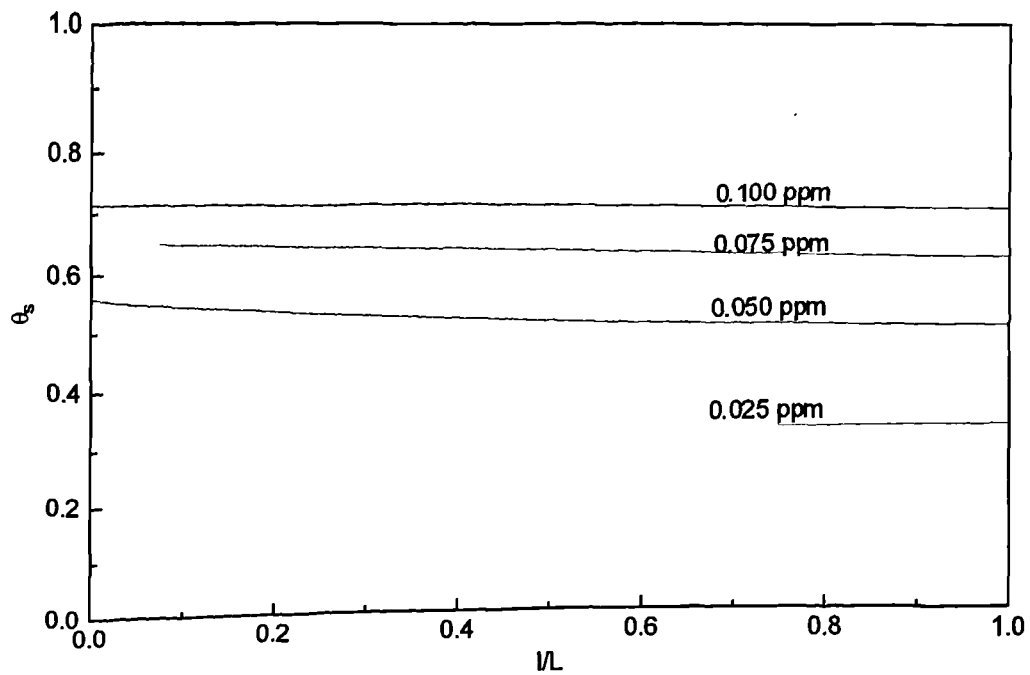
Fig.8.3 Comparison of axial profiles of H_2S coverage on catalyst at different H_2S level,
T=773 K, P_t=120 kPa, H_2O/CH_4=3, WF_{CH4}=133560 kg s/kmol
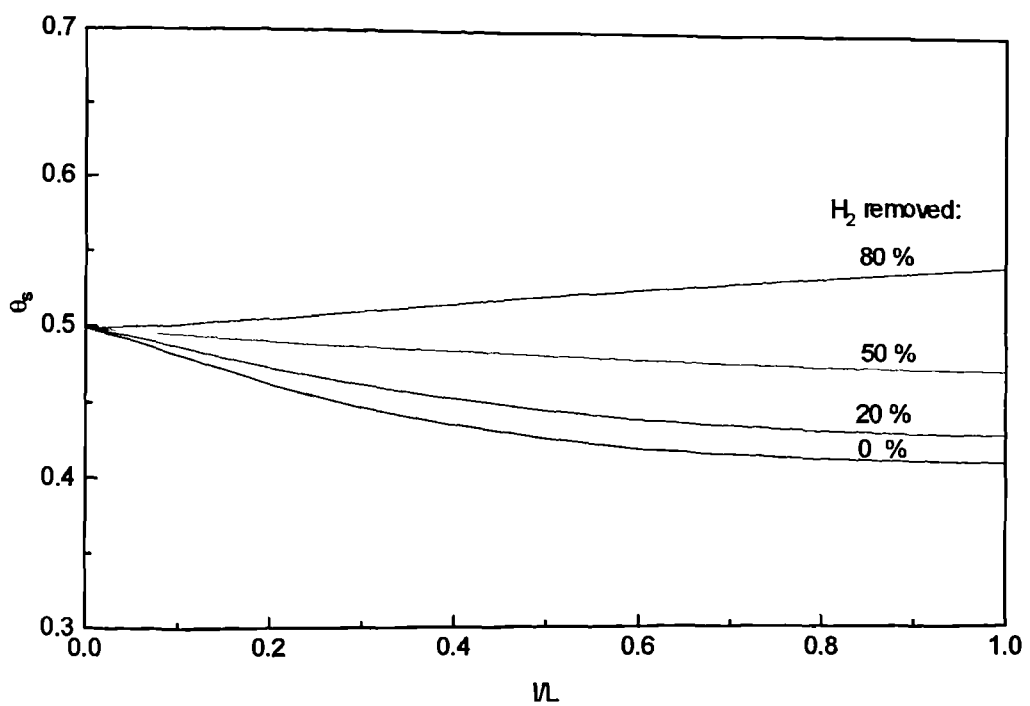
Fig.8.4 Effect of H_2 removed on axial profiles of H_2S coverage on catalyst, T=773 K,
y_{H2S}=0.04 ppm, P_t=120 kPa, H_2O/CH_4=3, WF_{CH4}=133560 kg s/kmol
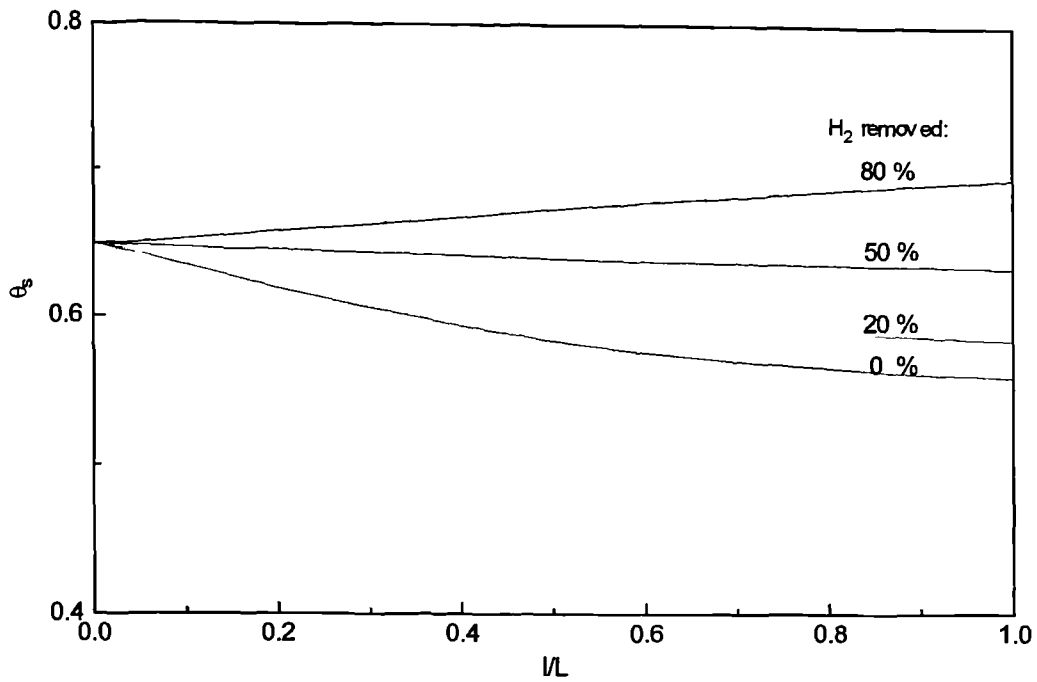
Fig.8.5 Effect of H_2 removed on axial profiles of H_2S coverage on catalyst, T=823 K,
y_{H_2S}=0.2 ppm, P_t=120 kPa, H_2O/CH_4=3, WF_{CH4}=133560 kg s/kmol
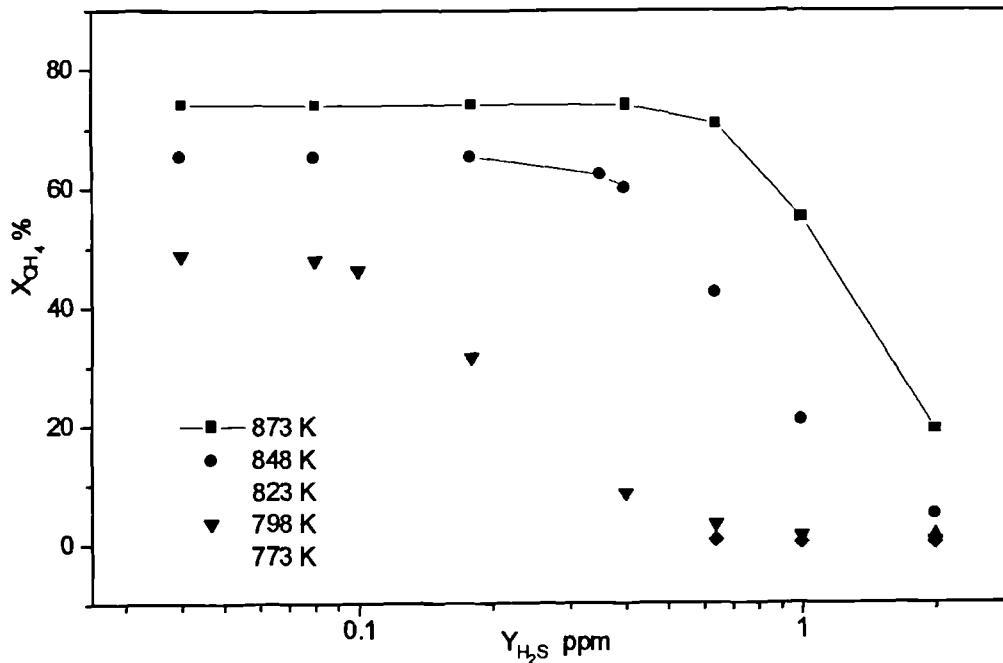
Fig.8.6 Effect of H_2S concentration on methane conversion, P_t=120 kPa,
H_2O/CH_4=3, WF_{CH_4}=133560 kg s/kmol, without H_2 removed
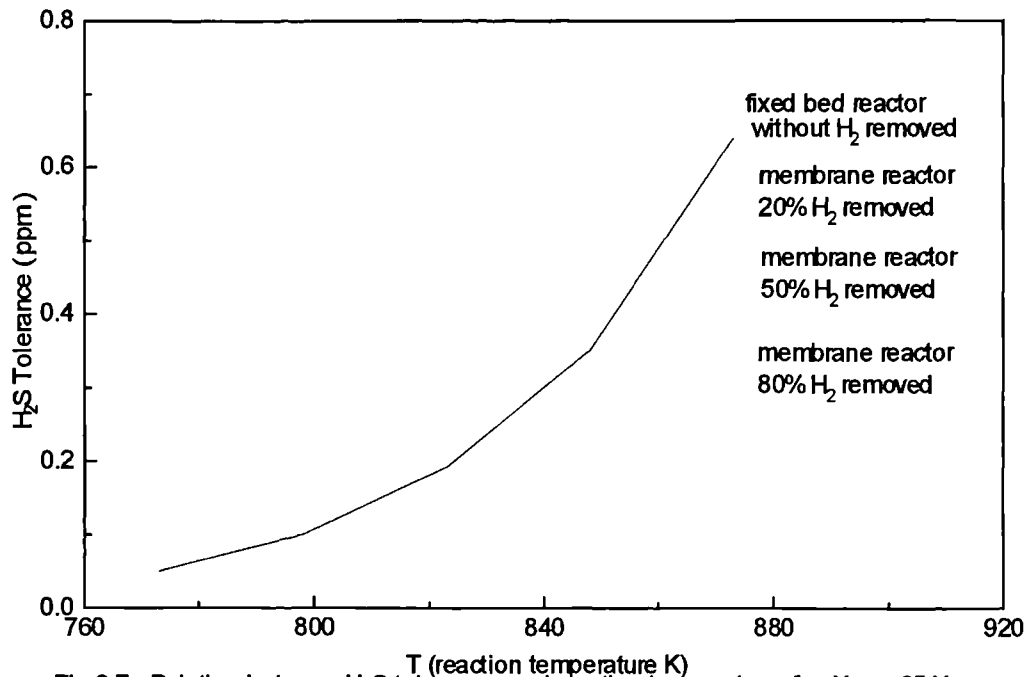
Fig.8.7   Relation between H_2S tolerance and reaction temperature, for $X_{CH_4}=.95\ X_{CH_4max}$, $P_t=120$ kPa, $H_2O/CH_4=3$, $WF_{CH_4}=133560$ kg s/kmol
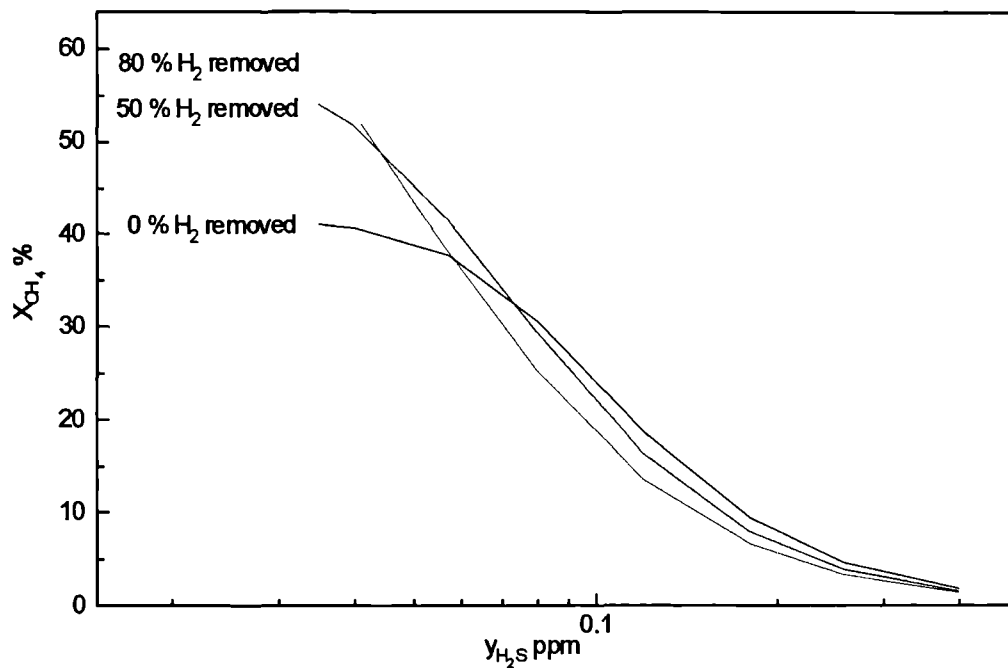
Fig.8.8 Comprison of effect of H_2S concentration on performances of fixed bed and membrane reactors, $T=773$ K, $P_t=120$ kPa, $H_2O/CH_4=3$, $WF_{CH_4}=133560$ kg s/kmol
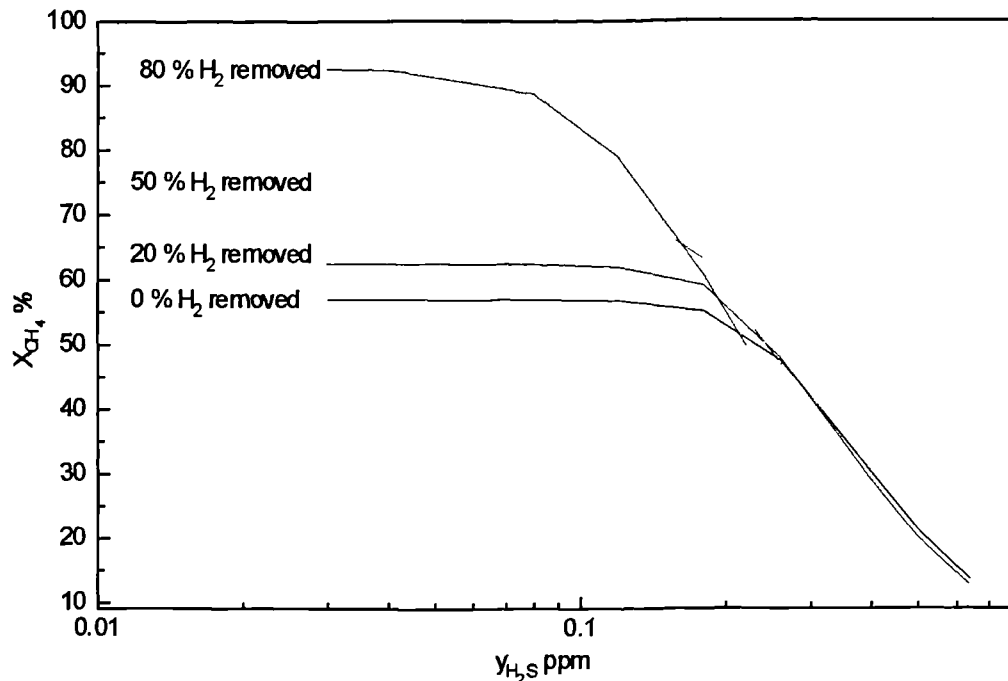
Fig. 8.9 Comprison of effect of H_2S concentration on performances of fixed bed and membrane reactors, T=823 K, P_t=120 kPa, H_2O/CH_4=3, WF_{CH_4}=133560 kg s/kmol
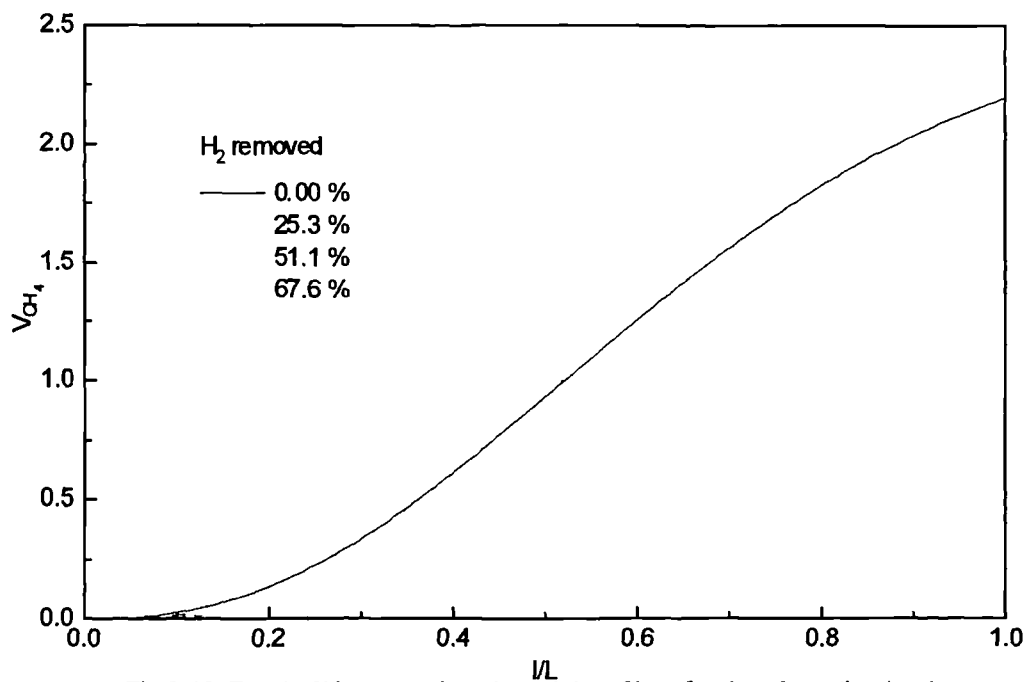
Fig.8.10 Effect of H_2 removed on the axial profiles of carbon formation tendency, T=823 K, y_{H_2S}=.192 ppm, P_t=120 kPa, H_2O/CH_4=3, WF_{CH_4}=133560 kg s/kmol
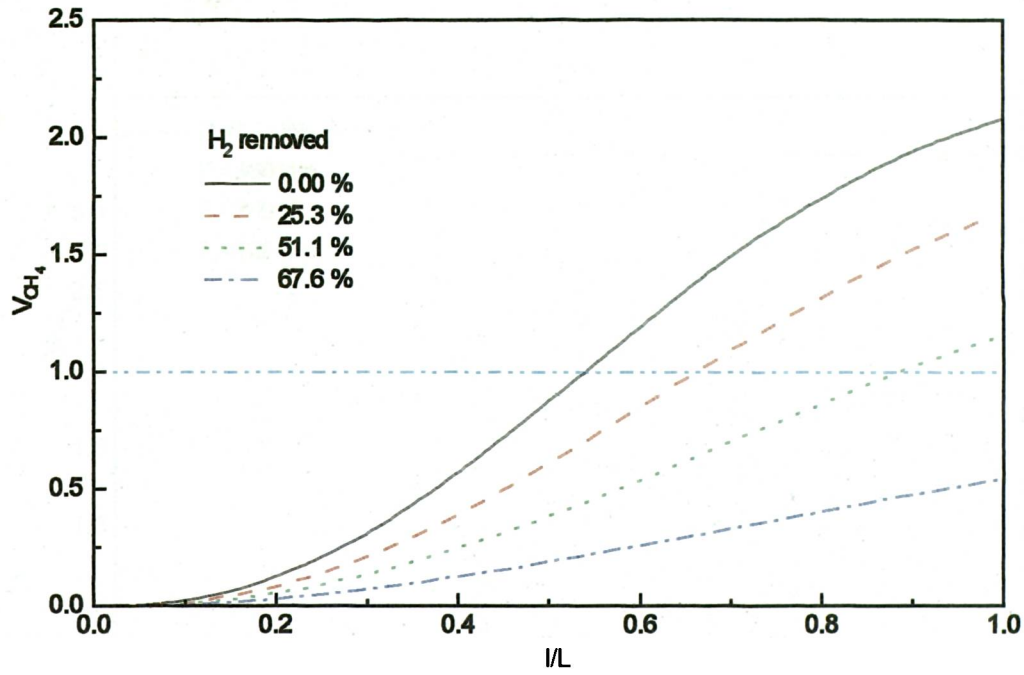
Fig. 8.11 Effect of H_2 removed on the axial profiles of carbon formation tendency, $T=773$ K, $y_{H_2S}=.05$ ppm, $P_t=120$ kPa, $H_2O/CH_4=3$, $WF_{CH_4}=133560$ kg s/kmol
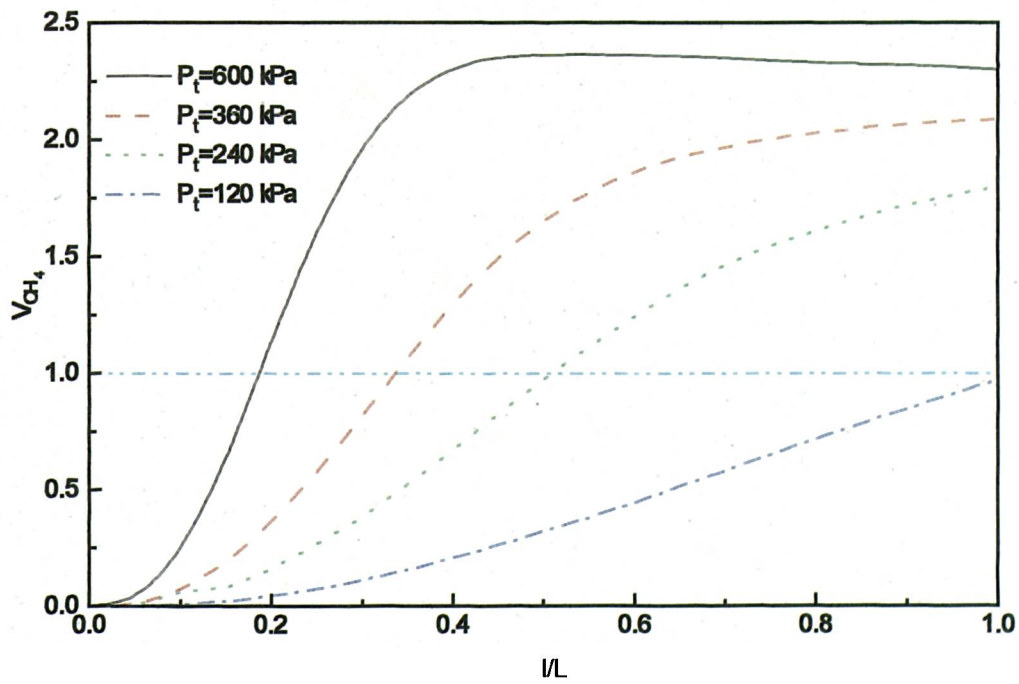
Fig. 8.12 Effect of reaction pressure on the axial profiles of carbon formation tendency, $T=773$ K, $y_{H_2S}=.05$ ppm, 50 % H_2 removed, $H_2O/CH_4=3$, $WF_{CH_4}=133560$ kg s/kmol
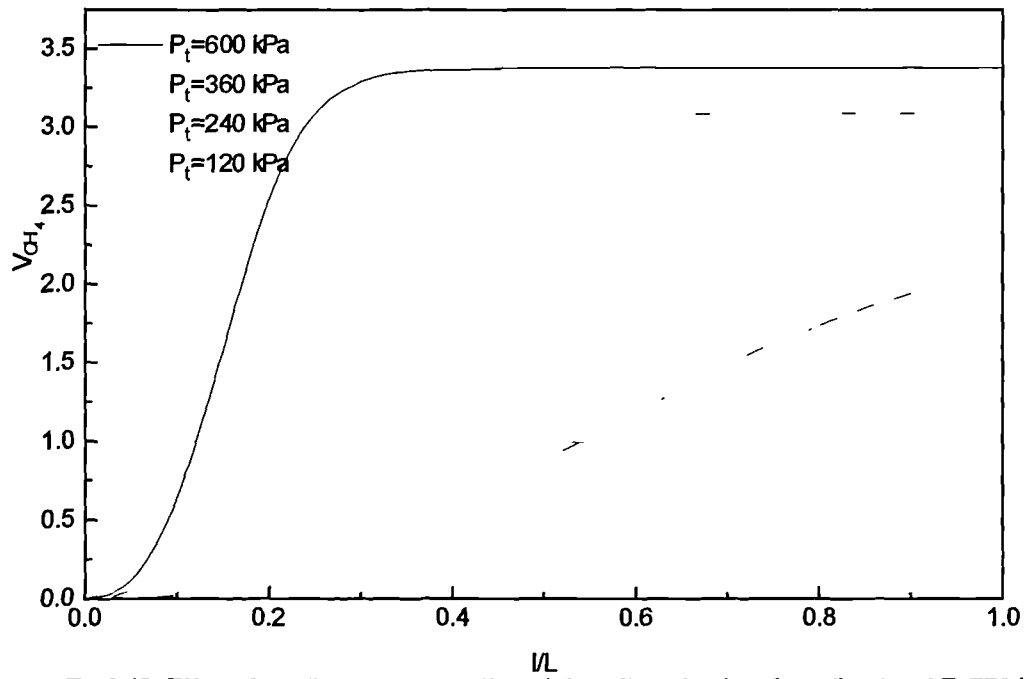
Fig. 8.13 Effect of reaction pressure on the axial profiles of carbon formation trend, T=773 K, y_{H_2S}=.05 ppm, without H_2 removed, H_2O/CH_4=3, WF_{CH_4}=133560 kg s/kmol

CHAPTER 9

CONCLUSIONS AND RECOMMENDATIONS FOR FUTURE WORK

The present work has been concerned with experimental diffusion and kinetics studies on methane steam reforming over a nickel/alumina catalyst. A Wicke-Kallenbach type diffusion cell was used for diffusion experiments, and an integral reactor and a single pellet reactor for kinetic experiments. A simulation study on the use of a catalytic membrane reactor for methane steam reforming has also been undertaken The diffusion study was mainly concerned with determining the effective diffusivities of gases present in methane steam reforming at different temperatures and pressures. The kinetic study has been focused on developing an intrinsic kinetics model (rate equations) for methane steam reforming on the catalyst used. The simulation study was devoted mainly to the effects of hydrogen removal on the performance of a membrane reactor for methane steam reforming.

This Chapter presents the conclusions which have been obtained from the results given in Chapters 4-8, and offers suggestions for future studies, which could supply useful information concerning methane steam reforming.

9.1 CONCLUSIONS

From the measurements of effective diffusivities, the following conclusions can be obtained:

1. The diffusion mode shifts with temperature and pressure changes. The experiments show that the effect of pressure on diffusion mode is greater than that of temperature. At ambient pressure, diffusion occurs in the transition region, whereas at pressures up to 1MPa, diffusion lies mainly in the bulk diffusion region.

2. The effects of temperature on the effective diffusivities of most of the gases measured (except for water vapour) increase with increase in pressure: at ambient pressure, the temperature exponent values range from 1.0 to 1.25, whereas at 1MPa, the values are in a range between 1.4 and 1.75. This is due to an increased contribution of bulk diffusion to the total diffusion with increase in pressure.

3. The effects of pressure on the effective diffusivities (expect for water vapour) decrease with increase in temperature: at room temperature, the pressure exponent values lie in the range of 0.5 to 0.85, while at 873 K, the values are between 0.4 and 0.67. However, the pressure exponents for hydrogen, methane and water vapour, which are the main components in methane steam reforming, approach stable values as the temperature exceeds 573 K.

4. Values of the pressure exponent and the temperature exponent of effective diffusivities for water vapour were nearly constant. This difference between water vapour and other permanent gases measured may be due to adsorption effect with water vapour.

5. The tortuosities estimated for the pellets varied from 1.8 to 2.50 for different gases at ambient pressure, but decreased with increase in pressure. The estimated tortuosity for

hydrogen and methane in the pressure range from 400-1000kPa tended to a constant value for the pellet.

From the study of the intrinsic kinetics of methane steam reforming, the following conclusions can be made:

1. Addition of hydrogen the feed can significantly inhibit catalyst deactivation resulting from the decomposition of methane.

2. The partial pressure of steam has a negative effect on the initial reaction rates, while the total pressure shows a positive effect.

3. Both CO and CO_2 are primary products of steam reforming but most of the CO is probably formed by the reverse water gas shift reaction under the present experimental conditions.

4. Methane steam reforming involves multiple steps, including steam adsorption with dissociation on the catalyst surface; methane adsorption with dissociation into radicals containing C on the catalyst surface, which react with adsorbed oxygen to yield an intermediate; surface reactions of the intermediate including decomposition or reaction with adsorbed oxygen; and desorption of products. The surface reactions are the slowest of these steps, and control the overall reaction rates.

5. A kinetic model for the catalyst used has been developed, which differs from that of Xu and Froment (1989) for a nickel on magnesium aluminate catalyst, and which includes

both Langmuir's ideal adsorption and Freundlich's non-ideal adsorption concepts. The kinetic model developed for the present catalyst fits the experimental results very well, and the parameters obtained are statistically significant and thermodynamically consistent.

6. The kinetic model shows a non-monotonic dependence upon steam partial pressure and first order dependence with respect to methane partial pressure for the reforming reaction, as does the model of Xu and Froment (1989)

From the simulation study on the effects of catalyst deactivation in fixed bed and membrane reactors, the following conclusions can be made:

1. Catalyst deactivation from both H_2S poisoning and carbon formation is very sensitive to hydrogen removal. Hydrogen removed by a membrane may cause more extensive catalyst deactivation, and also the H_2S tolerance drops. Similarly, the tendency to carbon formation increases as the proportion of hydrogen removed increases.

2. The simulation shows that the benefit of using a membrane reactor may be not achieved for feedstocks with a high H_2S level and in which a high proportion of hydrogen produced is removed, due to the severe catalyst deactivation.

3. A high-applied pressure can inhibit the methane decomposition reaction. Hence this will compensate for the negative influence of hydrogen removal on the catalyst activity for methane steam reforming in a membrane reactor.

4. To reduce the effect of catalyst deactivation from H_2S poisoning under significant hydrogen removal, a more efficient desuphurisation technique need to be employed for methane steam reforming in a membrane reactor operating at low temperature.

From the experiments of coupling reaction and diffusion in the single pellet reactor, the conclusions are as follows:

1. The experimental results show that the methane diffusion into the catalyst pellets possessing no holes, almost totally controls the reaction rate. Under such diffusion limitations, other factors, including the reaction temperature, the catalyst activity, and the contact time, did not show any apparent effects on the reaction.

2. The diffusion limitation lessened considerably for the catalyst pellets containing four holes; it was found that the effects of diffusion limitation on the catalyst pellets with higher activity were greater than on the catalyst pellets with lower activity. However, catalyst activity still did not play an important role in affecting the reaction.

3. Since the reaction rate of methane steam reforming over nickel/alumina catalyst is very fast at low conversion, and the diffusion rate controls the reaction, the effects of other factor on reaction are examined only with difficulty. Hence, a pellet reactor may be not suitable for measurements involving the coupling of reaction and diffusion during methane steam reforming.

9.2 RECOMMENDATIONS FOR FUTURE STUDY

Methane steam reforming is a complex process influenced by a such large number of variables that there are always areas which require further study. From the present study, as well as the review, the areas which are suggested for further investigation, include:

1. For the sake of accuracy, it is the best that the intrinsic kinetics derived on the catalyst used at present experimental conditions is confirmed experimentally under commercial conditions (i.e., at high temperatures and high pressures) before it is applied to the commercial usage

2. Since the change of catalyst composition and preparation method influences the mechanism of methane steam reforming greatly, individual kinetic studies have necessarily to be carried out for a specific catalyst.

3. Carbon formation is a major problem in maintaining the catalyst activity. Addition of alkalis can inhibit the carbon formation, but the effect of alkalis on catalyst activity used in industrial practice is not clear up to now. Hence, it is important to conduct an extensive study on this area.

4. The simulation has demonstrated that the hydrogen removal has a considerable influence on the catalyst activity. Because of the promising application of catalytic membrane reactors for methane steam reforming in industrial practice, it is suggested that experimental studies of catalyst deactivation from H_2S poisoning and carbon formation in

the presence of hydrogen removal and at low temperatures should be carried out to determine the H_2S tolerance and the carbon formation free region more reliably.

5. Since decreasing the steam/hydrocarbon ratio can lower the operating cost of reforming process, the development of catalysts with high stability at low ratios of steam/hydrocarbon could be an attractive future option.

6. An experimental study of the diffusion of the gases present in steam reforming over a wider pressure range of 1-3MPa would be very helpful to investigating the effects of pressure on effective diffusivities.

Notation

A   peak area of component detected by GC

A_j preexponential factor of rate constant, k_j

$A(K_i)$ preexponential factor of adsorption constant, K_i

a   constant used in equation (2.3)

a_i, a_i^* correlation coefficients in equations (7-18) and (7-22), respectively, $(kgcat\ s/kmol)^{-i}$

a_m outer surface of the catalyst, m^2/kg

b   constant used in equation (2.3), $(kPa)^{-1}$

b_i, b_i^* correlation coefficients in equations (7-19) and (7-23), respectively, $(kgcat\ s/kmol)^{-i}$

C   total concentration, $kmol/m^3$

C_i concentration of component i, $kmol/m^3$

C_{pm} heat capacity, $kJ/kg\ K$

C_s concentration of component on surface, $kmol/m^2$

D   diffusivity, m^2/s

$D_{AB,eff}$ effective diffusivity of component A in B, m^2/s

D_{KA} Knudsen diffusivity of component A, m^2/s

d_p diameter of the catalyst particle, m

E_i activation energy of reaction i, kJ/mol

f_c correction factor defined by equation (6.10)

F_i molar flow rate of component i, $kmol/s$

f_{H_2} permeability of hydrogen, $kmol/m^2\ s\ (kPa)^{0.5}$

$f(r_p)dr_p$ fraction of void volume occupied by pores with radii between

        r_p and r_p+dr_p

G   mass velocity, $kg/m^2\ s$

ΔH reaction heat, $kJ/kmol$

$\Delta H_{j,a}$ enthalpy change of adsorption, kJ/mol

h   heat transfer coefficient, kJ/m^2 s K

J_i^* molar flux of component i relative to the molar average velocity, $kmol/m^2$ s

j_d j factor of mass transfer

j_h j factor of heat transfer

K_{CH_4} adsorption coefficient of CH_4, $(kPa)^{-1}$

K_{CO} adsorption coefficient of CO, $(kPa)^{-1}$

K_{H_2O} adsorption coefficient of H_2O

K_{H_2S} adsorption constant of H_2S

K_M threshold constant for methane decomposition, kPa

K_{p1}, K_{p3} equilibrium constant of reaction 1 and 3, $(kPa)^2$

K_{p2} equilibrium constant of reaction 2

$K_1, K_2, K_3,$ adsorption coefficients used in equations (2.29), (2.36), (2.43), (2.44),

           (Dimensions depend on the corresponding adsorption term appearing

           in the equations)

k   reaction rate constant, dimension depended on which equation it appeared

k_1 reaction rate constant, kmol/kgcat s. $(kPa)^{1.404}$ in equation (2.45), kmol $(kPa)^{0.5}$

           /kgcat s in equation (2.55), kmol/kgcat s $(kPa)^{0.25}$ elsewhere

k_2 reaction rate constant, kmol/kgcat s $(kPa)^2$ in equation (2.46),

           kmol/kgcat s kPa elsewhere

k_3 reaction rate constant, kmol $(kPa)^{0.5}$/kgcat s in equations (2.57) and (2.60)

           kmol/kgcat s $(kPa)^{0.25}$ elsewhere

k_c mass transfer coefficient between bulk phase and catalyst surface, m/s

k_{CO} reaction rate constant used in equations (2.43) and (2.53), kmol kPa/kgcat s

k_{CO_2} reaction rate constant used in equations (2.44) and (2.54), kmol kPa/kgcat s

L   effective length of reactor, m

M   molecular weight

m_1, m_2, m_3 molar ratios of steam/methane, hydrogen/methane, and hydrogen/carbon dioxide, respectively

N_i molar flux of component i relative to stationary coordinates, kmol/m^2 s

n_i molar flow rate of component i, kmol/s

P_i partial pressure of component i, kPa

P, P_t total pressure, kPa

Pr   Prandtl number

R   universal gas constant

R_2 outer radius of substrate, m

Re_p Reynolds number

r   reaction rate, kmol/kgcat s

$r_{CH_4}^o$ rate of methane disappearance in steam reforming, kmol/kgcat s

$r_{CH_4}^{\bullet o}$ rate of methane formation in reverse water gas shift reaction, kmol/kgcat s

r_{CO}^o rate of CO formation in steam reforming, kmol/kgcat s

$r_{CO}^{\bullet o}$ rate of CO formation in reverse water gas shift reaction, kmol/kgcat s

$r_{CO_2}^o$ rate of CO$_2$ formation in steam reforming, kmol/kgcat s

$r_{CO_2}^{\bullet o}$ rate of CO$_2$ disappearance in reverse water gas shift reaction, kmol/kgcat s

r_p pore radius of catalyst, m

S_g surface of porous solid, m^2/kg

Sc   Schmidt number

S_V surface area per unit volume solid, m^2/m^3

$\Delta S^{o}_{j,a}$ entropy of species i in the adsorbed state, J/mol K

$\Delta S^{o}_{j,g}$ standard entropy of component i , J/mol K

s   active site of catalyst

T   temperature, K

t   time of collecting data from the beginning of the test

t_{1-2} the time duration from the beginning of the test to the end of the test

u_i molar velocity, m/s

$u^{\bullet}$ molar average velocity, m/s

$\overline{V_A}$ the equilibrium mean molecular velocity of component A, m/s

V_I defined by equation (7.17)

$(\sum v)$ diffusion volume of molecule

W   weight of catalyst, kg

X_{CH_4} methane conversion in steam reforming, and conversion of CO_2 into methane

in reverse water gas shift reaction respectively

X_{CO_2} CO_2 conversion in reverse water gas shift reaction, and conversion of

methane into CO_2 in steam reforming respectively

y   molar fraction

z   axial coordinate of pellet, m

Greek symbols

α defined in equation (3.7)

α_{AB} α_{ij} temperature dependence of effective diffusivity of component A in B

(i in j), α_{ij} also parameters in equations (7-27,28,29)

β_{AB} , β_{ij} pressure dependence of effective diffusivity of component A in B (i in j)

δ_1, δ_2 convergent criterion

$\epsilon_P, \epsilon_a, \epsilon_I$ porosity of particle, porosity in macropores and micropores respectively

          dimensionless

λ mean free path, cm

λ_f thermal conductivity of the catalyst, kJ/m s K

μ viscosity of fluid, kg/m s

ν_{ij} stochiometric coefficient of component i in reaction j

θ_s coverage fraction of hydrogen sulphide

ρ density of fluid, kg/m^3

ρ_p, ρ_B density of catalyst particle and catalyst bed, respectively, kg/m^3

σ molecular diameter of gas, cm

σ_{AB} collision diameter, $\overset{\circ}{A}$

$\sigma_i(k)$ standard derivation of parameter i estimation, dimensions as the same parameter i

τ tortuosity

Ω cross-sectional area of the catalyst bed, m^2

ω_{AB} collision integral, K

Superscripts

i   inlet of reactor

o   oulet of reactor

Subscripts

A   component A

a   macropore

B   component B

b   bulk phase

e   effective

g   gaseous state

i   component i , reaction i, or micropore

j   component j or reaction j

m   mixture

s   surface, or shellside

t   tubeside

REFERENCES

Adris, AM, Elnashaie, SSEH. and Hughes, R., 1991, A fluidized-bed membrane reactor for the steam reforming of methane, Can. J. Chem. Eng., Vol. 61, No.5, pp.1061-1070.

Agnelli, M.E., Demicheli, M.C. and Ponzi, E.N., 1987, Catalytic Deactivation on methane steam reforming catalysts: 2. Kinetics study, Ind. Eng. Chem. Res., Vol. 26, pp.1707-1713.

Akres, W.W. and Camp, D.P., 1955, Kinetics of methane-steam reforming, AIChEJ. Vol. 1, pp.471-475.

Al-Ubaid, A.S., 1984, Methane steam reforming activity, stability and characterisation of nickel catalysts, Ph.D. Thesis, University of Notre Dame, Indiana, USA.

Allen, D.W., Gerhard, E.R. and Likins, Jr.M.R., 1975, Kinetics of the methane-steam reaction, Ind. Eng. Chem. Pro. Des. Dev., Vol.14, No. 3, pp.256-259.

Arnold, M.R., Atwood, K., Baugh, H.M., and Smyser, H.D., 1952, Nickel catalysts for hydrocarbon-steam reforming, Ind. Eng. Chem., Vol. 44, pp.999-1006

Atroshchenko, V.I., Raman, Sh.K. and Zryagintsev, G.I., 1969, Kinetics of Conversion of natural gas by steam under pressure, J. Appl. Chem., USSR, Vol. 42, pp.1496-1503.

Baker, R.T.K. and Chludzinski, J.J.JR., 1980, Filamentous carbon growth on a nickel-iron surface: The effects of various oxide additives, J. Catal., Vol.64, pp.464.

Balder, J.R., Petersen, E.E., 1968, Poisoning studies in a single pellet reactor, Chem. Eng. Sci., Vol. 23, pp.1287.

Barbieri, G., Violante, V., DiMaio, FP., Criscuoli, A. and Drioli, E., 1997, Methane steam reforming analysis in a palladium-based catalytic membrane reactor, Ind. Eng. Chem. Res., Vol. 36, No. 8, pp. 3369-3374.

Barrer, R.M., 1953, A new approach to gas flow in a capillary, J. Phys. Chem., Vol. 57, pp.35.

Bartholomew, C.H. and Farrauto, R., 1976, Chemistry of nickel-alumina catalysts, J. Catal., Vol. 45, pp.41-53.

Bartholomew, C.H., Weatherbee, G.D. and Jarvi, G.A., 1979, Sulfur poisoning of nickel methanation catalysts: 1. In site deactivation by H_2S of nickel and nickel bimetalics, J. Catal., Vol. 60 , pp.257-269.

Bartholomew, C.H., Pannell, R.B. and Butler, J.L., 1980, Support and crystallite size effects in CO hydrogenation on nickel, J. Catal., Vol. 65, pp.335-347.

Bartholomew, C.H., 1982, Carbon deposition in steam reforming and methanation, Catal. Rev.-Sci. Eng. Vol. 24, pp.67-112

Beveridge, G.S., Goldie, P.J., 1972, A simple approach for the rapid estimation of the diffusibility of porous solids, Chem. Eng. J., Vol. 3, pp.232.

Bhatta, K.S.M. and Dixon, G.M., 1969, Roles of urania and alumina as support in the steam reforming of n-butane at pressure over nickel containing catalysts, Ind. Eng. Chem. Pro. Res. Dev., Vol. 8, pp.324.

Blue, R.W., Holm, V.C.F., Regier, R.B., Edwin Fast and Heckelsberg, L.F., 1952, Effect of granule size: in dehydrogenation and in hydrogen transfer reactions, Ind. Eng. Chem., Vol. 44 pp.2710-2715.

Blyhoder, G.D., and Boeen, D.O., 1962, Infrared spectra of sulfur compounds adsorbed on silics-supported nickel, J. Phys. Chem. pp.1288-1292.

Bodrov, N.M., Apelbaum, L.O. and Temkin, M.I., 1964, Kinetics of the reactions of methane with steam on the surface of nickel, Kinet. Catal. Vol. 5. pP.696-705.

Bodrov, N.M., Apelbaum, L.O. and Temkin, M.I., 1967, Kinetics of the reaction of methane with water vapour, catalyzed nickel on a porous carrier, Kinet. Catal. Vol. 8, pp.821-828.

Bodrov, N.M., Apelbaum, L.O. and Temkin, M.I., 1968, Kinetics of the reactions of methane with steam on the surface of nickel at 400-600°C, Vol. 9, pp.1065-1071.

Borowieck, T. and Golebiowski, A., 1994, Influence of molybdenum and tungsten additives on the properties of nickel steam reforming catalysts, Catal. Letters, Vol. 25, pp309-313.

Borowieck, T. and Golebiowski, A. and Stasinska, B., 1997, Effects of small MoO$_3$ additives on the properties of nickel catalysts for the steam reforming of hydrocarbons, Appl. Catal. A-General, Vol.153, pp.141-156.

British patent, 1927, 267535, to Farben, I.G..

Brown, L.F., Haynes, H.W., Maogue, W.E., 1969, The prediction of diffusion rates in porous materials at different pressures, J. Catal., Vol 14, pp.220.

Burghardt, A., Smith, J.M., 1979, Dynamic response of a single catalyst pellet, Chem. Eng. Sci.,Vol 34,pp.267.

Butt, J.B., 1980, Reaction kinetics and reactor design, Prentice-Hall., Englewood Cliffs, NJ, pp.169.

Chai, M., Machida, M., Eguchi, K. and Arai, H., 1993, Promotion of methane steam reforming using ruthenium-dispersed microporous alumina membrane reactor, Chemistry Letters, No.1, pp.41-44.

Christiansen, L.J., and Andersen, S.L., 1980, Transient profiles in sulphur poisoning of steam reformers, Chem. Eng. Sci. Vol. 35, pp.314-321.

Davis, B.R. and Scott, D.S., 1965, Measurement of the effective diffusivity of porous pellets, 58 th Ann. Mtg. of AIChE, Philadelphia, Dec.5-9, pp.48D.

De Deken, J.C., Devos, E.F. and Froment, G.F., 1982, Steam reforming of natural gas, Chem. Reaction Eng. ACS Symp. Ser., pp.196.

Den Besten, I.M., and Selwood, P.W., 1962, The chemisorption of hydrogen sulfide, methyl sulfide, and cyclohexene on supported nickel catalyst, J. Catal., Vol.1, pp.93-102.

Dirksen, H. A. and Riesz, C. H., 1953, Equilibrium in the steam reforming of Natural gas, Ind. Eng. Chem., Vol.45, No.7, pp.1562-1565.

Dogu, G., Smith, J.M., 1976, Rate parameters from dynamic experiments with single catalyst pellets, Chem. Eng. Sci., Vol. 31, pp.123.

Draper, N.R. and Smith, H., 1981, Applied regression analysis, Second edition, John Wiley and son, New york, pp.462.

Dullien, F.A.L., Scott, D.S., 1962, The flux-ratio for binary counterdiffusion of ideal gases, Chem. Eng. Sci., Vol. 17,pp.771.

Elnashaie, SSEH, Adris, A.M., Al-ubaid, A.S. and Soliman, M.A., 1990, On the non-monotonic behaviour of methane-steam reforming kinetics, Chem. Eng. Sci., Vol.45, pp.491

Evans, R.B., Watson, G.M. and Mason, E.A., 1961, Gaseous diffusion in porous media at uniform pressure, J. Chem. Phys., Vol. 35, pp.2076.

Fowler, R.W. and Bartholomew, C.H., 1979, Activity, adsorption, and sulfur tolerance studies of a fluidized bed methanation catalyst, Ind. Eng. Chem. Prod. Res. Dev., Vol. 18, No.4, pp. 339-347.

Froment, G.F. and Bischoff, K.B., 1979, Chemical Reactor Analysis, John Wiley and Sons Press, pp.146.

Fu, C.-C., Ramesh, M. S. P. and Haynes, Jr., H. W., 1986, Analysis of gas chromatography pulse dispersion data for the system n-butane- zeolite N_aY, AIChEJ., Vol. 32, pp.1846.

Fuller, E.N., Schettler, P.D.,and Giddings, J.C., 1966, A new method for prediction of binary gas phase diffusion coefficients, Ind. Eng. Chem., Vol. 58, pp.19.

Gardner, D.C. and Bartholomew, C.H., 1981, Kinetics of carbon deposition during methanation of carbon monoxide, Ind. Eng. Chem. Pro. Res. Dev., Vol.20, pp.80-87.

Garza, G. and Rosales, M. A., 1983, Adsorption and diffusion rate parameters from dynamic gravimetric techniques, Ind. Eng. Chem. Pro. Res. Dev., Vol. 22, pp.168-169.

Gobina, E. and Hughes, R., 1994, Ethane dehydrogenation using a high temperature catalytic membrane reactor, J. Membrane. Sci., 90, pp.11.

Goodknight, R.C., Fatt, I., 1961, The diffusion time-lag in porous media with dead-end pore volume, J. Phys. Chem., Vol. 65, pp.1709.

Growcock, F.B., et al, 1977-1978, Brookhaven National Laboratory Report to US NRC, BNL-NURGE-50683, 50883

Hahn, J.L., Petersen, E.E., 1970, Poisoning studies in a single pellet catalytic reactor, Can. J. Chem. Eng., Vol. 48, pp.147.

Haynes, Jr., H. W., and Sarma, P. N., 1973, A model for the application of gas chromatography to measurement of diffusion in bidisperse structured catalysts, AIChEJ., Vol. 19, pp.1043.

Haynes, Jr., H. W., 1986, An analyses of sorption heat effects in the pulse gas chromatography diddusion experiment, AIChEJ, Vol. 32, pp.1750.

Haynes, Jr., H. W., 1988, The experimental evaluation of catalyst effective diffusivity, Catal. Rev. –Sci. Eng., Vol.30, pp.563-627.

Heering, J., Kotter, M. and Reikert, L., 1982, Diffusion and catalytic reaction in zeolite ZSM-5, Chem. Eng. Sci., Vol. 37, pp.581-584.

Hirschfelder, J.O., Curtis, C.F. and Bird, R.B., 1954, Molecular theory of gases and liquid, Wiley, New York.

Hoogschagen, 1955, Diffusion in porous catalysts and adsorbents, Ind. Eng. Chem., Vol. 47,pp.906.

Hsiang, T. C.-S. and Haynes, Jr., H. W., 1977, Axial dispersion in small diameter beds of large, spherical particles, Chem. Eng. Sci., Vol. 32, pp.678.

Hsu, L.-K.P. and Haynes, Jr., H. W., 1981, Effective diffusivity by the gas chromatography technique: analysis and application to measurements of diffusion of various hydrocarbons in zeolite $N_a Y$, AIChEJ., Vol. 27, pp.81-91.

Hulburt, H.H. and Srini Vasan, C.D., 1961, Design of experiments on the kinetics of the water gas shift reaction, AIChEJ., Vol. 17, PP.143.

Ipatieff, V.N., Monroe, G.S. and Fisher, L.E., 1950, Low temperature hydrogen production, Ind. Eng. Chem., Vol. 42, pp.92-94.

Johnson, M.F.L., Stewart, W.E., 1965, Pore structure and gaseous diffusion in solid catalysts, J. Catal., Vol. 4, pp.248.

Kocirik, M., Zikanova, A. and Dubsky, J., 1973, Numerical solution of the adsorption kinetics with non-linear isotherm, Ind. Eng. Chem. Fund., Vol. 12, pp.440-443.

Kocirik, M. and Zikanova, A., 1974, The analysis of the adsorption kinetics in material with polydisperse pore structure, Ind. Eng. Chem. Fund., Vol. 13, pp.347-350.

Kondis, E. F. and Dranoff, J. S., 1971, Kinetics of isothermal sorption of ethane on 4A molecular sieve pellets, Ind. Eng. Chem. Proc. Des. Dev., Vol. 10, pp.108-114.

Kameyama, T., Dokiya, M., Fujishige, M, Yokokawa, H., and Fukuda, K., 1981, Possibility for effective production of hydrogen from hydrogen sulfide by means of a porous Vycor glass membrane, Ind. Chem. Fundam., Vol.20, pp.97.

Kester, K.B. and Falconer, J.L., 1984, CO methanation on low-weight loading Ni/Al_2O_3: Multiple reaction sites, J. Catal., Vol. 89, pp.380-391.

Kopsel, R., Richter, A. and Meyer, B., 1980, Catalyst deactivation and Kinetics of methane steam reforming, Chem. Tech., Vol.32, pp.460.

Laegsgaard Jorgensen, S., Hojlund Nielsen, P.E. and Lehrmann, P., 1995, Steam reforming of methane in a membrane reactor. Catalysis Today, Vol.25, pp.303

Leach, H.F., Mirodatos, C. and Whan, D.A., 1980, The exchange of methane, ethane, and propane with deuterium on silica-supported nickel catalyst, J. Catal., Vol. 63, pp.138-151.

Lee, Hong H., 1985, Heterogeneous reactor design, Butterworth Publishers, Stoneham, MA, pp.66.

Lewis,W.K., Gilliland, E.R. and Reed, W.A., 1949, Reaction of methane with copper oxide in a fluidized bed, Ind. Eng. Chem., Vol. 41, pp.1227-1237.

Ma, Y.H. and Roux, A.J., 1973, Multicomponent rates of sorption of SO_2 and CO_2 in sodium mordenite, AIChEJ., Vol. 19, 1055-1059.

Ma, Y. H. and Lee, T. Y., 1976, Transient diffusion in solids with a bipore distribution, AIChEJ., Vol. 22, pp.147-152.

Marquardt, D. W., 1963, An algorithm for the least-squares estimation of non-linear parameters, J. Soc. Ind. Appl. Math., Vol.11, pp.431-441.

McCarty, J.G. and Wise, H., 1980, Thermodynamics of sulfur chemisorption on metals. 1. alumina-supported nickel, J. Chem. Phys., Vol.72, No.12, pp.6332-6337.

Mears, D.E., 1971, Tests for transport limitations in experimental catalyst reactors, Ind. Eng. Chem. Pro. Des. Dev., Vol. 10, pp.541-547.

Ng, C.F., and Martin, G.A., 1978, Poisoning of Ni/SiO$_2$ catalyst with H$_2$S : Chemisorption of H$_2$, CO, C$_6$H$_6$ and C$_2$H$_2$ studied by magnetic methods, J. Catal. 54, pp.384-396.

Numaguchi, Toru and Katsutoshi, Kikuchi, 1988, Intrinsic kinetics and design simulation in a complex reaction network: steam-methane reforming, Chem. Eng. Sci., Vol.43, pp.2295-2301.

Oliphant, J.L., Foeler, R.W., Pannel, R.B., and Bartholomew, C.H., 1978, Chemisorption of hydrogen sulfide on nickel and ruthenium catalyst I. Desorption isothems, J. Catal. 51, pp.229-242.

Quach, P.T. and Rouleau, U.D., 1975, Kinetics of the methane-steam reaction over nickel catalyst in a continuous stirred tank reactor. J. Appl. Chem. Biotech. Vol.25, pp.445-459

Raymont, M.E.D., 1975, Make hydrogen from hydrogen sulphide, Hydrocarbon Proc., 54, pp.139.

Reed, E.M. and Butt, J.B., 1971, Surface diffusion of single sorbates at low and intermediate surface coverage, J. Phy. Chem., Vol.75, pp.133-141

Reitmeier, R.E., Kenton Atwood, Bennett, JR., H.A. and Baugh, H.M., 1948, Production of synthesis gas, Ind. Eng. Chem., Vol. 40, No. 4, pp.620.

Riekert, L., 1971, Rates of sorption and diffusion of hydrocarbons in zeolites, AIChEJ. Vol.17, pp.446-454.

Ross, J.R.H. and Steel, M.C.F., 1972, Mechanism of the steam reforming of methane over a copreciptated nickel alumina catalyst, J.Chem. Soc. Faraday. Trans., Vol. 1, pp.69.

Rostrup-Nielsen, J.R., 1968, Chemisorption of hydrogen sulphide on a supported nickel catalyst, J. Catal., Vol.11, pp.220-227.

Rostrup-Nielsen, J.R., 1974, Coking on nickel catalysts for steam reforming of hydrocarbons, J. Catal., Vol. 33, pp.184-201.

Rostrup-Nielsen, J.R., 1982, in "Progress in Catalyst Deactivation "(J.L. Figueiredo, ed.) Martinus Nijhoff Publ. The Hague, p.209.

Rostrup-Nielsen, J.R., 1984, Catalytic Steam Reforming,, Springer Verlag, Berlin.

Rostrup-Nielsen, J.R., 1984, Sulfur-passivated nickel catalyst for carbon free steam reforming of methane, J. Catal., 85, pp.31-43.

Rothfield, L., 1963, Gaseous Counterdiffusion in catalyst pellets, AIChEJ., Vol. 9, pp.19.

Ruthven, D. M. and Derrah, R. I., 1972, Sorption in Davison 5A molecular sieves, Can. J. Chem, Eng., Vol. 50, pp743-747.

Ruthven, D. M. and Lee, C. K., 1981, Kinetics of non-isothermal sorption: system with bed diffusion control, AIChEJ., Vol. 27, pp.654-663.

Ruthven, D. M., Lee, C. K. and Yucel, H., 1980, Kinetics of non-isothermal sorption in molecular sieve crystals, AIChEJ., Vol. 26, pp.16-23

Ruthven, D. M., Varlitis, A. and Coughlin, K., 1982, Diffusion of n-Decane in 5A zeolite crystals, AIChEJ., Vol. 28, pp.840-841

Sabastian, J.J.s., and Riesz, C.H., 1951, Sulfur-resistant catalysts for reforming of propane, Ind. Eng. Chem., Vol. 43, pp.860-866.

Saleh, J. M., Kemball, C. and Roberts, M. W., 1961, Trans. Farad. Soc. 57, pp.1771.

Sarmah, S.K. and Haynes, Jr. H.W. 1989, Effective diffusivity by pulse gas-chromatography at elevated pressures, AIChEJ, Vol.35, pp.1728-1734

Satterfield, C.N., 1968, Diffusion in commercially manufactured pelleted catalysts, Ind. Eng. Chem. Prod. Des. Dev., Vol. 7, pp.256.

Satterfield, C.N., 1970, Mass transfer in heterogeneous catalysis, M.I.T Press, pp.112.

Satterfield, C.N., 1980, Heterogeneous catalysis in practice, McGraw-Hill, pp.349.

Satterfield, C.N. and Frabetti, A.J. Jr, 1967, Sorption and diffusion of gases hydrocarbons in synthetic mordenite, AIChEJ. Vol. 13, pp.731-738

Satterfield, C.N. and Margetts, W.G., 1971, Diffusion in sodium mordenite, Vol. 17, pp.295-299

Schouten, F.C., Gijzeman, Q.L.J. and Bootsma, G.A., 1979, Interaction of methane with Ni(111) and Ni(100); Diffusion of carbon into nickel through (100) surface; An AES-LEED study, Surface Sci., Vol. 87, pp.1-12.

Scott, D.S., Dullien, F.A.L., 1962, Diffusion of ideal gases in capillaries and porous solids, AIChEJ., Vol. 8, pp.113.

Shaofen, Li, 1986, Chemstry and catalytic reaction engineering, Chemical industry press, Beijing, pp.197.

Shu, J., Grandjean, BPA.and Kaliaguine, S., 1994, Methane steam reforming in asymmetric Pd-Ag and Pd-Ag /Porous SS membrane reactors, Appl. Catal. A-General, Vol.119, No.2, pp.305-325.

Smith, J.M., Robertson, J.L., 1963, Flow and diffusion characteristics of alumina catalyst pellets, AIChEJ., Vol. 9, pp.342.

Soliman, M.A., Adris, M.A., Al-Ubaid, A.S. and El-Nashaie, S.S.E.H., 1992, Intrinsic kinetics of nickel/calcium aluminate catalyst for methane steam reforming, J. Chem. Tech. Biotechnol., Vol.55, pp.131-138.

Suzuki, M., Smith, J.M., 1971, Kinetics studies by chromatography, Chem. Eng. Sci., Vol. 26, pp.221-235.

Suzuki, M., Smith, J.M., 1972, Dynamics of diffusion and adsorption in a single catalyst pellet, AIChEJ., Vol.27, pp.326.

Trimm, DL., 1997, Coke formation and minimisation during steam reforming reactors, Catal. Today, Vol.37, pp.233-238.

Twigg, M. V., 1989, Catalyst handbook, Second enition, Wolfe Publishing Ltd, England

Uemiya, S., Sato, N., Ando, H., Matsuda,T. and Kikuchi, E., 1991, Steam reforming of methane in a hydrogen-permeable membrane reactor, Appl. Catal.,, 1991, Vol. 67, No.2 , pp.223-230.

Van Hook, J.P., 1980, Methane Steam Reforming, Catal. Rev.- Sci. Eng., Vol. 21, pp.1-51.

Wagner, E.S. and Froment, G.F., 1992, Steam reforming analyzed, Hydrocarbon Processing, 7, pp. 69-78.

Wakao, N., Smith, J.M., 1962, Diffusion in catalyst pellets, Chem. Eng. Sci., Vol. 17, pp.825.

Wakao, N. and Tanisho, S., !974, Chromatographic measurements of particle-gas mass transfer coefficients at low Reynolds number in packed bed, Chem. Eng. Sci., Vol. 29, pp.1991.

Wang, C.T., Smith, J.M., 1983, Tortuosity factors for diffusion in catalyst pellets, AIChEJ., Vol. 29, pp.132.

Wood, B.J., McCarty, J.G., Sheridan, D., Ablow, C.M. and Wise, H., 1980, Final report to DOE (DE-AC21-78ET11030), October 24.

Xu, J. and Froment, G.F., 1989, Methane-steam reforming, methanation, and water gas shift-I. Intrinsic kinetics, AIChEJ., Vol. 35, pp.88-96.

Yamazaki, O., Tomishige. And Fujimoto, K., 1996, Development of highly stable nickel-catalyst for methane steam reforming under low steam to carbon ratios, Appl. Catal. A-general, Vol.136, pp.49-56.

Yang, K.H. and Hougen, O.A., 1950, Determination of mechanism of catalyzed gaseous reactions, Chem. Eng. Prog., Vol. 46, No. 3, pp.147-157.

Yang, R.T., Liu, R.T., 1982, Gaseous diffusion in porous solids at elevated temperature, Ind. Eng. Chem. Fund., Vol 21. pp.262

Appendix A   Experimental Results for Methane Steam Reforming and the Reverse Water Gas Shift Reaction

Table 1   Experimental results for methane steam reforming (1)

W/ F_{CH4} kgcat. s/kmol	2160	4320	65161	8712	10872	13356
T K	X_{CH4} %					
748	2.65	5.36	7.45	9.56	12.14	14.06
773	4.17	8.54	12.25	16.62	20.25	22.94
798	7.36	13.55	19.05	23.48	28.35	31.56
823	12.80	22.80	29.61	34.92	40.87	43.53
	X_{CO2} %					
748	2.55	5.13	7.12	9.10	11.56	13.32
773	3.99	8.1	11.48	15.63	18.9	21.33
798	6.86	12.56	17.35	21.16	25.56	28.23
823	11.43	20.24	25.68	30.10	35.11	37.42
	S_{CO2}					
748	.9626	.9566	.9554	.9517	.9525	.9484
773	.9517	.9475	.9382	.9407	.9329	.9297
798	.9322	.9269	.9109	.9012	.9016	.8946
823	.8928	.8878	.8671	.8620	.8591	.8597

P_t=120 kPa, $H_2O/CH_4/H_2$= 4/1/1

Table 2 Experimental results for methane steam reforming (2)

W/ F_{CH4} kgcat s/kmol	2880	4320	6576	8712	10872	13356
T K	X_{CH4} %					
748	2.18	3.46	5.43	7.36	9.36	11.67
773	3.86	6.13	9.92	13.00	16.44	19.72
798	6.24	9.24	14.67	19.48	24.20	28.54
823	10.59	15.37	22.09	29.20	35.28	40.58
	X_{CO2} %					
748	2.13	3.36	5.26	7.10	9.00	11.25
773	3.71	5.83	9.40	12.39	15.57	18.79
798	5.96	8.68	13.75	18.21	22.89	26.45
823	9.82	14.13	19.88	26.46	31.92	36.26
	S_{CO2}					
748	.9662	.9699	.9681	.9643	.9625	.9634
773	.9606	.9506	.9542	.9533	.9471	.9529
798	.9542	.9398	.9372	.9346	.9276	.9268
823	.9276	.9200	.9001	.8888	.9050	.8927

P_t=120 kPa, $H_2O/CH_4/H_2$= 5.5/1/1

Table 3 Experimental results for methane steam reforming (3)

W/ F_{CH4} kgcat s/kmol	1.2	1.81	2.42	3.02	3.71
T K	X_{CH4} %				
748	3.61	5.64	7.89	9.87	12.10
773	5.50	8.50	11.67	14.50	17.19
798	8.13	12.61	16.45	20.23	24.50
823	13.50	20.50	28.08	33.76	38.33
	X_{CO2} %				
748	3.52	5.58	7.69	9.58	11.76
773	5.34	8.21	11.24	13.93	16.54
798	7.83	12.09	15.68	19.08	23.13
823	12.67	19.06	25.82	30.73	34.87
	S_{CO2}				
748	.9775	.9762	.9737	.9713	.9713
773	.9718	.9643	.9643	.9605	.9625
798	.9620	.9592	.9528	.9456	.9430
823	.9394	.9301	.9190	.9105	.9102

P_t=120 kPa, $H_2O/CH_4/H_2$= 7/1/1

Table 4 Experimental results for methane steam reforming (4)

W/ F_{CH4} Kgcat s/kmol	2880	4320	6576	8712	10872	13356
T K	X_{CH4} %					
748	3.08	5.06	7.91	10.45	12.39	15.43
773	5.57	8.80	12.78	16.50	18.75	22.75
798	8.79	13.85	20.53	23.38	28.72	32.55
823	11.64	18.32	24.85	31.11	37.18	39.84
	X_{CO2} %					
748	3.00	4.93	7.78	10.11	11.94	14.79
773	5.37	8.49	12.22	15.71	17.83	21.53
798	8.16	12.85	19.08	21.69	26.51	29.84
823	10.79	16.85	22.65	27.91	33.32	35.45
	S_{CO2}					
748	.9732	.9751	.9710	.9670	.9635	.9584
773	.9635	.9653	.9560	.9520	.9507	.9465
798	.9284	.9279	.9289	.9279	.9232	.9167
823	.9271	.9195	.9114	.8972	.8962	.8899

P_t= 300 kPa, $H_2O/CH_4/H_2$= 5.5/1/1

Table 5 Experimental results for methane steam reforming (5)

W/ F_{CH4} Kgcat s/kmol	0.50	0.75	1.00	1.25	1.50	1.75
T K	X_{CH4} %					
748	3.68	4.75	6.14	7.23	8.07	9.00
773	5.55	7.81	9.78	11.36	12.44	13.40
798	8.22	12.41	15.20	17.93	19.05	19.58
823	13.90	18.15	20.98	24.41	26.96	28.39
	X_{CO2} %					
748	3.56	4.67	6.00	7.06	7.85	8.76
773	5.36	7.53	9.42	10.91	11.93	12.81
798	7.47	11.52	14.16	16.71	17.81	18.26
823	12.10	16.17	18.72	21.96	24.40	25.74
	S_{CO2}					
748	.9674	.9832	.9778	.9765	.9727	.9733
773	.9658	.9641	.9632	.9604	.9590	.9560
798	.9088	.9283	.9316	.9320	.9349	.9326
823	.8705	.8909	.8923	.8996	.9050	.9067

P_t= 600 kPa, $H_2O/CH_4/H_2$= 5.5/1/1

Table 6 Experimental results for reverse of water gas shift reaction(1)

W/ F_{CO2} kgcat s/kmol	720	900	1080	1440	1800
T K	$X_{CO2}\%$				
598	2.54	2.84	3.12	3.50	3.91
623	4.46	5.07	5.54	6.26	6.98
648	8.15	8.77	9.32	10.45	11.16
673	12.16	13.00	14.36	15.06	15.66
	$X_{CH4}\%$				
598	0.54	0.65	0.75	0.94	1.16
623	1.06	1.28	1.51	1.86	2.29
648	2.04	2.36	2.67	3.39	4.14
673	3.18	3.74	4.93	5.86	6.98
	$X_{CO}\%$				
598	2.00	2.19	2.37	2.56	2.75
623	3.40	3.79	4.03	4.40	4.69
648	6.11	6.41	6.65	7.06	7.32
673	8.98	9.26	9.43	9.20	8.68

P_t=120 kPa, H_2/CO_2= 0.75/1

Table 7　Experimental results for reverse water gas shift reaction (2)

W/ F_{CO2} Kgcat s/kmol	720	900	1080	1440	1800
T K	X_{CO2}%				
598	2.30	2.57	2.81	3.24	3.77
623	4.17	4.58	4.99	5.75	6.30
648	7.16	7.84	8.29	8.93	9.64
673	10.36	11.07	11.60	12.00	12.48
	X_{CH4}%				
598	0.45	0.51	0.61	0.76	1.11
623	0.88	1.04	1.22	1.56	1.88
648	1.59	1.89	2.16	2.62	3.20
673	2.45	2.81	3.19	3.85	4.88
	X_{CO}%				
598	1.85	2.06	2.20	2.48	2.60
623	3.29	3.54	3.77	4.19	4.42
648	5.57	5.95	6.13	6.31	6.44
673	7.91	8.26	8.41	8.15	7.60

P_t=120 kPa, H_2/CO_2 = 0.50/1

Appendix B   Calculation of the Effects of Mass Transfer and Heat Transfer

B1   Calculation of effect of mass transfer

Component properties

	CH_4	H_2O	CO	CO_2	H_2
Molecular weight	6.043	18.015	28.010	44.010	2.016
Critical temperature T_C, K	190.6	647.3	132.9	304.2	33.3
Critical volume, V_C cm³/mol	99	56	93.1	94	65
Molecular diffusion volume ($\sum v$)	24.42	12.7	18.9	26.9	7.07

Basic conditions:

reaction temperation T= 823 K,   reaction pressure P_t= 120 kPa

catalyst weight W_{cat}= .3 g= 3× 10^{-4} kg   steam/methane/hydrogen=4/1/1

methane conversion X_{CH_4} = 0.4353   conversion of methane into CO_2, X_{CO_2} =.3742

methane flow rate F_{CH4}= 31.05 cm³/min =2.3103× 10^{-8} kmol/s

diameter of catalyst particle d_p=0.15 mm=0.00015 m

solid density of catalyst ρ_s = 2121 kg/m³

bed density of catalyst ρ_B= 1055 kg/m³

outer surface of catalyst a_s = 18.86 m²/kg

reactor cross section area A_R= 7.536 × 10^{-5} m²

composition of bulk phase: y_{CH_4} = .1244, y_{H2O} =.5655, y_{CO}= .0045,

y_{CO2}=.0272, y_{H2}= .2784

The total mass flow rate F_M= F_{CH4} (M_{CH4}+ M_{H2}) + 4 $F_{CH4}M_{H2O}$

= 2.079× 10^{-6} kg/s

The mass flow rate, $G = F_M/A_R$

$$= 0.0276 \text{ kg/m}^2 \text{ s}$$

The average molecular weight is calculated by

$$M_{ave} = \sum_{i=1}^{5} y_i M_i$$

$$= 14.07$$

The density of bulk phase ρ_b, obtained from

$$\rho_f = \frac{M_{ave}}{22.4} \frac{273}{T} \frac{P_t}{100}$$

$$= 0.249 \text{ kg/m}^3$$

Methane diffusivity D_{Am} in bulk phase is calculated by following equations:

$$D_{ij} = \frac{0.00001 \times T^{1.75} \left(\dfrac{1}{M_i} + \dfrac{1}{M_j} \right)^{1/2}}{P_t \left(\left(\sum v \right)_i^{1/3} + \left(\sum v \right)_j^{1/3} \right)^2}$$

$$D_{im} = \frac{1 - y_i}{\displaystyle\sum_{j \neq i} \frac{y_j}{D_{ij}}}$$

Substituting data in equations given above,

$$D_{Am} = 1.61 \times 10^{-4} \text{ m}^2/\text{s}$$

Mixture viscosity:

The viscosity of pure component is approximated with the Bromley-Wilke (1951) equation:

$$\mu_i = \frac{3.33 \times 10^{-6} \left(M_i T_{ri} \right)^{1/2}}{V_{Ci}^{2/3}} f(1.33 T_{ri})$$

where $\qquad T_{ri} = \dfrac{T}{T_{Ci}}$

and
$$f(1.33T_{ri}) = 1.058T_{ri}^{0.645} - \frac{0.261}{(1.9T_{ri})^{0.9 \lg(1.9T_{ri})}}$$

The mixture viscosity is obtained from

$$\mu_m = \frac{\sum \mu_i y_i M_i^{1/2}}{\sum y_i M_i^{1/2}}$$

$$= 2.45 \times 10^{-5} \text{ kg/m s}$$

The above results are used to calculated the mass transfer coefficient:

$$Sc = \frac{\mu_m}{\rho_f D_{Am}} = 0.6109$$

$$R_{ep} = \frac{d_p G}{\mu_m} = 0.1691$$

$$k_C = \frac{0.725}{R_{ep}^{0.41} - 0.15} \frac{G}{\rho_f} Sc^{-\frac{2}{3}} = 0.3349 \text{ m/s}$$

The criterion for the external mass transfer:

$$\frac{C_{CH_4 b} - C_{CH_4 s}}{C_{CH_4 b}} = \frac{F_{CH_4} X_{CH_4}}{a_s k_c C_{CH_4 b} W_{cat}}$$

$$= .0024$$

The value obtained for the percentage of reduction of methane across the film is negligible and it is concluded that the experiments during methane steam reforming were free of external mass transfer effects.

B2 Calculation of effect of heat transfer

The temperature difference between the bulk phase and the catalyst surface can be calculated by using the following equations:

(1)
$$T_s - T_b = \frac{r_{CH_4}(-\Delta H)}{ha_s}$$

(2)
$$T_s - T_b = \frac{j_d}{j_h}\left(\frac{Pr}{Sc}\right)^{2/3}\frac{(-\Delta H)(C_{Ab} - C_{As})}{\rho_f C_{pm}}$$

where $h = \dfrac{1.10GC_{pm}}{Pr^{0.67}(Re_p^{0.41} - 0.15)}$, heat transfer coefficient, kJ/m^2 s K

C_{pm}= mixture specific heat, kJ/kg K

ΔH= total reaction heat of complicated reaction, kJ/kmol CH$_4$

j_d = mass transfer j factor

j_h = heat transfer j factor

Pr = Prandti number, $\mu_m C_{pm}/\lambda_m$

λ_m =thermal conductivity of mixture, kJ/m s K

The mixture specific heat

The specific heat of component i, $C_{pi} = \sum\limits_{j=0}^{4} A_{ij}T^j$, kJ/kmol.

Then, the value of the mixture specific heat C_{pm} is calculated by

$$C_{pm} = \sum y_i C_{pi}/M_{ave}$$

$$= 2.84 \text{ kJ/kg K}$$

The reaction heat ΔH:

For complicated steam reforming, the total reaction heat per mole methane converted can be calculated as follows:

Let $S_{CO_2} = \dfrac{X_{CO_2}}{X_{CH_4}}$, the reaction can be considered

$$CH_4 + (1 + S_{CO_2})\, H_2O = S_{CO_2}\, CO_2 + (1 - S_{CO_2})\, CO + (3 + S_{CO_2})\, H_2$$
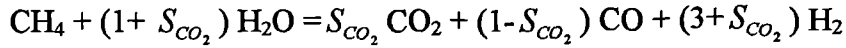
Then,

$$\Delta H^\circ = (1 - S_{CO_2})\Delta H_{CO,298} + S_{CO_2}\Delta H_{CO_2,298} + (3 + S_{CO_2})\Delta H_{H_2,298} - \Delta H_{CH_4,298} - (1 + S_{CO_2})\Delta H_{H_2O,298}$$

$$= 170671 \text{kJ/kmol}$$

$$\Delta C_p = (1 - S_{CO_2})C_{p,CO} + S_{CO_2}C_{p,CO_2} + (3 + S_{CO_2})C_{p,H_2} - C_{p,CH_4} - (1 + S_{CO_2})C_{p,H_2O}$$

So we can obtain

$$\Delta H = \Delta H^\circ + \int_{298}^{T} \Delta C_p\, dT = 189904 \text{ kJ/kmol}$$

The mixture thermal conductivity

The thermal conductivity of component i is determined by the Eucken equation

$$\lambda_i = \frac{\mu_i\left(C_{pi} + 10.37\right)}{M_i}$$

and the mixture thermal conductivity is obtained

$$\lambda_m = \frac{\sum y_i \lambda_i M_i^{1/3}}{\sum y_i M_i^{1/3}}$$

$$= 1.073 \times 10^{-4} \text{ kJ/m s K}$$

The preceding results are used to calculate the heat transfer coefficient.

$$\Pr = \frac{C_{pm}\mu_m}{\lambda_m}$$

$$= \frac{2.84 \times 2.45 \times 10^{-5}}{1.073 \times 10^{-4}} = 0.648$$

Thus

$$h = \frac{1.10 \times 0.0276 \times 2.84}{0.648^{0.67}\left(0.1691^{0.41} - 0.15\right)}$$

$$= 0.3465 \text{ kJ/m}^2 \text{ s K}$$

Therefore, the temperature difference between the bulk phase and the catalyst surface can be estimated by the equations (1) and (2).

From the equation (1)

$$T_s - T_b = -.97 \text{ K}$$

From the equation (2)

$$T_s - T_b = -1.03 \text{ K}$$

The near same values are obtained from the two equations. The small temperature difference is compared to the reaction temperature used. This indicates that the resistance of heat transfer is very small and the effect of temperature difference could be neglected in present study.

APPENDIX C: PROGRAM FOR THE PARAMETER ESTIMATION OF INTRINSIC KINETIC MODEL FOR METHANE STEAM REFORMING

```
C       A(i,j), A1(i,j)--- Martix used in the Gauss-Newton method
C       F(i,j)---Auxiliary function used in the Gauss-Newton method
C       F1(i)----Functions used in the Gauss-Newton method
C       FF1(i)---Functions used in the Gauss-Newton method
C       K(i)-----Parameter to be estimated
C       KE1,KE2--Equilibrium constants
C       M11(i)---Ratio of water vapour to methane
C       M12------Ratio of hydrogen to methane
C       P(i,j)---Partial pressure of component i
C       PT(i)----Total pressure of reaction
C       R(i,j)---Experimental reaction rate
C       RC(i,j)--Extimation reaction rate
C       X(i,j)---Molar fraction of component i


        REAL A(6,7),A1(6,7),F(2,6),FF1(2),F1(2),K(6),K0(6)
        REAL M11(29),P(5,29),PT(29),R(2,29),RC(2,29),X(2,29)
        REAL KE1,KE2,M12,M13


C       F FUNCTIONS
        FU1(P1,P2,P3,P4,P5,PA1,PA2,PA3,PA4,PA5,PA6,ke1,ke2)=(pa1*p1*
     $     p2**(.5)/p5**(2.5*.5)*(1-p3*p5**3/p1/p2/ke1)+pa3*p1*p2**
     $     (2*.5)/p5**(3.5*.5)*(1-p4*p5**4/p1/p2**2/ke2/ke1))
     $    /(1+pa4*p3+pa5*p5**.5+pa6*p2/p5)**2
        FU2(P1,P2,P3,P4,P5,PA1,PA2,PA3,PA4,PA5,PA6,ke1,ke2)=(pa3*p1
     $    *p2**(2*.5)/p5**(3.5*.5)*(1-p4*p5**4/p1/p2**2/ke2/ke1)+pa2
     $    *p3*p2**(.5)/p5**.5*(1-p4*p5/p2*p3/ke2))
     $    /   (1+pa4*p3+pa5*p5**.5+pa6*p2/p5)**2


C       N1 :PARAMETER NUMBER,N2:FUCNTION NUMBER,N3:EXPERIMENTS NUMBER

        open (unit=1,file='input.da',status='old',access=
     $       'sequential',form='formatted')
        READ(1,*) A1,X,R,m11,pt,K
        READ(1,*) N1,N2,N3,T
        close(1)

        ke1=exp(-26830/t+30.114)
        ke2=exp(4400/t-4.036)
        sum1=0
        do 10 i=1,n3
10      sum1=sum1+r(1,i)+r(2,i)
        rmean=sum1/2/n3
        DO 20 I=1,2
        DO 20 J=1,N3
        R(I,J)=R(I,J)/100
20      CONTINUE
        DO 30 I=1,2
        DO 30 J=1,N3
30      X(I,J)=X(I,J)/100
        DO 40 I=1,N3
        M12=1
        M13=M11(i)+M12+1+2*X(1,I)
        P(1,I)=(1-X(1,I))*PT(i)/M13
```

```
             P(2,I)=(M11(i)-X(1,I)-X(2,I))*PT(i)/M13
             P(3,I)=(X(1,I)-X(2,I))/M13*pt(i)
             P(4,I)=X(2,I)/M13*pt(i)
40           P(5,I)=(3*X(1,I)+X(2,I)+M12)/M13*pt(i)

C            CALCULATING MARTIX A
5000         DO 100 I=1,N1
             DO 100 J=1,N1+1
100          A(I,J)=A1(I,J)
             SUM=0
             SUM1=0
             DO 500 J=1,N3
             FF1(1)=FU1(p(1,j),p(2,j),p(3,j),p(4,j),p(5,j),k(1),K(2),K(3)
     $                 ,k(4),k(5),k(6),ke1,ke2)
             FF1(2)=FU2(p(1,j),p(2,j),p(3,j),p(4,j),p(5,j),k(1),K(2),K(3)
     $                 ,k(4),k(5),k(6),ke1,ke2)
             RC(1,J)=FF1(1)
             RC(2,j)=FF1(2)
             F1(1)=R(1,J)-FF1(1)
             F1(2)=R(2,J)-FF1(2)
             f11=ff1(1)-rmean
             f12=ff1(2)-rmean
             sum1=sum1+f11*f11+f12*f12
             SUM=SUM+F1(1)*F1(1)+F1(2)*F1(2)
C            CALCULATING MARTIX J,CAL DIFFERENTIATION BY DIFFERENCE METHOD
             DO 200 I2=1,N1
             K(I2)=K(I2)*1.02
             F(1,I2)=(FU1(p(1,j),p(2,j),p(3,j),p(4,j),p(5,j),K(1),K(2),K(3)
     $                 ,k(4),k(5),k(6),ke1,ke2)-FF1(1))/(0.02*K(I2))
             F(2,I2)=(FU2(p(1,j),p(2,j),p(3,j),p(4,j),p(5,j),K(1),K(2),K(3)
     $                 ,k(4),k(5),k(6),ke1,ke2)-FF1(2))/(0.02*K(I2))
             K(I2)=K(I2)/1.02
200          CONTINUE
             DO 300 I1=1,N1
             DO 350 J1=1,N1
             DO 400 I2=1,N2
400          A(I1,J1)=A(I1,J1)+F(I2,I1)*F(I2,J1)
350          CONTINUE
             DO 450 I2=1,N2
450          A(I1,N1+1)=A(I1,N1+1)+F(I2,I1)*F1(I2)
300          CONTINUE
500          CONTINUE
             ftest=sum1/4/(sum/(2*n3-5))


C            SOLVING LINEAR EQUATIONS,GAO SI XUAN ZU YUAN METHOD
C            D IS A FIXED DAMPING FACTOR
             D=.05
             DO 1000 I=1,N1
1000         A(I,I)=A(I,I)+D
             DO 1100 I=1,N1
             AKK=ABS(A(I,I))
             J1=I
             DO 1200 K1=I+1,N1
             IF(ABS(A(K1,I)).GT.AKK)THEN
             AKK=ABS(A(K1,I))
             J1=K1
             ENDIF
1200         CONTINUE
             DO 1300 K1=I,N1+1
             EM=A(I,K1)
```

```
           A(I,K1)=A(J1,K1)
1300       A(J1,K1)=EM
           AKK=A(I,I)
           DO 1400 K1=I,N1+1
1400       A(I,K1)=A(I,K1)/AKK
           DO 1500 I1=1,N1
           IF(I1.EQ.I) GOTO 1500
           DO 1600 K1=I+1,N1+1
1600       A(I1,K1)=A(I1,K1)-A(I1,I)*A(I,K1)
1500       CONTINUE
1100       CONTINUE


C          DETERMINING STEP LENGTH, P0 IS INITIAL STEP LENGTH
           P0=0.1
2500       DO 2100 I=1,N1
2100       K0(I)=K(I)+P0*A(I,N1+1)
           SUM1=0
           DO 2200 J=1,N3
           F1(1)=R(1,J)-FU1(P(1,J),P(2,J),P(3,J),P(4,J),P(5,J),K0(1)
      $         ,K0(2),K0(3),K0(4),K0(5),K0(6),KE1,KE2)
           F1(2)=R(2,J)-FU2(P(1,J),P(2,J),P(3,J),P(4,J),P(5,J),K0(1)
      $         ,K0(2),K0(3),K0(4),K0(5),K0(6),KE1,KE2)
2200       SUM1=SUM1+F1(1)*F1(1)+F1(2)*F1(2)
           IF(SUM1.LT.SUM) GOTO 2600
           P0=P0/2.
           If(p0.lt..00005) goto 2600
           GOTO 2500
c          STEP LENGTH IS OK


2600       SUM0=0
           DO 3000 I=1,N1
3000       SUM0=SUM0+ABS(A(I,n1+1)/K0(I))
           IF(SUM0.LT..01) GOTO 4000
           DO 3200 I=1,6
3200       K(I)=K0(I)
           GOTO 5000


4000       WRITE(*,*)'RC(1,i),R(1,i),RC(2,i),R(2,i)'
           DO 6000 i=1,n3
6000       WRITE(*,*)RC(1,i),R(1,i),RC(2,i),R(2,i)
           WRITE(*,*)'K0(1),K0(2),K0(3)',K0(1),k0(2),k0(3)
           WRITE(*,*)'K0(4),K0(5),K0(6)',K0(4),k0(5),k0(6)
           WRITE(*,*)'sum1,sum0,ftest',sum1,sum0,ftest
           END
```